FINDING COMMON GROUND TO TREAT PRIMARY AND METASTATIC CANCER: THE POTENTIAL OF TARGETING TUMOR STROMA

Albert Lo

A DISSERTATION

in

Cell and Molecular Biology

Presented to the Faculties of the University of Pennsylvania

In Partial Fulfillment of the Requirements for the Degree of Doctor of Philosophy

2016

Supervisor of Dissertation

Signature _____

Ellen Puré, Ph.D.

Grace Lansing Lambert Professor of Biomedical Science

Graduate Group Chairperson

Signature _____

Daniel S. Kessler, Ph.D.

Associate Professor of Cell and Developmental Biology

Dissertation Committee

Brian D. Keith, Ph.D., Adjunct Professor of Cancer Biology (Chairperson)

Steven M. Albelda, M.D., William Maul Measey Professor of Medicine

Carl H. June, M.D., Richard W. Vague Professor in Immunotherapy

Andy J. Minn, M.D., Ph.D., Assistant Professor of Radiation Oncology

ACKNOWLEDGEMENT

First and foremost, I would like to express my gratitude to my mentor Dr. Ellen Puré for her guidance and support. I am fortunate to have an advisor who allowed me the freedom to explore my own interests while providing guidance along the way. Her mentoring helped me explore my potential and enabled me to possess the experimental skills, critical thinking, experience and knowledge to continue my path towards becoming a rigorous scientist. Also, this work could not have been completed without the critical input and feedback from my thesis committee, Drs. Steve Albelda, Carl June, Brian Keith and Andy Minn. Their guidance and valuable advice have been indispensible. I am also grateful for the research funding provided by the Cancer Research Institute.

I wish to thank Steve Wang from Dr. Steven Albelda's lab for his collaboration on the FAP-CAR project. We worked closely together and I learned various technical skills and experience from him. I would like to thank the past and current members of my lab, James Monslow, Leslie Todd, John Chojnowski, Sonali Majumdar, Diana Avery, Rachel Blomberg, Priya Govindaraju, Allyson Lieberman and Mia Krolikoski for all their input and assistance throughout the course of my thesis work. I am also grateful to all the members from Pancreatic Cancer Working Group for their help and suggestions. I would like to acknowledge the histology core and clinical lab at the Ryan Veterinary Hospital of the University of Pennsylvania and the bioinformatics facility at the Wistar Institute for their support.

None of this would have been possible without the support of my family and friends, as these past few years have not been easy. I would like to dedicate this thesis to the memory of my father, who wished he could have witnessed me studying abroad.

ABSTRACT

FINDING COMMON GROUND TO TREAT PRIMARY AND METASTATIC CANCER: THE POTENTIAL OF TARGETING TUMOR STROMA

Albert Lo

Ellen Puré

Primary carcinomas and metastases are complex organ-like structures composed of malignant parenchymal epithelial tissues and a desmoplastic stroma formed by accumulation of hematopoietic cells, mesenchymal stromal cells and extracellular matrix. The crosstalk between malignant epithelial cells and tumor stroma is becoming increasingly appreciated as a key determinant in tumor development, progression and metastasis, as well as inducing resistance to various cancer treatments including chemotherapy, radiotherapy and immunotherapy. Mechanistic understanding of how the tumor-stromal interaction contributes to tumor progression and therapeutic resistance will advance cancer therapies and improve clinical management, especially for patients with metastatic disease. Fibroblast activation protein (FAP) is a membrane surface protease found overexpressed in cancer-associated stromal cells. Overexpression of FAP is associated with tumor progression, metastasis and recurrence, and predicts a poorer prognosis in many types of human tumors. The central goal of my thesis project is to investigate whether FAP protease and/or FAP protease-expressing stromal cells play

essential roles in tumor progression and metastasis. In collaboration with Drs. Steven Albelda and Carl June's groups, we generated chimeric antigen receptor (CAR) T cells redirected against FAP^+ stromal cells to study their impact on tumor progression. Conditional depletion of FAP^+ stromal cells by FAP-CAR T cells restrains tumor progression without causing severe toxicity. Mechanistic investigations revealed that FAP^+ stromal cells promote tumor growth via immune suppression and immune-independent remodeling of the stromal microenvironment. Additionally, using FAP-deficient mice, I found that FAP protease promotes early malignant cell seeding and pulmonary metastatic outgrowth, possibly through regulating coagulation pathways and the inflammatory response, respectively. Finally, I observed that FAP protease promotes pancreatic cancer development, as its deletion delays the progression of preneoplastic lesions and tumor formation in a genetically engineered mouse model of pancreatic ductal carcinoma. FAP protease is also essential for inducing pancreatic cancer resistance to necrotic cell death and promoting metastasis and outgrowth in multiple target organs. Together, these findings demonstrate that molecular and cellular targeting of FAP represents a promising therapeutic approach for a variety of solid tumors.

TABLE OF CONTENTS

LIST OF ILLUSTRATIONS

CHAPTER 1 – Introduction

Fibroblasts and desmoplastic response in cancer

Carcinogenesis is a multistep process that involves the crosstalk between parenchymal epithelial cells and various types of mesenchymal stromal cells, including fibroblasts, endothelial cells, inflammatory and immune infiltrates, that ultimately drives the development of clinically apparent tumors (Bhowmick et al., 2004b; Egeblad et al., 2010; Hanahan and Coussens, 2012; Jacob et al., 2012; Kalluri and Zeisberg, 2006). Across tumor types, this evolutionary process shares many aspects with the wound-healing response in which fibroblasts play critical roles in orchestrating inflammation, angiogenesis and generation of connective tissue stromal components required for tissue homeostasis and repair. Upon encountering tissue damage, fibroblasts become activated and synthesize extracellular matrix (ECM) components, including collagen, hyaluronic acid (HA) and fibronectin, and ECM remodeling proteases, resulting in a reactive stroma termed the desmoplastic response. This provisional stroma will eventually resolve when reactive fibroblasts undergo apoptosis after wound healing. Interestingly, tumors exhibit heightened accumulation of cancer-associated fibroblasts (CAFs) and deposition of ECM, and have been referred to as wounds that do not heal (Dvorak, 1986; Dvorak, 2015). Emerging evidence reveals that CAFs exhibit phenotypic and functional heterogeneity, and can regulate determinant processes of tumor initiation, progression and metastasis. Thus, it is critical to advance our understanding of CAF biology and develop successful strategies to target the epithelial-stromal cell interaction.

Molecular markers defining CAFs reveal their heterogeneity

CAFs are found in virtually all human carcinomas, but their prevalence can vary between tumor types and even within the same tumor type. In general, pancreatic, non-small-cell lung, colorectal, breast and prostate cancers usually contain high numbers of CAFs, whereas ovarian, thyroid, renal, brain, and head and neck cancers exhibit fewer (Garin-Chesa et al., 1990; Smith et al., 2013). Similar to fibroblasts, CAFs are often identified by their elongated fibroblastic appearance, a spindle-like shape. They are the nonvascular, nonepithelial and nonhematopoietic cells found in tumors. Currently, there is no consensus on the molecular definition of CAFs (Kalluri and Zeisberg, 2006; Ohlund et al., 2014; Orimo and Weinberg, 2007; Pietras and Ostman, 2010). Several molecular markers have been used to define CAFs including alpha-smooth muscle actin (α-SMA), fibroblast-specific protein 1 (FSP-1), cell membrane serine protease fibroblast activation protein (FAP), vimentin, desmin, neuron-glial antigen-2 (NG2), platelet-derived growth factor receptor-β (PDGFR-β), fibroblast-associated antigen, podoplanin, and prolyl 4-hydroxylase. Nonetheless, an emerging body of evidence reveals that CAFs are heterogeneous and that these markers do not necessarily identify the entire CAF population. Moreover, the expression of these markers is not restricted to CAFs or even to the fibroblast lineage. For instance, α-SMA is a well-established CAF marker that has been used to identify CAFs with a myofibroblast-like phenotype (Desmouliere et al., 2004). However, α-SMA expression can also be detected in various normal fibroblasts (Berdiel-Acer et al., 2014; Hawinkels et al., 2014), as well as other cell types including visceral smooth muscle cells, smooth muscle cells surrounding blood vessels, and pericytes (Wendling et al., 2009). Another commonly used CAF marker, FSP-1, is also

not limited to CAFs, as its expression can be detected in tumor cells undergoing epithelial-to-mesenchymal transition (EMT) or in macrophages during liver injury (Okada et al., 1997; Osterreicher et al., 2011). FAP is another robust CAF marker originally found highly expressed in various solid tumors but not most quiescent stromal cells (Garin-Chesa et al., 1990; Scanlan et al., 1994). However, its expression can be detected in mesodermal cells in multiple tissue types under homeostatic conditions and in tissues that undergo active remodeling (Acharya et al., 2006; Bae et al., 2008; Mathew et al., 1995; Niedermeyer et al., 2001; Wang et al., 2008). These observations indicate that CAF is a heterogeneous population and may also exhibit functional diversity to regulate tumor progression. Furthermore, since there is no single marker that can exclusively define the entire CAF population, it is possible that experimental findings targeting a certain CAF population may vary and may also depend on the tumor types studied.

Origin of CAFs

The origin of CAFs can be attributed to multiple sources (Jacob et al., 2012). Normal fibroblasts, stellate cells and mesenchymal stem cells (MSCs) within the parenchymal tissues contribute to the makeup of CAFs present within tumors (Bachem et al., 1998; Kojima et al., 2010; Kordes et al., 2009; Quante et al., 2011; Ronnov-Jessen and Petersen, 1993). CAFs may also derive from several cell types that undergo trans-differentiation. For instance, non-transformed epithelial cells can undergo EMT in response to stimuli derived from the tumor microenvironment and contribute to the generation of CAFs (Iwano et al., 2002; Petersen et al., 2001). Moreover, a lineage tracing study demonstrates that endothelial cells can undergo endothelial-to-

mesenchymal transition (EndMT), a process that involves downregulation of their CD31 expression and concomitant upregulation of FSP-1, and become CAFs to drive tumor progression (Zeisberg et al., 2007). α-SMA$^+$ or FSP-1$^+$ CAFs can also originate from adipocytes or adipose tissue-associated stromal cells (Bochet et al., 2013; Jotzu et al., 2010; Kidd et al., 2012). Additionally, bone marrow-derived fibrocytes or MSCs can be recruited into tumors and differentiate into CAFs (Direkze et al., 2004; Kidd et al., 2012; Mishra et al., 2008; Quante et al., 2011). Collectively, these studies demonstrate that preneoplastic epithelial cells or established tumors instigate local and/or systemic changes to drive the formation of heterogeneous CAFs to enable malignant progression. The contribution of CAFs from each source described above is likely to vary depending on the experimental conditions, specific tumor type, and stage of tumor progression.

Stromagenic switch to promote tumor initiation, progression, metastasis and therapeutic resistance

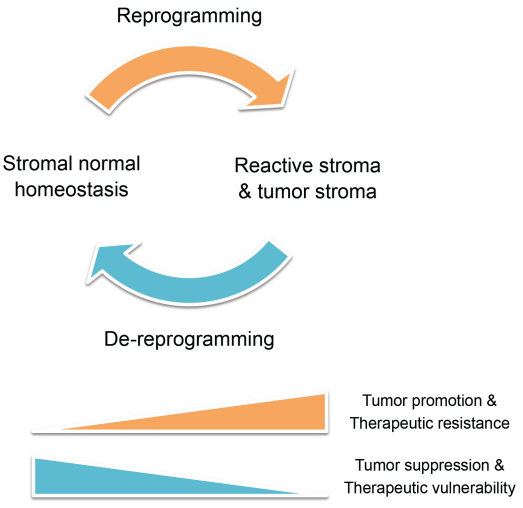

Figure 1-1. The stromagenic switch. During tumorigenesis, stromal fibroblasts can promote transition from tumor-resistant to tumor-permissive environment, drive neoplastic transformation of epithelial cells, promote tumor growth, progression, and metastasis and incite therapeutic resistance by regulating ECM remodeling, angiogenesis, inflammation and anti-tumor immunity. Such stromal-cell reprogramming can occur by transcriptional, genetic and epigenetic regulation. Targeting and/or re-engineering tumor-promoting stroma may have therapeutic implications across a broad spectrum of solid tumors.

During tumorigenesis, normal fibroblasts and MSCs may have the ability to keep the parenchymal epithelial compartments under surveillance. This concept was first illustrated by employing normal embryonic fibroblasts to inhibit growth of polyoma virus-transformed cells via a contact inhibition-dependent mechanism (Stoker et al., 1966). This observation was also noted in normal fibroblasts from other sources (Flaberg et al., 2011). Interestingly, conditional inactivation of the TGF-β type II receptor gene in mouse fibroblasts was shown to enable transgenic mice to develop lethally aggressive tumors derived from the forestomach and prostate epithelium. This finding provides compelling evidence that normal fibroblasts have the potential to prevent epithelia from becoming tumorigenic and that genetically modified fibroblasts can be sufficient to drive tumorigenesis (Bhowmick et al., 2004a). Subsequently, several reports revealed that PTEN, p53 and IKKβ signaling pathways in fibroblasts could play critical roles in restraining the tumorigenic potential of multiple solid tumors using genetically engineered mouse models (Lujambio et al., 2013; Pallangyo et al., 2015; Trimboli et al., 2009). In addition, fibroblast-derived HIF-1α and asporin were shown to inhibit breast cancer tumorigenesis and progression, respectively (Kim et al., 2012; Maris et al., 2015). Taken together, in addition to the immune-mediated tumor-suppressive mechanisms, the stromal surveillance programs may also explain why certain tumors found at autopsy appear to be in dormant states (Bissell and Hines, 2011).

Based on these observations, preneoplastic parenchymal tissues and/or established tumors must evolve to overcome the intrinsic stromal fibroblast-mediated barriers and transition

tumor-suppressive fibroblasts into tumor-supporting CAFs. Indeed, many studies have demonstrated that normal fibroblasts are functionally distinct from CAFs. Prostatic CAFs were found to be more proliferative and less prone to contact inhibition than normal prostate fibroblasts (Madar et al., 2009). Moreover, prostatic CAFs were shown to undergo increased anaerobic glycolysis and produced more lactate with respect to normal prostatic fibroblasts, a phenomenon known as the Warburg effect, to drive EMT and metastatic dissemination (Fiaschi et al., 2012). Colonic CAFs were demonstrated to enhance the proliferation and migration of tumor cells at a higher capacity compared to that of normal colonic fibroblasts (Berdiel-Acer et al., 2014). Breast CAFs exhibited higher capacity to synthesize matrix and contract collagen gels, a measure of their matrix remodeling ability, to enhance tumor cell invasion compared to normal mammary fibroblasts (Calvo et al., 2013). Gastric and dermal CAFs were found to be more capable of driving inflammation and angiogenesis than their normal counterparts (Erez et al., 2010; Quante et al., 2011). These functional differences between CAFs and their normal counterparts have been attributed to genetic or epigenetic changes that drive the malignant phenotypes. Although frequent somatic mutations in *PTEN* and *TP53* were reported in breast CAFs (Kurose et al., 2002; Patocs et al., 2007), experimental approaches utilized by these studies have been criticized. Isolation of limiting numbers of CAFs from microdissected formalin-fixed, paraffin-embedded tissues followed by highly multiplexed PCR-based analyses may have generated artifacts in these studies (Campbell et al., 2009). Some studies indicated lack no frequent somatic mutations in CAFs (Hosein et al., 2010; Qiu et al., 2008; Walter et al., 2008). Future studies with fully controlled and side-by-side comparison of the analytical procedures are required to address these issues

(Weinberg, 2008). On the other hand, several studies demonstrated that CAFs from multiple human solid tumors exhibited distinct promoter methylation patterns that distinguished them from their normal counterparts, indicating such stromagenic switch can occur by epigenetic regulation of gene expression (Hanson et al., 2006; Hu et al., 2005; Jiang et al., 2008).

Further studies demonstrated that normal fibroblasts could be reprogrammed into CAFs to drive tumor progression, invasion, metastasis and therapeutic resistance by modulating various aspects of the tumor microenvironment including ECM remodeling, angiogenesis, inflammatory and immune responses (Bronisz et al., 2012; Jacobetz et al., 2013; Lee et al., 2015; Mitra et al., 2012; Procopio et al., 2015; Provenzano et al., 2012; Shimoda et al., 2014; Valencia et al., 2014; Zhang et al., 2015). Intriguingly, once normal fibroblasts were reprogrammed, the CAF phenotype could persist *in vitro* even in the absence of continued exposure to the stimuli (Orimo et al., 2005). Nonetheless, it should be noted that CAFs might still remain some tumor inhibitory mechanisms that can impede tumor progression. For instance, certain primary human breast CAF lines secreted Slit ligands and when they bound to their cognate receptors, Robo1, expressed by human breast cancer cells, activation of Robo1 signaling restrained tumor growth via inhibiting PI3K/Akt pathway (Chang et al., 2012).

CAFs remodel ECM and promote angiogenesis

One of the distinguishing features of CAFs is their ability to synthesize various matrix components and remodel the tumor stroma by expressing matrix modification enzymes.

By regulating the synthesis and remodeling of the tumor stroma, CAFs can drive tumor progression, metastasis and therapeutic resistance through cell-autonomous and non-cell-autonomous fashions. HA and collagen, two of the major matrix components produced by CAFs, could induce tumor cell proliferation, invasion and metastasis through the CD44 or collagen receptors, respectively (Aguilera et al., 2014; Draffin et al., 2004; Valencia et al., 2012; Wang and Bourguignon, 2006; Zhang et al., 2013). Expression of HA and versican could also potentiate lymphangiogenesis, angiogenesis and macrophage recruitment to promote tumor growth (Kobayashi et al., 2010; Koyama et al., 2007; Koyama et al., 2008). Another ECM component, fibronectin, plays an important role in the formation of the premetastatic niche. Increased pulmonary fibroblast fibronectin expression was observed in the lung critical for the recruitment of bone marrow-derived cells to form a permissive niche for incoming tumor cells (Kaplan et al., 2005). Additionally, enrichment of CAFs and deposition of matrix proteins in highly desmoplastic tumors, such as PDA, contributes to hypoperfusion and resistance to chemotherapy and radiotherapy, and predicts poorer disease outcome (Garrido-Laguna et al., 2011). For instance, CAFs could promote radioprotection of pancreatic cancer cells by direct upregulation of β1-integrin signaling and abrogation of this signaling in pancreatic cancer cells induced radiosensitivity (Mantoni et al., 2011). Moreover, heightened accumulation of HA resulted in increased tissue solid stress and interstitial fluid pressures, both of which led to vascular compression and dysfunction, thereby impairing drug delivery into tumors. Degradation of stromal HA by pegylated hyaluronidase was shown to induce a transient increase in vessel density and perfusion, and led to increased delivery of gemcitabine to tumors, thereby augmenting efficacy of

chemotherapy in pancreatic cancer (Jacobetz et al., 2013; Olive et al., 2009; Provenzano et al., 2012; Stylianopoulos et al., 2012).

In addition to increased synthesis of matrix components, CAFs also express ECM remodeling lysyl oxidase (LOX) and lysyl hydroxylase 2 (LH2), enzymes that are responsible for collagen crosslinking. Enhanced collagen-crosslinking has been shown to increase tumor stiffness, thereby driving tumor invasion and metastasis (Chen et al., 2015; Levental et al., 2009). Although the role of CAF-derived LOX in the formation of premetastatic niche has not been investigated, tumor-derived LOX was shown to promote collagen IV-crosslinking essential for $CD11b^{+}$ myeloid cell recruitment, thereby enhancing tumor cell invasion and metastasis (Erler et al., 2009). Furthermore, studies indicated that FAP protease-mediated collagen and fibronectin fiber organization could enhance tumor cell migration by activation of the β1-integrin signaling pathway (Lee et al., 2011). CAFs have also been shown to promote and lead collective tumor cell invasion in an organotypic culture by Rho-dependent signaling pathways (Gaggioli et al., 2007; Goetz et al., 2011; Sanz-Moreno et al., 2011). This observation suggests that generation of migratory tracks by the CAFs in the matrix is sufficient to drive neighboring neoplastic cells to follow. Caveolin-1 (Cav-1) and JAK signaling pathways in CAFs was identified to play an essential role for Rho-dependent cytoskeletal remodeling, thereby promoting actomyosin contractility and enhancing invasion (Gaggioli et al., 2007; Goetz et al., 2011; Sanz-Moreno et al., 2011). Furthermore, expression of Cav-1 also could contribute to remodeling of CAF-derived matrix to enhance tumor cell migration (Goetz et al., 2011).

On the other hand, CAFs can also regulate turnover of the matrix molecules by expression of matrix metalloproteinases (MMPs), which have been demonstrated to play pivotal roles in enhancing tumor growth, invasion, and metastasis (Poulsom et al., 1992; Sternlicht et al., 1999; Zigrino et al., 2009). Moreover, MMP-mediated ECM remodeling plays an active role in tumor angiogenesis and metastasis. For instance, ECM can sequester and hence acts as a "local depot" for a wide range of growth factors and cytokines. MMP13 expressed by CAFs was found essential to release VEGF sequestered from the ECM to promote angiogenesis and invasion of skin squamous cell carcinomas (Lederle et al., 2010). Another cytokine transforming growth factor-beta (TGF-β), which is secreted as a latent form associated with a Latency Associated Peptide (LAP), is also sequestered in ECM to limit its bioavailability. Cell surface-localized MMP-9 activated TGF-β by proteolytically processing of LAP and promoted tumor invasion and angiogenesis (Yu and Stamenkovic, 2000). CAFs have also been shown to secrete SDF-1α/CXCL12 to promote angiogenesis by recruiting endothelial progenitor cells into tumors (Orimo et al., 2005).

CAFs modulate inflammatory and immune responses

Inflammation is becoming increasingly appreciated as an important contributing factor in promoting the development of a wide range of malignancies, including colon, gastric, liver, lung and pancreatic cancers (Guerra et al., 2007; Peek and Crabtree, 2006; Pikarsky et al., 2004; Pine et al., 2011; Terzic et al., 2010). Crosstalk between inflammatory cells and tumor stroma regulates the desmoplastic response in tumor and vice versa. CAFs

have been shown to orchestrate the inflammatory response by secreting cytokines such as IL-6 and IL1-β and by recruiting tumor-associated neutrophils and macrophages through chemokines, CXCL1 and CXCL2 (Erez et al., 2010; Torres et al., 2013). CAF-dependent proinflammatory gene signatures were found in various human solid tumors including breast cancer, lung cancer and pancreatic cancer (Erez et al., 2010; Rudisch et al., 2015; Vicent et al., 2012). CAF-dependent proinflammatory gene signatures have been demonstrated to be dependent on the NF-κB signaling as knocking down of IKKβ, a protein that is essential for NF-κB activation, abrogated the recruitment of macrophage and decreases angiogenesis essential for tumor progression (Erez et al., 2010). Moreover, CAFs could also promote the survival and polarization of tumor-associated myeloid cells to a M2 macrophage phenotype (Stairs et al., 2011). The alternative activation of macrophages was likely due to the overexpression of IL-6, TGFβ and CCL2 by CAFs (Comito et al., 2014; Gong et al., 2012; Sierra-Filardi et al., 2014).

Conversely, inflammatory myeloid cells have been suggested to promote CAF activation and desmoplastic response. IL-6 or SDF-1α/CXCL12 secreted by M2 macrophages has been shown to promote human prostatic fibroblast activation as determined by α-SMA expression (Comito et al., 2014). Moreover, treatment with the anti-inflammatory drug dexamethasone was shown to reduce the recruitment of Gr-1^+ $CD11b^+$ cells, to decrease CAF accumulation and collagen deposition, thereby attenuating tumor progression in a spontaneous squamous carcinoma model (Stairs et al., 2011). Additionally, CAFs and M2 macrophages have been shown to collaborate in activating endothelial cells to enhance

angiogenesis, promoting the escape of cancer cells from the primary tumor and ultimately driving metastatic dissemination (Comito et al., 2014).

CAFs and desmoplastic stroma have been observed to promote tumor growth by modulating the anti-tumor immune response. Desmoplastic stroma can act as a physical barrier to preclude T cells from actively migrating and infiltrating into the human lung cancers. Degradation of matrix by collagenase treatment has been shown to augment the T cell mobilization, thereby increasing their accessibility to the proximity of tumor cell nests *ex vivo* (Salmon et al., 2012). Based on studies of human pancreatic samples and an autochthonous model of pancreatic cancer, it has been shown that activated pancreatic stellate cells (PSCs) can secret SDF-1α/CXCL12 to promote $CD8^+$ T cells chemotaxis towards the juxtatumoral stromal compartment, thereby preventing the access of $CD8^+$ T cells to cancer cells. Knocking down of SDF-1α/CXCL12 or treatment of activated PSCs with all-trans retinoic acid (ATRA), a drug that renders PSCs quiescent, can abrogate $CD8^+$ T cells chemotaxis towards PSCs. Moreover, ATRA treatment can enhance $CD8^+$ T cells infiltration to the proximity of the neoplastic cells in an autochthonous model of pancreatic cancer (Ene-Obong et al., 2013). In contrast, SDF-1α/CXCL12 derived from FAP^+ CAFs has been shown to bind pancreatic cancer cells, and thereby excluding T cells from neoplastic cells through an unknown mechanism. Inhibition of CXCR4, a receptor of SDF-1α/CXCL12 , by AMD3100 can reverse the immune suppression and potentiates the efficacy of checkpoint-blockade immunotherapy to restrain the growth of pancreatic tumors (Feig et al., 2013). Additionally, cancer-associated PSCs are able to promote the differentiation of peripheral blood mononuclear cells into myeloid-derived

suppressor cells (MDSCs) by secreting proinflammatory cytokines including IL-6, macrophage colony-stimulating factor, VEGF and SDF-1α/CXCL12. IL-6/STAT3-mediated signaling is critical for PSC-induced MDSC differention. PSC-induced MDSCs are able to inhibit T-cell activation, thereby contributing to tumoral immune suppression (Mace et al., 2013). Furthermore, targeted depletion of granulocytic MDSCs by an anti-Ly6G antibody promotes intra-tumoral accumulation of activated $CD8^+$ T cells, enhances tumor cell apoptosis and remodels the tumor stroma in pancreatic tumors (Stromnes et al., 2014). Furthermore, CAFs have been shown to secrete immune modulatory enzyme including prostaglandin E2 and indoleamine 2,3-dioxygenase that can impair the activation, cytokine production and cytotoxicity of NK cells to enable progression of skin and liver cancers (Balsamo et al., 2009; Li et al., 2012). Taken together, CAFs and desmoplastic stroma maintain a proinflammatory and immune-suppressive microenvironment to support tumor progression and therapeutic resistance.

In the following chapters, I will describe investigations into the potential influences of FAP-expressing stromal cells and FAP protease in driving primary tumor progression and metastasis.

CHAPTER 2 – Fibroblast activation protein-expressing stromal cells can promote tumor growth by adaptive immunity-independent remodeling of the stromal microenvironment

Introduction

Discovery of FAP

Solid tumors recruit and activate a heterogeneous population of non-transformed stromal cells to promote desmoplasia, inflammation and immune suppression in the tumor microenvironment. Crosstalk between tumor cells and tumor-associated stromal cells can promote tumor progression and metastasis, as well as induce therapeutic resistance leading to treatment failure. Therefore, there has been considerable interest in identifying and validating suitable candidate markers to develop stromal cell-targeted therapies against cancer. One attractive stromal cell target that is receiving significant attention is the fibroblast activation protein (FAP), a transmembrane serine protease that was originally discovered by Dr. Lloyd L. Old's group at the Ludwig Institute at Memorial Sloan-Kettering Cancer Center in New York, USA (Rettig et al., 1986). FAP was initially designated F19 antigen based on its reactivity with the F19 monoclonal antibody isolated from a mouse immunized with human lung fibroblasts. Using immunohistochemical analysis with F19 monoclonal antibody, they found that F19 antigen was expressed on most astrocytomas and sarcomas, as well as on cultured fibroblasts and a subset of melanomas. In addition, studies from the same group also showed that F19 antigen was highly expressed in cancer-associated stromal cells of various primary and metastatic

carcinomas but not most quiescent stromal fibroblasts. Further analysis of dermal incision wounds revealed that F19 antigen was strongly induced during scar formation (Garin-Chesa et al., 1990; Scanlan et al., 1994). The conclusion from these findings was that expression of F19 antigen was restricted to cells of mesenchymal origin, mostly activated fibroblasts and a subset of neuroectodermal cells. Therefore, F19 antigen was later designated as "fibroblast activation protein", or FAP (Rettig et al., 1993).

Subsequently, FAP expression was also detected during embryonic development as well as within mesenchymal stem cells and in chronic inflammatory and fibrotic conditions such as liver cirrhosis and idiopathic pulmonary fibrosis (Acharya et al., 2006; Bae et al., 2008; Mathew et al., 1995; Niedermeyer et al., 2001; Wang et al., 2008). To better trace and identify FAP-expressing cells *in vivo*, we and others have developed FAP-reporter mice for non-invasive bioluminescent imaging of FAP^+ stromal cells (Jacob et al., 2012; Roberts et al., 2013). FAP^+ stromal cells were found to reside in many tissues of the adult mouse, including skin, bone marrow, skeletal muscle, pancreas, adipose and lymph node. Moreover, FAP^+ stromal cells were found to accumulate in transplanted tumors. Recent phenotypic analysis of FAP^+ stromal cells in human breast cancer specimens demonstrated that a majority of intratumoral FAP^+ stromal cells expressed CD90 but did not express the hematopoietic cell marker CD45; a minor population of M2-like macrophages also expressed FAP (Tchou et al., 2013). These findings demonstrate that FAP-expressing cells or FAP protease may have homeostatic functions and may regulate a wide spectrum of human diseases that involve active tissue remodeling, including inflammation, fibrosis and cancer.

FAP expression correlates with poor prognosis in various human carcinomas

Since its discovery, several research groups have investigated whether FAP can be used as a cancer biomarker to predict patient outcome. Notably, a clinicopathological study demonstrated that FAP overexpression was associated with worse clinical outcome in PDA. FAP overexpression correlated with increased risk of lymph node metastasis, tumor recurrence and death (Cohen et al., 2008). In patients with non-small cell lung cancer, elevated FAP expression was identified as a predictor of worse overall survival and might be associated with inflammation and suppressed lymphocyte-dependent immune response (Liao et al., 2013). In patients with colon cancer, FAP expression was found to inversely correlate with tumor stage, suggesting that stromal FAP may play a greater role in the early stage of the tumor development. Furthermore, for patients with known metastatic disease, increased FAP expression was demonstrated to associate with decreased survival (Henry et al., 2007). These observations have raised an interesting question as to whether the FAP-expressing cells or FAP protease itself may regulate tumorigenesis, invasion, and/or metastasis.

FAP-expressing stromal cells are promising targets in the tumor microenvironment

To evaluate the potential impact of FAP at a cellular level within the tumor microenvironment, Dr. Eli Gilboa's group employed an immunotherapeutic approach using a dendritic cell vaccine to target FAP^+ stromal cells in multiple tumor types. This approach resulted in tumor growth inhibition without morbidity or mortality associated with anti-FAP vaccination, except for a small delay in wound healing (Lee et al., 2005).

Subsequent experiments with an oral vaccine targeting FAP demonstrated suppression of primary tumor growth and metastasis of mouse colon and breast carcinoma (Loeffler et al., 2006). Moreover, tumor tissues of FAP-vaccinated mice showed significantly decreased collagen levels and enhanced uptake of chemotherapeutic drugs. No overt toxicity or impact on wound healing was observed (Loeffler et al., 2006). Other studies utilizing immunoconjugate (Ostermann et al., 2008) and enzyme-activated pro-drug therapy (Brennen et al., 2012) also achieved tumor growth inhibition without causing obvious toxicity or side effects. Collectively, these studies demonstrate that FAP^+ stromal cells are attractive targets and have therapeutic implications across a broad spectrum of solid tumors.

Development of chimeric antigen receptor (CAR) T cells redirected against FAP^+ stromal cells

The adoptive transfer of T cells engineered with chimeric antigen receptor (CAR) has achieved unprecedented clinical responses in both adults and children with chronic or acute leukemia (Garfall et al., 2015; Grupp et al., 2013; Maude et al., 2014; Porter et al., 2015; Porter et al., 2011). Given the potential efficacy and translational value of adoptive T cell therapy, we and others hypothesized that using engineered T cells to target FAP^+ stromal cells would be more effective than therapeutic vaccination (Kakarla et al., 2013; Schuberth et al., 2013; Tran et al., 2013). In collaboration with Dr. Carl June's and Dr. Steven Albelda's labs, we generated CAR T cells redirected against FAP^+ stromal cells. We hypothesized that depletion of FAP^+ stromal cells and disruption of stromal

cell/ECM-dependent pathways would alter the tumor microenvironment, thereby inhibit tumor growth and reduce resistance to therapy.

In this chapter, I describe using FAP-CAR T cells as an approach to deplete FAP^+ stromal cells in human tumor xenografts and poorly immunogenic pancreatic tumors, as well as investigating the potential immune-independent mechanism by which FAP^+ stromal cells promote tumor growth.

Materials and methods

Cell lines

A mouse AE17 mesothelioma cell line expressing chicken ovalbumin (AE17.OVA) was obtained from Dr. Delia Nelson (University of Western Australia). Syngeneic 4662 pancreatic cancer cells were derived from a pancreatic tumor isolated from a fully backcrossed C57BL/6 *Kras*^{G12D}:*Trp53*^{R172H}:*Pdx-1-Cre* (KPC) mouse (Hingorani et al., 2005). A human A549 lung adenocarcinoma cell line and 3T3 fibroblastic line were obtained from the American Type Culture Collection. The human sarcomatoid type mesothelioma cell line I45 was provided by Dr. J. Testa (Fox Chase Cancer Center, Philadelphia, PA). M30 and EM cell lines were derived from the pleural effusion of patients with malignant mesothelioma. EM-meso cells were generated via transduction of a lentivirus encoding human mesothelin (Crisanti et al., 2009; Moon et al., 2011). Cells were tested mycoplasma-free and frozen and were used less than 1 month after resuscitation.

Animals

C57BL/6 mice and NOD/SCID/IL2-receptor γ chain knockout (NSG) mice were purchased from Charles River Laboratories Inc. (Wilmington, MA), Jackson Labs (Bar Harbor, ME) and the Children's Hospital of Philadelphia. FAP-deficient mice (*Fap*$^{LacZ/LacZ}$) provided by Boehringer Ingelheim (Niedermeyer et al., 2000) were backcrossed 12 generations onto a C57BL/6 genetic background. These mice were then crossed with NSG mice to generate NSG FAP-deficient mice. KPC mice were provided by the Mouse Hospital at the University of Pennsylvania. Experimental protocols were

approved by the Institutional Animal Care and Use Committee and were in compliance with guidelines for the care and use of animals.

Generation of anti-mouse FAP-CAR constructs

Total RNA from the 73.3 hybridoma was isolated and reverse-transcribed to obtain cDNA. Variable heavy (V_H) and light (V_L) chains of the 73.3 immunoglobulin were PCR-amplified and sequenced (**Fig. 2-4A and B**). The V_H and V_L sequences were fused with a CAR construct encoding CD8α hinge, CD8α transmembrane domain, human 4-1BB and CD3ζ intracellular signaling domains (Milone et al., 2009). This CAR construct was then inserted into the pELNS lentiviral vector or an internal ribosome entry site (IRES)-containing the retroviral MigR1 vector (**Fig. 2-4C**) (Pear et al., 1998). A fully mouse FAP-CAR construct was also generated by fusing the 73.3 scFv with the mouse CD3ζ chain and the mouse CD28 ICD. This construct was inserted into another retroviral vector MSGV (**Fig. 2-4D**). Two additional control FAP-CAR constructs, encoding either human CD3ζ or mouse CD3ζ ICD, were also generated to evaluate the function of the costimulatory domains.

Recombinant lentivirus preparation

The anti-mouse FAP-CAR was subcloned into a third-generation self-inactivating lentiviral expression vector (pELNS). High-titer replication-defective lentiviruses were produced and concentrated as described previously (Moon et al., 2011). Briefly, 293T cells were transfected with 18 μg of pRSV.REV (Rev expression plasmid), 18 μg of pMDLg/p.RRE (Gag/Pol expression plasmid), 7 μg pVSV-G (VSV glycoprotein

expression plasmid) and 15 μg of pELNS transfer plasmid using Express Inn transfection reagents (Open Biosytems). Viral supernatant was harvested and concentrated for T cell transduction.

Isolation, transduction, and expansion of primary human T lymphocytes

Primary human T cells isolated from healthy volunteer donors were purchased from the Human Immunology Core at University of Pennsylvania. All specimens were collected under a university Institutional Review Board-approved protocol, and written informed consent was obtained from each donor. Human T cells expressing CAR were prepared as described (Parry et al., 2003). T cells were cultured in RPMI 1640 supplemented with 10% heat-inactivated fetal bovine serum, 100 U/mL penicillin, 100 μg/mL streptomycin sulfate and 10 mM HEPES, and stimulated with anti-CD3/anti-CD28-coated magnetic beads (Invitrogen) at a 3:1 bead-to-cell ratio. Approximately 24 hours after activation, T cells were transduced with lentiviral vectors at a multiplicity of infection of 5. Cells were counted and nourished with fresh culture medium containing 30 U/mL of recombinant human interleukin-2 every two days. Once the T cells appeared to rest down, as determined by both decreased growth kinetics and cell size, they were either used for functional assays or cryopreserved.

Recombinant retrovirus preparation

Anti-mouse FAP-CAR was subcloned into MigR1 or MSGV retroviral vectors. 293T cells were transfected with 9 μg of pHIT (Rev expression plasmid), 9 μg of pCGP

(Gag/Pol expression plasmid) and 18 μg of MigR1 transfer plasmid using Lipofectamine 2000 (Thermo Fisher Scientific). Viral supernatant was harvested for T cell transduction.

Isolation, transduction and expansion of primary mouse T cells

Mouse splenic T cells were isolated using negative selection (Miltenyi Biotec). T cells were then cultured in RPMI 1640 supplemented with 10% heat-inactivated fetal bovine serum, 100 U/mL penicillin, 100 μg/mL streptomycin sulfate, 10 mM HEPES and 100 U/mL IL-2 and activated by plate-bound anti-CD3 (1 μg/mL) and anti-CD28 (2 μg/mL). After 48 hours, cells were mixed with retrovirus and transferred to a 24-well plate coated with retronectin (50 μg/mL; Clontech) and were then centrifuged, without braking, at room temperature for 45 minutes at 1200G. After overnight incubation, cells were expanded with 50 U/mL of IL-2 for an additional 48 hours. Cells were then harvested for functional assays or adoptive transfer.

Cytokine release and cytotoxicity assays

3T3 and 3T3.FAP fibroblasts were transduced with a lentivirus to force expression of GFP and luciferase. FAP-CAR T cells and control T cells were co-cultured with 3T3 or 3T3.FAP fibroblasts at various effector-to-target ratios. After 18 hours, the culture supernatants were collected for IFNγ analysis using an ELISA (BD Bioscience). Cytotoxicity of transduced T cells was determined by detecting the remaining luciferase activity from the adherent fibroblasts using a luciferase assay system (Promega). Results were shown as percent of cytolysis by normalizing the luciferase signal obtained from co-culture experiments to that obtained from 3T3 and 3T3.FAP fibroblast cultures only.

Intravenous transfer of FAP-CAR T cells in mice bearing established tumors

NSG or NSG-FAP null mice were injected subcutaneously with 2×10^6 A549, M30 or I45 cells mixed with matrigel (BD Biosciences). Mice bearing established tumors were then intravenously injected with one dose of 1×10^7 FAP-CAR human T cells or non-transduced T cells, or left untreated. NSG mice were injected subcutaneously with 2×10^6 EM-meso cells. Mice bearing established tumors were then intravenously injected with one dose of 5×10^6 FAP-KIR, DAP-12 or non-transduced human T cells. C57BL/6 mice and NSG mice were injected subcutaneously with 3×10^5 4662 tumor cells mixed with matrigel. Tumor-bearing mice were randomly assigned to three groups that received FAP-CAR or MigR1-transduced (control) mouse T cells or that remained untreated. KPC mice were monitored by ultrasound and randomly assigned for treatment when they had established pancreatic tumors with volumes of 95 to 270 mm^3. Mice bearing established tumors were treated intravenously with two weekly doses of 1×10^7 FAP-CAR mouse T cells. At the endpoint, tumors were harvested for flow cytometric or histopathological analyses.

Antibodies

Monoclonal anti-mouse FAP antibody was generated and characterized by our lab. Briefly, FAP-deficient mice were immunized and boosted twice by intraperitoneal injection of 3T3 fibroblasts expressing FAP. Splenocytes were harvested and fused with myeloma cells to generate hybridomas three days after the final boost. Supernatant derived from each hybridoma was collected and screened for reactivity with 3T3.FAP

fibroblasts and activated primary FAP-intact fibroblasts but not the parental 3T3 fibroblasts or the activated primary fibroblasts from FAP-deficient mice. The 73.3 hybridoma was selected and further characterized by ELISA and by immunoblotting with purified recombinant mouse FAP extracellular domain (rFAP-ECD) provided by Dr. Jonathan Cheng (Fox Chase Cancer Center, Philadelphia, PA). 73.3 antibody does not cross-react with human FAP expressed by human foreskin fibroblasts or with primary human tumor-associated stromal cells.

Purified anti-mouse CD3ε (145-2C11), anti-mouse CD28 (37.51) and anti-mouse CD16/32 antibodies were purchased from eBioscience. Anti-CD45 (30-F11; PE-Cy7), anti-CD90 (53-2.1; FITC, PE), anti-F4/80 (BM8; APC) and anti-CD206 (C068C2; FITC) antibodies were purchased from Biolegend. Anti-CD8α (53-6.7; APC) was purchased from BD Bioscience. A polyclonal sheep anti-human antibody that cross-reacts with mouse FAP was purchased from R&D and the specificity was confirmed based on its reactivity with A549 human lung cancer xenografts derived from wild-type but not FAP-deficient NSG mice.

Surface staining and flow cytometry analysis

Tumor tissues were harvested and dissected into small pieces, after which the tissues were enzymatically dissociated with collagenase type I (100 U/mL, Worthington), II (100 U/mL, Worthington) and IV (100 U/mL, Worthington), as well as DNase I (100 U/mL, Worthington), in Leibovitz's L-15 Medium (Thermo Fisher Scientific) at 37°C for one hour. Digested tumors were then filtered through 70 μm nylon mesh cell strainers (BD

Bioscience), and red blood cells lysed by ACK buffer (BD Bioscience). Fc receptors were blocked by incubating cells with anti-mouse CD16/CD32 antibody for 15 minutes and then stained with primary antibodies at 4°C for 30 minutes, followed by incubation with streptavidin-APC or BV421 for another 15 minutes. Dead cells were excluded using propidium iodide (Thermo Fisher Scientific). Cell acquisition was performed on LSR-II using FACSDiva software (BD Bioscience). Data were analyzed using FlowJo software (Tree Star).

Histopathological, histochemical and immunohistochemical analysis

Tumors were harvested, fixed with Prefer (Anatech), dehydrated and paraffin-embedded. Tissue sections were deparaffinized, rehydrated and stained with Masson's trichrome, Alcian blue or H&E. H&E stained tumor sections were evaluated by two board-certified veterinary pathologists at the Ryan Veterinary Hospital of the University of Pennsylvania (Amy C. Durham and Elizabeth L. Buza). For each sample, 9 to 10 consecutive 40X HPF images were evaluated and scored based on the predominant tumor phenotype (greater than 50% of the field of view): necrotic, well-differentiated, moderately differentiated, and poorly differentiated. For immunohistochemical staining, tissue sections were further subjected to 10 mM sodium citrate or Tris-EDTA buffer for antigen retrieval, followed by quenching endogenous peroxidases with 3% H_2O_2. Sections were then blocked with 10% goat or rabbit serum in 1% BSA/PBS at room temperature for an hour, and then incubated with avidin-biotin or streptavidin-biotin block (Vector Labs). Primary antibodies were applied overnight at 4°C and incubated with biotinylated secondary antibody at room temperature for an hour. Bound antibodies were detected with

horseradish peroxidase (HRP), using either streptavidin-HRP (Jackson ImmunoResearch) or Vectastain Elite ABC (Vector Laboratories), followed by counterstaining with hematoxylin. Digital images were captured using a Nikon E600 microscope at 20X HPF, with at least 5 images per sample. Computer-based quantification was performed using Fiji software. Proliferation or apoptotic indices were calculated by the ratio of Ki-67$^+$ cells or cleaved-caspase-3$^+$ cells to hematoxylin$^+$ cells. Histochemical-reactive or immuno-reactive signals were calculated and normalized to the total area of 20X HPF images (n = 3 to 6 per group).

Statistical Analyses

Statistics were calculated using GraphPad Prism 6. For studies comparing two groups, the Student's *t*-test was used. For studies comparing more than two groups, one-way ANOVA with post-hoc Tukey testing was used. Data are represented as mean ± SEM. Differences were considered significant when $p < 0.05$.

Results

Mouse and human tumors exhibit varying degrees of desmoplasia which correlate with the prevalence of intratumoral FAP^+ stromal cells

We investigated the extent of desmoplasia in multiple mouse tumors and human xenografts by histopathological, histochemical and immunohistochemical analyses. ECM components, including collagen, total glycosaminoglycans (GAGs), hyaluronic acid (HA) and a proteoglycan versican, were overexpressed in 4662 and A549 tumors. In contrast, mouse mesothelioma AE17.OVA tumors and human mesothelioma I45 xenografts displayed moderate and sparse desmoplasia, respectively (**Fig. 2-1**). Moreover, these matrix components were found to accumulate and be confined to the juxtatumoral stromal regions in 4662 and A549 tumors. On the contrary, all matrix components investigated were dispersed throughout the AE17.OVA and I45 tumors.

Next, we determined the phenotypes of FAP^+ stromal cells and whether there was a correlation between the degree of tumor desmoplasia and the accumulation of FAP^+ stromal cells within the tumors. In established A549 lung cancer xenografts, most FAP^+ stromal cells were found to be $CD45^-$ $CD90^+$, though a minor population of FAP^+ stromal cells was found to be $CD45^+$ (**Fig. 2-2A**). These $CD45^+$ FAP^+ cells were further characterized as $F4/80^+$ $CD206^+$ (M2-like) macrophages (**Fig. 2-2B**). Interestingly, we found that the number of both intratumoral $CD45^-$ $CD90^+$ FAP^+ stromal cells and $CD45^+$ FAP^+ cells correlated with the degree of desmoplasia in mouse tumors and human xenografts (**Fig. 2-3**). In 4662 tumors and A549 xenografts, approximately 8% to 12% of total cells were $CD45^-$ $CD90^+$ FAP^+, compared to only 0.3% to 1.2% in AE17.OVA

tumors and I45 xenografts. About 0.34% to 1.65% of total cells in 4662 tumors and A549 xenografts were $CD45^+$ FAP^+, compared to only 0.1% in AE17.OVA tumors and I45 xenografts. These results raised the possibility that intratumoral FAP^+ stromal cells may play critical roles in the formation and/or maintenance of desmoplastic tumor stroma.

Development of chimeric antigen receptor (CAR) T-cells redirected against FAP-expression stromal cells

To test whether FAP^+ stromal cells are required for the formation and/or maintenance of desmoplastic tumor stroma, we utilized a specific mouse monoclonal antibody 73.3 generated in our lab to generate murine FAP-specific chimeric antigen receptors. Briefly, variable heavy (V_H) and light (V_L) chains of the 73.3 immunoglobulin were determined by PCR amplification and sequencing using RNA from 73.3 hybridomas (**Fig. 2-4A** and **B**). The V_H and V_L sequences were cloned into a CAR construct including CD8α hinge, CD8α transmembrane domain, and two human intracellular signaling domains (ICD) derived from 4-1BB and CD3ζ. This CAR was then cloned into a lentiviral vector pELNS for transducing human T cells or an internal ribosome entry site (IRES)-GFP containing retroviral MigR1 vector for transducing mouse T cells (**Fig. 2-4C**). A fully mouse FAP-CAR construct was also generated using 73.3 variable heavy and light chains with the mouse CD3ζ chain and mouse CD28 ICD. This construct was inserted into a retroviral vector MSGV for transducing mouse T cells (**Fig. 2-4D**). We were able to transduce activated mouse T cells with FAP-CAR or MigR1 vector control with high efficiency (**Fig. 2-5A**). To evaluate the effector functions, transduced mouse T cells were co-cultured with 3T3 fibroblasts or with 3T3 fibroblasts expressing mouse FAP

(3T3.FAP) (**Fig. 2-5B**). After 18 hours of co-incubation, FAP-CAR T cells secreted IFNγ and killed 3T3.FAP fibroblasts in a dose-dependent fashion, but exhibited no activity against parental 3T3 fibroblasts (**Fig. 2-5C and D**).

FAP-CAR T cells inhibit growth of desmoplastic human cancer xenografts

To investigate whether host FAP^+ stromal cells are essential for growth of human tumors, we evaluated the impact of FAP-CAR T cells on the growth of established A549 human lung cancer xenografts in NSG and FAP-deficient NSG mice. Administration of FAP-CAR human T cells directed against murine FAP^+ stromal cells reduced tumor growth by 42% at 8 days post-adoptive T-cell transfer (**Fig. 2-6A**). Interestingly, we noticed that the adenocarcinoma ductal-like structure of the tumor nodules was disrupted and also observed an increase in necrotic cell death following FAP-CAR T-cell transfer. Immunohistochemical staining indicated that treatment with FAP-CAR human T cells decreased tumor cell proliferation and increased apoptotic cell death (**Fig. 2-6C**). In contrast, FAP-CAR T cells did not affect growth of A549 tumors in FAP-deficient NSG hosts, demonstrating that FAP expression in stromal cells is critical for FAP-CAR T-cell-dependent anti-tumor activity and unlikely due to direct targeting of tumor cells themselves (**Fig. 2-6B**). Further experiments also showed that FAP-CAR T cells inhibited growth of highly desmoplastic human M30 and EM-meso mesothelioma xenografts (**Fig. 2-7A and B**), but had no impact on the growth of poorly-desmoplastic human I45 mesothelioma xenografts (**Fig. 2-7C**). These data demonstrate that human tumors exhibit varying degrees of desmoplasia and that it is the desmoplastic tumor types that are susceptible to the anti-tumor activity of FAP-CAR T cells. Furthermore, although initial

studies indicated that FAP^+ stromal cells might subvert anti-tumor immune response to promote tumor growth (Kraman et al., 2010), our human xenograft studies revealed that FAP^+ stromal cells could also enhance tumor growth in the absence of host adaptive immunity.

FAP-CAR T cells disrupt stromagenesis and angiogenesis and reduce desmoplasia in highly-desmoplastic human lung cancer xenografts

To study the potential non-immune mechanisms by which FAP^+ stromal cells support growth of desmoplastic human tumors, we investigated the impact of their depletion on the composition and architecture of the stromal microenvironment in A549 xenografts. Administration of FAP-CAR T cells reduced the number of FAP^+ stromal cells by 84%. In addition, we found that the number of SMA^+ myofibroblasts was reduced by 83%.

As mentioned earlier, we found that the prevalence of FAP^+ stromal cells correlated with the degree of desmoplasia (**Fig. 2-1 and 2-3)**. Therefore, we next determined whether depletion of FAP^+ stromal cells altered the tumor desmoplasia in established A549 tumors. Treatment with FAP-CAR T cells resulted in 72% decrease in collagen content, 57% reduction in total GAGs, 75% decrease in HA, and 93% depletion in versican (**Fig. 2-8B**).

We also examined the impact of FAP-CAR T cells on tumor angiogenesis, as angiogenesis is known to be important for tumor progression and dependent on stromal cells and ECM. CD31 (endothelial cell) and NG2 (pericyte) immunohistochemical

staining showed that administration of FAP-CAR T cells resulted in a 53% decrease in tumor endothelial cells and 92% decrease in pericytes in A549 tumors (**Fig. 2-8A**). These data indicate that FAP^+ stromal cells are essential for synthesis and/or maintenance of tumor desmoplasia. We therefore posit that the immune-independent tumor-promoting effect of FAP^+ stromal cells in this model is dependent on the extrinsic signals or provisional matrix derived from FAP^+ stromal cells.

FAP-CAR T cells also inhibit growth of non-immunogenic but highly desmoplastic pancreatic tumors through immune-independent stromal remodeling of the tumor microenvironment

To further determine whether FAP^+ stromal-cell-mediated immune-independent remodeling of the tumor microenvironment is a general tumor-promoting mechanism, and can even uncover this potential non-immune mechanism in the immune competent hosts, we studied the roles of FAP^+ stromal cells in mouse models of pancreatic cancer, as it is one of the most desmoplastic and least immunogenic tumor types described to date. We first employed the 4662 tumor cell line generated by Dr. Vonderheide's lab. This line was derived from a tumor that spontaneously developed in a $Kras^{LSL\text{-}G12D/+}$, $Trp53^{LSL\text{-}R172H/+}$ and *Pdx-1-Cre* (KPC) mouse. Interestingly, 4662 tumors were found to be non-immunogenic as the growth of this tumor did not significantly change when implanted subcutaneously into syngeneic C57BL/6 versus NSG mice (**Fig. 2-9A**). Further studies from Dr. Vonderheide's lab using antibody-mediated depletion of either $CD4^+$ or $CD8^+$ T cells did not impact tumor growth compared to isotype-treated controls. Forcing expression of a nominal antigen ovalbumin in 4662 cells resulted in

complete rejection in syngeneic C57BL/6 mice, demonstrating that the 4662 line is antigenic but non-immunogenic.

We treated established 4662 tumor-bearing C57BL/6 or NSG mice with two doses (one week apart) of FAP-CAR or MigR1 T cells. At the endpoint, we found that FAP-CAR T-cell treatment reduced the growth of 4662 tumors in immune-competent C57BL/6 mice by 36% (**Fig. 2-9B**). Importantly, FAP-CAR T-cell treatment had a similar impact on the growth of 4662 tumors in NSG mice. These results demonstrate that FAP-CAR T cells impact 4662 tumor growth via immune-independent mechanisms (**Fig. 2-9B**). Histopathological and immunohistochemical analyses showed that FAP-CAR T-cell treatment altered tumor architecture, reduced proliferation and increased apoptosis in 4662 tumors (**Fig. 2-9C**). As discussed above, as FAP^+ stromal cells can modulate the immune response, we also characterized the impact of FAP-CAR T-cell treatment on immune infiltrates. We found that the number of $CD11b^+$ $Ly6G^+$ cells was slightly reduced in tumors from FAP-CAR T-cell treated C57BL/6 mice (**Fig. 2-10A,** $p<0.05$), and that there was a very modest increase of total GFP^- $CD8^+$ host T cells (**Fig. 2-10B,** $p<0.05$). We also observed that GFP^+ FAP-CAR T cells were able to traffic into 4662 tumors (**Fig. 2-10B**).

Furthermore, we extended these studies to the autochthonous KPC mouse model of pancreatic ductal adenocarcinoma (PDA). KPC mice were monitored by high-resolution ultrasound and randomly assigned for treatment when they had established pancreatic tumors with volumes of 95 to 270 mm^3. Tumor-bearing mice were treated with two

weekly doses of FAP-CAR T cells or MigR T cells. Tumor progression was monitored pre- and post-adoptive T-cell transfer over a two-week period. FAP-CAR T-cell treatment significantly inhibited tumor growth in KPC mice (**Fig. 2-11A**). Interestingly, we again observed that the adenocarcinoma ductal-like structure of the tumor nodules was disrupted and resulted in poorly differentiated tumors, as defined by loss of tumor stroma, following FAP-CAR T-cell transfer. Immunohistochemical staining demonstrated that treatment with FAP-CAR T cells decreased tumor cell proliferation and increased apoptotic cell death as seen in the transplanted 4662 models (**Fig. 2-11B**).

We investigated tumor stromagenesis, angiogenesis and desmoplasia following FAP-CAR T-cell transfer in transplanted and autochthonous mouse models of PDA. We found that FAP-CAR T-cell treatment decreased FAP^+ stromal cells by 62% and 91% in 4662 tumors and autochthonous PDAs, respectively (**Fig. 2-12A and 13A**). Similar to the finding from FAP-CAR T treated A549 tumors, we also observed 70% reduction of SMA^+ cells in both models of PDA (**Fig. 2-12A and 13A**). Based on dual immunofluorescence staining, we observed that FAP and SMA defined distinct, yet overlapping, subsets of stromal cells in A549 tumors (**Fig. 2-14A)**. Moreover, flow cytometry analysis demonstrated that FAP^+ stromal cells isolated from A549 tumors expressed varying levels of the MSC marker CD105 and CD44 (**Fig. 2-14B)**. Similarly, immunofluorescence staining revealed that FAP and SMA identified distinct subsets of stromal cells, with few FAP and SMA double expressing cells in either mouse or human pancreatic tumors. FAP^+ stromal isolated from human pancreatic tumors also expressed the MSC marker CD105 (**Fig. 2-14C)**. Additionally, we found that majority of cancer-

associated stromal cells isolated from human tumor explants expressed FAP, whereas few stromal cells expressed SMA (**Fig. 2-14D)**. These observations demonstrate the stromal cells are highly heterogeneous. Depletion of FAP^+ stromal cells by FAP-CAR T cells also altered tumor angiogenesis, resulting in 50% reduction in $CD31^+$ endothelial cells and 70% decrease in $NG2^+$ pericytes in both models (**Fig. 2-12A and 13A**). Collagen was decreased by 70-80%, and HA and versican were reduced by 34% and 52% respectively following treatment with FAP-CAR T cells (**Fig. 2-12B and 13B**).

Combined FAP-CAR T cells with gemcitabine treatment provide an additive anti-tumor effect in 4662 tumors

Prior studies showed that accumulation of HA in pancreatic tumors increased tissue solid stress and interstitial fluid pressures, which prevented drug delivery into tumor by causing vascular compression and dysfunction (Jacobetz et al., 2013; Provenzano et al., 2012; Stylianopoulos et al., 2012). Enzymatic targeting of stromal HA by pegylated hyaluronidase transiently restored vessel density and perfusion for delivery of gemcitabine into tumors, thereby augmenting efficacy of chemotherapy in a highly desmoplastic mouse model of pancreatic cancer (Jacobetz et al., 2013; Provenzano et al., 2012). Having determined that FAP-CAR T cells can disrupt and resolve tumor desmoplasia, we sought to test whether it can facilitate drug delivery into pancreatic tumors to further inhibit tumor progression. We treated 4662 tumors with FAP-CAR T cells and gemcitabine. Our initial results showed that the combination therapy provided an additive anti-tumor effect compared to treatment with the single agent (**Fig. 2-14**).

Conclusions and discussion

Tumor cells exhibit intra-tumor heterogeneity and high levels of genomic instability, rendering tumors resistant to therapeutic intervention and ultimately causing treatment failure. Developing therapeutic strategies to target non-transformed cancer-associated stromal cells is appealing but requires an in-depth understanding of the targeted population, as distinct stromal cell populations may have opposing effects on tumor growth, progression and metastasis. It is likely that depletion of specific stromal cell populations may have either therapeutic or detrimental effects. For instance, accumulation of SMA^+ myofibroblasts was shown to correlate with better prognosis, and depletion of these cells enhanced hypoxia and accelerated tumor progression in mouse models of pancreatic cancer (Ozdemir et al., 2014). Importantly, depletion of SMA^+ myofibroblasts in this study did not alter the prevalence of FAP^+ stromal cells in pancreatic tumors, indicating these two stromal cell populations are, for the most part, non-overlapping in this model (Ozdemir et al., 2014). In contrast, we found that depletion of FAP^+ stromal cells by adoptive transfer of FAP-CAR T cells could restrain growth of desmoplastic human lung cancer and mesothelioma xenografts and syngeneic murine pancreatic cancers (Lo et al., 2015). Studies by another group also showed that targeting FAP^+ stromal cells in pancreatic tumors resulted in an anti-tumor response (Feig et al., 2013). These data indicate that deleting FAP^+ stroma cells and SMA^+ myofibroblasts can have opposing effects, highlighting the phenotypic and functional heterogeneity of tumor stromal cells, at least in pancreatic cancer.

For many years, investigators have been equating SMA^+ myofibroblasts with cancer associated fibroblasts/stromal cells. However, as mentioned earlier, recent data from several groups, including ours, demonstrated that tumor stromal cells could exhibit phenotypic and functional heterogeneity (Feig et al., 2013; Lo et al., 2015; Ozdemir et al., 2014; Quante et al., 2011). In fact, although virtually all desmoplastic carcinomas contain FAP^+ stromal cells, as well as SMA^+ myofibroblasts, nonetheless, these two populations are not coincident. Depending on the tumor type, and also with variability between tumors of a particular type, the overlap between FAP^+ and SMA^+ cells can be as little as <5% (eg. human breast cancer and human pancreatic cancer, as well as the mouse autochthonous model of PDA utilized in this study), or as great as near 100% (eg. in squamous cell lung carcinomas, unpublished observation). These findings are consistent with a recent study in which gastric tumors from SMA promoter-driven RFP reporter mice were shown to contain multiple phenotypically distinct subsets of tumor stromal cells, including SMA^- MSCs, (Quante et al., 2011), while others showed that MSC expressed FAP (Bae et al., 2008). Therefore, MSCs likely account for at least a portion of the FAP^+ SMA^- cells we, and others, have observed in the microenvironment of many human and murine carcinomas. Interestingly, these cells were shown to have the capacity to both self-renew, as well as differentiate into SMA^+ myofibroblasts both in the wound healing and the tumor microenvironment (Lee et al., 2010; Quante et al., 2011), suggesting a lineage relationship exists between some terminally differentiated SMA^+ myofibroblasts and mesenchymal progenitor cells that at some stage may express both SMA and FAP, but at least some of which at a later stage, down regulate or lose FAP expression but express SMA. This being the case, the elimination of terminally

differentiated SMA^+ myofibroblasts would not be expected to deplete the SMA^- but FAP^+ progenitor population consistent with the results reported (Ozdemir et al., 2014). Therefore, based on this paradigm and consistent with the results we present in this study, FAP^+ cell depletion, would be expected to target and deplete not only the $FAP^+ SMA^-$ and $FAP^+ SMA^+$ subsets, but also to result in the loss of $SMA^+ FAP^-$ myofibroblasts derived from FAP^+ progenitors, as we indeed observed. Another, not mutually exclusive explanation, is that FAP^+ cells might be required to support the recruitment and/or differentiation of a distinct FAP^+ progenitor population to SMA^+ myofibroblasts.

To further investigate the impact of FAP^+ stroma cells on tumor-promoting desmoplastic response, we screened several mouse and human tumors and found that the extent of matrix accumulation correlated with the prevalence of intratumoral FAP^+ stromal cells, consistent with prior studies showing that stromal cells are an important source of ECM (Egeblad et al., 2010; Hanahan and Coussens, 2012; Jacob et al., 2012; Kalluri and Zeisberg, 2006). Experimental depletion studies revealed markedly depleted intratumoral ECM including reduced levels of collagen, HA and versican. These observations confirm that FAP^+ stromal cells are essential for the formation and/or maintenance of provisional tumor stroma and for promoting angiogenesis. While initial studies have attributed the FAP^+ stromal cell-mediated tumor-promoting effect to the immune suppression (Arnold et al., 2014; Feig et al., 2013; Kraman et al., 2010), our finding here indicates there is indeed an immune-independent mechanism in action. This immune-independent stromal remodeling and tumor-promoting angiogenesis effect was uncovered in the highly desmoplastic tumor types, as depletion of FAP^+ stromal cells resolved desmoplasia and

reduced angiogenesis, and therefore inhibited tumor progression (Lo et al., 2015). Along with a recent study of the impact of SMA^+ myofibroblast depletion (Ozdemir et al., 2014), the data presented herein indicate that while both FAP^+ and SMA^+ stromal cells regulate intratumoral collagen content, only FAP^+ stromal cells are important for the maintenance of intratumoral HA, suggesting that either FAP^+ stromal cells are the major source of HA or that FAP^+ stromal cells are required to drive SMA^+ myofibroblast deposition of HA. We also observed that depletion of FAP^+ stromal cells and loss of matrix components reduced tumor cell proliferation and increased apoptosis. Moreover, FAP-CAR T-cell treatment disrupted ductal adenocarcinoma-like structure, suggesting that extrinsic signals provided by tumor stroma are critical to the spatial orientation of tumor cells. Finally, as it is well established that tumor stroma can limit drug delivery and confer resistance to chemotherapeutics, we postulate that depletion of FAP^+ stromal cells can ameliorate desmoplastic response and hence reduce therapeutic resistance. Our data to date indicate that the combination of stromal cell depletion with gemcitabine treatment provides at least additive anti-tumor effects in 4662 tumors.

In summary, intratumoral FAP^+ stromal cells are attractive targets in the tumor microenvironment and can be therapeutically targeted by FAP-CAR T cells. FAP^+ stromal cells are essential in promoting immune-independent remodeling of tumor stroma and angiogenesis in highly desmoplastic tumors. Developing combinatorial strategies that incorporate targeting FAP^+ stromal cells may offer therapeutic advantages in cancer treatment.

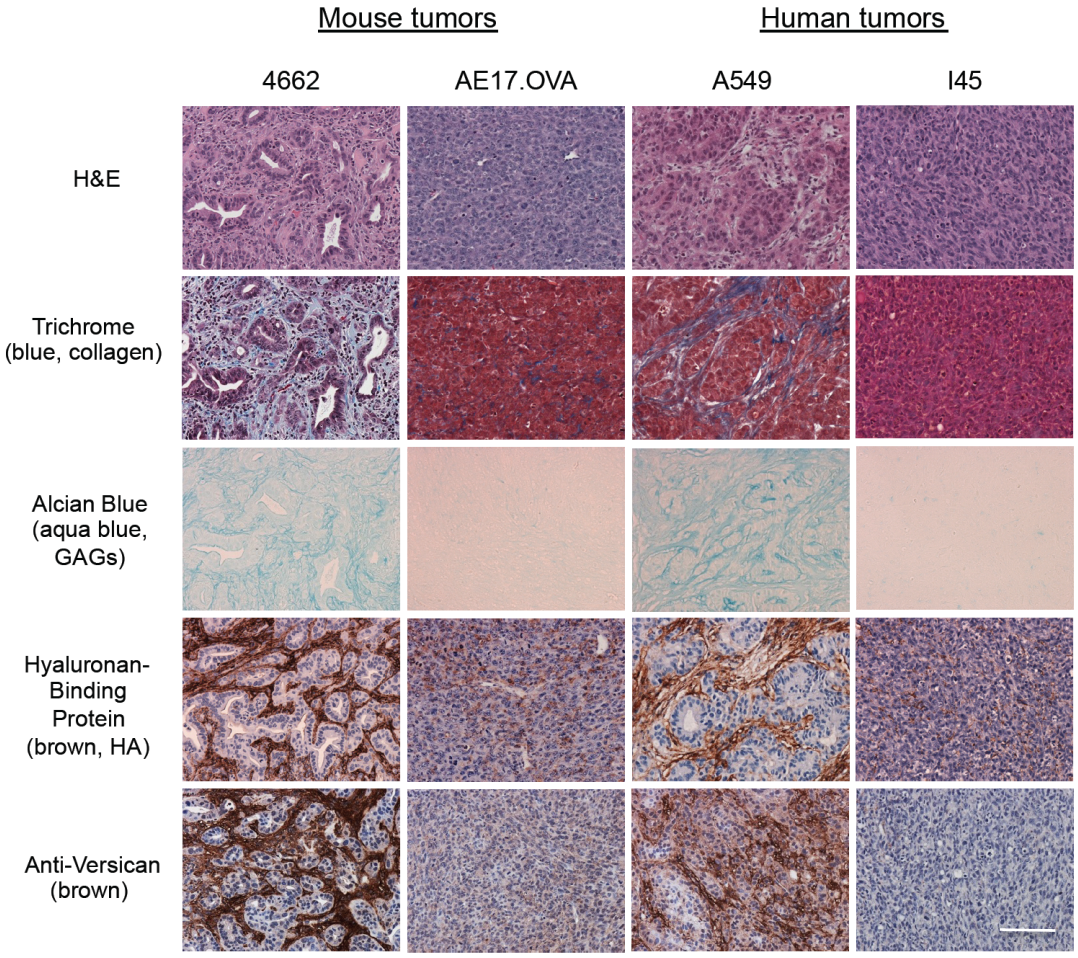

Figure 2-1. Mouse tumors and human tumor xenografts exhibit varying degrees of desmoplasia. C57BL/6 mice bearing established syngeneic 4662 pancreatic tumors and AE17.OVA mesotheliomas and NSG mice bearing established human A549 lung tumors and I45 mesotheliomas were harvested to evaluate the extent of desmoplasia. Collagen deposition was revealed by trichrome staining (blue). The total amount of glycosaminoglycans was determined by Alcian blue staining (aqua blue). IHC staining was performed with hyaluronan-binding protein (HABP) or anti-versican to reveal the total amount of HA and versican, respectively. n>5 per group, scale: 100 μm.

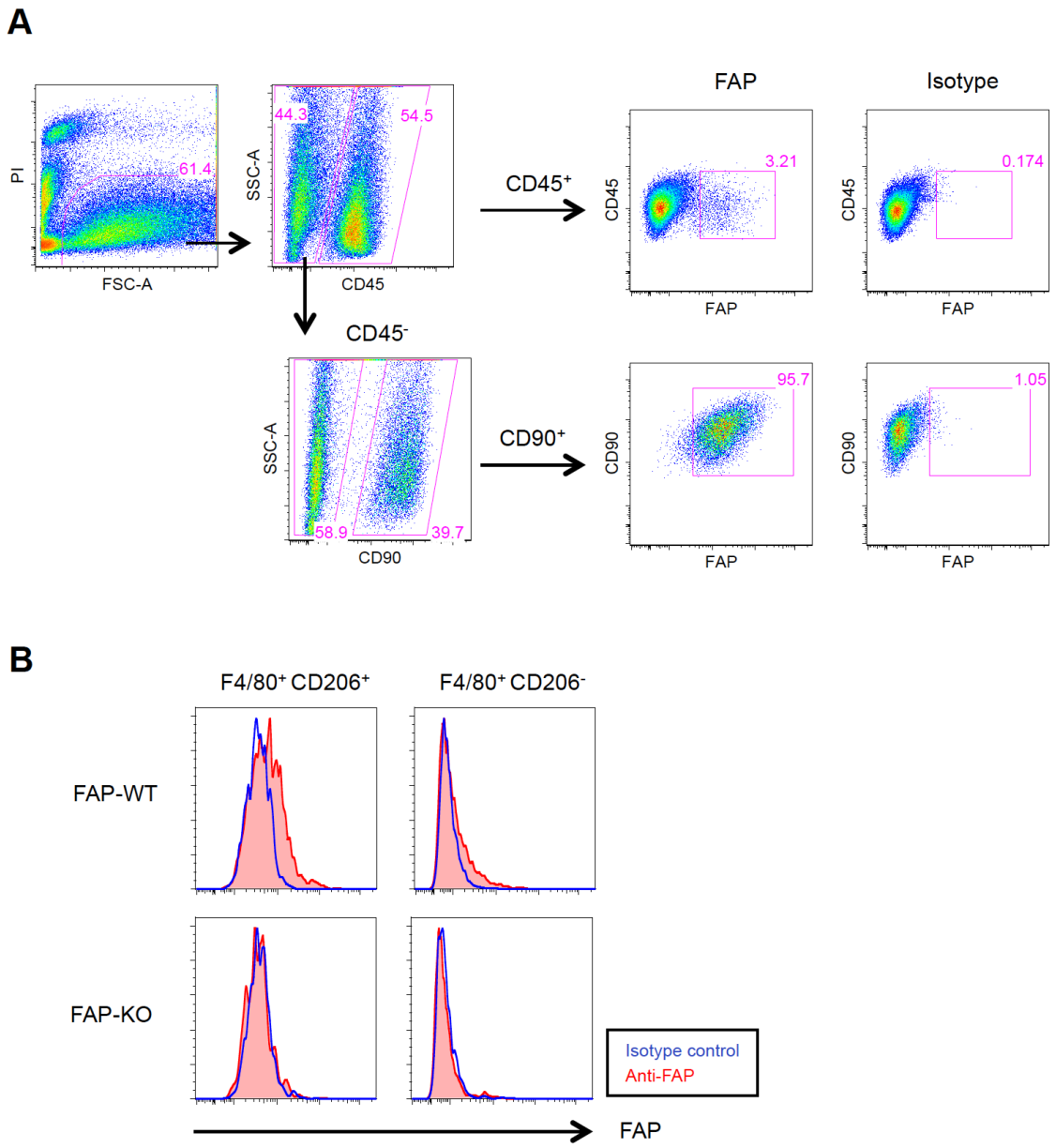

Figure 2-2. Identification of FAP$^+$ stromal cells in A549 human lung adenocarcinoma xenografts. Established A549 xenografts from NSG FAP-WT and FAP-KO mice were harvested and digested with a collagenase cocktail to obtain single-cell suspensions. (A) Cells were stained with anti-CD45, anti-CD90, anti-F4/80, anti-CD206 and anti-FAP antibodies, and flow cytometry was performed to identify FAP$^+$ stromal cells. Live cells were gated using propidium iodide exclusion. (B) A subset of CD11b$^+$ CD206$^+$ M2 macrophages express FAP.

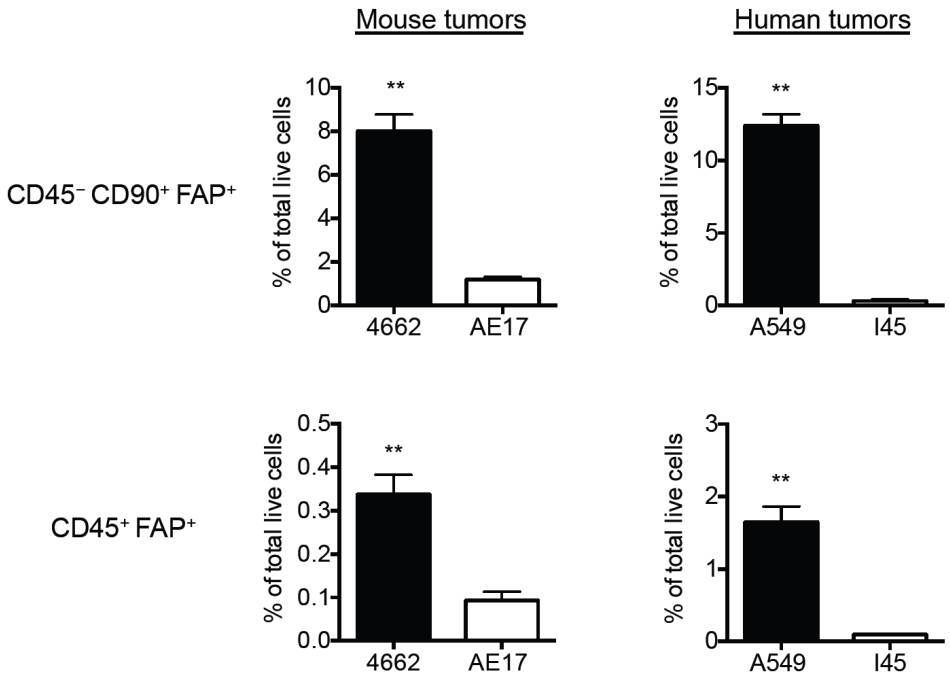

Figure 2-3. The extent of desmoplasia in mouse tumors and human tumor xenografts correlates with the abundance of intratumoral FAP$^+$ stromal cells. C57BL/6 mice bearing established highly desmoplastic 4662 pancreatic tumors and moderately desmoplastic AE17.OVA mesotheliomas and NSG mice bearing established highly desmoplastic human A549 lung tumors and poorly desmoplastic I45 mesotheliomas were harvested and dissociated using a collagenase cocktail to obtain single-cell suspensions. Flow cytometry was performed to identify CD90$^+$ stromal cells and CD45$^+$ hematopoietic cells that express FAP. Results are shown as mean ± SEM (n>5 per group), **p<0.01.

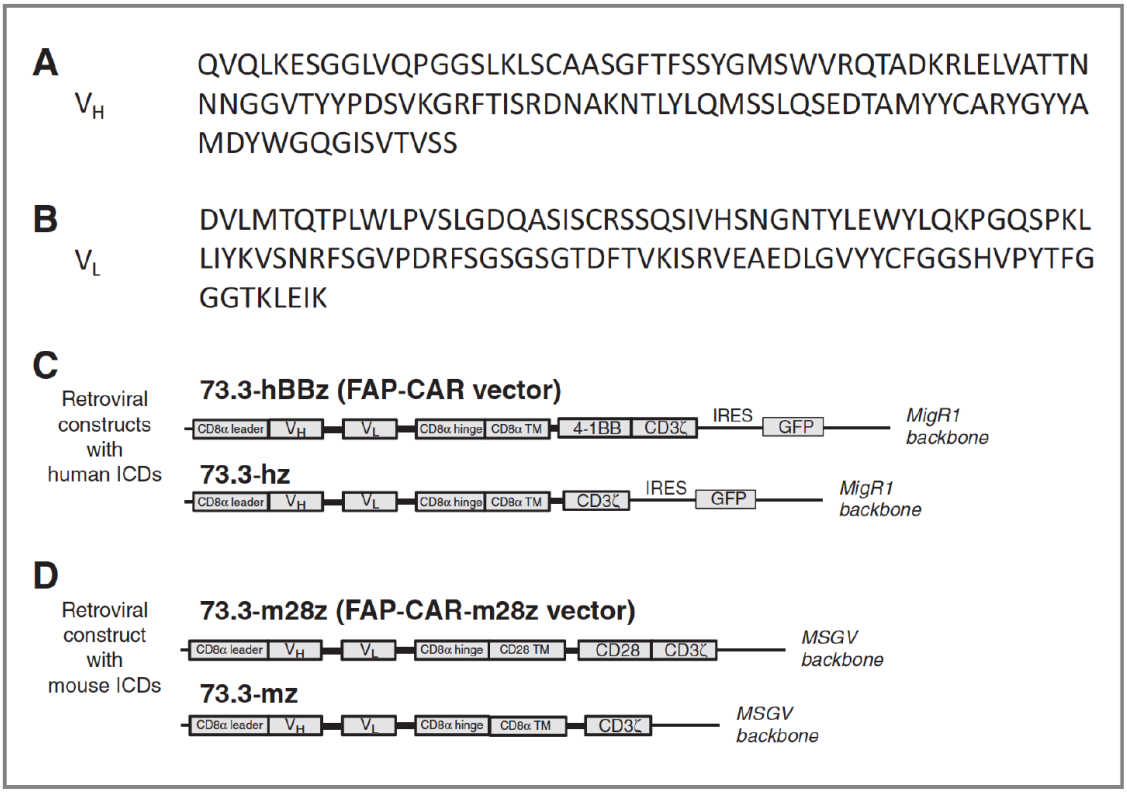

Figure 2-4. Development of FAP-specific chimeric antigen receptors. A monoclonal antibody (73.3) against murine FAP was generated by immunization of FAP-KO mice with 3T3 fibroblast-expressing FAP. Total RNA from the 73.3 hybridoma was extracted and reverse-transcribed to generate cDNA. The immunoglobulins were PCR-amplified to obtain the sequences of (A) variable heavy (V_H) and (B) light (V_L) chains. The FAP-CAR construct was synthesized by fusing the V_H and V_L sequences of 73.3 antibody with a CD8α hinge and transmembrane (TM) domain, plus human CD3ζ and human 4-1BB domains (73.3-hBBz), and was cloned into the MigR1 retroviral vector (C) to transduce mouse T cells or was cloned into the pELNS lentiviral vector to transduce human T cells. (D) A fully murine FAP-CAR construct was also synthesized by fusing the V_H and V_L sequences of 73.3 antibody with CD8α hinge, CD28 transmembrane domain and mouse CD28 and CD3ζ intracellular signaling domains (73.3-m28z), and was cloned into the MSGV retroviral vector to transduce mouse T cells.

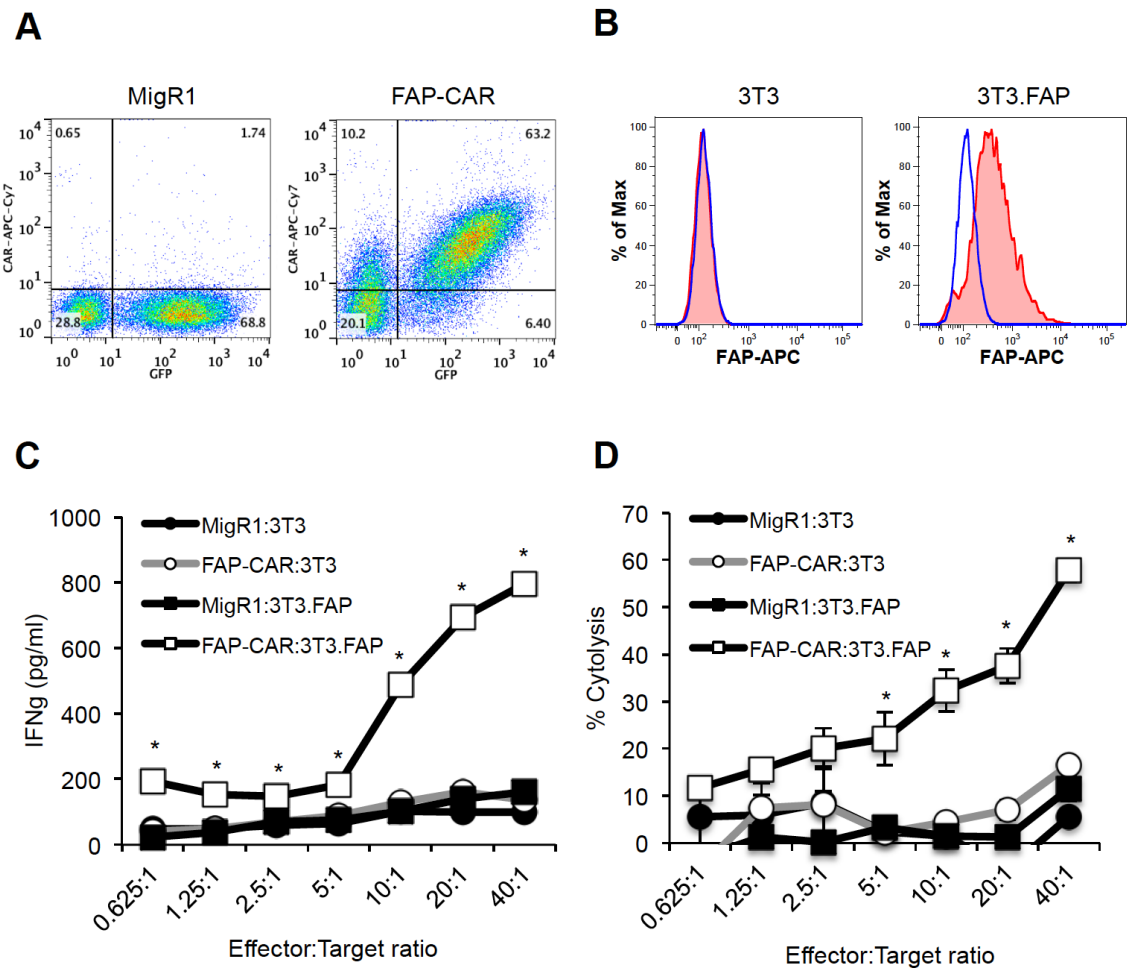

Figure 2-5. Ex-vivo characterization of murine FAP-CAR T cells using 3T3 fibroblasts. (A) Mouse T cells were transduced with a retroviral vector expressing GFP (MigR1) or GFP and anti-murine FAP-CAR. FAP-CAR was detected using goati anti-mouse IgG antibody conjugated with fluorochrome APC-Cy7. Transduction efficiency was evaluated by flow cytometry. (B) Flow cytometry analysis of FAP expression in 3T3 fibroblasts, or 3T3 fibroblasts transfected of murine FAP (3T3.FAP). (C) FAP-CAR T cells and MigR1 T cells were used to determine their IFNγ production and (D) cytolytic activity upon reacting with 3T3 or 3T3.FAP fibroblasts at various effector-to-target ratio. Results are shown as mean ± SEM (n=3 per group), *$p<0.05$.

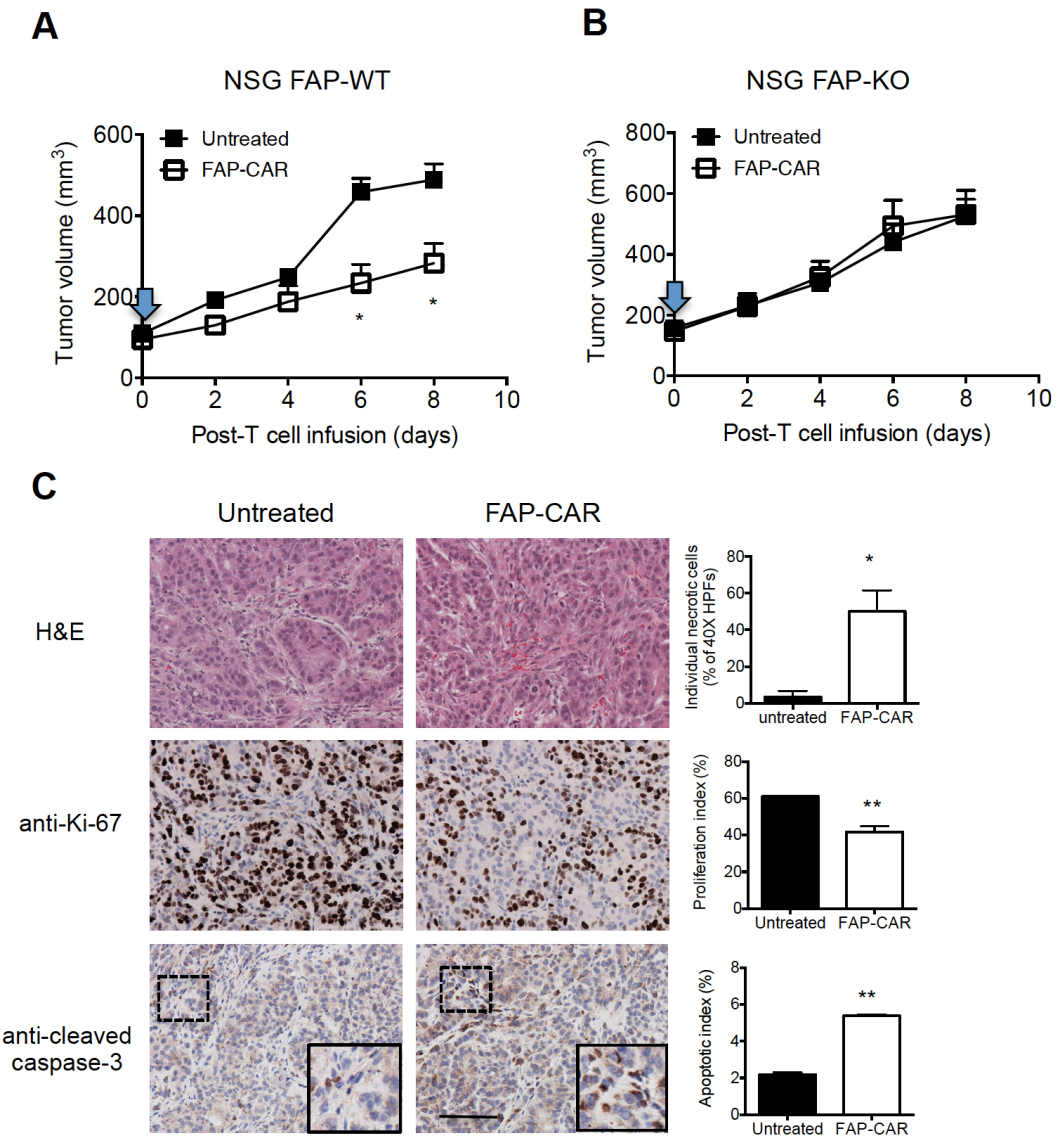

Figure 2-6. FAP-CAR T cells inhibit growth of desmoplastic A549 xenografts by inhibiting proliferation and increasing apoptosis in a target-specific fashion in the absence of adaptive immunity. (A) NSG mice bearing established A549 tumors were intravenously injected with 1×10^7 FAP-CAR human T cells or left untreated (n=5 per group). (B) To determine the target specificity, NSG FAP-KO mice bearing established A549 tumors were treated with 1×10^7 FAP-CAR human T cells through tail vein or left untreated (n=5 per group). Tumor growth was monitored by electronic caliper. The blue arrow indicates the time of adoptive T-cell transfer. (C) Tumor tissues were harvested 8 days post T-cell transfer for H&E, Ki67 and cleaved-caspase 3 staining. Computer-based quantification was performed using Fiji software. Results are shown as mean ± SEM (n=3 per group), *p<0.05; **p<0.01. Scale: 100 μm.

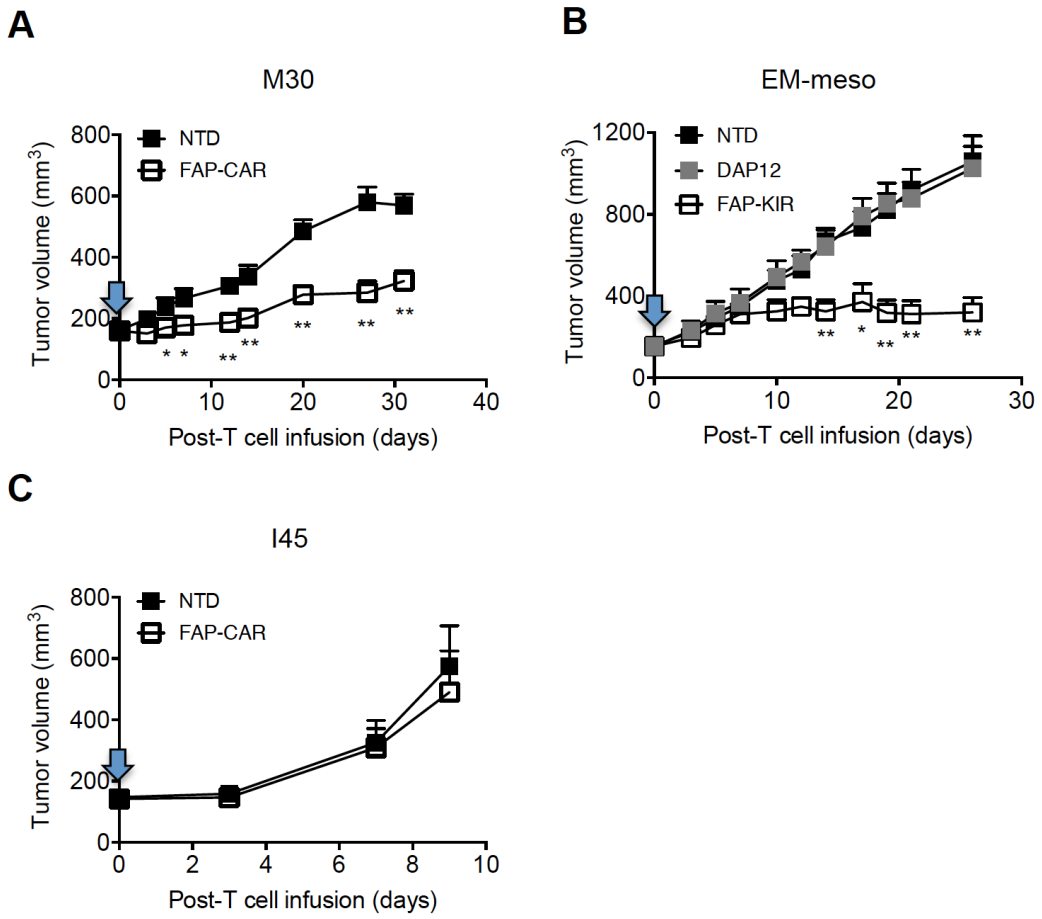

Figure 2-7. FAP-CAR T cells inhibit growth of desmoplastic M30 and EM-meso but not poorly-desmoplastic I45 xenografts. (A) NSG mice bearing highly desmoplastic M30 were intravenously injected with 1×10^7 FAP-CAR human T cells (FAP-CAR) or untransduced T cells (NTD). (B) NSG mice bearing highly desmoplastic EM-meso xenografts were intravenously injected with 5×10^6 enhanced FAP-CAR human T cells (killer immunoglobulin-like receptor-based FAP-CAR, also known as FAP-KIR), control vector T cells (DAP12) or untransduced T cells (NTD). (C) NSG mice bearing poorly desmoplastic I45 human mesothelioma xenografts were intravenously injected with 1×10^7 FAP-CAR human T cells (FAP-CAR) or untransduced T cells (NTD). Tumor growth was monitored by electronic caliper. The blue arrow indicates the time of adoptive T-cell transfer (n=5 per group). *$p<0.05$; **$p<0.01$.

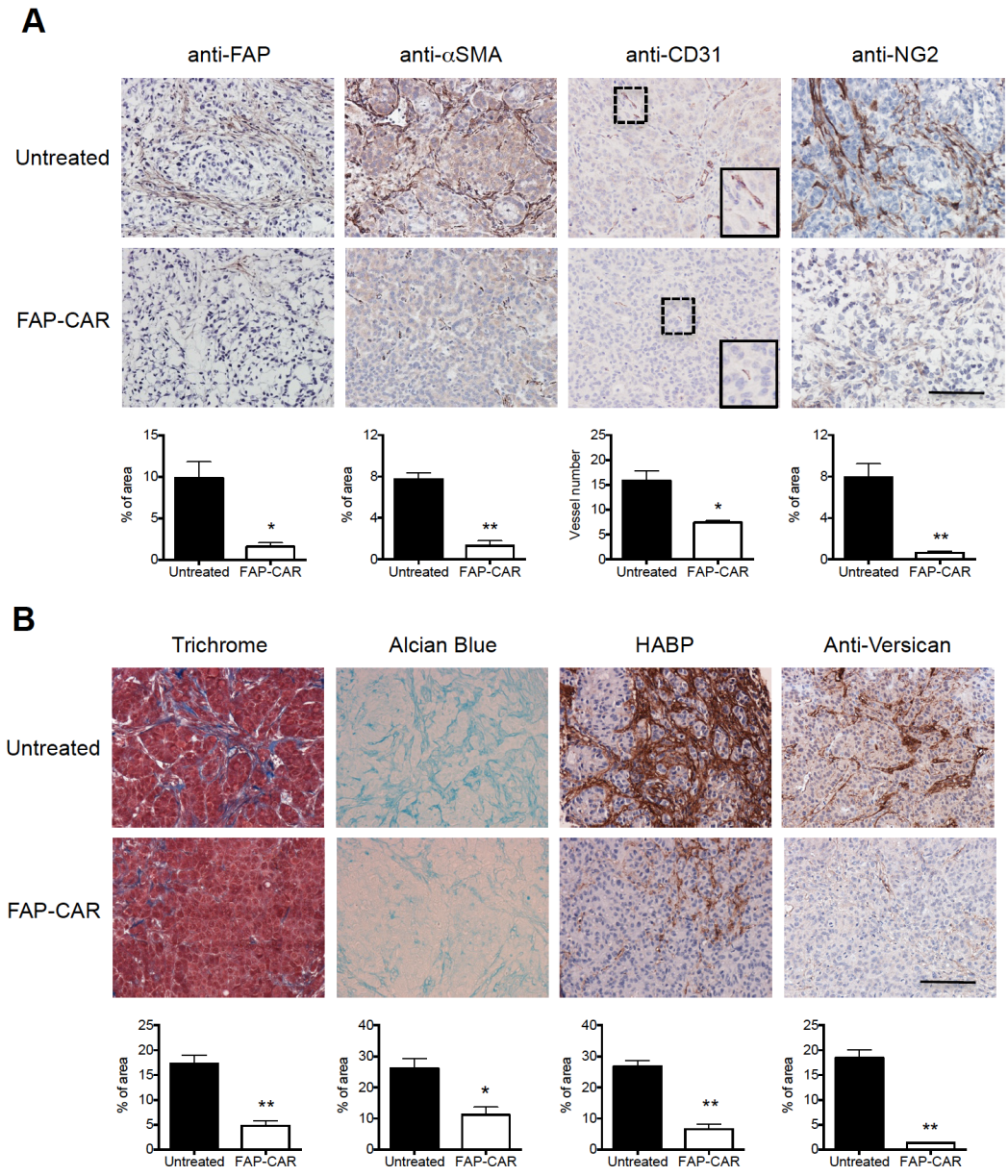

Figure 2-8. FAP-CAR T-cell-induced anti-tumor activity is associated with disrupted stromagenesis and angiogenesis in desmoplastic A549 xenografts. NSG mice bearing established A549 tumors were intravenously injected with 1×10^7 FAP-CAR human T cells through tail vein or left untreated as described in Figure 2-6. (A) Tumors were harvested 8 days post-adoptive T-cell transfer and sections were stained with anti-FAP, anti-αSMA, anti-CD31 and anti-NG2 antibodies to assess the impact of FAP-CAR T cells on tumor stromagenesis and angiogenesis. (B) The impact of FAP-CAR T cells on tumor stroma was evaluated by Masson's trichrome staining (collagen), Alcian blue staining (GAGs), and IHC staining for HA and versican. Computer-based quantification was performed using Fiji software. Results are shown as mean ± SEM (n=3 per group), *p<0.05; **p<0.01. Scale: 100 μm.

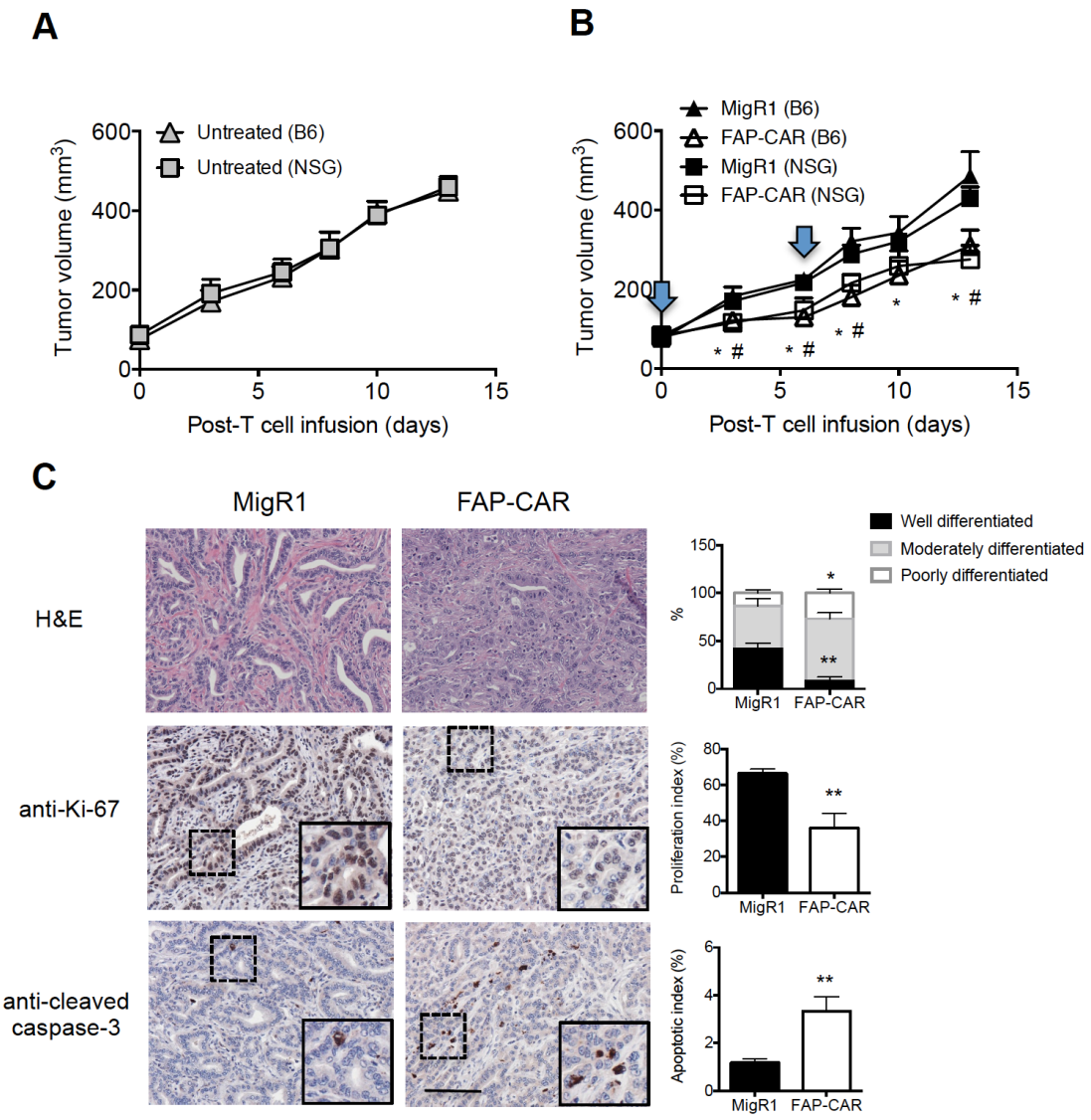

Figure 2-9. FAP-CAR T cells inhibit the growth of non-immunogenic but highly desmoplastic syngeneic PDAs by inhibiting proliferation and increasing apoptosis. (A) 4662 PDA growth was comparable in untreated B6 and NSG mice. (B) Established 4662 tumor-bearing C57BL/6 and NSG mice were intravenously injected with 2 doses of 1×10^7 FAP-CAR or MigR1 mouse T cells (n=5 per group). Tumor growth was monitored by electronic caliper. The blue arrow indicates the time of adoptive T-cell transfer. Tumor tissues were harvested for flow analysis shown in Fig. 2-10. (C) In another independent experiment, established 4662 tumor-bearing C57BL/6 mice were treated with 2 doses of 1×10^7 FAP-CAR or MigR1 mouse T cells (n=6 per group). Tumor tissues were harvested 3 days after the second dose of transferred T cells for H&E, Ki-67 and cleaved-caspase 3 staining. FAP-CAR T cell-induced anti-tumor effect is comparable to that shown in (B). Computer-based quantification was performed using Fiji software. Results are shown as mean ± SEM (n=6 per group), *p<0.05; **p<0.01. Scale: 100 μm.

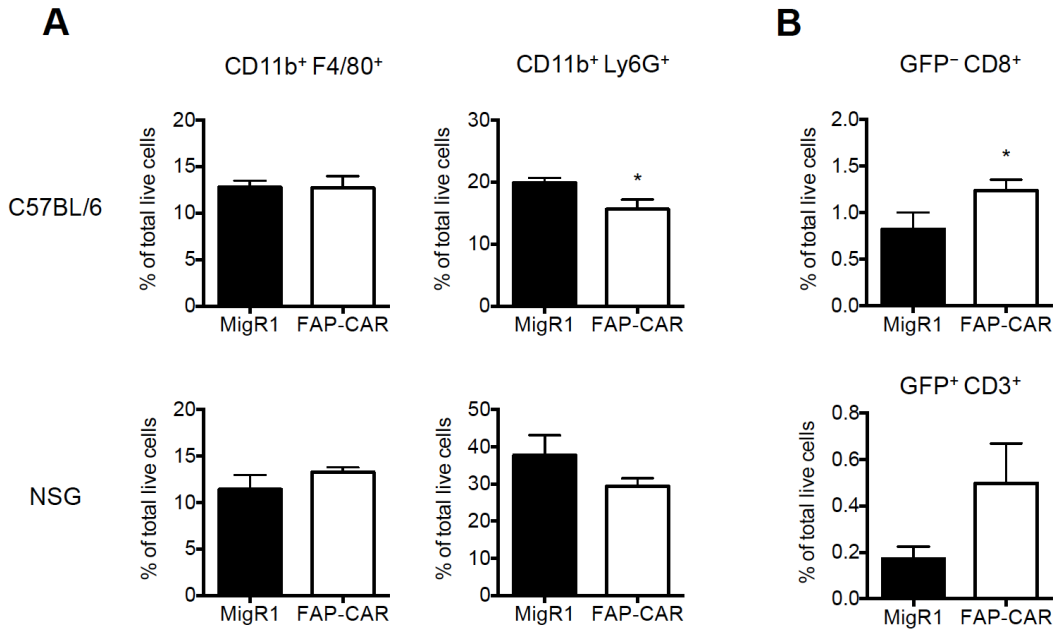

Figure 2-10. Depletion of FAP$^+$ stromal cells alters CD8$^+$ T cell and CD11b$^+$ Ly6G$^+$ cell infiltration in desmoplastic syngeneic PDAs. Established 4662 tumor-bearing C57BL/6 and NSG mice were intravenously injected with 2 doses of 1×10^7 FAP-CAR or MigR1 mouse T cells as described in Figure 2-9. Tumor tissues were harvested 7 days after the second dose of T-cell transfer and dissociated using a collagenase cocktail to obtain single-cell suspensions. (A) Flow cytometry was performed to identify CD11b$^+$ F4/80$^+$ macrophages, CD11b$^+$ Ly6G$^+$ neutrophils and (B) GFP$^-$ CD8$^+$ host T cells and GFP$^+$ adoptive transferred FAP-CAR T cells or MigR1 T cells. Results are shown as mean ± SEM (n=6 per group), *p<0.05.

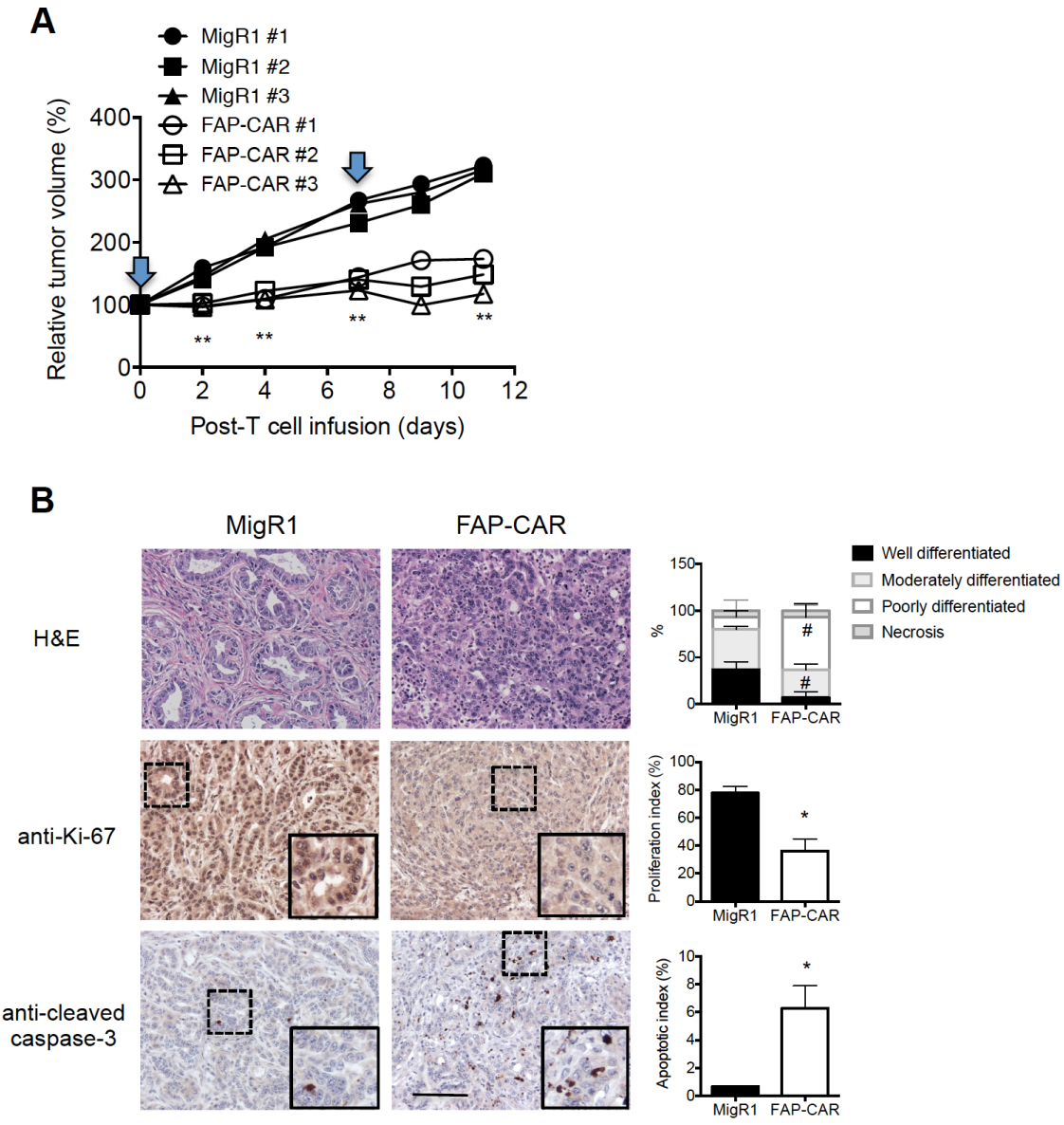

Figure 2-11. FAP-CAR T cells restrain tumor progression in an autochthonous mouse model of pancreatic cancer. (A) KPC mice bearing autochthonous PDA were intravenously injected with 2 doses of 1×10^7 FAP-CAR or MigR1 mouse T cells (n=3 per group). Tumor progression was followed by ultrasound. The blue arrow indicates the time of adoptive T-cell transfer. (B) Tumor tissues were harvested 4 days after the second dose of T-cell transfer for H&E, Ki-67 and cleaved-caspase 3 staining. Computer-based quantification was performed using Fiji software. Results are shown as mean ± SEM (n=3 per group), # p-value=0.05; * $p<0.05$. Scale: 100 μm.

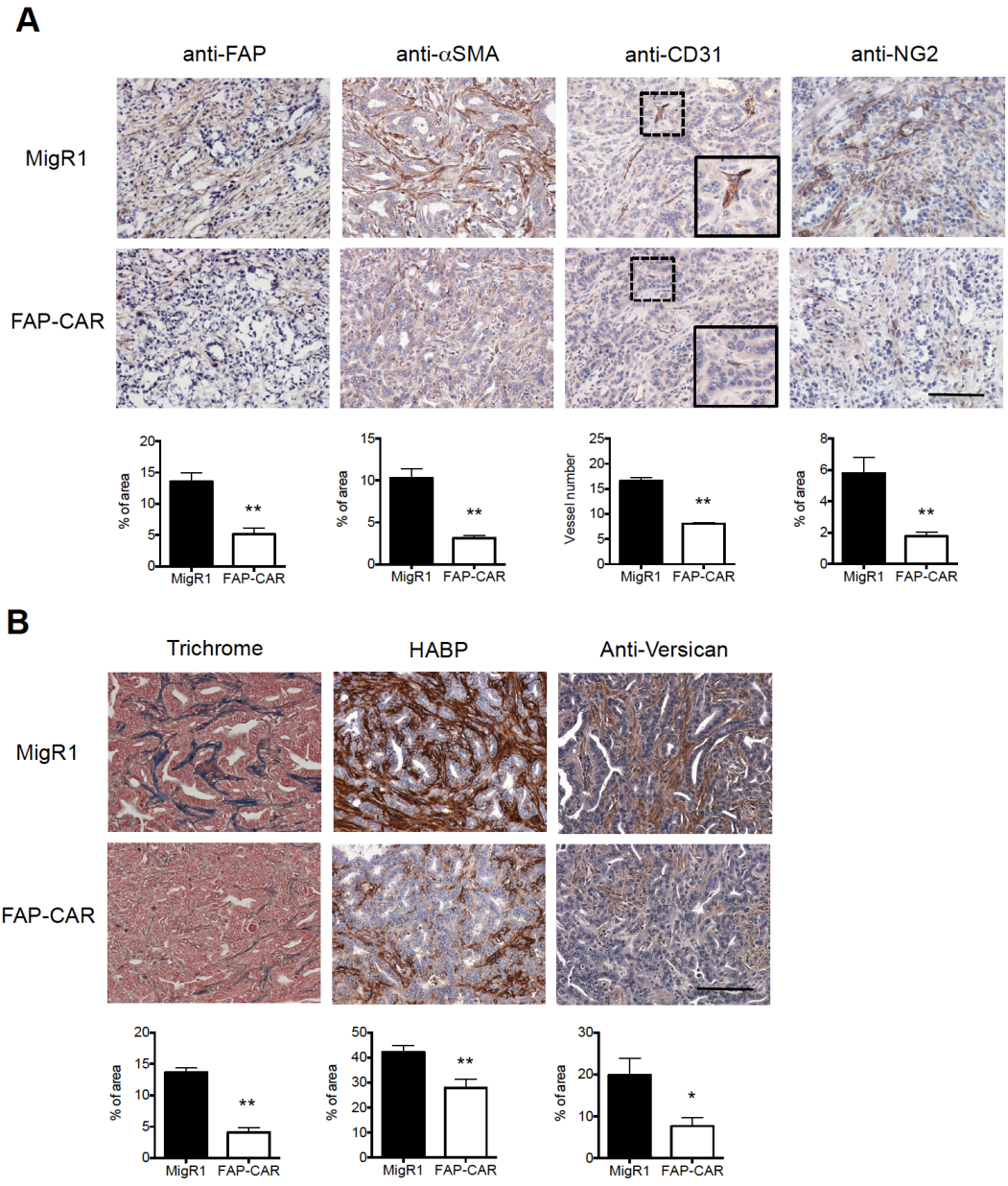

Figure 2-12. FAP-CAR T cells disrupt stromagenesis and angiogenesis in non-immunogenic but highly desmoplastic syngeneic PDAs. Established 4662 tumor-bearing C57BL/6 mice were intravenously injected with 2 doses of 1×10^7 FAP-CAR or MigR1 mouse T cells. Tumor tissues were harvested 3 days after the second dose of T-cell transfer and sections were stained with anti-FAP, anti-αSMA, anti-CD31 and anti-NG2 antibodies to determine the impact of FAP-CAR T cells on tumor stromagenesis and angiogenesis. Masson's trichrome staining and immunohistochemical staining for HA and versican were also performed to evaluate the tumor stroma. Computer-based quantification was performed using Fiji software. Results are shown as mean ± SEM (n=6 per group), *p<0.05; **p<0.01. Scale: 100 μm.

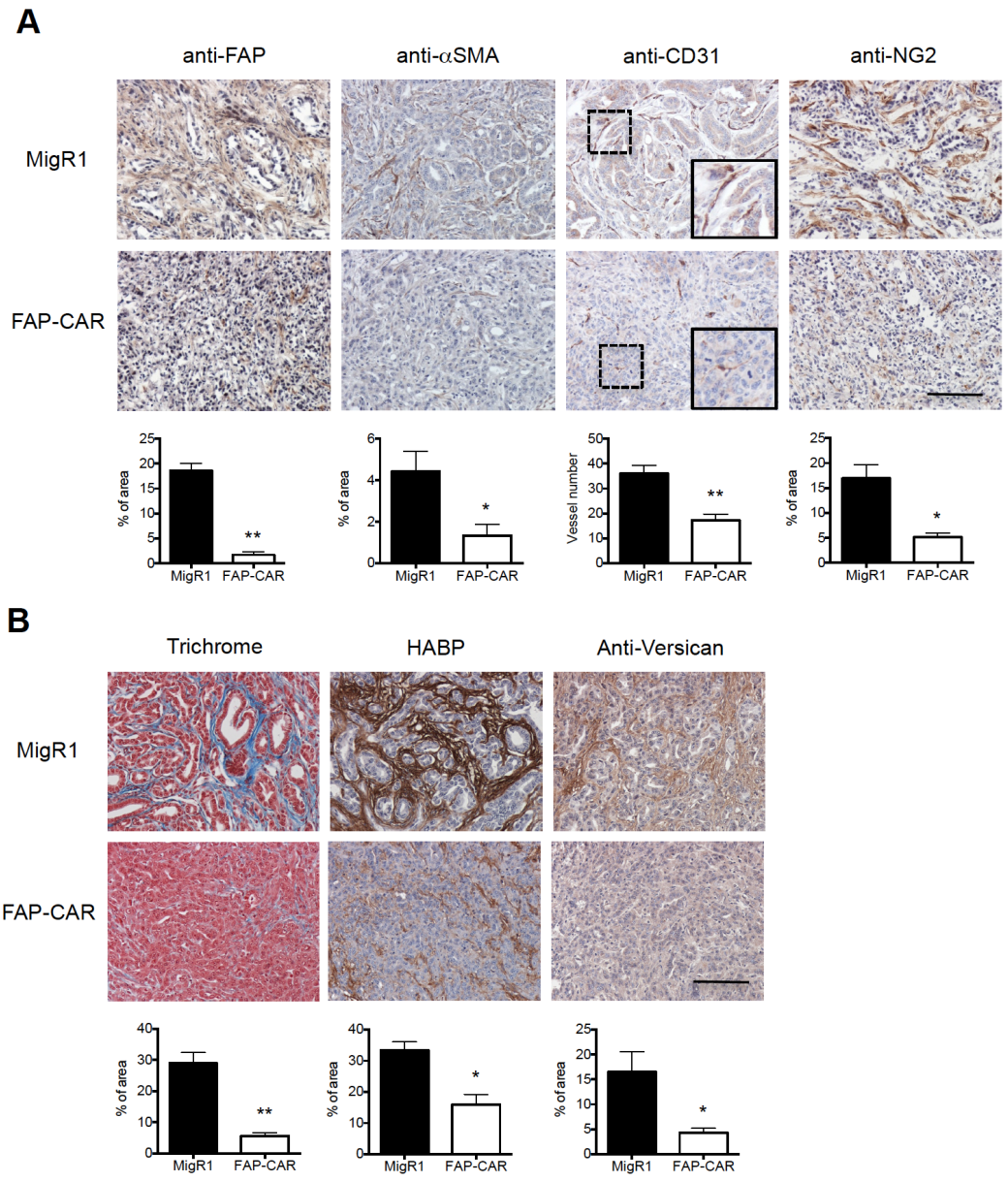

Figure 2-13. Depletion of FAP$^+$ stromal cells disrupts tumor-promoting desmoplasia in an autochthonous mouse model of pancreatic cancer. KPC mice bearing autochthonous PDA were intravenously injected with 2 doses of 1×10^7 FAP-CAR or MigR1 mouse T cells as described in Figure 2-11. Tumor tissues were harvested 3 days post the second dose of T-cell transfer and sections were stained with anti-FAP, anti-αSMA, anti-CD31 and anti-NG2 antibodies to determine the impact of FAP-CAR T cells on tumor stromagenesis and angiogenesis. Masson's trichrome and immunohistochemical staining for HA and versican were also performed to evaluate the impact of FAP-CAR T cells on the tumor stroma. Computer-based quantification was performed using Fiji software. Results are shown as mean ± SEM (n=3 per group), *p<0.05; **p<0.01. Scale: 100 μm.

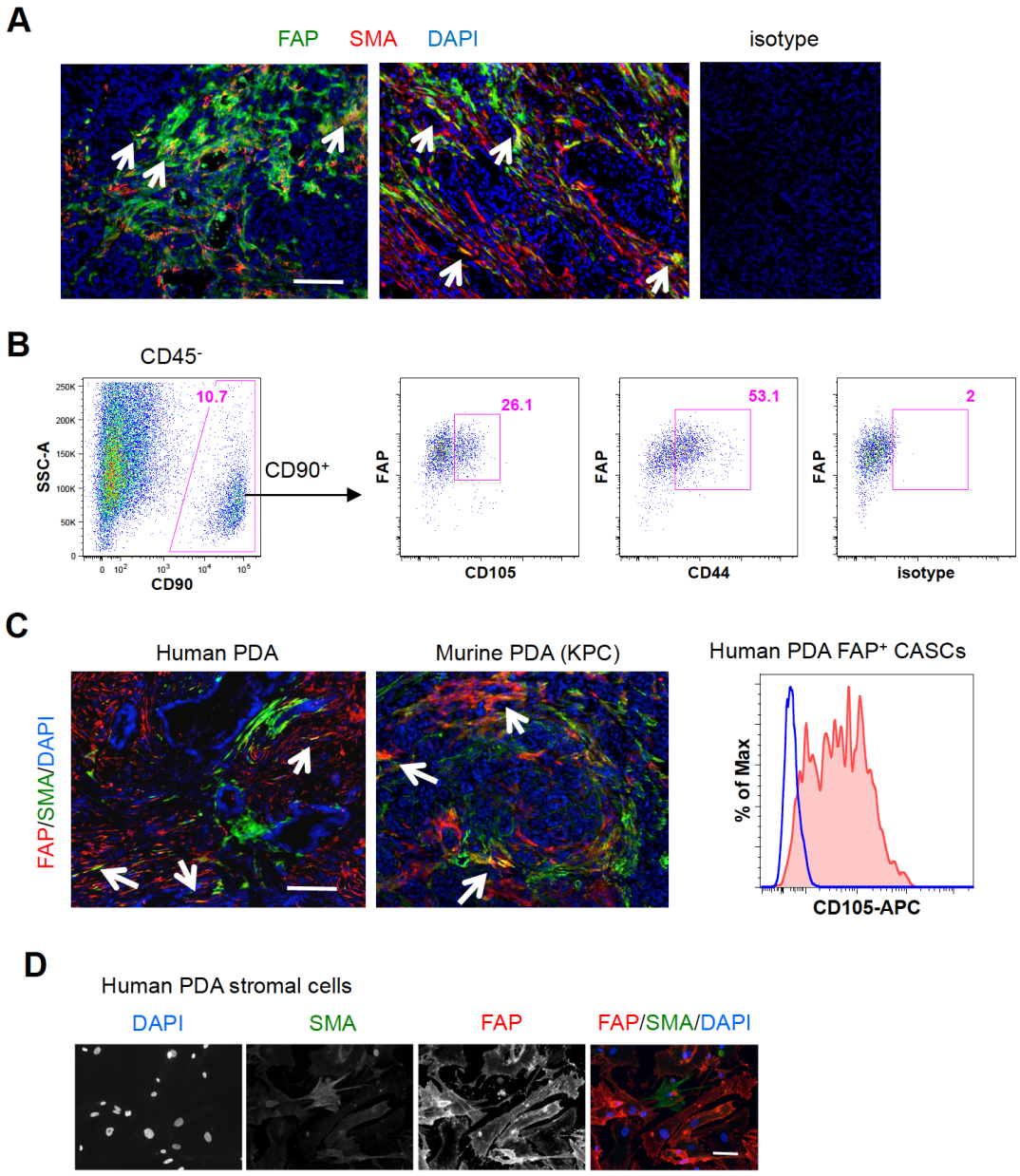

Figure 2-14. Identification of tumor stroma by FAP and SMA reveals stromal cell heterogeneity. (A) Established A549 lung xenografts were harvested and tumor sections were stained with FAP and SMA to identify mesenchymal tumor stromal cells. Arrows indicate cells that express both FAP and SMA. Scale: 100 μm. (B) A subpopulation of $CD45^{-}$ $CD90^{+}$ FAP^{+} cells in A549 tumor xenografts express mesenchymal stem cell marker CD105 and CD44. (C) Human and murine PDA tumors were stained with FAP and SMA. Arrows indicate cells that express both FAP and SMA. Scale: 100 μm. Expression of CD105 in human PDA FAP^{+} stromal cells. (D) Cancer-associated stromal cells were isolated from human PDA explants and stained with FAP and SMA. Scale: 50 μm.

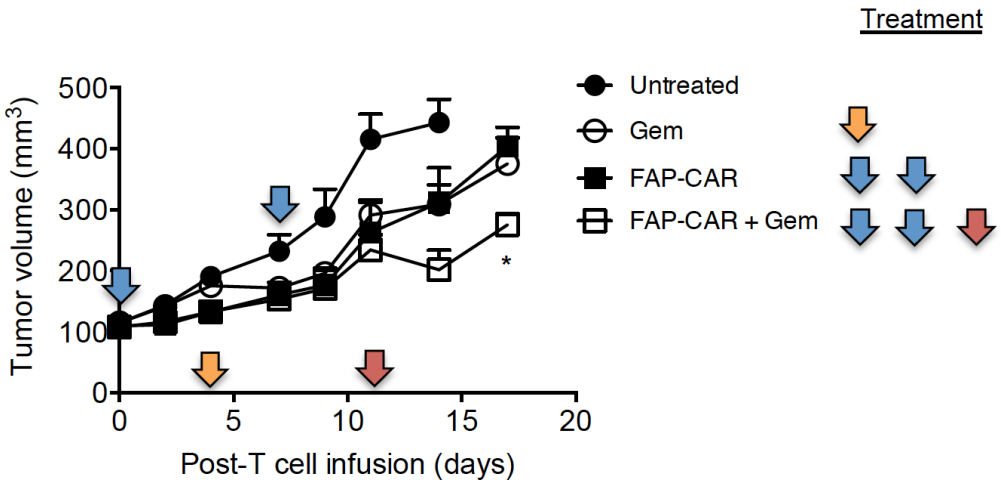

Figure 2-15. Combination of FAP-CAR T cells and chemotherapy provides additive anti-tumor response in desmoplastic syngeneic PDAs. Established 4662 tumor-bearing C57BL/6 mice were randomly grouped and assigned to the following treatments: (1) a cohort of mice were intravenously injected with two doses of 1×10^7 FAP-CAR T cells (blue arrows); (2) a cohort of mice received gemcitabine (120 mg/kg) treatment (intraperitoneal) on day 4 (orange arrow); (C) a cohort were given gemcitabine 4 days after the second dose of FAP-CAR T cells (red arrow); and (4) left untreated. Tumor growth was followed. Results are shown as mean ± SEM (n=5 per group); * denotes a significant difference between FAP-CAR, gemcitabine and the combo groups ($p<0.05$).

CHAPTER 3 – Depletion of fibroblast activation protein-expressing stromal cells can enhance host adaptive anti-tumor immunity

Introduction

FAP-expressing cells regulate anti-tumor immunity

The first indirect indication of the potential influence of FAP^+ stromal cells in modulating anti-tumor immunity was eluded by Dr. Eli Gilboa's group. Specifically, they demonstrated that depletion of $CD8^+$ T cells partially abrogated the anti-tumor effects induced by anti-FAP vaccination (Lee et al., 2005). However, their approach could not determine whether the loss of anti-tumor activity was due to elimination of FAP^+ stromal cell-specific $CD8^+$ T cells induced by anti-FAP vaccination, or it was due to loss of the tumor-reactive $CD8^+$ T cells that could contribute to the anti-tumor response. To better understand the impact of FAP^+ stromal cell on host anti-tumor immune response, a Bac transgenic mouse expressing the human diphtheria toxin receptor (DTR) driven by the *Fap* promoter was developed by Dr. Fearon's group to study the effects of FAP^+ stromal cell ablation on anti-tumor immunity (Kraman et al., 2010). They reported that elimination of FAP^+ stromal cells inhibited growth of Lewis lung carcinoma cells forced to express a nominal antigen ovalbumin (LLC-OVA). The anti-tumor effect of FAP^+ stromal cell ablation was abolished in RAG-1-deficient mice or by administration of anti-TNF-α and IFN-γ antibodies, indicating that FAP^+ stromal cells can induce immune suppression to enable tumor growth. Using this genetic approach, heme-oxygenase-1 (HO-1) and stromal-derived factor-1 alpha (SDF-1α), secreted by the hematopoietic and mesenchymal FAP^+ stromal cells, respectively, were shown to inhibit anti-tumor

immunity (Arnold et al., 2014; Feig et al., 2013). Notably, genetic ablation of FAP^+ stromal cells or pharmacologic targeting of HO-1 and SDF-1α overcame immune suppression and potentiated an anti-tumor immune response to control the growth of transplanted and autochthonous pancreatic tumors, respectively.

In this chapter, I describe using FAP-CAR T cells as an approach to deplete FAP^+ stromal cells in multiple syngeneic mouse tumor models, and investigate the potential immune-dependent mechanism by which FAP^+ stromal cells promote tumor growth. We also explored several approaches to enhance FAP-CAR T-cell-mediated anti-tumor activity by repeated dosing, enhancing FAP-CAR T-cell persistence and/or effector functions, and combining treatment with a cancer vaccine.

Materials and methods

Cell lines

A mouse mesothelioma cell line AE17.OVA was obtained from Dr. Delia Nelson (University of Western Australia). TC1 lung cancer cells derived from mouse lung epithelial cells immortalized with human papillomavirus (HPV)-16 E6 and E7 antigens, and then transformed with the c-Ha-*ras* oncogene (Lin et al., 1996), were acquired from Dr. Steven Albelda at the University of Pennsylvania. A mouse LKR cell line was derived from an explant of a pulmonary tumor from an autochthonous mutant *Kras*-induced lung cancer generated by the laboratory of Tyler Jacks at MIT (Johnson et al., 2001). The mouse 4T1 mammary carcinoma cell line and CT26 colon cancer cell line were purchased from the American Type Culture Collection. Cells were tested mycoplasma-free and frozen and were used less than one month after resuscitation.

Animals

Sources and generation of the C57BL/6, NSG FAP-WT and FAP-deficient mice were described in the methods section of Chapter 2. Additionally, C57BL/6:129pf/j hybrid mice were generated for LKR lung cancer studies. BALB/c mice were purchased from Charles River Laboratories Inc. (Wilmington, MA). DGKζ-knockout (Riese et al., 2013) and Thy1.1 congenic C57BL/6 mice were obtained from Dr. Gary Koretzky at the University of Pennsylvania and Dr. Wayne Hancock at the Children's Hospital of Philadelphia, respectively. Experimental protocols were approved by the Institutional Animal Care and Use Committee and were in compliance with guidelines for the care and use of animals.

Intravenous transfer of FAP-CAR T cells in mice bearing established tumors.

Mice were injected subcutaneously with 2×10^6 AE17.OVA (FAP-WT and FAP-KO C57BL/6 mice), 1×10^6 TC1 (C57BL/6 mice), 2×10^6 LKR (C57BL/6:129pf/j hybrid mice), 0.5×10^6 4T1 (BALB/c mice), or 1×10^6 CT26 (BALB/c mice) tumor cells into the dorsolateral flank. Tumor-bearing mice were randomly assigned to three groups that either received one dose of 1×10^7 WT FAP-CAR or MigR1-transduced mouse T cells or were left untreated. Established AE17.OVA tumor-bearing mice were treated with either one dose or two doses of 1×10^7 WT FAP-CAR (one week apart), or left untreated. In another experiment, AE17.OVA tumor-bearing mice were treated with one dose of 1×10^7 WT FAP-CAR or DGKζ-KO FAP-CAR T cells, or left untreated. To test if FAP-CAR T cells can increase the efficacy of cancer vaccination, large TC1 tumor-bearing mice were subcutaneously injected with saline or a vaccine consisting of 10^9 plaque-forming units (pfu) of an adenovirus expressing the HPV-E7 antigen. Four days later, one dose of 1×10^7 FAP-CAR T cells was administered intravenously. At the endpoint, tumors were harvested for flow cytometric or histopathological analyses.

Antibodies

Purified anti-mouse CD3ε (145-2C11), anti-mouse CD28 (37.51), anti-mouse CD16/32 and anti-Thy1.1 (HIS51; APC) antibodies were purchased from eBioscience. Anti-CD45 (30-F11; PE-Cy7) and anti-CD90 (53-2.1; FITC, PE) antibodies were purchased from Biolegend. Anti-CD8α (53-6.7; APC, PE), anti-CD69 (H1.2F3; PE), anti-TNF (MP6-XT22; PE) and anti-IFNγ (XMG1.2; PE) antibodies were purchased from BD Bioscience.

H-2K^b tetramer loaded with ovalbumin peptide (SIINFEKEL; APC) was purchased from iTag^{TM} MHC Tetramer (Beckman Coulter). H-2D^b tetramer loaded with E7 peptide (RAHYNIVTF; PE) was purchased from the National Institute of Allergy and Infectious Diseases Tetramer Core. A polyclonal sheep anti-human antibody that cross-reacts with mouse FAP was purchased from R&D.

Surface staining and flow cytometry analysis

This experimental method is described in detail in the methods section of Chapter 2.

Intracellular Staining.

Surface staining was first performed as described in the methods section of Chapter 2 using anti-CD8α (53-6.7; APC, PE) antibody. Cells were washed and incubated with a viability probe (Thermo Fisher Scientific) for 30 minutes. Cells were then fixed and permeabilized for another 45 minutes at 4°C, followed by staining with anti-TNFα or anti-IFNγ antibody.

Histopathological, histochemical and immunohistochemical analysis

These experimental methods are described in detail in the methods section of Chapter 2.

Cytokine release and cytotoxicity assays

FAP-CAR T cells encoding different intracellular signaling domains including the mouse CD3ζ chain (73.3-mz), mouse CD3ζ along with mouse CD28 domains (73.3-m28z), human CD3ζ chain (73.3-hz), and human CD3ζ along with human 4-1BB domains (73.3-

hBBz) were co-cultured with 3T3 or 3T3.FAP fibroblasts expressing GFP and luciferase at various effector-to-target ratios. After 18 hours, the culture supernatants were collected for IFNγ analysis using an ELISA (BD Bioscience). The cytotoxicity of transduced T cells was determined using a luciferase assay system (Promega).

Activation-induced T cell death assay

Recombinant FAP-extracellular domain (residues 99–761) or bovine serum albumin (BSA) was chemically crosslinked to tosylactivated 4.5 μm Dynabeads (Thermo Fisher Scientific). Mouse MigR1 or FAP-CAR T cells encoding different intracellular signaling domains including mouse CD3ζ along with mouse CD28 domains (m28z) and human CD3ζ along with human 4-1BB domains (hBBz) were cultured with FAP-ECD or BSA-coated beads. The number of live cells was determined at various time points using trypan blue exclusion.

Statistical Analyses

Statistics were calculated using GraphPad Prism 6. For studies comparing two groups, Student's *t*-test was used. For studies comparing more than two groups, one-way ANOVA with post-hoc Tukey testing was used. Data are represented as mean ± SEM. Differences were considered significant when $p < 0.05$.

Results

FAP-CAR T cells inhibit growth of multiple moderately-desmoplastic solid tumors in syngeneic hosts

In the previous chapter, we specifically tested whether FAP^+ stromal cells can augment growth of highly desmoplastic human tumors and syngeneic mouse models of PDA via immune-independent stromal remodeling of the tumor stroma. Consistent with the data described in those studies, we observed that syngeneic tumors, including AE17.OVA, TC1 and LKR, all exhibited moderate desmoplasia and recruited FAP^+ stromal cells into the tumor microenvironment in immune-competent hosts (**Fig. 2-1 and 3-2**). Here, we explore the capability of FAP-CAR T cells to inhibit tumor growth using three different tumor lines that do not express FAP: AE17.OVA mesothelioma cells and TC1 and LKR lung cancer cells and investigate the contribution of immune-dependent and immune-independent mechanisms to their anti-tumor activity in these models.

Adoptive transfer of FAP-CAR T cells, but not MigR1 T cells, significantly reduced the growth of AE17.OVA tumors (**Fig. 3-1A**), TC1 tumors (**Fig. 3-1C**), LKR tumors (**Fig. 3-1D**) and 4T1 tumors (**Fig. 3-1E**) by 35-50%. FAP-CAR T cell treatment inhibited the growth of CT26 tumors at day 1 to day 3 post-adoptive transfer, but tumor resurged at the later time point (**Fig. 3-1F**). To confirm specificity, AE17.OVA-bearing FAP-deficient C57BL/6 mice were treated with FAP-CAR T cells. In contrast to the effect on AE17.OVA tumors in FAP-intact C57BL/6 mice, FAP-CAR T cells had no effect on the growth of AE17.OVA tumors in FAP-deficient mice (**Fig. 3-1B**).

At the endpoint, around 7-9 days post-T-cell transfer, FAP-CAR T-cell treatment decreased the number of $CD45^{-}$ $CD90^{+}$ FAP^{+} and $CD45^{+}$ FAP^{+} populations by about 50% compared to those in the untreated group of AE17.OVA tumors, TC1 tumors and LKR tumors (**Fig. 3-2**). To further characterize this FAP-CAR T-cell-mediated depletion of intratumoral FAP^{+} stromal cells, we treated AE17.OVA tumors with FAP-CAR T cells and evaluated the prevalence of FAP^{+} stromal cells at 3 days post-T-cell transfer. At this earlier time point, we observed a dramatic decrease of $CD90^{+}$ FAP^{+} stromal cells (a reduction of 82%) and $CD45^{+}$ FAP^{+} leukocytes (a reduction of 56%), whereas MigR1 T cells had no impact on the numbers of either population (**Fig. 3-3A**). We also identified both low- and high-FAP-expressing cells in both the $CD45^{-}$ $CD90^{+}$ and $CD45^{+}$ populations in untreated tumors. When we gated on these specific populations, we noted that the FAP-CAR T cells selectively depleted the FAP-high expressers but had little effect on FAP-low expressers (**Fig. 3-3B and C**).

FAP-CAR T cells alter tumor angiogenesis and desmoplastic response in syngeneic AE17.OVA tumors

Having established that FAP^{+} stromal cells are required for the formation and maintenance of a provisional tumor stroma in multiple desmoplastic tumor models described in chapter 2, we also sought to investigate the impact of FAP-CAR T cells on the tumor microenvironment in moderately-desmoplastic AE17.OVA tumors by histochemical and immunohistochemical analyses. FAP-CAR T-cell treatment showed altered tumor morphology and nuclear condensation, reduced tumor cell proliferation and increased tumor cell apoptosis. The tumor stroma was also remarkably changed. The

number of $CD31^+$ vessels was decreased by 30% following FAP-CAR T-cell transfer. Collagen and HA content were reduced by 57% and 83%, respectively (**Fig. 3-4**). Although AE17.OVA tumors are not as desmoplastic as the other tumor types examined (**Fig. 2-1 and 2-3**), these data indicate that FAP^+ stromal cell-mediated immune-independent stromal remodeling may have contributed to tumor growth.

Role of the adaptive immune response in FAP-CAR T-cell-induced anti-tumor activity

As discussed above, depletion of FAP^+ stromal cells may have induced anti-tumor activity by abrogating immune-independent stromal remodeling and reducing angiogenesis, nonetheless, we also aimed to investigate the potential contribution of host adaptive anti-tumor immunity in these immunogenic tumors in the immune-competent mice. We examined the potential impact of FAP^+ stromal cells on host anti-tumor immunity using AE17.OVA and TC1 tumor cells that are highly immunogenic due to expression of human papilloma virus (HPV) oncoproteins E6 and E7. Interestingly, we found a significant increase of total $CD8^+$ T cells within the AE17.OVA and TC1 tumors at 8 days following FAP-CAR T-cell treatment (**Fig. 3-5**). Further analyses using tetramer staining showed that FAP-CAR T-cell-treated tumors had a higher number of OVA-specific T cells and E7-specific T cells within AE17.OVA tumors and TC1 tumors, respectively (**Fig. 3-5**).

To further study the impact of FAP^+ stromal cell depletion on host adaptive anti-tumor immunity, we treated AE17.OVA tumor-bearing mice with FAP-CAR T cells and

analyzed the endogenous (non-GFP-expressing) T cells at 3 and 8 days post T-cell transfer. We found that the number of intratumoral $CD3^+$ T cells did not change at 3 days post T-cell transfer (**Fig. 3-6A**), consistent with a previous report in which a genetic approach was used to ablate FAP^+ stromal cells (Kraman et al., 2010). Nevertheless, we found that at this time point, the number of $CD4^+$ T cells producing TNFα was significantly higher in tumors that received FAP-CAR T-cell treatment (**Fig. 3-6C**), while the numbers of activated $CD69^+$ T cells and IFNγ-producing $CD8^+$ T cells remained unchanged (**Fig. 3-6D and E**). Interestingly, the number of $CD3^+$ T cells was higher in tumors at 8 days following treatment with FAP-CAR T cells (**Fig. 3-6B**). At this time point, the numbers of $CD69^+$ and $IFN\gamma^+$ $CD8^+$ T cells had increased (**Fig. 3-6D and E**), while the numbers of TNFα-producing T cells remained similar between FAP-CAR T cell- and MigR T cell-treated group (**Fig. 3-6C**). Taken together, these data show that depletion of intratumoral FAP^+ stromal cells might augment the anti-tumor immune response by initially activating intratumoral host $CD4^+$ T cells, followed by enhanced $CD8^+$ T-cell infiltration and activation at the later time point.

To further elucidate the relative contributions of FAP^+ stromal-cell-mediated immune suppression and immune-independent remodeling of the tumor microenvironment to the inhibition of AE17.OVA tumor growth, we compared the impact of FAP-CAR T cells in AE17.OVA tumor-bearing C57BL/6 (**Fig. 3-7A**) and immunodeficient NSG mice (**Fig. 3-7B**). Notably, AE17.OVA tumors grew much more rapidly in NSG mice than in C57BL/6 mice, indicating that tumors were highly immunogenic and that the endogenous anti-tumor activity was lost in NSG mice. As above, administration of FAP-CAR T cells

significantly inhibited the growth of AE17.OVA tumors in immune-competent C57BL/6 mice, but this anti-tumor effect was not observed in immune-deficient NSG mice (**Fig. 3-7**). This loss in activity was not due to the loss of FAP expression in the NSG tumor microenvironment, as we confirmed that AE17.OVA tumors recruited comparable levels of FAP^+ stromal cells in C57BL/6 and NSG mice. Therefore, the impact of FAP-CAR T cells on tumor growth in this model is dependent on endogenous anti-tumor immunity.

FAP-CAR T-cell therapy augments the efficacy of a cancer vaccine

As FAP^+ tumor cell depletion can augment endogenous adaptive anti-tumor immunity, we hypothesized that the combination of tumor vaccination and FAP-CAR T-cell treatment may increase therapeutic efficacy compared to either approach alone. To test this possibility, mice bearing established large TC1 tumors (approximately $200mm^3$) were treated with a tumor vaccine consisting of an adenovirus expressing HPV-E7 (Ad.E7) to augment the T-cell response against E7-expressing TC1 tumor cells (**Fig. 3-8**, red arrow). FAP-CAR T cells were then administered intravenously (**Fig. 3-8**, blue arrow) four days after injection with the Ad.E7 vaccine. Individually, the Ad.E7 cancer vaccine and FAP-CAR T cells each only resulted in modest effects on these large established tumors. However, the combination treatment suppressed tumor growth for up to two weeks before further tumor progression (**Fig. 3-8**).

Enhancement of FAP-CAR T-cell therapy

We noticed that tumors that received a single infusion of FAP-CAR mouse T cells eventually progressed 6-8 days after T-cell transfer (**Fig. 3-1**). We reasoned that the rapid

loss of FAP-CAR T cells was due to their limited persistence and/or suppression of their effector functions in an immune-suppressive tumor microenvironment, thereby leading to tumor resurgence. To address the first possibility, we assessed the number of intratumoral FAP-CAR T cells in the AE17.OVA model at various time points after adoptive transfer. We found that the number of FAP-CAR T cells peaked at day 3 post-infusion and had diminished by 7 to 10 days by approximately 65% (**Fig. 3-9**). To confirm that this rapid loss of T cells was not due to abnormal function of the human 4-1BB and CD3ζ intracellular signaling domains in the context of mouse T cells, we engineered a fully mouse FAP-CAR construct encoding the mouse CD28 cytoplasmic domain and the mouse CD3ζ chain (73.3m28z) (**Figure 2-4D**). When transduced into mouse T cells, 73.3-hBBz FAP-CAR and 73.3m28z FAP-CAR T cells released comparable levels of IFNγ (**Fig. 3-10A**) and induced comparable levels of cytotoxicity when co-cultured with 3T3.FAP fibroblasts (**Fig. 3-10B**). To further evaluate the importance of the co-stimulatory cytoplasmic domains, we synthesized two additional FAP-CAR constructs that lack these co-stimulatory domains, i.e. 73.3-human CD3ζ and 73.3-mouse CD3ζ. Neither the mouse nor the human CD3ζ construct was sufficient to induce IFNγ production (**Fig. 3-10A**) or cytotoxicity (**Fig. 3-10B**) when co-cultured with 3T3.FAP fibroblasts. Moreover, FAP-CAR T cells employing either human or mouse ICDs were able to traffick into tumors (**Fig. 3-10C**) and induced comparable anti-tumor activity in AE17.OVA tumors (**Fig. 3-10D**). These data demonstrate that mouse CAR T cells injected into syngeneic hosts persisted for only a short time, regardless of the origin of cytoplasmic co-stimulatory domains. Additionally, mouse CAR T cells may undergo activation-induced cell death (ACID) as they are highly activated, a requirement for

retroviral transduction. We observed that FAP-CAR T cells employing either human or mouse ICDs were equally susceptible to activation-induced cell death (**Fig. 3-11**), ruling out the possibility that human ICD-based FAP-CAR T cells were prone to AICD and therefore resulted in tumor resurgence. Therefore, since FAP-CAR mouse T cells only persisted for only a short period of time *in vivo*, we hypothesized that a second infusion of FAP-CAR T cells may enhance therapeutic efficacy. Indeed, administration of a second dose of FAP-CAR T cells prevented the resurgence of tumor in AE17.OVA tumors (**Fig. 3-12**).

Another, not mutually exclusive, explanation for the lack of tumor regression may be related to suboptimal CAR signaling in mouse T cells and/or functional suppression of CAR T cells in the immune-suppressive tumor microenvironment. Recent studies from showed that mesothelin-targeted CAR mouse T cells deficient in the inhibitory enzyme diacylglycerol kinase zeta (DGKζ) exhibited enhanced effector functions *in vitro* and *in vivo,* as well as increased persistence (Riese et al., 2013). Therefore, we generated DGKζ-deficient FAP-CAR T cells and found that these DGKζ-deficient FAP-CAR T cells released more IFNγ (**Fig. 3-13A**) and induced higher cytotoxicity (**Fig. 3-13B**) when co-cultured with 3T3.FAP fibroblasts. DGKζ-deficient FAP-CAR T cells induced more potent anti-tumor activity compared to the WT FAP-CAR T cells (**Fig. 3-13C**). At the endpoint, we also observed more numbers of DGKζ-deficient FAP-CAR T cells in the AE17.OVA tumor cells, indicating DGKζ-deficiency increased the persistence of FAP-CAR T cells (**Fig. 3-13D**).

Conclusions and discussion

The host adaptive immune response possesses great potential to restrain the growth of solid tumors. Nevertheless, immune suppression often occurs to prevent the efficient arrest of tumor growth (Leach et al., 1996). Checkpoint-blockade antibodies antagonizing CTLA-4, PD-1 and PD-L1 have been shown to promote sustained and heightened T-cell activation and achieve favorable clinical outcomes in a subset of cancer patients. Nevertheless, many patients fail to respond to these treatments (Brahmer et al., 2015; Brahmer et al., 2012; Hamid et al., 2013; Hodi et al., 2010; Larkin et al., 2015; Le et al., 2015; Motzer et al., 2015; Royal et al., 2010; Wolchok et al., 2013). Further understanding of the molecular and cellular components that govern tumoral immune suppression will offer new opportunities to invigorate the adaptive immune system to inhibit tumor progression.

Using FAP-CAR T cells, we observed that depletion of FAP^+ stromal cells inhibited tumor growth in multiple syngeneic tumor models. We again confirmed that the FAP-CAR T-cell-induced anti-tumor response was lost in FAP-deficient mice, indicating that the anti-tumor activity is dependent on FAP expression by host stromal cells. Consistent with the reported immune-suppressive functions of FAP^+ stromal cells (Arnold et al., 2014; Feig et al., 2013; Kraman et al., 2010), we found that the impact on growth of immunogenic but moderately-desmoplastic AE17.OVA tumors depended on anti-tumor immunity, as the effect of FAP-CAR T cells was associated with enhanced infiltration of tumor-reactive T cells and the effect was abrogated in immune-deficient mice. In addition, we detected pronounced alterations in the tumor stroma, demonstrating that

FAP^+ stromal cells are required for the formation and/or maintenance of desmoplasia. We expected that the alteration in tumor stroma and angiogenesis induced by FAP-CAR T cells might partially contributed to the anti-tumor activity in AE17/OVA tumors observed in FAP-CAR T cell-treated desmoplastic human tumors and syngeneic pancreatic tumors. Nonetheless, the drastic growth increase in highly-immunogenic, modestly-desmoplastic AE17.OVA tumors in NSG mice may have overwhelmed the potential for FAP-CAR T-cell-induced immune-independent effects.

Moreover, it will be interesting in future studies to determine whether FAP-CAR T cell-induced stromal changes contribute to the enhanced infiltration of endogenous T cells into tumors. We hypothesize that FAP-CAR T-cell-mediated matrix destruction may permit more efficient T cell recruitment and infiltration, and likely enhances anti-tumor immunity to restrict tumor progression. A recent study demonstrating that matrix architecture excludes T cells from migrating and infiltrating into the tumor cell nests supports this idea (Salmon et al., 2012). T cell accumulation was more pronounced in the stroma than in tumor islets of human lung tumors. Matrix degradation by collagenase enhanced mobilization of T cells and increased the accessibility of T cells to cancer cells *ex vivo*. Intriguingly, another study showed that expression of heparanase, which degrades heparan sulfate proteoglycans in the ECM, promoted tumor infiltration and augmented the anti-tumor activity of CAR-redirected T cells (Caruana et al., 2015). Identification of an immunogenic and highly desmoplastic syngeneic tumor model will enable further studies into the relationship between tumor desmoplasia and anti-tumor immunity.

We evaluated the endogenous T cells within the tumors at 3 days and 8 days post CAR-T cell infusion. At the earlier time point, we observed no difference between the total number of T cells and activated $CD8^+$ T cells, but found an increase in the number of TNFα-producing $CD4^+$ T cells, consistent with similar findings using a genetic ablation mouse model (Kraman et al., 2010). Interestingly, at the later time point, we observed an increase in total $CD8^+$ T cells as well as antigen-specific $CD8^+$ T cells in AE17.OVA and TC1 tumors. Moreover, these $CD8^+$ T cells displayed a more activated phenotype, as there were more IFNγ-producing $CD8^+$ T cells and $CD69^+$ T cells. Given the potential immune activation with conditional depleting of FAP^+ stromal cells, we tested the combination of FAP-CAR T cells and an Ad.E7 cancer vaccine. This combination therapy was able to induce synergistic effects to control the growth of established large tumors, while either monotherapy did not induce significant anti-tumor activity. Similarly, a strategy combining tumor and stromal cell-targeted CAR T cells also resulted in an augmented therapeutic efficacy (Kakarla et al., 2013). Moreover, combination of an anti-FAP DNA vaccination with doxorubicin inhibited breast cancer metastasis by reducing proinflammatory cytokine IL-6 and by shifting of the immune microenvironment from a Th2 to Th1 polarization (Liao et al., 2009). These observations demonstrate that conditional depletion of FAP^+ stromal cells can augment anti-tumor immune response and reduce tumor-promoting inflammation, and therefore reduce therapeutic resistance. Further studies are needed to fully understand the mechanisms by which FAP^+ stromal cells modulate inflammatory and immune responses.

We also noted that limited persistence of the FAP-CAR T cells eventually led to tumor resurgence. To determine if the FAP-CAR T-cell-induced anti-tumor effect can be further extended, a second dose of T cells was administered one week after the initial infusion. The repeated dosing also demonstrated increased efficacy. This finding suggests that enhanced persistence of FAP-CAR T cells may augment therapeutic efficacy. Our prior observations indicated that genetic deletion of DGKζ, an enzyme that limits T-cell activation, augmented the cytotoxic potential and persistence of mouse CAR T cells targeted to mesothelin (Riese et al., 2013). Similarly, we now found that FAP-CAR T cells deficient in DGKζ exhibited an enhanced ability to control tumor growth. Collectively, these data demonstrate that optimizing the persistence and potency of FAP-CAR T cells may further increase their therapeutic efficacy.

In summary, we conclude that depletion of FAP^+ stromal cells can enhance the host adaptive immune response in controlling growth of immunogenic tumors, and that depletion of FAP^+ stromal cells can render the tumor vulnerable to other treatments including immunotherapy and/or chemotherapy.

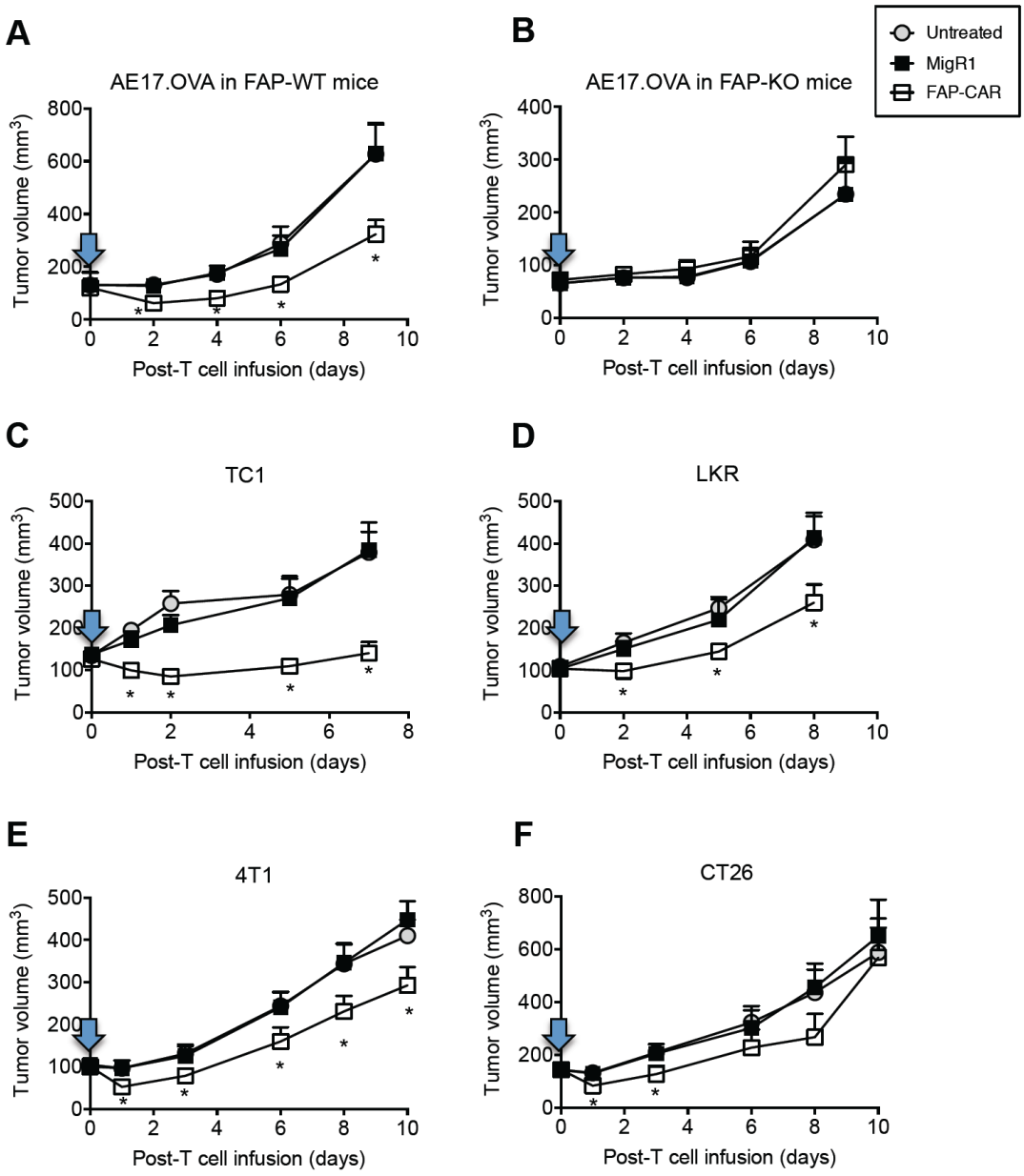

Figure 3-1. FAP-CAR T cells inhibit growth of multiple syngeneic solid tumors in a target-specific fashion. Mice were injected subcutaneously with 2×10^6 AE17.OVA, 1×10^6 TC1, 2×10^6 LKR, 0.5×10^6 4T1, or 1×10^6 CT26 tumor cells into the dorsolateral flank of FAP-WT or FAP-KO syngeneic mice. Mice bearing established tumors derived from AE17.OVA (A), TC1 (C), LKR (D), 4T1 (E) and CT26 (F) were injected intravenously with 1×10^7 FAP-CAR or MigR1 T cells. (B) AE17.OVA-bearing FAP-KO mice were given 1×10^7 FAP-CAR or MigR1 T cells. The blue arrows indicate the time of adoptive T-cell transfer. Results are shown as mean ± SEM (n=4~5 per group); *denotes statistical significance between untreated, MigR1 and FAP-CAR-treated specimens, $p<0.05$.

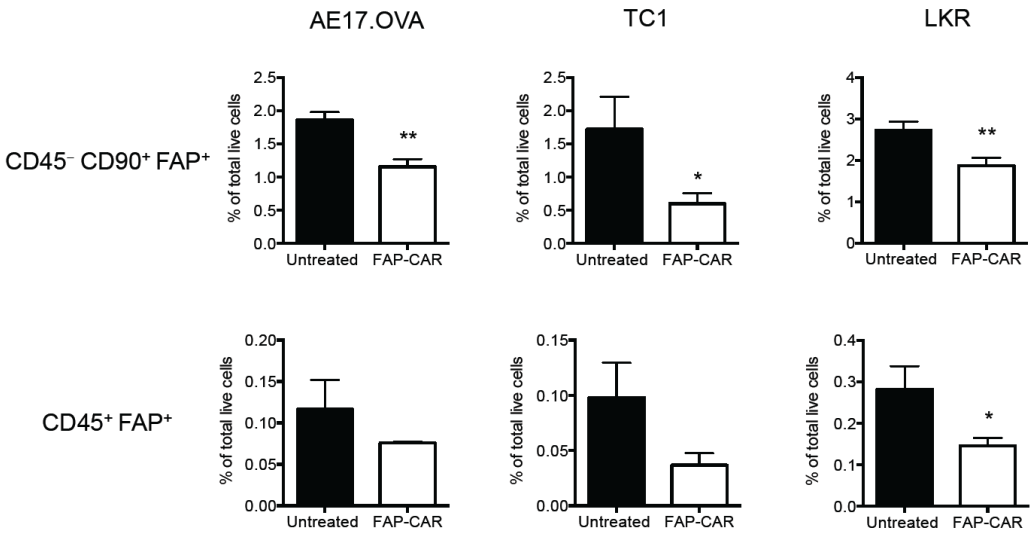

Figure 3-2. Adoptive transfer of FAP-CAR T cells depletes intratumoral FAP$^+$ stromal cells in multiple syngeneic solid tumor models. C57BL/6 mice bearing established AE17.OVA tumors, TC1 tumors or LKR tumors were intravenously injected with 1×10^7 FAP-CAR T cells or left untreated. Tumors were harvested 7-9 days post-adoptive T-cell transfer to assess depletion of FAP$^+$ stromal cells. Results are shown as mean ± SEM (n=3~5 per group), *p<0.05; **p<0.01.

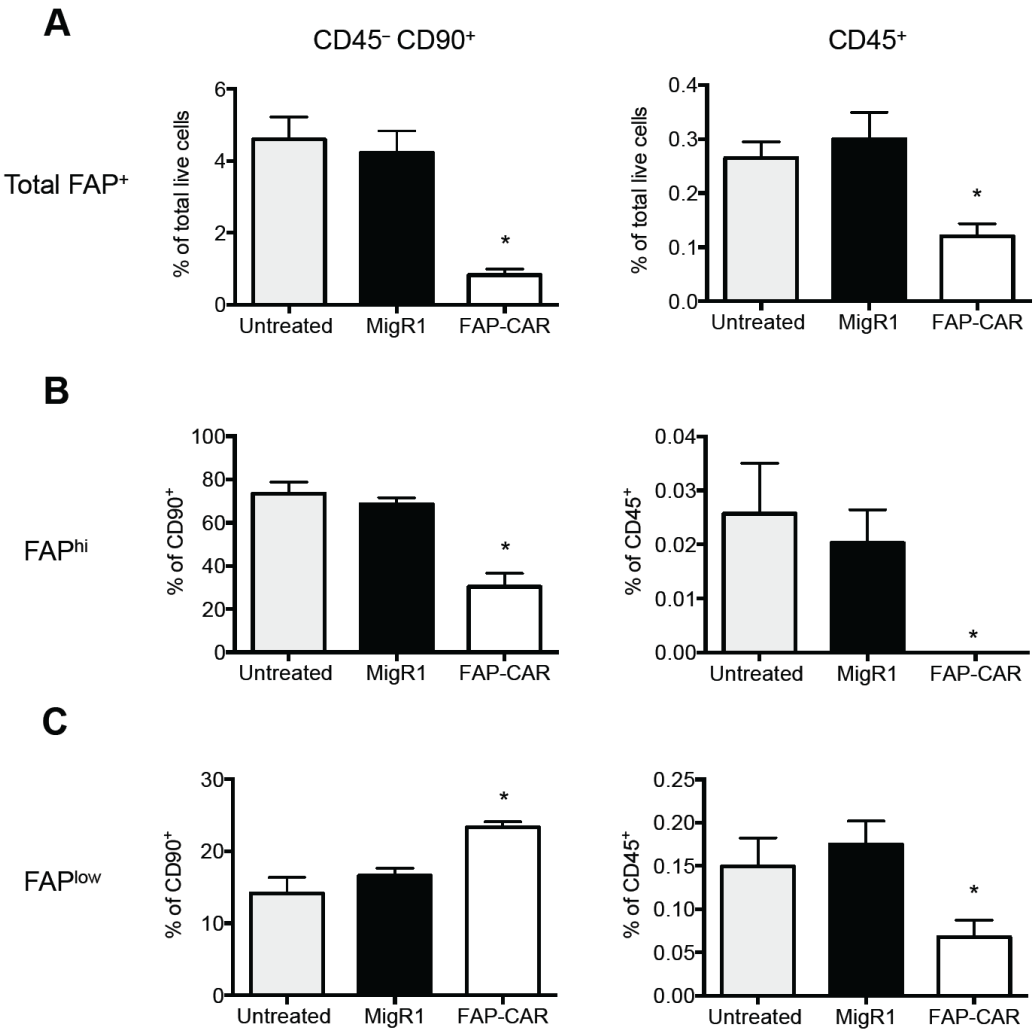

Figure 3-3. Preferential acute depletion of intratumoral FAP^{hi} stromal cells by FAP-CAR T cells in syngeneic AE17.OVA tumors. Established AE17.OVA tumor-bearing mice were intravenously injected with 1×10^7 FAP-CAR or MigR1 T cells. At 3 days post-adoptive T-cell transfer, tumors were harvested and dissociated with a collagenase cocktail to obtain single-cell suspensions. Flow cytometry was performed to evaluate depletion of (A) total FAP$^+$ stromal cells, (B) FAP^{hi} cells and (C) FAP^{lo} cells by FAP-CAR T cells. Results are shown as mean ± SEM (n=5 per group); *indicates statistical significance between untreated, MigR1 and FAP-CAR-treated samples, $p<0.05$.

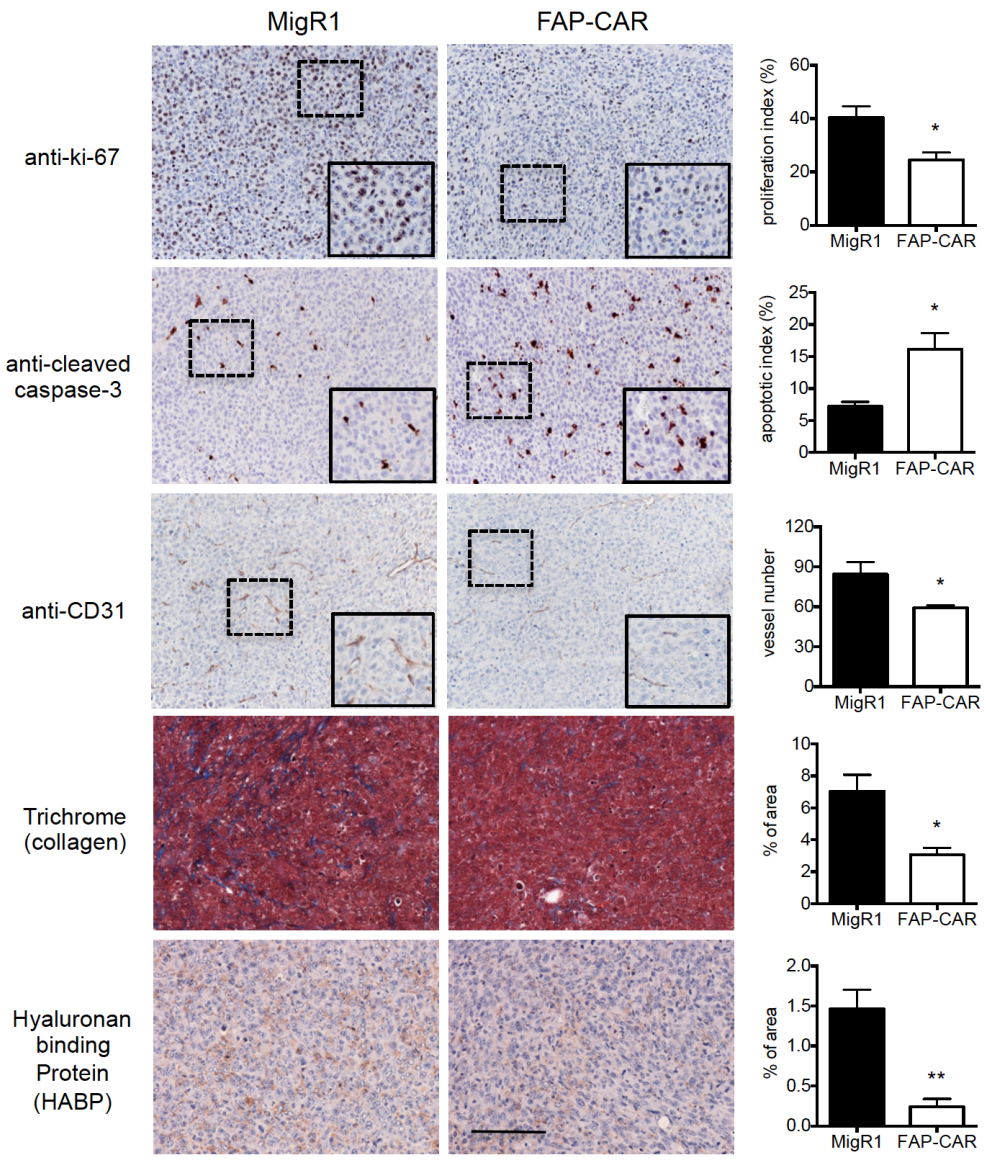

Figure 3-4. FAP-CAR T cells inhibit growth of moderately desmoplastic AE17.OVA tumors by inhibiting proliferation, increasing apoptosis and altering tumor stroma. Syngeneic C57BL/6 mice bearing AE17.OVA tumors were injected intravenously with 1×10^7 FAP-CAR or MigR1 T cells. Tumor tissues were harvested and sections were stained with antibodies against Ki-67, cleaved-caspase3 and CD31. Trichome and HABP stains were performed to reveal the tumor stroma. Computer-based quantification was performed using Fiji software. The proliferation index was calculated by the ratio of Ki-67^+ cells to hematoxylin$^+$ cells. The apoptotic index was calculated by the ratio of CC-3^+ cells to hematoxylin$^+$ cells. CD31 was quantified by the number of immunoreactive vessels. Trichrome and HA were determined by blue or brown colors normalized to the total area; n=3 per group, *$p<0.05$, **$p<0.01$. Scale: 100 μm.

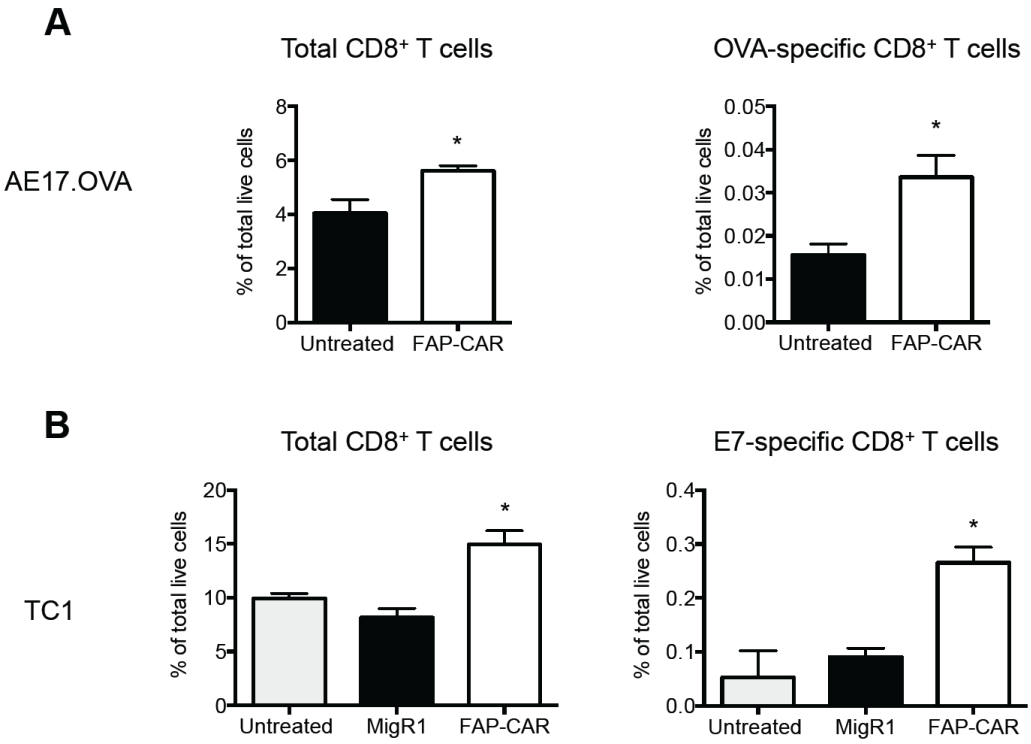

Figure 3-5. FAP-CAR T-cell-induced anti-tumor activity in AE17.OVA and TC1 tumors is associated with enhanced CD8 T-cell response. C57BL/6 mice bearing (A) AE17.OVA or (B) TC1 tumors were intravenously injected with 1×10^7 FAP-CAR or MigR1 T cells or left untreated. Tumors were harvested 8 days after T-cell infusion and digested with a collagenase cocktail to prepare single-cell suspensions. Cells were stained with anti-CD8 antibody and fluorochrome-conjugated tetramer loaded with HPV E7 or OVA peptide. Flow cytometry was performed to determine the total intratumoral CD8 and antigen-specific T cells. Results are shown as mean ± SEM (n=5 per group); *$p<0.05$.

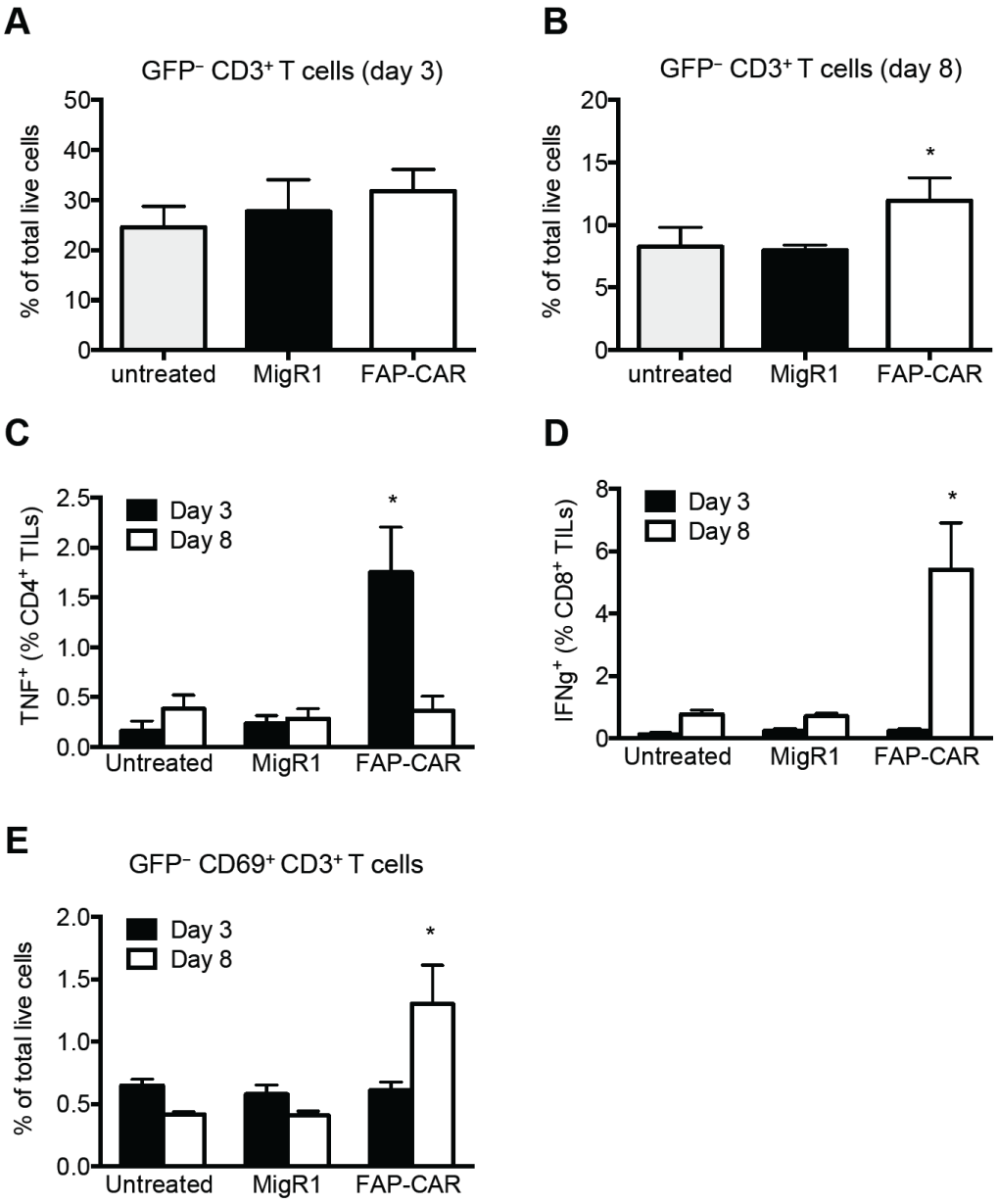

Figure 3-6. Depletion of intratumoral FAP$^+$ stromal cells recruits and/or activates endogenous T cells expressing TNFα or IFNγ at distinct kinetics in AE17.OVA tumors. Established AE17.OVA tumor-bearing mice were intravenously injected with 1×10^7 FAP-CAR or MigR1 T cells. Tumors were digested to evaluate the number of total host CD3$^+$ T cells 3 days (A) and 8 days (B) post-adoptive T-cell transfer. Endogenous CD4$^+$ T cell expressing TNFα (C), CD8$^+$ T cell expressing IFNγ (D) CD3$^+$ T cell expressing CD69 (E) were analyzed at 3 and 8 days after adoptive T-cell transfer. Results are shown as mean ± SEM (n=5 per group); *denotes statistical significance between untreated, MigR1 and FAP-CAR-treated groups, $p<0.05$.

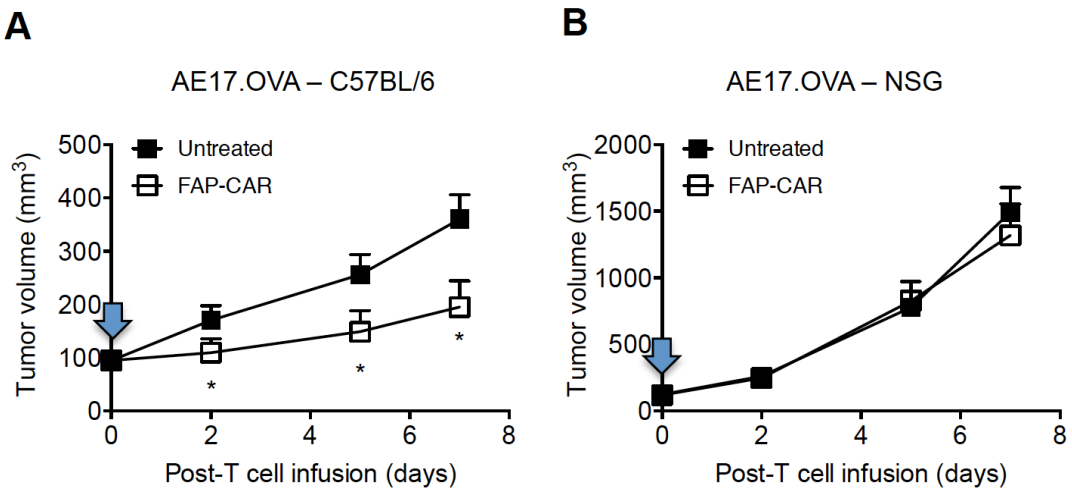

Figure 3-7. Adaptive immunity is critical for FAP-CAR T-cell-induced anti-tumor response to AE17.OVA tumors. Established AE17.OVA tumor-bearing C57BL/6 mice (A) and NSG mice (B) were intravenously injected with 1×10^7 FAP-CAR or left untreated. Tumor growth was followed. Blue arrows indicate the time of adoptive T-cell transfer. Results are shown as mean ± SEM (n=5 per group), *$p<0.05$.

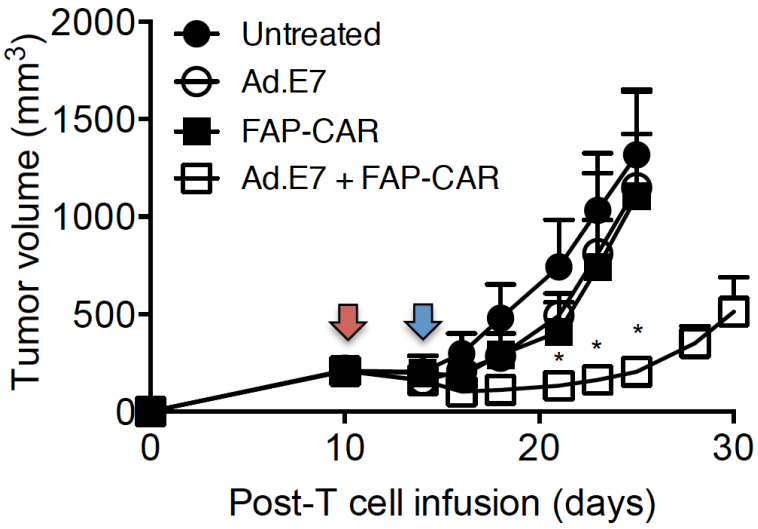

Figure 3-8. FAP-CAR T cells enhance the efficacy of tumor antigen vaccination in the TC1 tumor model. TC1 tumor cells were injected into the right flanks of C57BL/6 mice. When tumors reached 200 mm^3 in volume, 10^9 pfu adenovirus-encoding HPV E7 (Ad.E7) was injected subcutaneously to the contralateral side of the flank tumors (red arrow). 1×10^7 FAP-CAR T cells were intravenously injected 4 days later (blue arrow). Results are shown as mean ± SEM (n=5 per group); *indicates a significant difference between the combined treatment group and untreated or single-regimen treated groups, $p<0.05$.

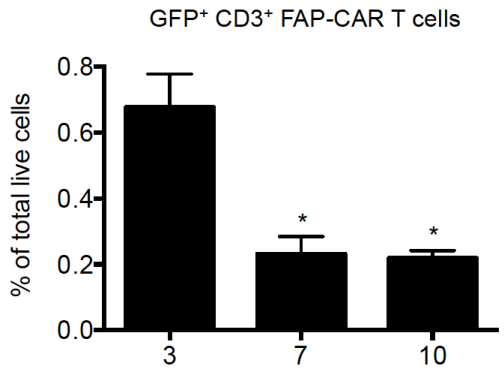

Figure 3-9. Murine FAP-CAR T cells do not persist *in vivo*. Established AE17.OVA tumor-bearing C57BL/6 mice were intravenously injected with 1×10^7 FAP-CAR T cells. Tumors were harvested at 3, 7 and 10 days post-T cell transfer to determine the frequency of GFP^+ $CD3^+$ FAP-CAR T cells. Results are shown as mean ± SEM (n=5 per group), *$p<0.05$.

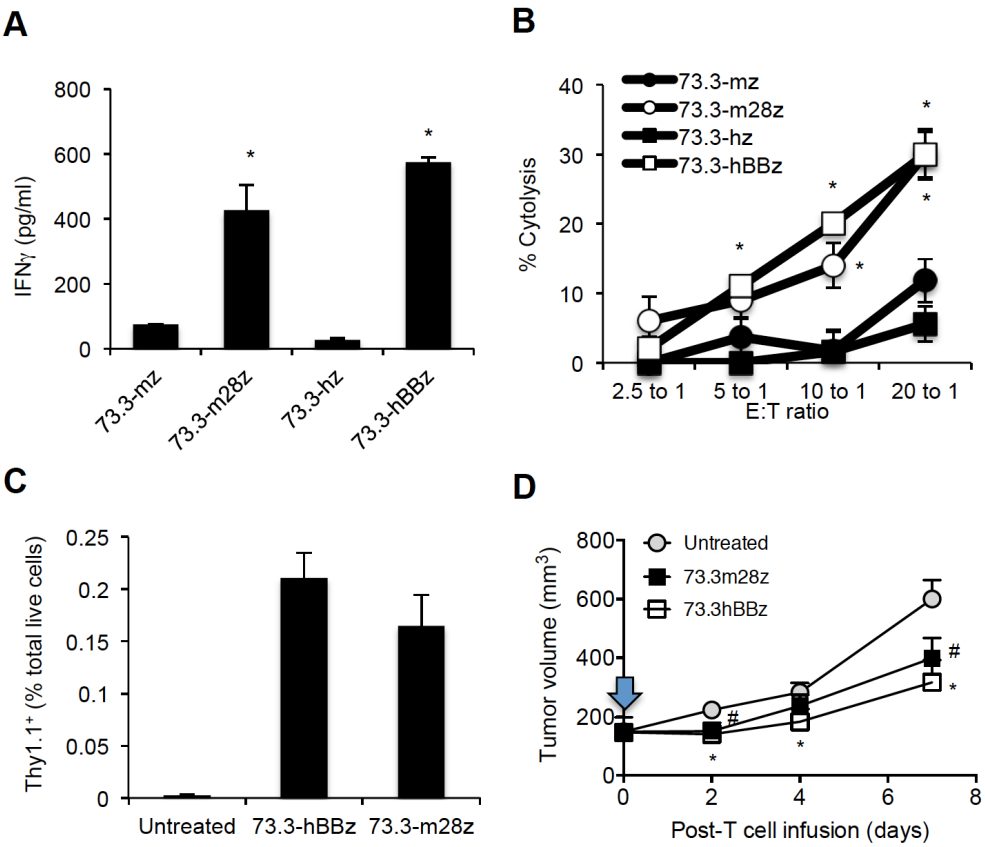

Figure 3-10. Murine FAP-CAR T cells employing either human 4-1BB (hBBz) or mouse CD28 (m28z) exhibit comparable effector functions, trafficking and anti-tumor activity in AE17.OVA tumors. Mouse FAP-CAR T cells encoding different intracellular signaling domains including the mouse CD3ζ chain (73.3-mz), the mouse CD3ζ along with mouse CD28 domains (73.3-m28z), the human CD3ζ chain (73.3-hz), and the human CD3ζ along with human 41BB domains (73.3-hBBz) were used to react with 3T3 or 3T3.FAP to (A) determine their ability to secrete IFNγ at an effector-to-target ratio of 10:1 and (B) determine their cytolytic activity at various effector-to-target ratios, 18 hours after co-culture. Results are shown as mean ± SEM (n=3 per group); *indicates statistical significance between the first generation (CD3ζ constructs) and second generation (CD28ζ and 4-1BBζ constructs), $p<0.05$. (C) To determine if different costimulatory domains may govern trafficking and persistence in vivo, Thy1.1^{+} C57BL/6 mouse T cells were transduced with FAP-CAR constructs encoding CD28ζ or 4-1BBζ and injected into Thy1.2 C57BL/6 mice bearing established AE17.OVA tumors. Tumors were harvested 3 days after adoptive T-cell transfer to evaluate the presence of FAP-CAR T cells by flow cytometry using fluorochrome-conjugated anti-Thy1.1 and anti-CD3 antibodies. (D) Established AE17.OVA tumor-bearing mice were intravenously injected with 1×10^{7} FAP-CAR T cells encoding CD28ζ or d 4-1BBζ domains. Tumor growth was followed. Blue arrows indicate the time of adoptive T-cell transfer. Results are shown as mean ± SEM (n=5 per group); * and # represent statistical significance between untreated and FAP-CAR-treated samples, $p<0.05$.

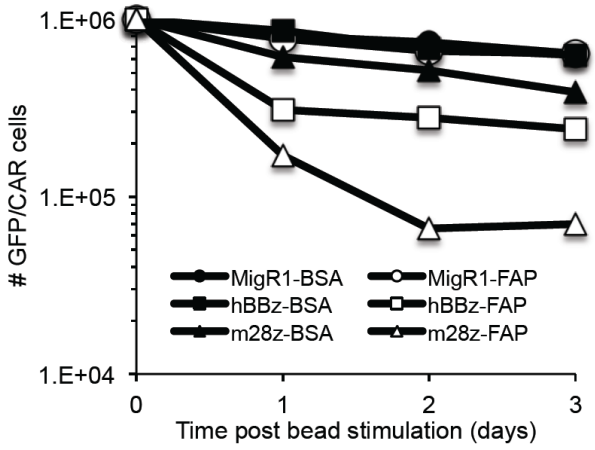

Figure 3-11. Murine FAP-CAR T cells undergo activation-induced cell death. Mouse MigR1 or FAP-CAR T cells encoding different signaling intracellular signaling domains including the mouse CD3ζ along with mouse CD28 domains (m28z), and the human CD3ζ along with human 4-1BB domains (hBBz), were exposed to either BSA- or FAP-ECD-coated beads. Live cells were determined by trypan blue exclusion.

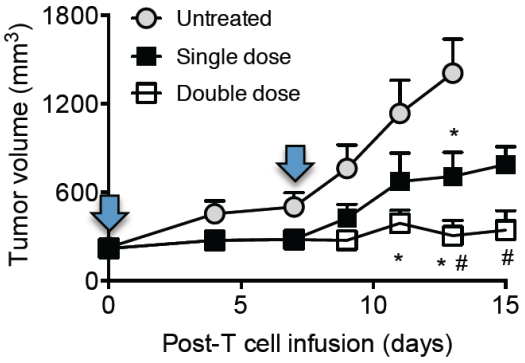

Figure 3-12. Enhancement of FAP-CAR T-cell-mediated anti-tumor activity by repeated dosing. Established AE17.OVA tumor-bearing mice were intravenously injected with 1×10^7 FAP-CAR T cells. Anti-tumor efficacy was further enhanced by a second dose of FAP-CAR T-cell infusion given a week after the initial dose. Tumor growth was monitored by electronic caliper. Blue arrows indicate the time of adoptive T-cell transfer. Results are shown as mean ± SEM (n=5 per group); *indicates statistical significance between untreated and FAP-CAR-treated samples, $p<0.05$; $^{\#}$denotes statistical significance between the single-dose FAP-CAR treated group versus the double-dose group.

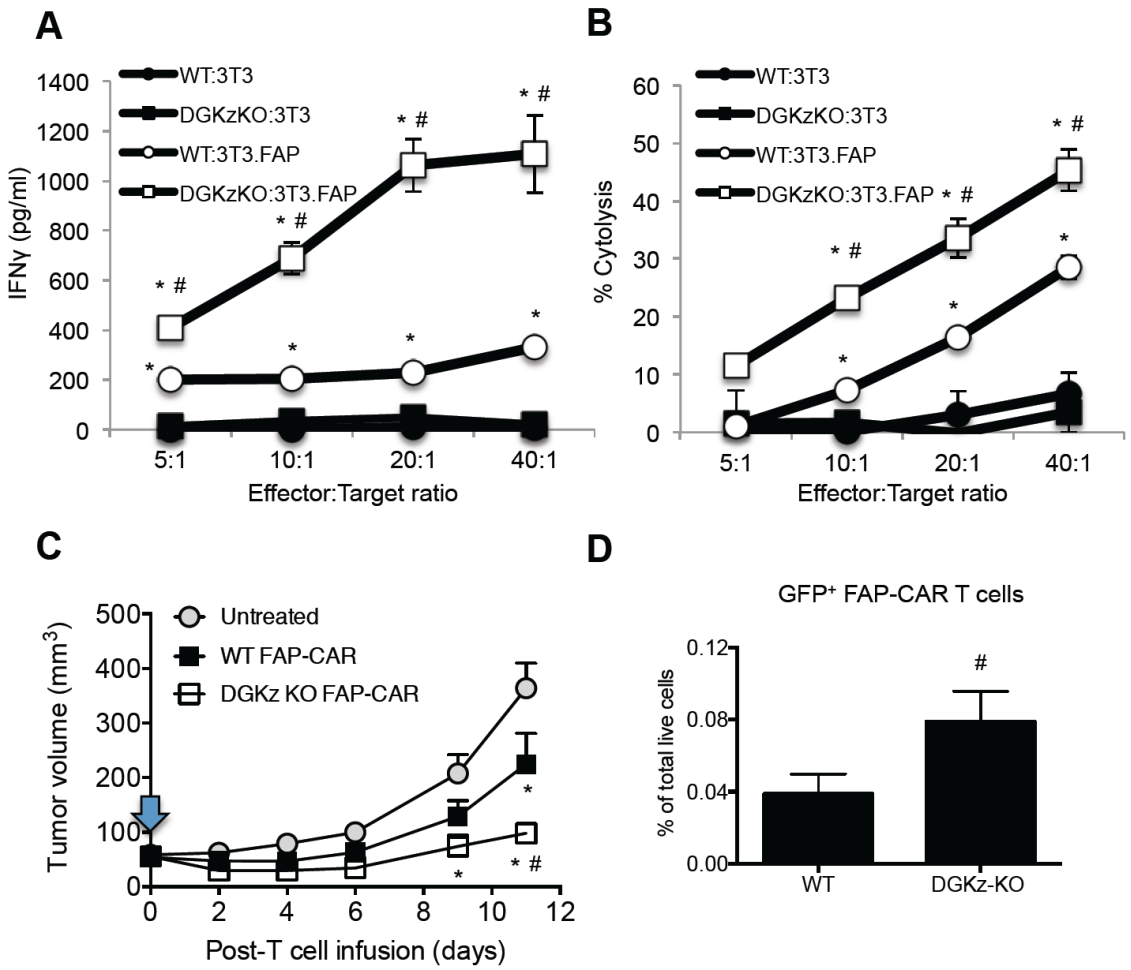

Figure 3-13. Enhancement of FAP-CAR T-cell-mediated anti-tumor activity through increased effector functions and persistence. Wild-type FAP-CAR T cells (WT) and DGKζ knockout FAP-CAR T cells (DGKzKO) were used to react with 3T3 or 3T3.FAP to (A) determine their ability to secrete IFNγ and (B) determine their cytolytic activity at various effector-to-target ratios, 18 hours after co-culture. Results are shown as mean ± SEM (n=3 per group); *indicates statistical significance between non-reactive (FAP-CAR T cells co-cultured with 3T3) and reactive samples (FAP-CAR T cells co-cultured with 3T3.FAP), $p<0.05$. #indicates statistical significance between WT and DGKζ KO FAP-CAR-treated samples, $p<0.05$. (C) Established AE17.OVA tumor-bearing mice were intravenously injected with 1×10^7 WT or DGKζ-KO FAP-CAR T cells. Tumor growth was monitored by electronic caliper. Blue arrows indicate the time of adoptive T-cell transfer. (D) Tumors were harvested 11 days post-T cell transfer. Intratumoral GFP^+ FAP-CAR T cells were determined using flow cytometry. Results are shown as mean ± SEM (n=5 per group). *indicates statistical significance between untreated and FAP-CAR-treated samples, $p<0.05$; #denotes statistical significance between the WT FAP-CAR T cell-treated samples versus the DGKζ-KO FAP-CAR T-cell-treated samples, $p<0.05$.

CHAPTER 4 – Therapeutic window exists for adoptive T-cell therapy against fibroblast activation protein-expressing stromal cells

Introduction

One of the major determinants of tumor-targeted therapy, including cancer immunotherapy using CAR T-cell technology, is identifying a target antigen that is differentially expressed in the tumor versus normal tissues. Targeting antigens that are overexpressed in the tumor milieu with minimal or no expression in essential normal tissues would help minimize toxicity. FAP expression has been detected in the somite of the mouse embryo (Niedermeyer et al., 2001), in the placenta and uterus (Dolznig et al., 2005) and in mesenchymal stem cells from multiple origins (Bae et al., 2008; Jeong et al., 2005; Jeong et al., 2007). Therefore, it is important to understand the normal physiological functions of FAP^+ stromal cells and study the potential impact and potential adverse effects of their depletion in normal tissues.

FAP-expressing cells in normal tissues and their homeostatic functions

In the past, studies of the distribution of FAP^+ stromal cells in tumors or normal tissues were largely relied on immunohistochemistry or immunofluorescence analyses, capturing areas of interest at a tissue-section level. To better understand FAP expression at an organism level, we and others have developed FAP-reporter mice, enabling noninvasive bioluminescent imaging of FAP^+ stromal cells in normal tissues (Jacob et al., 2012;

Roberts et al., 2013). FAP^+ stromal cells were found to reside in many tissues of the adult mouse, including skin, bone marrow, skeletal muscle, pancreas, adipose and lymph nodes. Genetic ablation (Roberts et al., 2013) or immune-targeting studies by using FAP-CAR, based on the FAP5 anti-FAP antibody (Tran et al., 2013), showed that depletion of FAP^+ stromal cells induced bone marrow hypoplasia, cachexia and anemia. FAP^+ stromal cells from skeletal muscle were found to be the major cell population to produce follistatin, a protein that can promote muscle growth. Moreover, FAP^+ stromal cells in the bone marrow were shown to produce SDF-1α and KitL, which are essential in regulating B-lymphopoiesis and erythropoiesis (Roberts et al., 2013). Further studies revealed that fibroblastic reticular cells in lymph nodes also expressed FAP, and experimental ablation of these cells in mice disrupted lymph node homeostasis and impaired launching an effective immune response to clear influenza virus infection (Denton et al., 2014). These studies demonstrate that FAP^+ stromal cells are important in the maintenance of normal muscle mass, lymph node homeostasis and hematopoiesis.

Conditional depletion of FAP-expressing cells can achieve tumor inhibition without inducing severe toxicities

As described in the literature, targeting FAP^+ stromal cells via several approaches, including vaccine, immunoconjugate and enzyme-activating prodrug therapies (Brennen et al., 2012; Lee et al., 2005; Loeffler et al., 2006; Ostermann et al., 2008), as well as two independent CAR T-cell therapies (Kakarla et al., 2013; Schuberth et al., 2013), resulted in therapeutic efficacy without inciting severe toxicities such as bone marrow destruction, muscle wasting or anemia, and did not induce a significant impact on the wound healing

response. In contrast, genetic ablation (Roberts et al., 2013) or FAP5-CAR T-cell therapy, which induced little anti-tumor effects (Tran et al., 2013), were shown to trigger bone marrow hypoplasia and cachexia in mice. These variations in toxicity raise serious concerns as to whether FAP^+ stromal cells are indeed good cancer targets; perhaps alternative strategies should be taken, such as targeting the molecular mediators secreted by FAP^+ stromal cells (Arnold et al., 2014; Feig et al., 2013), or targeting the protease activity of FAP itself (Santos et al., 2009) as will be discussed in later chapters.

In this chapter, I address the potential toxicity versus safety of 73.3 FAP-CAR T cells as an approach to deplete FAP^+ stromal cells in the mouse tumor models described earlier in chapters 2 and 3, as well as in the mouse models of wound healing and atherosclerosis. We also conducted experiments to understand differences in the efficacy and toxicity profiles of 73.3 FAP-CAR T cells versus FAP5-CAR T cells.

Materials and methods

Animals

C57BL/6, BALB/c and C57BL/6:129pf/j F1 hybrid mice were used for the experiments as described in chapter 2 and 3. Apolipoprotein E-deficient C57BL/6 mice were purchased from Charles River Laboratories Inc. (Wilmington, MA). Experimental protocols were approved by the Institutional Animal Care and Use Committee and were in compliance with guidelines for the care and use of animals.

Body weight monitoring

The body weights of mice treated with FAP-CAR T cells or control T cells were monitored by electronic scale.

Amylase assay

Blood from mice treated with FAP-CAR T cells or control T cells was obtained by cardiac puncture. Serum amylase levels were measured in the clinical laboratory of the Ryan Veterinary Hospital of the University of Pennsylvania.

Hematocrit assay

Blood from mice treated with FAP-CAR T cells or control T cells was obtained by cardiac puncture. Hematocrit levels were measured in the clinical laboratory of the Ryan Veterinary Hospital of the University of Pennsylvania.

Generation of full-thickness excisional wounds

C57BL/6 mice were anesthetized with intraperitoneal administration of 70 mg/kg ketamine and 7 mg/kg xylazine. Hair was removed from the skin using Nair. Exposed skin was sterilized with betadine and cleaned with 70% ethanol before creating excisional wounds with a 4 mm disposable biopsy punch.

Intravenous transfer of FAP-CAR T cells in wounded mice or apoE-deficient mice

Wounded mice were randomly assigned to two groups and treated with 1×10^7 FAP-CAR T cells or MigR1 T cells at 2 hours and 3 days post-wounding. Wound closure was followed using the IVIS Imaging 200 system. Mice were monitored daily for signs of distress caused by toxicity of the T cells. At day 8, wounded tissue and visceral organs were collected for further analysis. In another experiment, 24-week-old female apoE-KO mice were randomly grouped to receive 1×10^7 FAP-CAR T cells or MigR1 T cells. The second dose was administered one week after the first dose. The aorta was harvested 3 days after the second dose of T cells.

Oil red staining for evaluating total atherosclerotic lesion burden in the aorta

Each aorta was fileted with the aid of a dissecting microscope to allow better penetration of the Oil Red O dye into lesions. Aortas were equilibrated in 60% isopropanol for 5 minutes at room temperature. Each specimen was then immersed in 0.3% Oil Red O staining solution (Sigma) for 10 minutes at room temperature. Following this, samples were briefly washed with 60% isopropanol and distilled water. The lumenal side of the aorta was positioned on a sheet of dental wax and then imaged using a tripod-mounted

SLR camera (Canon). The total lesion area was calculated as a percentage of total lumenal surface area using Fiji computer-based quantification software.

H&E staining for evaluating atherosclerotic lesion burden in the aortic root

Quantification of the atherosclerotic lesion burden in the aortic root was performed as previously described (Cuff et al., 2001), with some minor modifications. Briefly, 10 μm serial sections of each frozen OCT-embedded aortic root were collected across 16 Superfrost Plus slides (Thermo Fisher Scientific) with 3 sections per slide, totaling approximately 450-500 μm. Six sections (equally spaced throughout the entire aortic root) were stained with hematoxylin and eosin, and imaged at 10X magnification using an Olympus BX51 upright microscope with a SPOT RT2540 camera. Computer-based quantification was performed to quantify lesion areas across the six representative sections to determine the average atherosclerotic burden across the entire aortic root.

Statistical Analyses

Statistics were calculated using GraphPad Prism 6. For studies comparing two groups, Student's *t*-test was used. For studies comparing more than two groups, one-way ANOVA with post-hoc Tukey testing was used. Data are represented as mean ± SEM. Differences were considered significant when $p < 0.05$.

Results

Conditional depletion of FAP$^+$ stromal cells by FAP-CAR T cell therapy provides anti-tumor efficacy without causing severe toxicity in multiple solid tumor models

Recent studies have raised concerns that depletion of normal FAP$^+$ stromal cells by either genetic ablation or FAP-CAR T cells might induce severe toxicities including weight loss, bone marrow destruction and anemia (Roberts et al., 2013; Tran et al., 2013). Therefore, we carefully assessed off-tumor/on-target adverse side effects following FAP-CAR T-cell infusion. In contrast to those studies, we observed no toxicity or anemia in any CD3ζ-based 73.3 FAP-CAR T-cell therapy in multiple solid tumor models. The body weights of tumor-bearing mice remained constant or increased throughout each experiment (**Fig. 4-1**). We further evaluated toxicities in visceral organs post FAP-CAR T-cell therapy. The heart, lungs, pancreas, liver, spleen, kidneys, skeletal muscle, and bone marrow were harvested, sectioned, stained and analyzed in a blinded fashion by a board-certified pathologist. We did not observe any significant abnormality in mice that received CD3ζ-based FAP-CAR T cells. Specifically, we did not observe bone marrow hypoplasia (**Fig. 4-2A**), skeletal muscle wasting or an increased incidence of lung metastasis, consistent with the findings of other groups (Lee et al., 2005; Loeffler et al., 2006; Ostermann et al., 2008), and the studies that employed two independently-generated FAP-CAR constructs (Kakarla et al., 2013; Schuberth et al., 2013). Interestingly, we found that treatment with hyperactive DGKζ-deficient FAP-CAR T cells in AE17.OVA tumor-bearing mice, which induced more potent anti-tumor activity as described in chapter 3 (**Fig. 3-12B**), resulted in limited focal perivascular and peri-islet lymphocytic infiltration in the pancreas (**Fig. 4-2B**). These changes were not seen in the

tumor-bearing mice treated with wild-type FAP-CAR T cells. No other abnormalities were found.

In order to reconcile the differences in the efficacy and toxicity profiles between our 73.3 FAP-CAR construct and the FAP5-CAR construct (Tran et al., 2013), we compared the antibodies used as the foundation for the scFv to generate the respective CAR constructs. The 73.3 antibody and FAP5 antibody proved to have similar affinities for mouse FAP. The affinity of the FAP5 antibody has been reported to be 0.6 nmol/L. Biacore analysis reveals that the affinity of the 73.3 antibody is less than 1 nmol/L (0.1-0.3 nmol/L), which is modestly less than that reported for FAP5 and therefore we think unlikely to explain the dramatic difference in their efficacy and toxicity profiles.

As a potential alternative, we investigated the relationship between the epitope specificity of two monoclonal antibodies against FAP. We found that 73.3 specifically reacted with mouse FAP while FAP5 bound to an epitope shared by both mouse and human FAP, indicating they are reactive with distinct epitopes (**Fig. 4-3**). Interestingly, the position of the targeted epitope of a scFv has previously been shown to determine the efficacy of activation of CAR T cells (Hombach et al., 2007). We therefore hypothesized that this distinct epitope specificity may allow our FAP-CAR T cells to efficiently eliminate the intratumoral FAP-high expressers (**Fig. 3-3**) while sparing FAP-low expressers that are more prevalent in normal tissues. Specifically, flow cytometry analysis indicated that tumor-associated stromal cells exhibited higher FAP expression than pancreatic stromal cells (**Fig. 4-4**). Based on these observations, we concluded that the limited persistence of

73.3 FAP-CAR T cells *in vivo* (**Fig. 3-9**) and the preferential depletion of FAP^+ stromal cells (**Fig. 3-3**) provide for a therapeutic window with limited toxicity for specific FAP-CAR constructs.

FAP-CAR T-cell therapy does not impact wound healing response nor exacerbates atherosclerotic lesion development and architecture in apoE-deficient mice

Since stromal fibroblasts play critical roles in tissue regeneration and FAP^+ stromal cells have been demonstrated to present in injury sites and atherosclerotic lesions (Brokopp et al., 2011; Garin-Chesa et al., 1990; Scanlan et al., 1994), it is imperative to study the potential impacts of FAP-CAR T-cell therapy on these processes as this could limit the use of FAP-CAR in cancer patients. We tested whether FAP-CAR T-cell therapy may alter the wound-healing response or progression of atherosclerosis. Wounded mice were treated with two doses of FAP-CAR T cells at 2 hours and 3 days post-wounding (**Fig. 4-5A**). We monitored the wound healing and body weight over an 8-day period. We found that FAP-CAR T-cell therapy did not alter wound closure (**Fig. 4-5B**) or cause changes in body weight (**Fig. 4-5C**) or circulating amylase levels (**Fig. 4-5D**). We employed apoE-deficient mice, which spontaneously develop atherosclerotic lesions at 4-6 months of age, to test whether FAP-CAR T cells would cause any adverse effect on the development or progression of atherosclerotic lesions. 24-week-old female apoE-deficient mice were treated with two weekly doses of FAP-CAR T cells or MigR1 T cells (**Fig. 4-6A**). We found that FAP-CAR T-cell therapy did not exacerbate atherosclerotic lesion development and morphology (**Fig. 4-6B**) or cause changes in body weight (**Fig. 4-6C**), circulating amylase levels (**Fig. 4-6D**) or hematocrit levels (**Fig. 4-6E**). These data

support a regimen that offers anti-tumor activity, as seen in several solid tumor models, that does not impact atherosclerosis or the wound-healing response, which is consistent with other studies (Kakarla et al., 2013; Loeffler et al., 2006).

Complete depletion of FAP$^+$ stromal cells using enhanced FAP-CAR T-cell therapy offers potent anti-tumor activity but is associated with increased toxicities

In an attempt to enhance the efficacy of FAP-CAR T-cell therapy using a killer immunoglobulin-like receptor (KIR)-based CAR system described in **Fig. 2-7B**, we found that the growth of highly desmoplastic EM-meso tumors was completely abrogated. However, this response was associated with bone marrow hypocellularity (**Fig. 4-7B**), weight loss (**Fig. 4-7C**), reduced circulating amylase (**Fig. 4-7D**) and anemia (**Fig. 4-7E**). These observations are consistent with the toxicities reported in a genetic model of complete FAP ablation and the FAP5 CAR T-cell study (Roberts et al., 2013; Tran et al., 2013). In fact, we found that the KIR-based FAP-CAR T-cell system achieved complete depletion of intratumoral FAP$^+$ stromal cells for up to 26 days following T-cell transfer (**Fig. 4-7A**), which was much protracted and more potent than what we have observed using any CD3ζ-based FAP-CAR T-cell therapy.

Conclusions and discussion

Given the potential on-target/off-tumor toxicity in normal tissues, we carefully examined the tumor-bearing mice that received FAP-CAR T-cell therapy. Using a regimen of one dose or two doses of 1×10^7 WT FAP-CAR T cells, we observed conditional depletion of intratumoral FAP^+ stromal cells and anti-tumor effects in multiple solid tumor models in both immune-competent and immune-deficient mice without associated bone marrow destruction or changes in total body weight. These results are consistent with prior findings that targeting FAP^+ stromal cells could induce anti-tumor activity without toxicity in either immune-competent or immune-deficient mice (Kakarla et al., 2013; Lee et al., 2005; Loeffler et al., 2006; Ostermann et al., 2008; Schuberth et al., 2013). In contrast, another study that used FAP5-CAR T cells demonstrated negligible anti-tumor effects but severe toxicities (Tran et al., 2013).

We hypothesize that the differences in efficacy can be attributed to the following. Firstly, FAP5-CAR T-cell-induced host anti-tumor immune responses may have been lost as the result of the lymphodepletion protocol by systemic radiation used by Tran et al (Tran et al., 2013) that was not part of our regimen. Moreover, the differences in efficacy of the FAP-CAR T cells may be due to the differences in epitope specificity of the anti-FAP antibodies used to generate the scFv regions of the CARs in different studies. Recent studies revealed that the target epitopes of CARs might dictate their efficacy (Hombach et al., 2007), supporting this hypothesis, and we found that 73.3 and FAP5 reacted with different epitopes of murine FAP. It will therefore be critical to define the epitope

specificity of anti-FAP antibodies to understand how they contribute to the different efficacies and associated toxicities observed among the various FAP-CARs.

Additionally, we attribute the lack of toxicity to the ability of 73.3 FAP-CAR T cells to only transiently deplete FAP^+ stromal cells, and/or the fact that 73.3 FAP-CAR T cells preferentially depleting cells that express high levels of FAP (such as intratumoral stromal cells) but not cells expressing low levels of FAP (for example, basal levels of FAP in normal cells). Recent studies demonstrating the antigen-dependent threshold of CAR redirected T cells support this hypothesis. ErbB2-specific CAR T cells were shown to release IFNγ and induced target-cell toxicity when co-cultured with $ErbB2^{hi}$ tumor cells, while co-culturing ErbB2-specific CAR T cells with $ErbB2^{lo}$ tumor cells did not induce IFNγ secretion nor cytolytic activity (Chmielewski et al., 2011). Interestingly, we found that intratumoral stromal cells in our multiple tumor models expressed higher levels of FAP compared to normal pancreatic stromal cells. Therefore, the differential surface-antigen density between intratumoral FAP^+ stromal cells and normal FAP^+ stromal cells may determine the activation and effector functions of FAP-CAR T cells, thereby allowing FAP-CAR T cells to specifically eliminate intratumoral FAP^+ stromal cells, while protecting normal FAP^+ stromal cells, which express physiological levels of FAP antigen, from T-cell attack.

Furthermore, we demonstrated that the same FAP-CAR T-cell regimen did not impact wound closure, exacerbate atherosclerosis or induce systemic toxicities including bone marrow destruction, muscle wasting or anemia. Nevertheless, when we attempted to

increase the potency and persistence of the T cells, for example with DGKζ-deficient FAP-CAR T cells, we began to observe some histological abnormalities in the pancreas. Furthermore, when we utilized killer immunoglobulin-like receptor-based FAP-CAR, also known as FAP-KIR (Wang et al., 2015), growth of highly-desmoplastic mesothelioma was abolished likely due to complete depletion of intratumoral FAP^+ stromal cells. However, this complete response was associated with systemic toxicities including bone marrow hypoplasia, anemia, decreased circulating amylase and loss of body weight.

Based on these results, we propose that there may be an optimal therapeutic window i.e. maximum efficacy in the face of minimum/tolerable toxicity of intratumoral FAP^+ stromal cell depletion using appropriate CAR constructs. Results from other research groups (Lee et al., 2005; Loeffler et al., 2006; Ostermann et al., 2008), including two independently-generated FAP-CAR constructs (Kakarla et al., 2013; Schuberth et al., 2013), also support this concept. In addition, we showed that conditional depletion of FAP^+ stromal cells could augment the efficacy of immune- and chemotherapy. Lastly, many novel approaches have been developed to regulate the duration, location and timing of CAR activity, which can limit the potential on-target/off-tumor toxicity (Desnoyers et al., 2013; Fedorov et al., 2013; Kloss et al., 2013; Wu et al., 2015; Zhao et al., 2010). We conclude that FAP-CAR T-cell therapy is a promising strategy to disrupt tumor-promoting desmoplasia and augment anti-tumor immunity across many types of human malignancies.

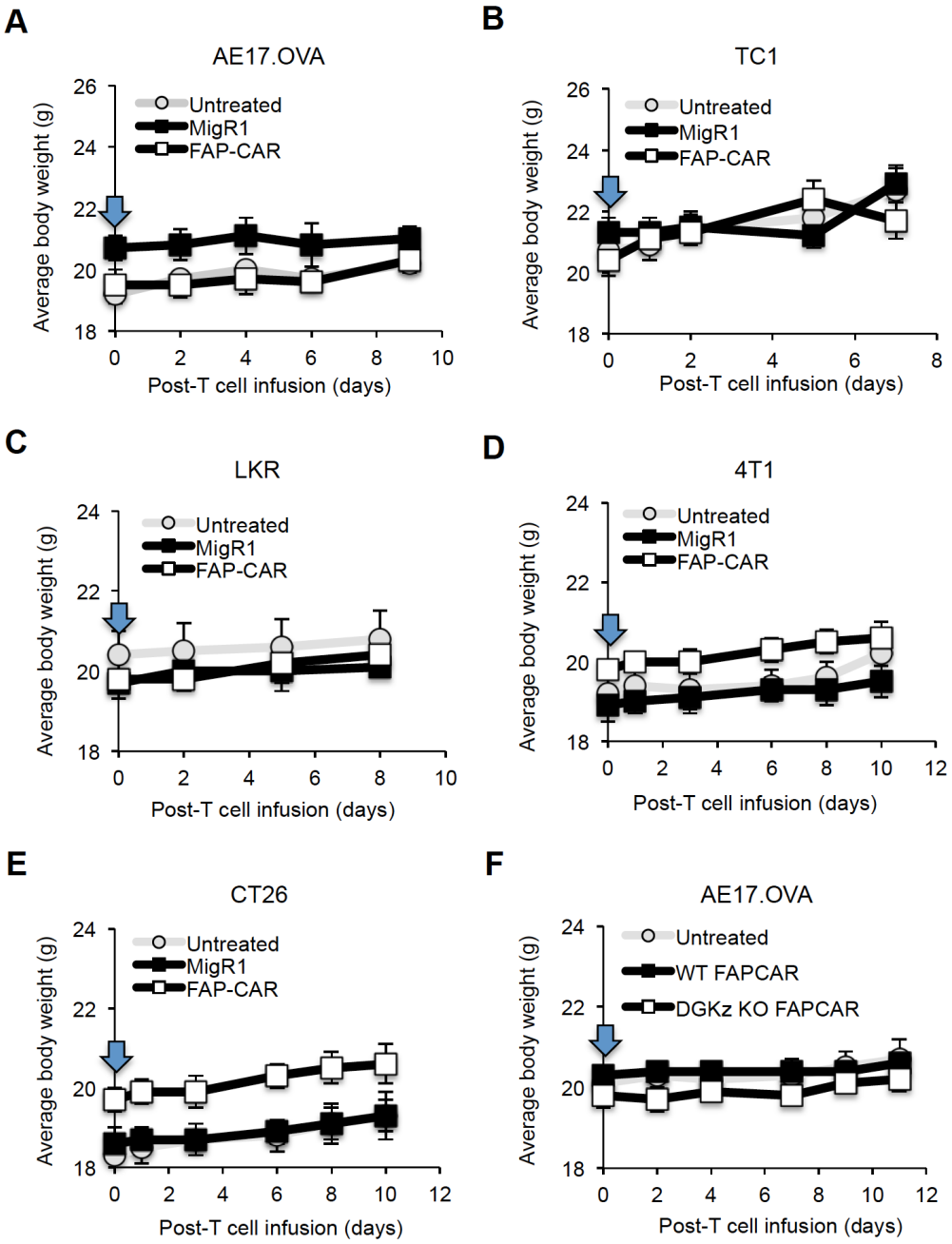

Figure 4-1. FAP-CAR T-cell therapy does not cause weight loss in multiple syngeneic flank tumor models. Mice bearing established tumors derived from AE17.OVA (A), TC1 (B), LKR (C), 4T1 (D) and CT26 (E) were injected intravenously with 1×10^7 wild-type FAP-CAR or MigR1 T cells. (F) Mice bearing AE17.OVA tumors were injected with 1×10^7 wild-type FAP-CAR T cells or DGKζ-knockout FAP-CAR T cells. Body weight was measured by electronic scale following adoptive T-cell transfer. Blue arrows indicate the time of adoptive T-cell transfer. Results are shown as mean ± SEM (n=5 per group).

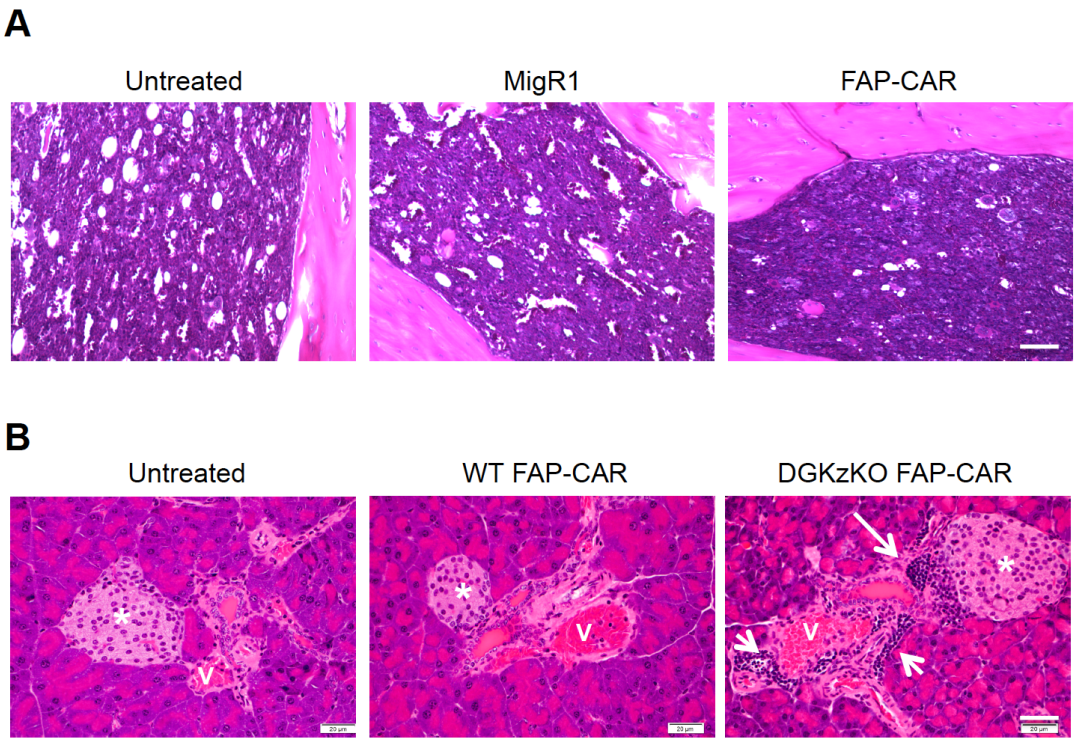

Figure 4-2. FAP-CAR T-cell therapy does not trigger bone marrow or pancreatic destruction. (A) AE17.OVA tumor-bearing mice were injected intravenously with one dose of 1×10^7 wild-type FAP-CAR or MigR1 T cells. Femurs were harvested one week after adoptive T-cell transfer. H&E staining was performed to assess the integrity of the bone marrow. (B) Mice bearing AE17.OVA tumors were injected with one dose of 1×10^7 wild-type FAP-CAR T cells or DGKζ-knockout FAP-CAR T cells. Pancreatic tissues were harvested and evaluated by H&E staining. Islets of Langerhans are marked by asterisks; blood vessels are labeled with "v". No significant changes were detected in the pancreas in the wild-type FAP-CAR T-cell-treated group. Mice that received hyperactive DGKζ-knockout FAP-CAR T cells had focal lymphocytic aggregates in peri-islet (arrow) and perivascular (arrowheads) regions. Scale: 20μm.

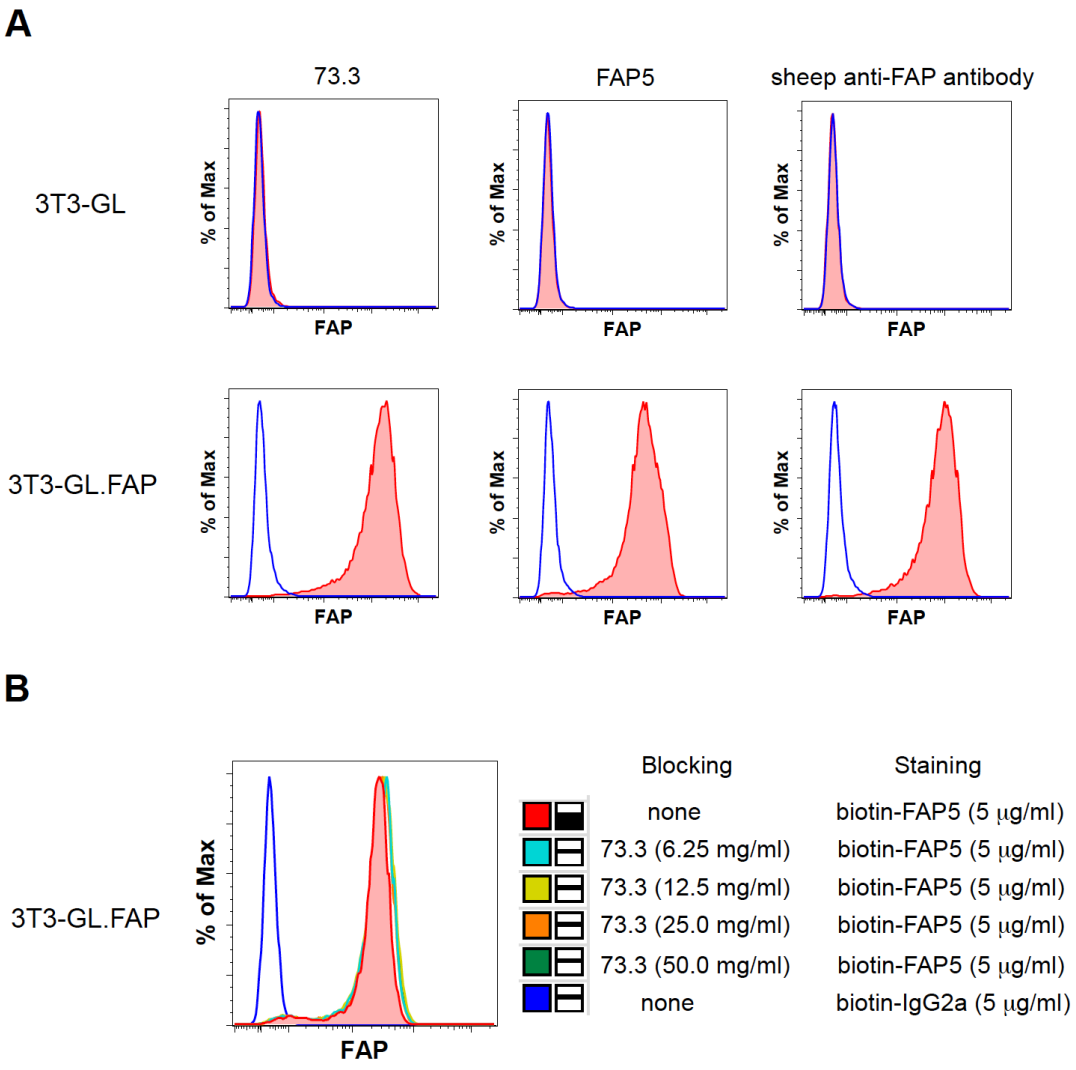

Figure 4-3. mAb 73.3 and mAb FAP5 bind to distinct epitopes of murine FAP expressed by fibroblasts. (A) Flow cytometry analysis was performed to detect FAP expression in 3T3 and 3T3.FAP cells using following anti-FAP antibodies: 73.3, FAP5 acquired from Boehringer Ingelheim and sheep polyclonal anti-human FAP that cross-reacts with murine FAP purchased from R&D. (B) Pre-incubation with the indicated concentrations of 73.3 did not impact the binding of FAP5 to 3T3.FAP cells.

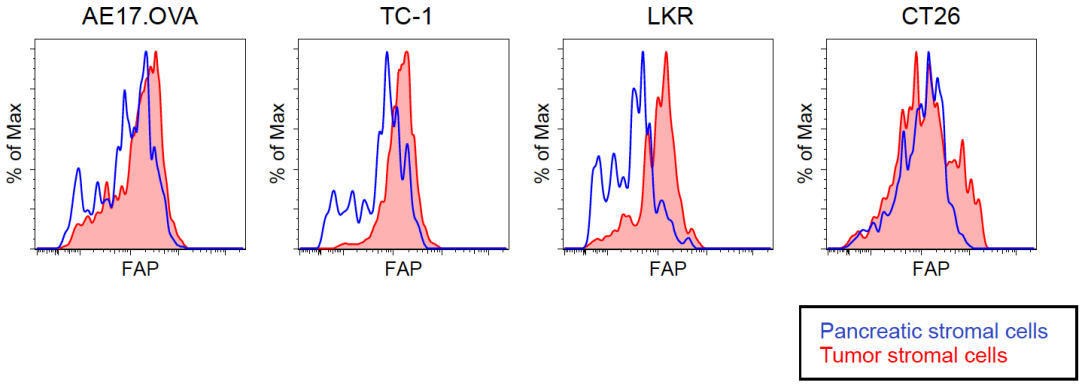

Figure 4-4. Tumor and pancreatic stromal cells express different levels of FAP. Tumor and pancreas tissues from multiple tumor-bearing mice were harvested and digested with a collagenase cocktail to obtain single-cell suspensions. Cells were then stained with biotin-conjugated anti-FAP polyclonal antibody and streptavidin-conjugated fluorochrome, together with anti-CD90 and anti-CD45 antibodies. Live cells were gated by propidium iodide exclusion. Representative figures demonstrate FAP expression on $CD90^{+}$ $CD45^{-}$ stromal cells in tumors (red) and pancreatic tissue (blue).

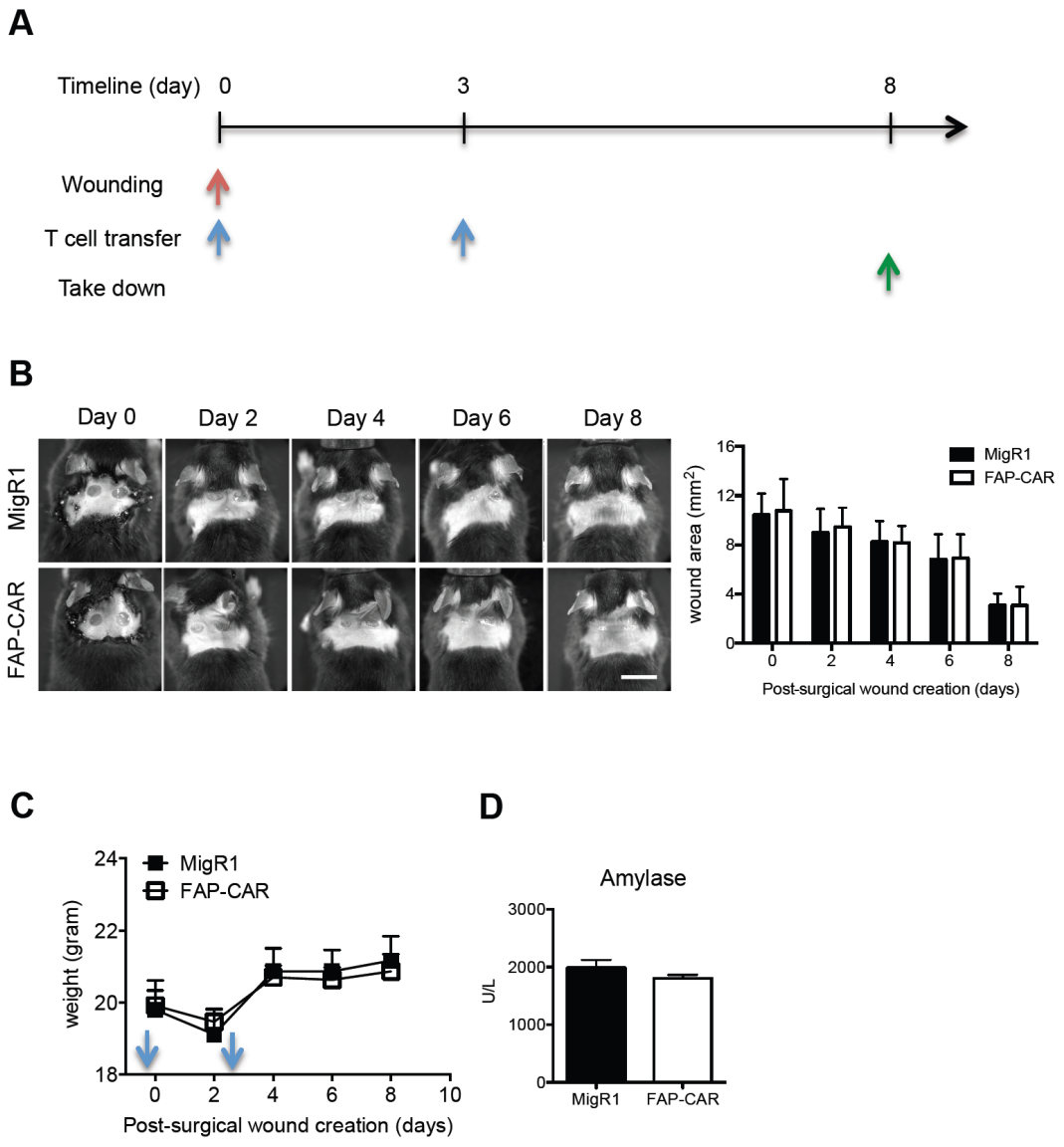

Figure 4-5. FAP-CAR T-cell therapy does not impact skin wound healing. (A) Schematic illustration of the experimental design. Full-thickness excisional wounds were created by biopsy punches in the dorsal skin of the C57BL/6 mice on day 0. Wounded mice were intravenously injected with 1×10^7 FAP-CAR or MigR1 T cells 2 hours post-wounding. A second dose of 1×10^7 FAP-CAR or MigR1 T cells was intravenously injected on day 3. Wound closure and body weight were monitored every other day from day 0 to day 8. (B) Representative images showing wound closure in mice treated with FAP-CAR or MigR1 T cells, scale: 1 cm. Wound closure was measured by computer-based quantification using Fiji software. Blue arrows indicate the time of adoptive T-cell transfer. (C) Body weight was monitored post T-cell infusion. (D) Serum amylase levels were measured at the endpoint. Results are shown as mean ± SEM (n=6 per group).

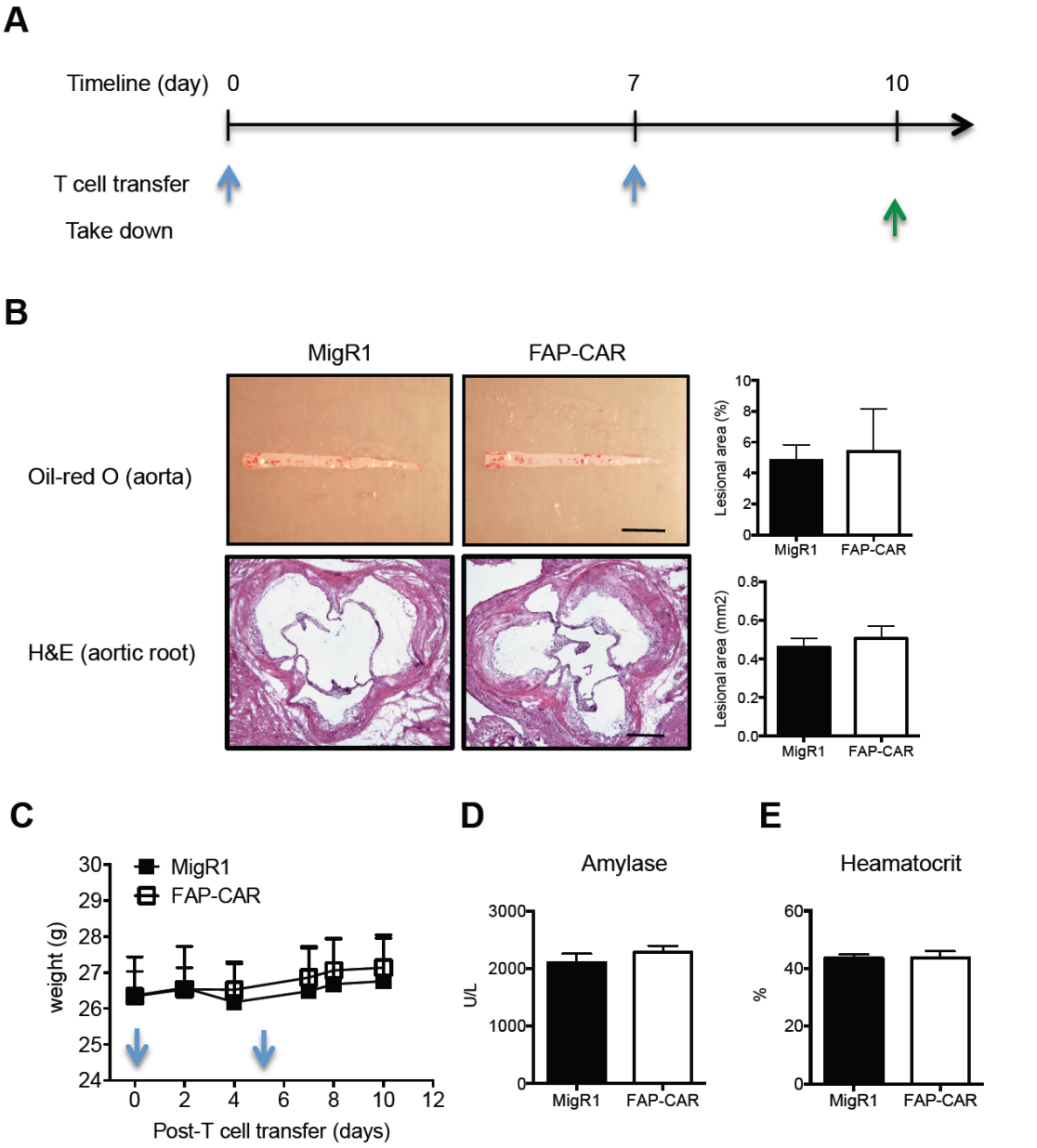

Figure 4-6. FAP-CAR T-cell therapy does not exacerbate atherosclerosis in APOE-deficient mice. (A) Schematic illustration of the experimental design. 24-week-old female apoE-deficient mice were intravenously injected with 1×10^7 FAP-CAR or MigR1 T cells. A second dose of 1×10^7 FAP-CAR or MigR1 T cells was administered intravenously one week after the initial dose. Mice were taken down on day 10. (B) The aorta was harvested to assess total atherosclerotic lesions by Oil Red staining (scale: 1 cm) and H&E staining (scale: 250 μm). Computer-based quantification was performed using Fiji software. (C) Body weight was monitored post T-cell infusion. (D) Serum amylase and hematocrit levels (E) were assessed at the endpoint. Results are shown as mean ± SEM (n=5 per group).

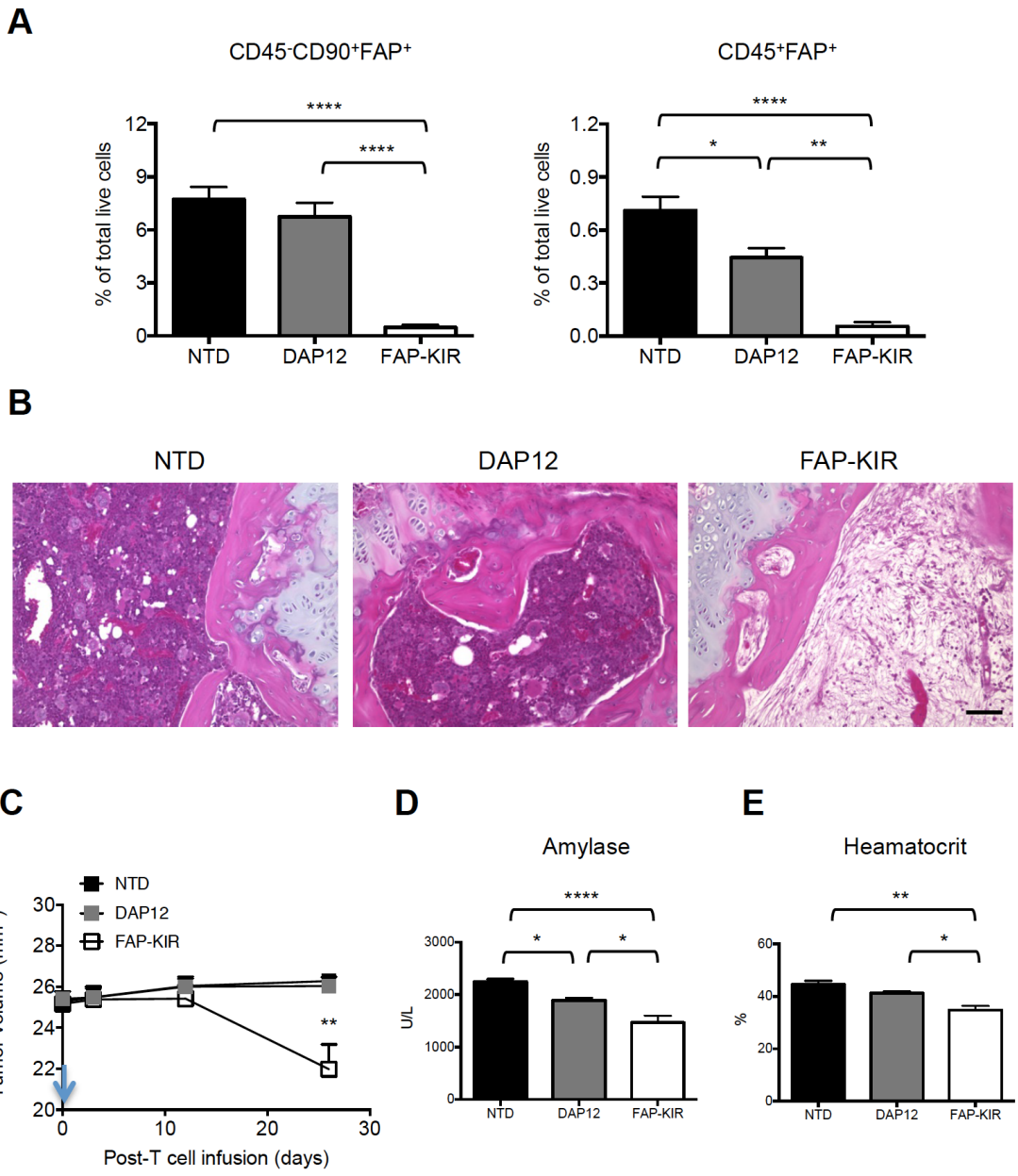

Figure 4-7. Enhanced FAP-CAR T-cell therapy results in complete intratumoral FAP$^+$ stromal depletion and is associated with systemic toxicities. EM-meso xenografts were intravenously injected with 5×10^6 enhanced FAP-CAR human T cells (FAP-KIR T cells), control vector T cells (DAP12) or untransduced T cells as shown in Fig. 2-7C. (A) Tumors were harvested 26 days post T-cell transfer and dissociated with a collagenase cocktail to obtain single-cell suspensions. Flow cytometry was performed to evaluate depletion of FAP$^+$ stromal cells. (B) Representative H&E stains of the bone marrow from each group; scale: 20μm. (C) Body weight was monitored post T-cell infusion. (D) Serum amylase and hematocrit levels (E) were analyzed at the endpoint. Results are shown as mean ± SEM (n=5 per group); *p<0.05; **p<0.01; ****p<0.0001.

CHAPTER 5 – Fibroblast activation protein governs malignant cell colonization and outgrowth to drive pulmonary metastasis

Introduction

In the previous chapters, I described using CAR T cells redirected against FAP^+ stromal cells to study the tumor-promoting effects of FAP at a cellular level. An alternative approach to target the tumor stroma is by disrupting specific molecular stromal cell/ECM-dependent pathways that are critical for tumor progression and therapeutic resistance. In the following two chapters, I will discuss the potential impacts of FAP on tumor development, progression and metastasis at a molecular level, specifically using FAP-deficient mice.

FAP protease regulates proteolysis that may potentially influence the tumor microenvironment

FAP is a type II transmembrane cell surface proteinase belonging to the prolyl dipeptidyl aminopeptidase (DPP) family, which cleaves amino-terminal dipeptides from polypeptides with proline or alanine in the penultimate position (P1Pro or P1Ala) (Park et al., 1999). FAP also exhibits endopeptidase activity that preferentially cleaves after the Gly-Pro sequence motif (P2GlyP1Pro) (Edosada et al., 2006). Although FAP was initially discovered in a membrane-bound form, low concentrations of circulating soluble FAP, also known as α2-antiplasmin-cleaving enzyme (APCE), in human and mouse serum have also been reported (Keane et al., 2013; Lee et al., 2004; Lee et al., 2006). While

FAP protease activity *in vitro* has been studied extensively, its substrate repertoire *in vivo* is not fully defined. *In vitro* screening of natural substrates has demonstrated that FAP DPP activity can efficiently process neuropeptide Y, B-type natriuretic peptide, substance P and peptide YY. Moreover, CCL22/MDC, CXCL2/Groβ and CXCL12/SDF-1α can be cleaved by FAP, albeit less efficiently (Keane et al., 2011). FAP also has an endopeptidase activity that is capable of modifying gelatin, type I and type III collagens, FGF21 and α2-antiplasmin (Christiansen et al., 2007; Keane et al., 2013; Lee et al., 2004; Lee et al., 2006; Levy et al., 1999; Zhen et al., 2015). Many of these substrates have been implicated in tumor progression; for instance, CXCL12/SDF-1α is crucial for promoting tumor cell invasion, angiogenesis and T-cell exclusion (Ene-Obong et al., 2013; Feig et al., 2013; Maroni et al., 2007; Orimo et al., 2005); collagen is important in enhancing tumor cell proliferation, invasion and metastasis (Aguilera et al., 2014; Valencia et al., 2012; Zhang et al., 2013). Nonetheless, the functional consequences of FAP-dependent proteolytic processing in the context of the tumor microenvironment are poorly understood.

Expression of FAP in parenchymal epithelial tissues may promote tumor growth, invasion or metastasis in a cell-autonomous fashion

FAP expression has been detected mostly in tumor stromal fibroblasts but not tumor epithelial cells; however, several groups have ectopically overexpressed FAP, or an enzymatically inactive mutant, in tumor cells to study the potential influence of FAP in the tumor microenvironment (Cheng et al., 2002; Cheng et al., 2005; Huang et al., 2004). Although initial results from these studies have demonstrated that FAP promotes tumor

growth *in vivo*, the experimental approaches failed to recapitulate the cardinal features of the tumor microenvironment, and mechanistic investigations were not performed. Importantly, the impact of ectopic overexpression of FAP on tumor cell proliferation *in vitro* was not determined (Cheng et al., 2002; Cheng et al., 2005). Further *in vitro* studies also suggested that FAP overexpression in HT-1080 fibrosarcoma cells might increase metastatic potential by upregulation of the integrin-mediated signaling pathway (Baird et al., 2015). Interestingly, a recent report described that FAP expression in the parenchyma of human oral squamous cell carcinoma (OSCC) was associated with poor prognosis (Wang et al., 2014a). Loss-of-function studies, employing two human primary OSCC cells that endogenously express FAP, revealed that FAP could enhance tumor cell proliferation, EMT, migration, invasion and metastasis through regulating PTEN/PI3K/AKT, Ras-ERK pathways. Since FAP only has a short cytoplasmic tail, it is intriguing how FAP potentiates signal transduction pathways in cancer cells. In summary, it is likely that FAP expression in tumor cells can drive malignant progression in a cell-autonomous fashion.

Expression of FAP in mesenchymal stromal cells enhances tumor growth and migration

One approach that has been taken to explore the potential non-cell-autonomous tumor-promoting functions mediated by FAP was employing rabbit anti-FAP polyclonal antibodies to inhibit FAP protease activity (Cheng et al., 2002). *In vitro*, polyclonal anti-FAP antibodies significantly inhibited murine FAP DPP activity. HT-29 colon cancer xenografts treated with these inhibitory anti-FAP antisera resulted in reduced tumor

growth compared to those treated with preimmunization antisera. Subsequent studies demonstrated that a pharmacologic inhibitor targeting the endopeptidase activity of FAP also attenuated the growth in the same xenograft model (Cheng et al., 2005). These results suggest that FAP may promote tumor growth through its DPP and endopeptidase activity. Nevertheless, the mechanisms involved were not investigated and the approaches taken did not distinguish the potential inhibitory effects on other DPP members e.g. DPP-IV, which has been detected in HT-29 colon cancer cells (Darmoul et al., 1992), and/or other proteins that exhibit endopeptidase activity that may have contributed to the tumor growth. To investigate whether mesenchymal FAP plays a determinant role in tumorigenesis, Dr. Puré's lab utilized FAP-deficient mice and showed that genetic deletion of FAP inhibited the growth of mutant *Kras*-induced lung cancers and CT26 colon cancer syngeneic transplants (Santos et al., 2009). Pharmacological targeting of DPP and the endopeptidase activity of FAP also replicated this finding. Tumor inhibition induced by FAP deficiency was attributed to decreased tumor angiogenesis and altered ECM remodeling that resulted in increased accumulation of collagen associated with altered integrin signaling in residual tumors. Collectively, these studies indicate that FAP is not merely a marker for tumor-associated stromal cells, but indeed plays a significant role in the growth of primary tumors.

Interestingly, a recent study indicated that FAP-dependent matrix remodeling could augment tumor cell migration though β1-integrin signaling (Lee et al., 2011), suggesting that endogenous FAP may promote tumor invasion and metastasis. In this chapter, I describe the investigations of the requirement for FAP protease expressed by

mesenchymal stromal cells in driving the formation of pulmonary metastasis. I also explored the potential mechanisms by which FAP regulates tumor cell seeding and metastatic outgrowth.

Materials and methods

Cell lines

Murine Lewis lung carcinoma cells (LLC), human A549 lung adenocarcinoma cells and MDA-MB-231 human breast cancer cells (231) were purchased from the American Type Culture Collection. MDA-MD-231 cells expressing firefly luciferase (231-luc) were provided by Dr. Qihong Huang (Wistar Institute, Philadelphia, PA). A549 cells expressing GFP and luciferase (A549-GL) were generated as described (Moon et al., 2015). Mouse adult lung fibroblasts (MAF) were isolated from 8-12 week old C57BL/6 wildtype and FAP-deficient mice.

Animals

C57BL/6 mice and NOD/SCID/IL2-receptor γ chain knockout (NSG) mice were purchased from Charles River Laboratories Inc. (Wilmington, MA) and Jackson Labs (Bar Harbor, ME). FAP-deficient mice ($Fap^{LacZ/LacZ}$) provided by Boehringer Ingelheim (Niedermeyer et al., 2000) were backcrossed 12 generations onto a C57BL/6 genetic background. These mice in turn were crossed with NSG mice to generate NSG FAP-deficient mice. Experimental protocols were approved by the Institutional Animal Care and Use Committee and were in compliance with guidelines for the care and use of animals.

In vivo tumor growth assay

NSG or NSG FAP-KO mice were subcutaneously injected with 2×10^5 A549-GL cells mixed with matrigel (BD Biosciences), or were orthotopically implanted into mammary

fat pad with 2×10^5 MDA-MB231-luc cells mixed with matrigel. C57BL/6 or C57BL/6 FAP-KO mice were subcutaneously injected with 2×10^5 LLC lung cancer cells. Tumor growth was followed using bioluminescence imaging or caliper measurements. Tumor volume was calculated using the formula: length × width^2 × $\pi/6$.

Experimental metastasis assay

NSG or NSG FAP-KO mice were intravenously injected with 1 to 6×10^5 A549 parental cells, A549-GL cells, 231 cells or 231-luc cells. C57BL/6 or C57BL/6 FAP-KO mice were intravenously injected with 4×10^5 LLC cells. The presence of pulmonary metastasis was determined by sectioning and H&E staining of Prefer (Anatech)-fixed paraffin-embed lung tissue at three different levels at the endpoint or followed over time by bioluminescence imaging.

Bioluminescence imaging

The IVIS Lumina III Bioluminescence and Fluorescence Imaging System (Perkin Elmer, Waltham, MA) was used for *in vivo* bioluminescent imaging. Primary tumor or pulmonary metastasis-bearing animals were injected intraperitoneally with 150mg/kg body D-luciferin (Gold Biotechnology, St. Louis, MO, USA) suspended in PBS. Mice were imaged under isoflurane anesthesia 15 minutes post D-luciferin injection as kinetic studies demonstrated peak bioluminescent intensity of tumors around this time. Bioluminescent signal from tumor cells expressing luciferase was quantified by Living Image software and reported as units of tissue radiance (photons/second).

Isolation of lung matrisome for proteomic study

FAP-heterozygous and FAP-deficient mice were gently perfused with PBS. Lung tissues were harvested, washed twice with PBS, and dissected into small pieces. Tissue fragments were incubated with 10 mL decellularization buffer composed of 1% SDS, 20 mM EDTA and protease inhibitor (Roche) in PBS for 24 hours at 4°C. Tissue fragments were further incubated with new 10 mL of decellularization buffer for another 24 hours at 4°C. Tissue fragments were washed with 10 mL washing buffer composed of 20 mM EDTA and protease inhibitor in distilled water for 24 hours at 4°C. Decellularized lung tissues were homogenized and sonicated with protein extraction buffer (Sigma), and then spun at 15000 rpm for 10 minutes at 20°C. Tissue supernatant was used for electrophoresis and mass spectrometry.

Prothrombin Time and Partial Thromboplastin Time assay

Blood from NSG-FAP-intact and NSG-FAP-deficient mice was obtained by cardiac puncture. Prothrombin time and partial thromboplastin time were measured at the clinical lab of the Ryan Veterinary Hospital of the University of Pennsylvania.

Vascular permeability and leakage assay

Assays for lung and liver vascular permeability and leakage were performed as previously described with minor modifications (Hiratsuka et al., 2011; Radu and Chernoff, 2013). NSG or NSG FAP-KO mice were intravenously injected with 10 mg/kg of Evans blue (EB, Sigma) in PBS. Mice were sacrificed and perfused gently with PBS at 4 hours post EB injection. Lung and liver tissues were harvested and dissected for EB

extraction. Formamide (Sigma) was added to dissected tissues for 20-hour incubation at 55°C. Tissue EB content (μg EB/g lung) was calculated by correcting A620 for the presence of heme pigments from the supernatant: A620 (corrected) = A620 − (1.426 × A740 + 0.030) (Hiratsuka et al., 2011).

Antibodies

Purified anti-mouse CD16/32 antibody was purchased from eBioscience. Anti-CD45 (30-F11; PE-Cy7, biotin), anti-CD90 (53-2.1; FITC, PE), anti-CD11b (M1/70, PE-Cy7, Pacific blue), anti-F4/80 (BM8; APC), anti-CD206 (C068C2; FITC, PE), anti-CD8α (53-6.7; PECy7) and anti-CD4 (GK1.5; FITC) antibodies were purchased from Biolegend. A polyclonal sheep anti-human antibody that cross-reacts with mouse FAP was purchased from R&D and the specificity was confirmed based on its reactivity with A549 human lung cancer xenografts derived from wild-type but not FAP-deficient NSG mice.

Surface staining and flow cytometry analysis

Normal mice and pulmonary metastasis-bearing mice were gently perfused with PBS. Lung tissues were harvested, washed twice with PBS, and dissected into small pieces. Lung tissues were enzymatically dissociated with collagenase type I (100 U/mL, Worthington), II (100 U/mL, Worthington) and IV (100 U/mL, Worthington) as well as DNase I (100 U/mL, Worthington), in Leibovitz's L-15 Medium (Thermo Fisher Scientific) for an hour at 37°C. Digested tissues were then filtered through 70 μm nylon mesh cell strainers (BD Bioscience), and red blood cells were lysed by a ACK buffer (BD Bioscience). Fc receptors were blocked by incubating cells with anti-mouse CD16/CD32

antibody for 15 minutes and then stained with primary antibodies at 4°C for 30 minutes, followed by incubation with streptavidin-BV421 for another 15 minutes. Dead cells were excluded using propidium iodide (Thermo Fisher Scientific). Cell acquisition was performed on LSR-II using FACSDiva software (BD Bioscience). Data were analyzed using FlowJo software (Tree Star).

Intracellular Staining

Cells were incubated with a viability probe (Thermo Fisher Scientific) for 30 minutes and then fixed with 4% formaldehyde for 10 min. The cells were then permeabilized and blocked with 10% rabbit serum/ 1% BSA/ 15mM glycine in 0.1% PBS-Tween for 20 minutes. Cells were stained with Alexa Fluor 647-conjugated anti-human APOE antibody (Abcam) or Alexa Fluor 647-conjugated isotype-matched control for 30 minutes.

RNA extraction, gene expression profiling and bioinformatics analysis of microarray data

Serially transplanted A549-GL tumor cells (WT.p1, WT.p3, KO.p1, KO.p3) were sorted from single-cell suspensions derived from 4 to 8 pulmonary metastasis-bearing mice. RNA was extracted with TriZol (Invitrogen). Subsequently, RNA was purified and DNase treated on RNeasy (Qiagen) columns. The eukaryote total RNA nano bioanalyzer (Agilent) assay confirmed the quality of RNA, and all RNA used for the following steps had a RIN > 8. Equal amounts of total RNA for each sample (400 ng) were amplified as recommended by Illumina and hybridized to the Human-HT12 v4 human whole genome bead arrays. Illumina GenomeStudio software was used to export expression levels and

detection p-values for each probe of each sample. Signal intensity data was quantile-normalized and genes that showed insignificant detection p-value ($p>0.05$) in all samples were excluded from further analysis. Genes different by at least 2-fold between any two of four samples (WT.p1, WT.p3, KO.p1, KO.p3) were included in further analysis. Gene expression was used to calculate Pearson correlation coefficient with each of 38 distinct expression patterns and the gene was assigned to a pattern that resulted in the maximum absolute correlation coefficient. Gene set enrichment analysis for canonical pathways and upstream regulators was performed using QIAGEN's Ingenuity Pathway Analysis software (IPA, QIAGEN Redwood City,www.qiagen.com/ingenuity), and the significance of enrichment was defined at FDR<10% for pathways and $p<10^{-5}$ for upstream regulators.

Online dataset-based gene expression and survival analysis

Data was acquired from publicly available microarray databases from Oncomine and cancer survival analyses (Gyorffy et al., 2013; Rhodes et al., 2004). APOE expression in lung adenocarcinomas and normal lung tissues was compared in the following microarray datasets: the Okayama dataset, composed of 20 normal lung tissues and 226 stage I-II lung adenocarcinomas treated at National Cancer Center Hospital, Tokyo (Okayama et al., 2012); the Stearman dataset, composed of 10 pairs of adjacent normal lung tissues and invasive lung adenocarcinomas treated at University of Colorado Cancer Center (Stearman et al., 2005); the Su dataset, composed of 27 pairs of adjacent normal lung tissues and lung adenocarcinomas treated at the Taipei Veterans General Hospital, Taiwan; two commercially available human normal lung tissues; and one immortalized,

non-tumorigenic human bronchial epithelial cell line (Su et al., 2007). Large cohort survival analysis of lung adenocarcinoma patients was performed using the APOE Affymetrix ID 203382_s_at. (the 2015 version of the database was used). Patients with lung adenocarcinoma were divided by the best cutoff, and no further restrictions were applied. Both the hazard ratio and log-rank test *p*-value are provided.

Histopathological, histochemical and immunohistochemical analysis.

Mice were gently perfused with PBS, and lung tissues were inflated intratracheally and fixed with Prefer (Anatech), followed by dehydration and paraffin embedding. Four-micron sections were cut at three different levels and stained with H&E. The percentage of total lung area occupied by tumor in each of the five lobes was quantified by computer-based morphometry using either Image-Pro 6.2 or Fiji on H&E-stained sections. For immunohistochemical staining, tissue sections were further subjected to 10 mM sodium citrate buffer for antigen retrieval, followed by quenching endogenous peroxidases with 3% H_2O_2. Sections were then blocked with 10% goat serum in 1% BSA/PBS at room temperature for one hour, and then incubated with avidin-biotin or streptavidin-biotin block (Vector Labs). Rabbit monoclonal anti-human APOE antibody (Novus Biologicals) was applied overnight at 4°C and incubated with biotinylated secondary antibody at room temperature for an hour. Bound antibodies were detected with horseradish peroxidase (HRP) using Vectastain Elite ABC (Vector Laboratories), followed by counterstaining with hematoxylin.

Statistical Analyses

Statistics were calculated using GraphPad Prism 6. For studies comparing two groups, Student's *t*-test was used. For studies comparing more than two groups, one-way ANOVA with post-hoc Tukey testing was used. Data are represented as mean ± SEM. Differences were considered significant when $p < 0.05$.

Results

Accumulation of FAP-expressing cells in pulmonary metastasis

To determine whether host expression of FAP can regulate pulmonary metastasis, we employed three commonly used pulmonary metastasis models including A549 human lung adenocarcinoma, MDA-MB-231 human breast adenocarcinoma (231) and Lewis lung cancer (LLC). Flow cytometry analysis demonstrated that these cells did not express detectable FAP *in vitro*, while mouse adult lung fibroblasts exhibited basal-level FAP expression (**Figure 5-1**). We first compared the primary tumor growth in these models and found that genetic deletion of FAP decreased growth of subcutaneous A549 and LLC flank tumors and 231 orthotopic tumors (**Figure 5-2**), consistent with our previous finding that FAP enhances primary tumor growth (Santos et al., 2009). As this would complicate any data obtained in spontaneous metastasis in these models, we instead conducted our subsequent experiments using an experimental metastasis approach i.e. intravenous injection of tumor cells for hematogenous spread to circumvent the potential impact of FAP on primary tumor growth. Interestingly, we observed abundant $CD90^+$ FAP^+ tumor-associated mesenchymal stromal cells accumulated in the pulmonary metastases compared to the normal lung tissues (**Figure 5-3**). This finding raised the interesting possibility that FAP protease or FAP^+ stromal cells are in a position to regulate pulmonary metastasis.

FAP protease enhances tumor cell seeding and metastatic outgrowth in lung

To test whether FAP protease plays a role in regulating pulmonary metastasis, A549, 231 or LLC cells were intravenously injected into FAP-intact or FAP-deficient hosts. We

found that FAP deficiency resulted in decreased tumor burden, colony number and colony size in A549, LLC and 231 pulmonary metastasis models (**Figure 5-4**). To better get a first estimate of what stage FAP impacts the metastatic process, specifically tumor cell seeding and metastatic tumor outgrowth, we performed non-invasive bioluminescent imaging using A549 cells expressing GFP/Luciferase (A549-GL) and 231 cells expressing luciferase (231-luc) and conducted a kinetic analysis. Notably, the tumor cell-derived luciferase activity from lung tissue was significantly reduced in the FAP deficiency mice one hour post-intravenous inoculation in both models (**Figure 5-5**, **upper panel**). Moreover, the luciferase activity remained markedly decreased at later time points in the FAP deficiency mice in both models (**Figure 5-5**, **bottom panel**). Along with observations that the colony size was significantly reduced in the FAP deficiency mice (**Figure 5-4B**), these data indicate that FAP may regulate the early steps of tumor cell colonization and the outgrowth of metastatic tumor colonies.

FAP protease may govern fibrinolysis to permit tumor cell seeding

To understand how FAP promotes tumor cell seeding in the lung, I analyzed the proteomic data of the matrisomes isolated from FAP-heterozygous and FAP-deficient mice performed by a former postdoctoral fellow in the lab (**Figure 5-6A**). Gel electrophoresis demonstrated that various differentially-expressed proteins were evident in the FAP-heterozygous and FAP-deficient lung matrisomes (**Figure 5-6B**). Proteomic analysis revealed that several coagulation proteins known to regulate pulmonary metastasis were altered in the lung matrisome derived from FAP-deficient mice (**Figure 5-6C**). Among these candidates, we focused on fibrinogen, which has been implicated as

a key determinant in governing tumor cell seeding without interfering with metastatic tumor outgrowth in the lung (Palumbo et al., 2000). Analyses of prothrombin time and partial thromboplastin time indicated that the integrities of extrinsic, intrinsic and common coagulation pathways were not altered in the homeostatic condition between FAP-intact and FAP-deficient mice (**Figure 5-7**). These results rule out the possibility that FAP may directly regulate the levels of circulating hemostatic factors that play critical roles in the formation of tumor cell-fibrin clot complexes to enable metastatic seeding. Additionally, we did not observe any differences in lung vascular permeability between FAP-intact and FAP-deficient mice, suggesting that FAP does not increase vascular perfusion to facilitate tumor cell seeding (**Figure 5-8**). Given that FAP can convert native Met-α2 antiplasmin into Asn-α2 antiplasmin, which is 10 to 15 times more potent than its native form in inhibiting plasmin function (Lee et al., 2004; Lee et al., 2006), and that FAP has been shown to promote tissue plasminogen activator turnover (Koczorowska et al., 2016), we hypothesize that FAP deficiency would render tumor cell-fibrin clots more susceptible to plasmin-mediated fibrinolysis, thereby reducing tumor cell colonization in the lung (**Figure 5-6D**). Further experiments will be performed to test this hypothesis.

FAP protease is dispensable for the recruitment and/or retention of CD90$^+$ mesenchymal stromal cells in pulmonary metastasis

Prior studies have shown that endogenous FAP protease is essential for the migration of bone-marrow-derived stem cells (Chung et al., 2014), suggesting that knocking out FAP may impede tumor stromagenesis by abrogating the recruitment and/or retention of

tumor-associated mesenchymal stroma cells and therefore potentially inhibiting pulmonary metastasis. To evaluate this possibility, we dissociated metastasis-bearing lung tissues and performed flow cytometry. We did not find any differences in the numbers of $CD90^+$ tumor-associated mesenchymal stromal cells between FAP-intact and FAP-deficient mice in our metastasis models (**Figure 5-9**), making this unlikely to be the relevant mechanism.

FAP protease promotes inflammatory M2 macrophage response to enable tumor metastatic outgrowth

In contrast, we constantly observed a decrease of $CD45^+$ hematopoietic cells in the pulmonary metastasis derived from FAP-deficient mice. Flow analyses demonstrated that the number of $CD11b^+$ $F4/80^+$ macrophages, also known as metastasis-associated macrophages (MAMs), was decreased in the pulmonary metastasis derived from FAP-deficient mice, while the level of $CD11b^+$ $Ly6G^+$ neutrophils remained unchanged. This decreased population was further characterized as $CD206^+$ $CD11b^+$ $F4/80^+$ M2-like macrophages (**Figure 5-10**). These data demonstrate that genetic deletion of FAP inhibits the M2 macrophage response in pulmonary metastasis. In future studies, it will be important to assess whether targeting M2 macrophages suppresses pulmonary metastatic outgrowth.

Serial transplantation in FAP deficient mice reduces the lung metastatic potential of A549 tumor cells

To determine whether propagation in a FAP-deficient microenvironment could reprogram the metastatic potential of tumor cells, we performed serial transfer experiments designed to address three questions: 1) whether the residual tumor cells derived from initial passage in FAP-deficient mice are capable of propagating in a permissive microenvironment, and 2) test whether these residual tumor cells may still be subjected to FAP-inhibition, whether serial transplantation could imprint tumor cells with a reduced metastatic phenotype. A549-LG tumor cells were recovered from the lungs after a single passage through FAP-intact and FAP-deficient mice and designated as WT.p1 and KO.p1, respectively (**Figure 5-11A, upper panel**). These tumor cells were briefly expanded *in vitro*, sorted based on GFP expression and then transferred into either FAP-intact or FAP-deficient mice for an additional two *in vivo* passages. Cells recovered from the third passage were designated as WT.p3 and KO.p3, respectively (**Figure 5-11A, bottom panel**). Interestingly, regardless of prior conditioning in FAP-intact (e.g. WTp.1 and WTp.2) or FAP-deficient environments (e.g. KOp.1 and KOp.2), A549 tumor cells transferred into FAP-deficient hosts in the second or third transplants showed reduced seeding at one hour post tumor-cell transfer (**Figure 5-11B, upper panel**). These observations indicate that serial transplantations in FAP-deficient microenvironment may not alter the pulmonary seeding capacity of A549-LG tumor cells. Notably, we found that A549 tumor cells that had been passaged twice in FAP-deficient hosts (KO.p2) grew less efficiently than WT.p2 when transferred into FAP-intact hosts (**Figure 5-11B, bottom panel**), indicating that serial transplantations in FAP-deficient microenvironment might impact the metastatic outgrowth of A549-LG tumor cells. Nevertheless, the conditioning of tumor cells in FAP-intact and FAP-deficient hosts did not alter their growth potential

in vitro (**Figure 5-12**). Collectively, these data suggest that tumor cell conditioning in a FAP-deficient environment might impose either genetic and/or epigenetic alterations in the tumor cells such that these tumor cells lose their ability to grow in a permissive microenvironment.

APOE is a candidate target for FAP-dependent enhancement of tumor metastatic outgrowth and may serve as a potential negative prognostic marker in human lung cancer.

To further explore the molecular mechanisms by which FAP targeting restricts tumor outgrowth in the lung, we performed a microarray analysis to compare the gene expression profiles of WT.p1, KO.p1, WT.p3 and KO.p3 recovered by cell sorting. Principal component analysis demonstrated that tumor cells that underwent *in vivo* transplantation exhibited marked changes in gene expression (**Figure 5-13A**). More genes are differentially expressed in the third transplant compared to the first transplant (**Figure 5-13A**). Microarray analysis identified two expression patterns that may reflect FAP-dependent genetic and/or epigenetic alterations (**Figure 5-13B**). APOE was decreased 3-fold and 9-fold during a single and three serial passages in FAP-deficient hosts, respectively. On the other hand, miRNA-1974 was found to increase 9.1-fold after three serial passages in FAP-deficient hosts. Further canonical pathways and upstream regulators analyses indicated that "atherosclerosis" and "inflammatory" signaling were altered (**Figure 5-13C**). Moreover, we found that the number of $CD11b^{+}$ $F4/80^{+}$ macrophages was decreased in FAP-deficient mice in the serial transplants (**Figure 5-14**), reflecting that FAP-dependent tumor metastatic outgrowth gene signature may correlate

with its ability to regulate the recruitment, retention and/or alternative activation of macrophage to drive proinflammatory response.

Given that APOE has been suggested to be a candidate marker for lung cancer progression (Liu et al., 2014; Su et al., 2011), we chose to study the pro-tumorigenic activity of APOE in our model. We first assessed the clinical relevance of APOE expression in publicly available lung adenocarcinoma databases. Bioinformatic analyses via the Oncomine platform confirmed that APOE was overexpressed in multiple human lung adenocarcinoma gene expression datasets (**Figure 5-15**). Kaplan-Meier analyses of lung adenocarcinoma datasets showed that APOE overexpression correlated with tumor progression and decreased patient survival (**Figure 5-16**). These data highlight the importance of APOE in progression of lung adenocarcinoma. Immunohistochemical staining (**Figure 5-17A**) and flow cytometry analysis (**Figure 5-17B**) confirmed that APOE expression was downregulated in A549 tumors in the FAP-deficient mice following intravenous transfer, suggesting that APOE may play a role in the outgrowth of the A549 tumors. Further gain-of-function and loss-of-function experiments will be performed to determine the role of APOE in the growth of A549 tumor and to test if exogenous APOE expression can rescue A549 tumor growth in the FAP-deficient mice.

Conclusions and discussion

Metastasis is the major cause of cancer-related deaths and represents one of the most difficult challenges in the clinical management of cancer patients. Despite improvements in surgical procedures, chemotherapy and radiation therapy, the prognosis for patients with distant metastases remains dismal. This challenge underlies the importance of advancing our mechanistic understanding of how metastasis occurs.

Cancer metastasis is a complex multistep process that involves local tumor cell invasion and dissemination from the primary tumor, intravasation into the circulation, adhesion to the vascular endothelium of distant organs, extravasation into those tissues, and finally growth at distant sites (Gupta and Massague, 2006). The current paradigm is that primary tumor-host interactions establish a pre-metastatic niche in distant target organs (Kitamura et al., 2015a; McAllister and Weinberg, 2014; Psaila and Lyden, 2009), and/or that disseminated metastatic cells guide the formation of early metastatic niches during hematogenous dissemination and colonization (Gay and Felding-Habermann, 2011; Labelle and Hynes, 2012). Therefore, it is crucial to understand how mesenchymal stromal cells are involved in regulation of the metastatic cascade. Herein, I describe that FAP protease is crucial in governing the early steps of tumor cell seeding and metastatic outgrowth to drive pulmonary metastasis.

Metastatic colonization and outgrowth is a highly inefficient process, as less than 0.1% of tumor cells that enter the circulation eventually form pulmonary metastasis (Luzzi et al., 1998). Our data demonstrate that deficiency in FAP protease further decreased the initial

tumor cell seeding, suggesting that FAP has an essential role in governing the early steps of metastatic colonization (**Figure 5-5**). Multiple hemostatic factors have been linked to the formation of early metastatic niches to promote pulmonary metastasis. Prior studies using molecular, cellular and pharmacological approaches as well as gene-targeted mice unequivocally demonstrated that tumor-cell-associated tissue factor, circulating prothrombin and multiple downstream thrombin pro-coagulant targets including platelets and fibrinogen, robustly enhanced the metastatic potential of tumor cells. (Camerer et al., 2004; Horowitz et al., 2011; Mueller et al., 1992; Mueller and Ruf, 1998; Palumbo et al., 2000; Palumbo et al., 2002; Palumbo et al., 2007; Yokota et al., 2014). Importantly, genetic deletion of fibrinogen abrogated tumor cell seeding without affecting the outgrowth of seeded tumor colonies in both spontaneous and experimental pulmonary metastasis models (Palumbo et al., 2000; Palumbo et al., 2002). These studies indicate that tumor cell-clot formation is one of the key rate-limiting steps for the establishment of early metastatic niches, in which interactions among tumor cells, platelets and inflammatory cells collectively drive pulmonary metastatic colonization and outgrowth (Gay and Felding-Habermann, 2011; Labelle and Hynes, 2012). Nonetheless, less is known about the regulatory mechanisms involved in the maintenance of the tumor cell-fibrin clot after its formation. Interestingly, our proteomic analysis of the lung matrisome showed that fibrinogen was downregulated in FAP-deficient mice (**Figure 5-6C**). This led us to consider the possibility that FAP might play an active role in regulating fibrin/fibrinogen turnover to impact pulmonary metastasis. *In vitro*, FAP protease has been implicated to prevent plasmin-mediated fibrinolysis by abrogating the synthesis and activity of plasmin via regulation of proteolytic processing of α2-antiplasmin and

turnover of tissue plasminogen activator, respectively (Koczorowska et al., 2016; Lee et al., 2004; Lee et al., 2006). Thus, we hypothesize that FAP is a key determinant in enhancing tumor-fibrin clot resistance to plasmin-mediated fibrinolysis *in vivo*, thereby promoting tumor cell colonization in the lung (**Figure 5-6D**). The rationale of this hypothesis is supported by a recent study demonstrating that plasminogen activator inhibitor-1 deficiency reduced the number but not growth of pulmonary metastasis (Yan and DeMars, 2014). Our initial studies showed that levels of hemostatic factors required for fibrin clot formation were not altered under homeostatic conditions in FAP-deficient mice. Further experiments will be performed to determine if the levels of Met-α2 antiplasmin and tissue plasminogen activator and clot dissociation time are altered in FAP-deficient mice.

Growing evidence indicates that macrophages play active roles in the development of pulmonary metastasis (Kitamura et al., 2015a). Experimental targeting of these metastasis-associated macrophages (MAMs) at different stages of the metastatic cascade demonstrated their supportive roles in tumor cell seeding and persistent outgrowth (Kitamura et al., 2015b; Qian et al., 2009; Qian et al., 2011; Qian et al., 2015). Interestingly, we observed that FAP deficiency reduced the number of MAMs in our pulmonary metastasis models (**Figure 5-10**). Serial transplant and microarray studies also revealed that FAP-dependent metastatic tumor outgrowth programs correlated with the recruitment and/or retention of MAMs (**Figure 5-13 and 5-14**). These data indicate that FAP may augment the inflammatory response to drive persistent metastatic tumor outgrowth. A recent report employing unbiased proteomic approaches demonstrated that

FAP protease activity could have a strong impact on the secreted CAF proteome. Notably, TGFβ and CCL2 were found downregulated in FAP-deficient CAFs or CAF-expressing endopeptidase inactive mutant ($FAP^{S624}A$) (Koczorowska et al., 2016). Given the established roles of TGFβ and CCL2 in macrophage recruitment, retention and alternative activation as well as their potential roles in stromagenesis and pulmonary metastasis (Gong et al., 2012; Kitamura et al., 2015b; Pang et al., 2013; Qian et al., 2011; Sierra-Filardi et al., 2014), we postulate that FAP may impact metastatic tumor outgrowth by driving the inflammatory response and/or stromagenesis via TGFβ and CCL2. Further experiments will be performed to test this hypothesis.

The tumor microenvironment and host milieu have considerable influence on the establishment of pulmonary metastasis, and targeting pro-metastatic niches may offer an opportunity to control the growth of these lesions. As with any other anti-cancer therapy, tumor cells may eventually develop acquired resistance, even for stroma-targeted therapies. Therefore, we performed a serial transplant study using A549-LG cells to explore whether persistent FAP inhibition may induce cancer resistance. Our data indicated that serial transplantation in the FAP-deficient hosts might not alter the pulmonary seeding ability of A549-LG tumor cells, but rather restrained their outgrowth capacity to drive the formation of pulmonary metastasis (**Figure 5-11**). Taken together, these data suggest that sustained exposure to a FAP-deficient environment does not drive the development of FAP-independent growth in the residual tumors, but rather, it may impose genetic and/or epigenetic alterations to inhibit metastatic outgrowth, at least in this model. We have identified several candidates that may drive tumor metastatic

outgrowth (**Figure 5-12**). Notably, APOE, was found highly upregulated and correlated with poor outcome in lung adenocarcinomas (**Figures 5-13, 5-15 and 5-16**). We confirmed that APOE expression was downregulated in A549 experimental pulmonary metastasis in the FAP-deficient mice (**Figure 5-17**), indicating that APOE is indeed a FAP-dependent molecular target. It remains to be investigated how FAP protease modulates APOE expression. It may either directly activate the upstream LXR/RXR signaling pathway or indirectly regulate macrophage recruitment, retention, and alternative activation to potentiate APOE expression. Further gain-of-function and loss-of-function experiments employing APOE overexpression or knockdown are underway to determine the role of APOE in pulmonary metastatic outgrowth.

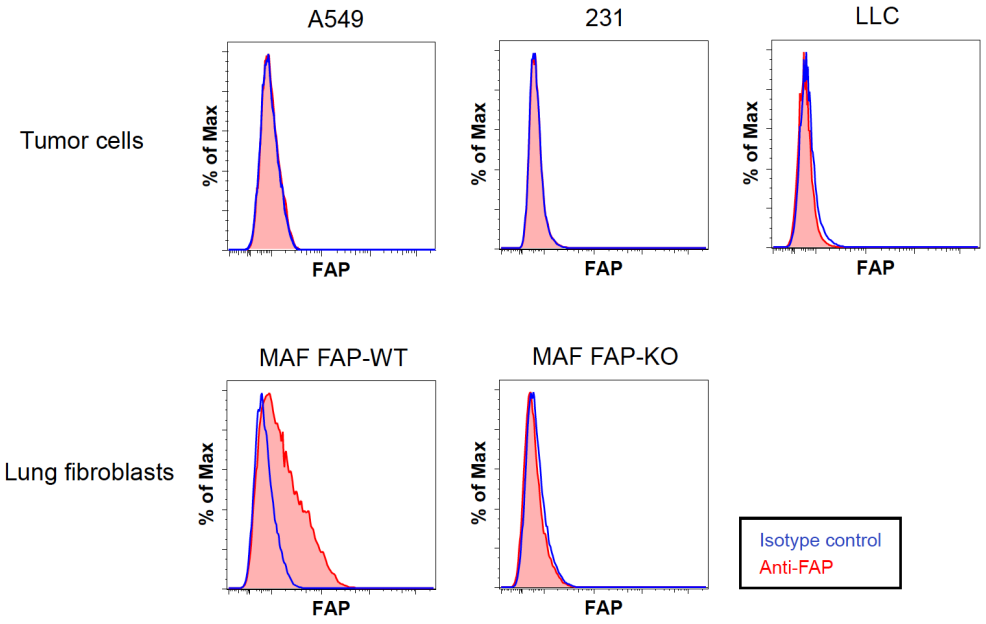

Figure 5-1. Flow cytometry analysis of FAP expression in A549, 231 and LLC tumor cells and mouse lung fibroblasts. A549 human lung adenocarcinoma cells, MDA-MB-231 human breast cancer cells (231), Lewis lung mouse lung cancer cells (LLC) and mouse adult lung fibroblasts (MAF) isolated from FAP-intact (FAP-WT) C57BL/6 mice or FAP-deficient mice (FAP-KO) were stained with sheep polyclonal anti-human/mouse FAP and analyzed by flow cytometry.

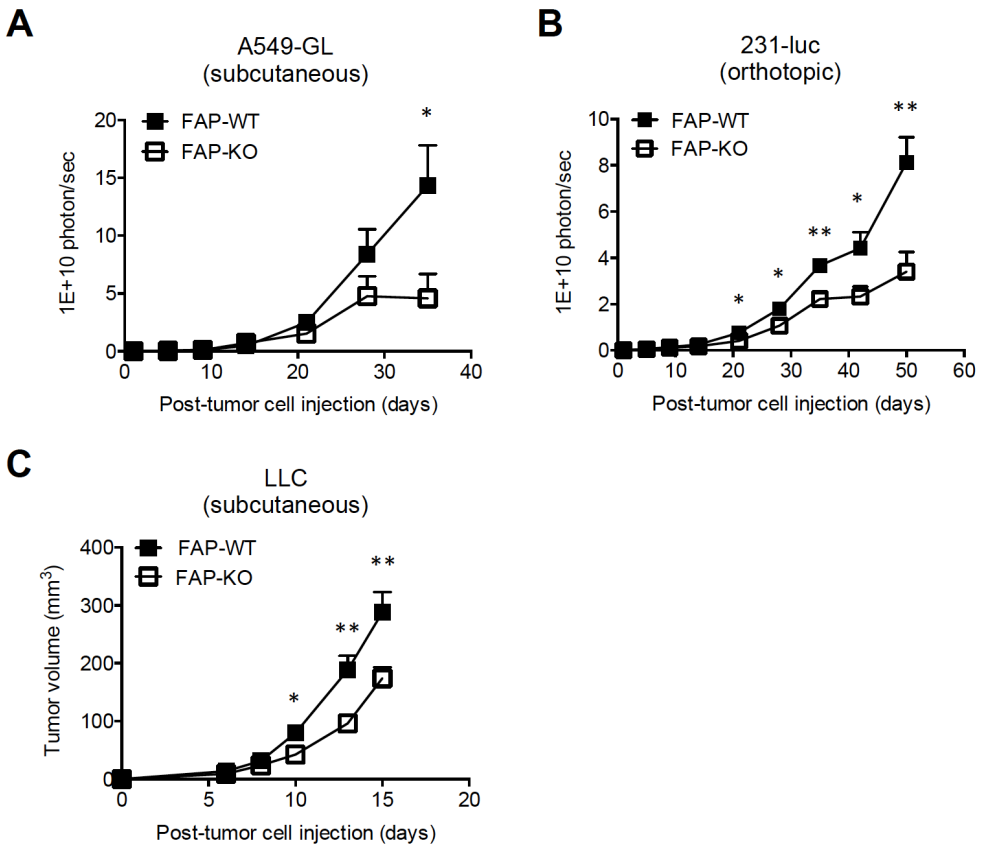

Figure 5-2. FAP protease enhances growth of primary A549, 231 and LLC tumors. (A) A549 cells expressing GFP and luciferase (A549-GL) were inoculated subcutaneously into the right flank of the FAP-WT and FAP-KO NSG mice (n=5). (B) MDA-MB-231 cells expressing luciferase (231-luc) were injected orthotopically into the mammary fat pad of the FAP-WT and FAP-KO NSG mice (n=7). Tumor growth was monitored by bioluminescence imaging. (C) LLC cells were injected subcutaneously into the right flank of the FAP-WT and FAP-KO C57BL/6 mice (n=8). Tumor growth was monitored by electronic caliper. Results are shown as mean ± SEM; *p<0.05, **p<0.01.

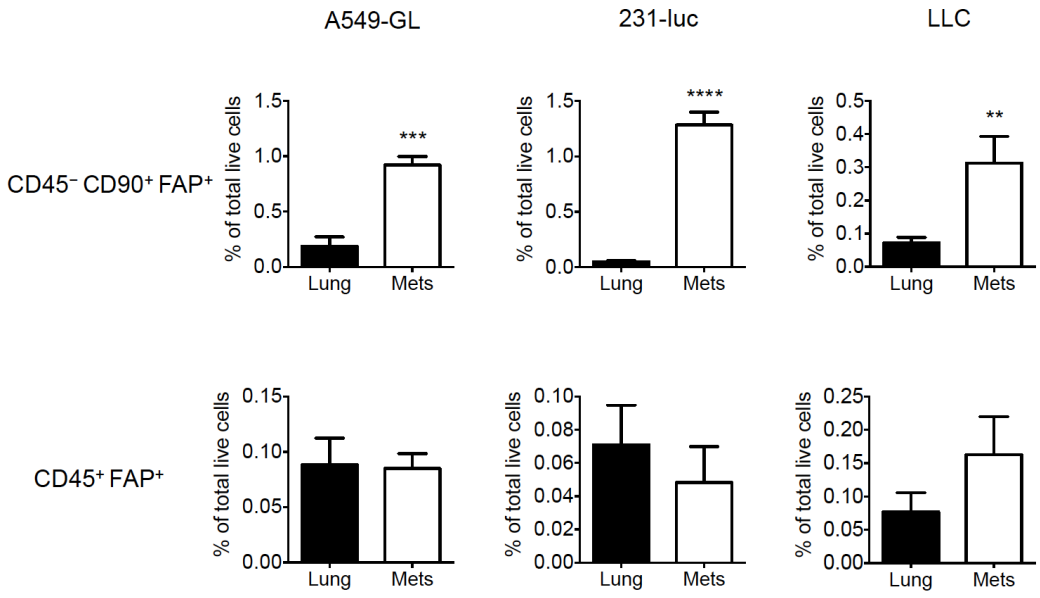

Figure 5-3. Accumulation of FAP-expressing stromal cells in A549, 231 and LLC pulmonary metastasis models. NSG or C57BL/6 mice were intravenously injected with A549-GL, 231-luc or LLC tumor cells or were left untreated. Tumor-bearing lung metastases (Mets) and normal lung tissues were harvested and dissociated with a collagenase cocktail to obtain single-cell suspensions. Flow cytometry was performed to identify $CD90^+$ stromal cells and $CD45^+$ hematopoietic cells that express FAP. Results are shown as mean ± SEM (n=5~7 per group); **p<0.01, ***p<0.001, ****p<0.0001.

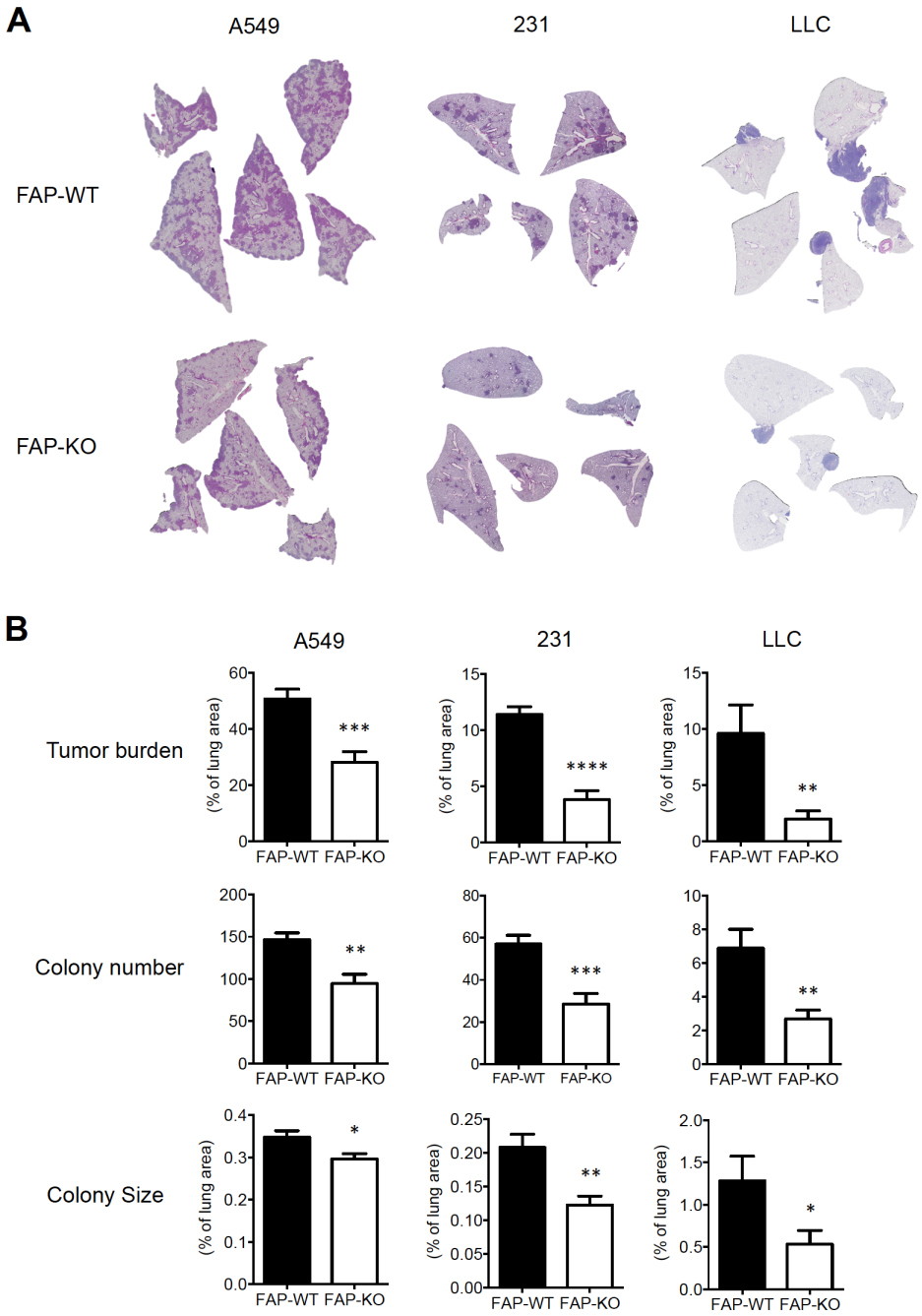

Figure 5-4. FAP protease promotes A549, 231 and LLC pulmonary metastasis. (A) FAP-WT and FAP-KO NSG or C57BL/6 mice were injected intravenously with A549 cells, MDA-MB-231 or LLC cells. Tumor-bearing lung tissues were harvested and stained with H&E to determine the tumor burden. (B) Computer-based quantification was performed using Fiji or imageJ software. The tumor burden was determined by the tumor-to-lung area ratio at three different levels of lung sections from each genotype. Colony size was calculated by dividing the total tumor burden by the colony number. Results are shown as mean ± SEM (n≥6 per group); *p<0.05, **p<0.01, ***p<0.001, ****p<0.0001.

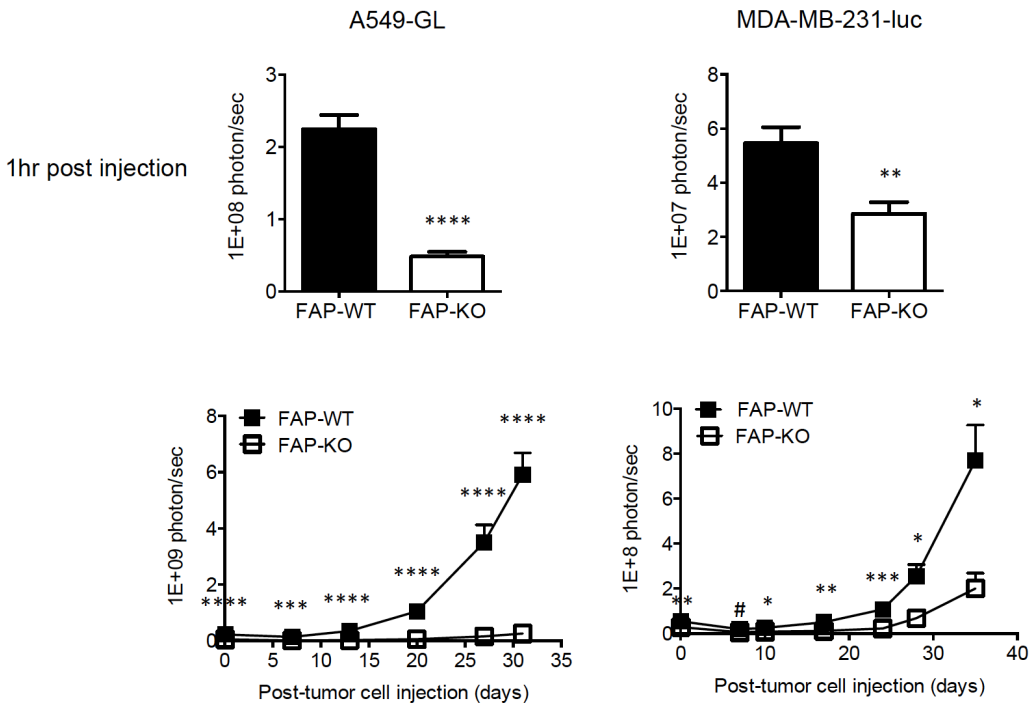

Figure 5-5. FAP protease enhances A549 and 231 tumor-cell seeding and metastatic outgrowth. FAP-WT and FAP-KO NSG mice were injected intravenously with A549-GL (n=8 per group) or 231-luc tumor cells (n=5-6 per group). Tumor cell colonization and metastatic outgrowth were monitored by bioluminescence imaging. Results are shown as mean ± SEM; #p=0.05, *p<0.05, **p<0.01, ***p<0.001, ****p<0.0001.

A

de-cellularization

lung matrisome

Electrophoresis & mass spec

B

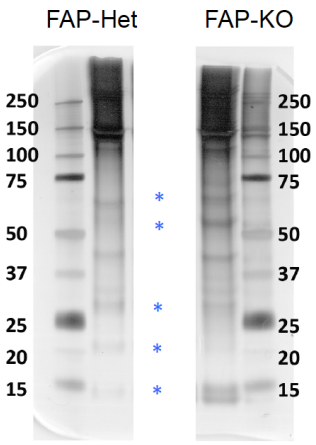

C

Candidate Protein	Metastasis regulator	FAP-Het	FAP-KO
Fibrinogen alpha peptide	+	72	29
Fibrinogen beta chain	+	124	16
Fibrinogen gamma chain	+	89	34
Annexin A2	+	9	2
Serpin B12	+	7	1
Annexin A5	-	1	5
Von Willebrand factor	-	1	9

D

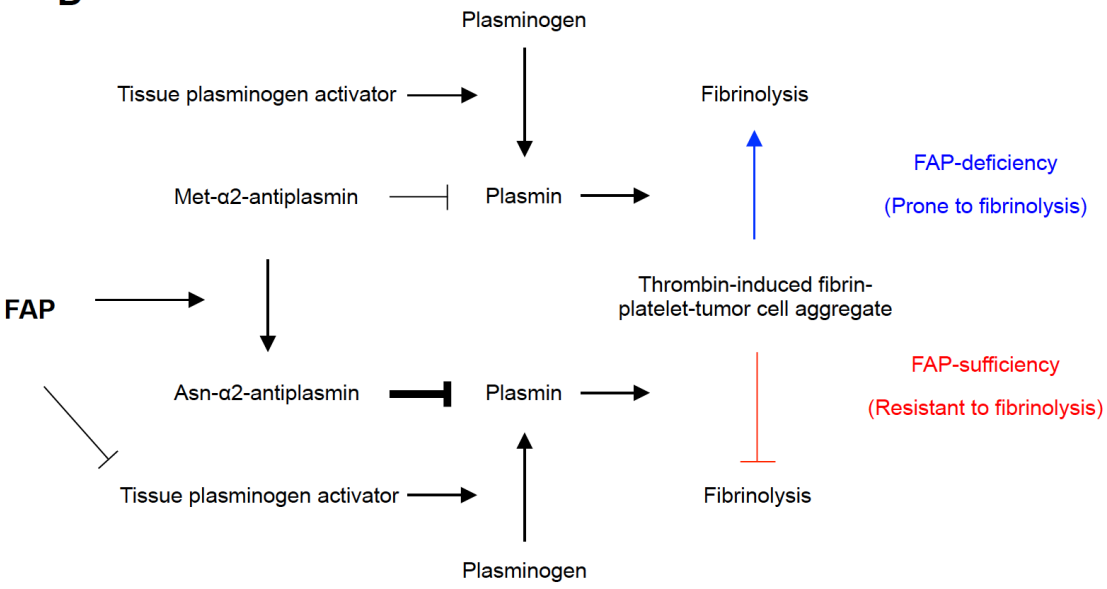

Figure 5-6. Proteomic analysis of the lung matrisome uncovers altered coagulation pathways in FAP-deficient mice. (A) Schematic illustration of the experimental design. Normal lung tissues from $FAP^{+/-}$ (FAP-Het) and $FAP^{-/-}$ (FAP-KO) mice were de-cellularized to extract the lung extracellular matrix. Lung matrisomes were subjected to electrophoresis and mass spectrometry to identify global FAP-dependent matrix remodeling candidate targets. (B) Results of the lung matrisome electrophoresis using 4-12% bis-tris gel; *indicates potential differential expression of matrix molecules between FAP-Het and FAP-KO. (C) Various coagulation molecules that have been demonstrated to positively or negatively govern lung metastasis are down-regulated or up-regulated in the FAP-deficient lung matrisome. (D) Hypothetical mechanisms by which FAP regulates the synthesis and activity of plasmin via regulation of proteolytic processing of α2-antiplasmin and turnover of tissue plasminogen activator for the maintenance of the tumor cell-fibrin clots during metastatic seeding. Note: lung matrisome extraction and the proteomic assay were performed by a former post-doctoral fellow Lisa Chang.

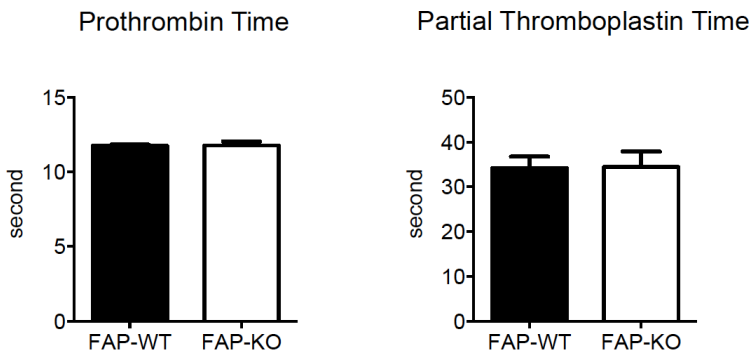

Figure 5-7. FAP is dispensable for fibrin clot formation under homeostatic conditions. Serum from FAP-WT and FAP-KO NSG mice were obtained by cardiac puncture after euthanasia. The integrity of extrinsic, intrinsic and common coagulation pathways was assessed using prothrombin time and partial thromboplastin time, respectively. Results are shown as mean ± SEM (n=5 per group).

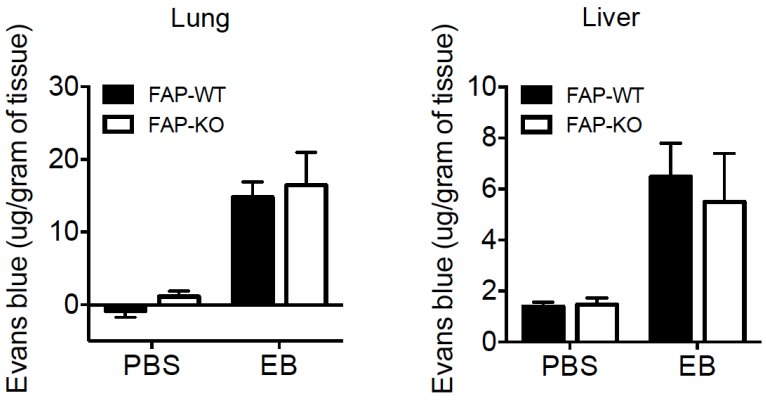

Figure 5-8. Genetic deletion of FAP does not affect lung or liver permeability. FAP-WT and FAP-KO NSG mice were injected intravenously with evans blue (EB) or PBS. At 4 hours post-injection, lung and liver tissues were harvested to determine evans blue microvascular leakage. Results are shown as mean ± SEM (n=3 per group).

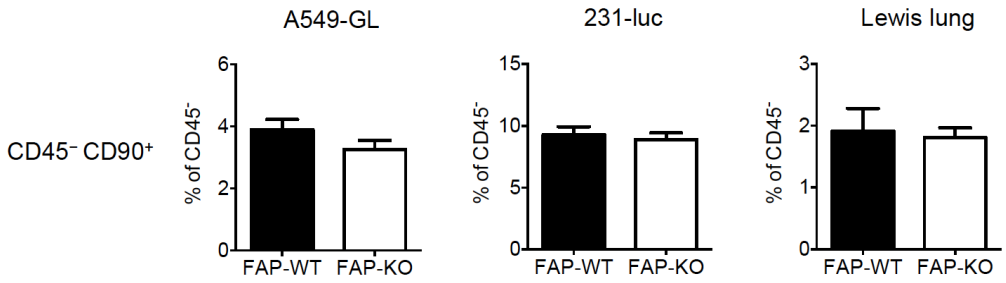

Figure 5-9. Genetic deletion of FAP does not impact the recruitment of CD45$^-$ CD90$^+$ cancer-associated stromal cells in A549, 231 and LLC pulmonary metastases. FAP-WT and FAP-KO NSG or C57BL/6 mice were injected intravenously with A549-GL, 231-luc or LLC cells. Tumor-bearing lung tissues were harvested and digested with a collagenase cocktail to obtain single-cell suspensions. Flow cytometry was performed to identify total CD45$^-$ CD90$^+$ stromal cells. Results are shown as mean ± SEM (n≥5 per group).

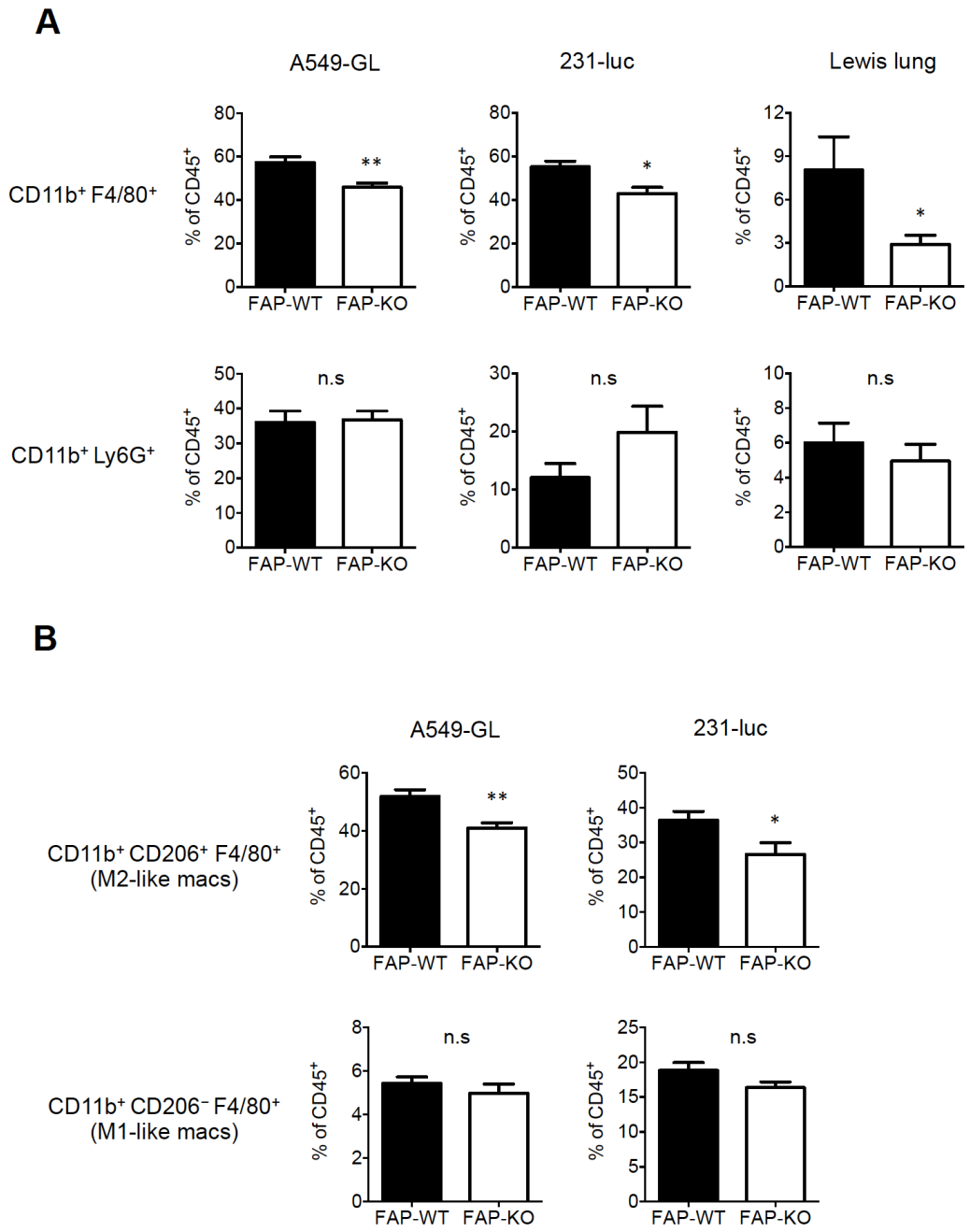

Figure 5-10. FAP-dependent A549, 231 and LLC tumor metastatic outgrowth in the lung correlates with macrophage infiltration. FAP-WT and FAP-KO NSG or C57BL/6 mice were injected intravenously with A549-GL, 231-luc or LLC cells. Tumor-bearing lung tissues were harvested and digested with a collagenase cocktail to obtain single-cell suspensions. (A) Flow cytometry was performed to identify $CD11b^+$ $F4/80^+$ macrophages and $CD11b^+$ $Ly6G^+$ neutrophils. (B) M2 macrophages were further defined by gating $CD206^+$ macrophages. Results are shown as mean ± SEM (n≥5 per group); *p<0.05, **p<0.01.

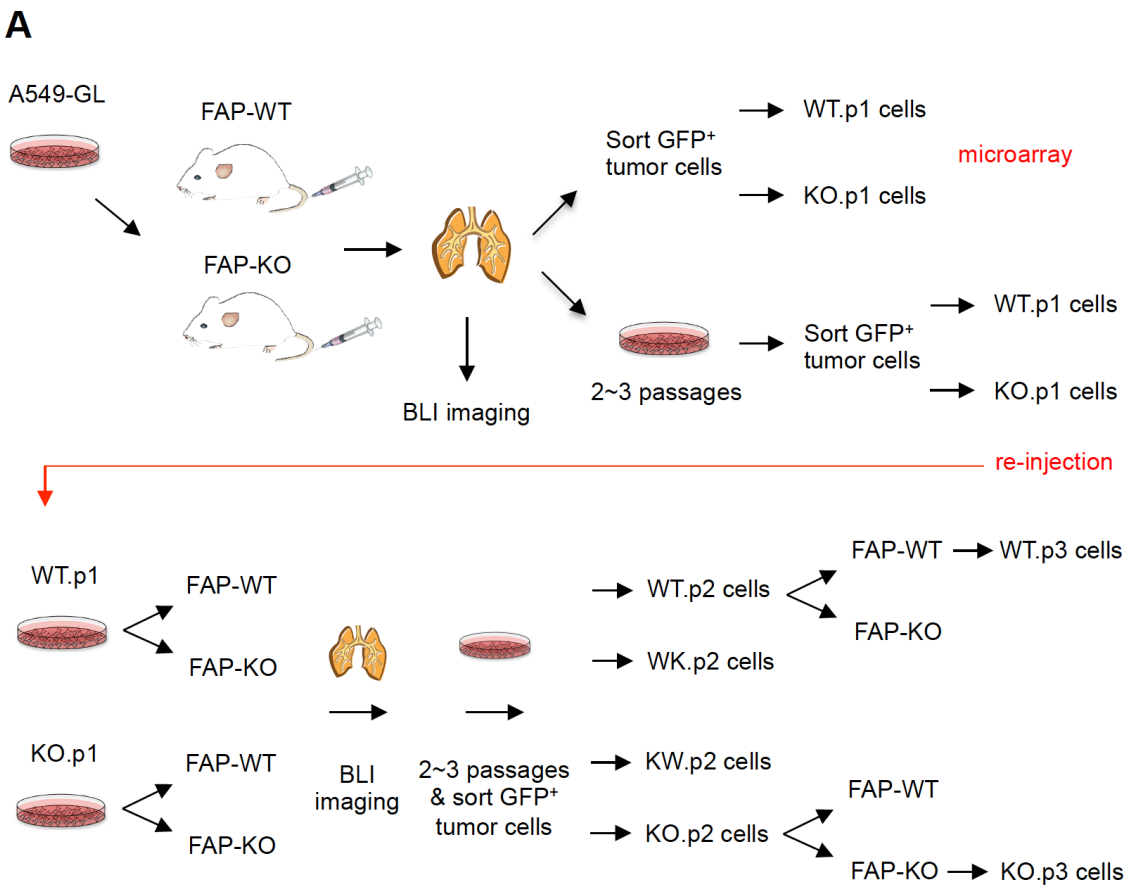
A
A549-GL
FAP-WT
FAP-KO
BLI imaging
Sort GFP+ tumor cells
WT.p1 cells
KO.p1 cells
microarray
2~3 passages
Sort GFP+ tumor cells
WT.p1 cells
KO.p1 cells
re-injection
WT.p1
FAP-WT
FAP-KO
KO.p1
FAP-WT
FAP-KO
BLI imaging
2~3 passages & sort GFP+ tumor cells
WT.p2 cells
WK.p2 cells
KW.p2 cells
KO.p2 cells
FAP-WT
WT.p3 cells
FAP-KO
FAP-WT
FAP-KO
KO.p3 cells

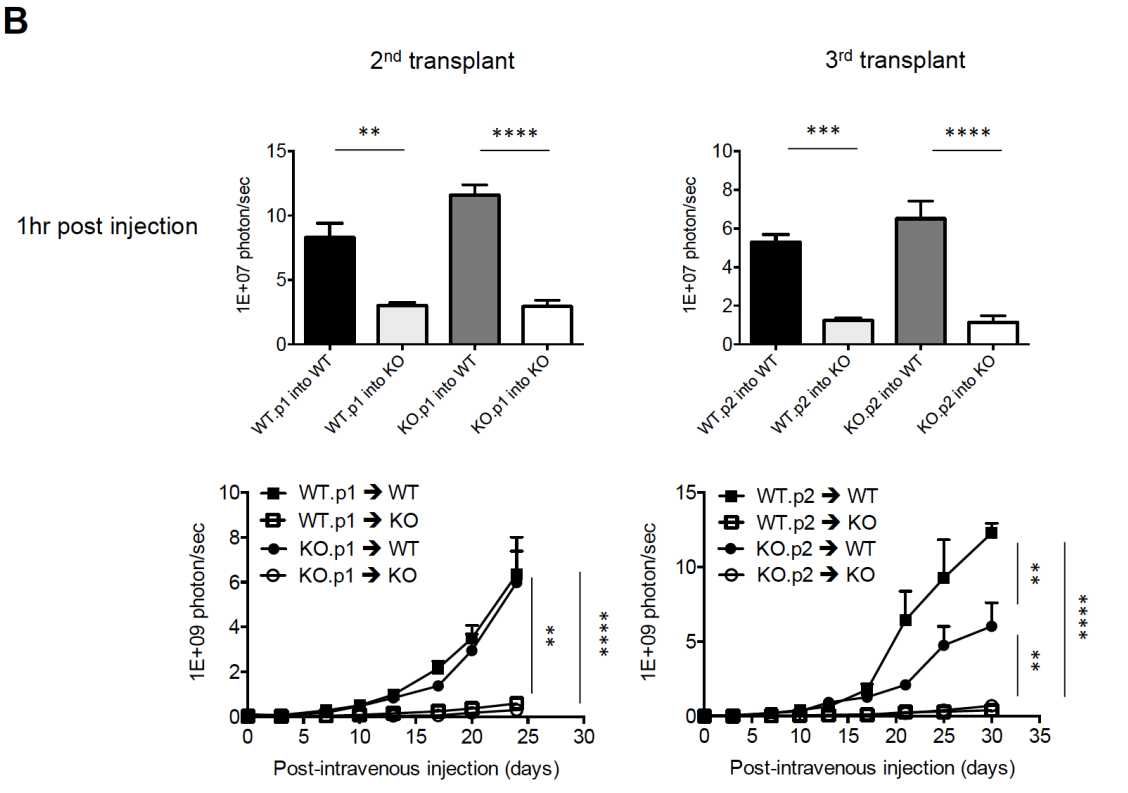
B
2nd transplant
3rd transplant
1hr post injection
1E+07 photon/sec
WT.p1 into WT
WT.p1 into KO
KO.p1 into WT
KO.p1 into KO
WT.p2 into WT
WT.p2 into KO
KO.p2 into WT
KO.p2 into KO
1E+09 photon/sec
WT.p1 → WT
WT.p1 → KO
KO.p1 → WT
KO.p1 → KO
WT.p2 → WT
WT.p2 → KO
KO.p2 → WT
KO.p2 → KO
Post-intravenous injection (days)

Figure 5-11. FAP protease promotes A549 pulmonary metastasis in a serial transplant study. (A) Schematic illustration of the experimental design. FAP-WT and FAP-KO NSG mice were injected intravenously with A549-GL. Tumor cell colonization and metastatic outgrowth were monitored by bioluminescence imaging. Tumor-bearing lung tissues were digested, and A549GL cells were sorted directly by FACS for microarray analysis or briefly expanded for 2-3 passages, followed by sorting and reinjecting recovered cells into FAP-WT and FAP-KO NSG mice for serial transplantation. (B) Tumor cell colonization and metastatic outgrowth in the second and third serial transplants were monitored by bioluminescence imaging. Results are shown as mean ± SEM ($n \geq 4$ per group); $^{**}p<0.01$, $^{***}p<0.001$, $^{****}p<0.0001$.

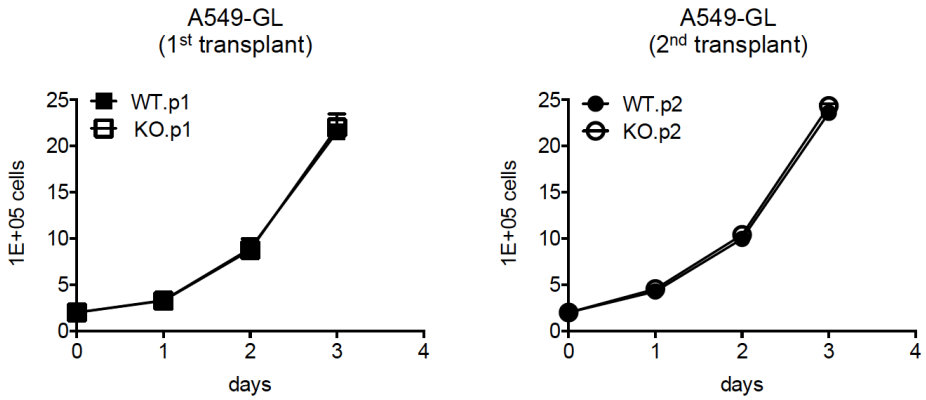

Figure 5-12. Conditioning of A549 tumor cells in FAP-intact and FAP-deficient hosts by serial transplantation does not impact their growth in vitro. A549-GL cells that underwent serial transplants were recovered from FAP-WT and FAP-KO lung tissues by cell sorting. Tumor cell growth from the first transplant (WT.p1 and KO.p1) and second transplant (WT.p2 and KO.p2) were determined by trypan blue exclusion. Results are shown as mean ± SEM (n=3 per group).

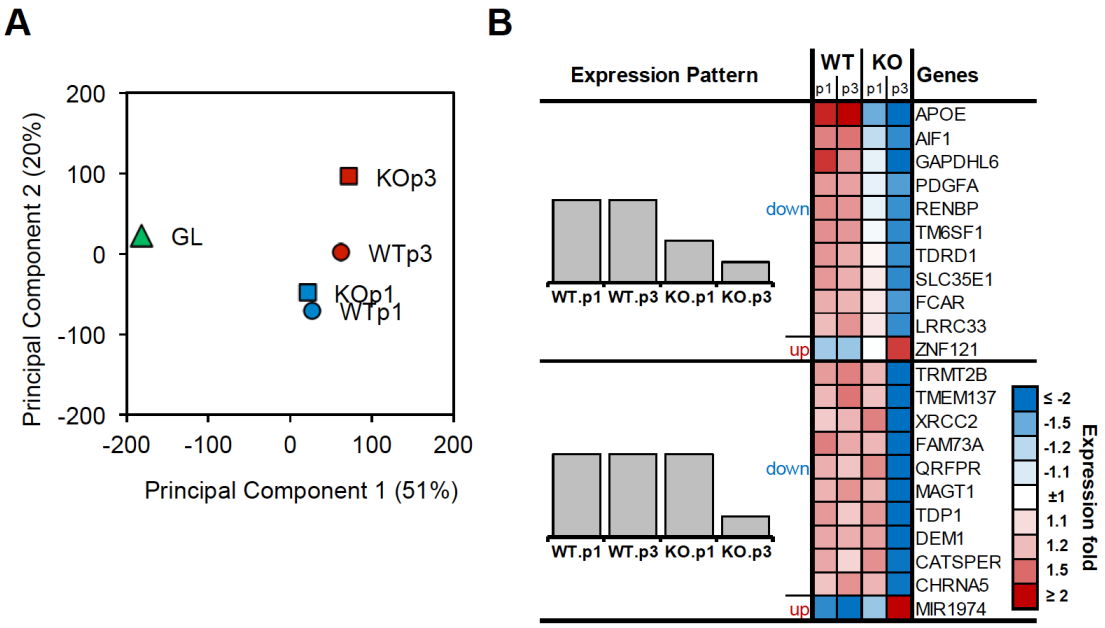

C

Pathways	p value	Regulators	p value
Atherosclerosis signaling	2.8E-08	IFN-γ	3.0E-15
LXR/RXR activation	2.2E-06	IL1-β	3.0E-14
IL-10 signaling	1.7E-04	TNF	9.0E-11
IL-6 signaling	5.4E-04	TGF-β1	6.0E-10
FXR/RXR activation	4.0E-03	IL-17A	2.0E-09
PPAR signaling	5.8E-03	IL-6	1.0E-05

Figure 5-13. Identification of potential molecular targets implicated in FAP-mediated metastatic tumor outgrowth using A549 pulmonary metastasis model. (A) Principal component analysis of samples based on expression of all detected probes. (B) Two expression patterns of interest and heatmap of expression levels of genes that demonstrated the pattern. down=genes that were downregulated at KO.p3, up=genes that were upregulated at KO.p3. Expression fold was calculated vs averaged across samples. (C) Canonical pathways and upstream regulators enriched with 311 genes had an at least 2-fold difference between any two KO/WT samples.

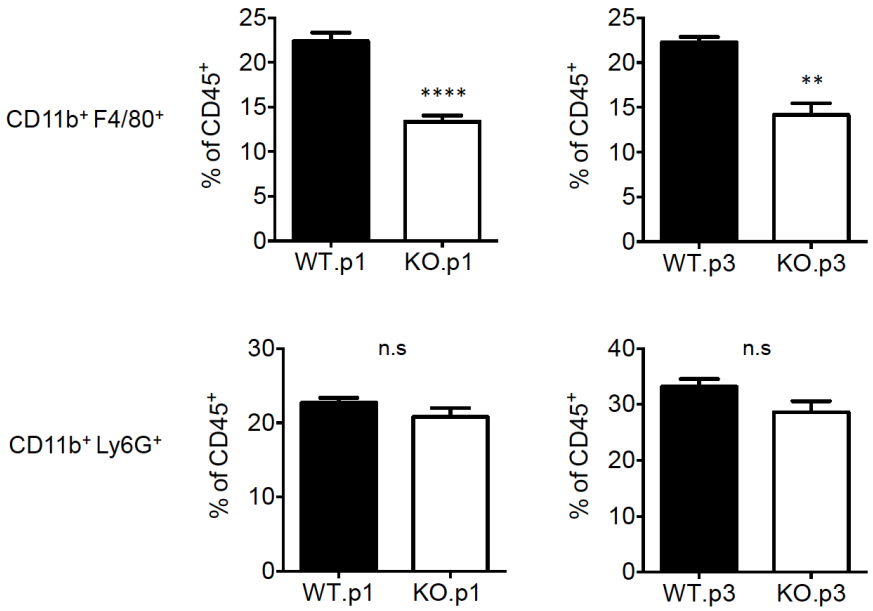

Figure 5-14. FAP-mediated tumor metastatic gene signature is associated with altered macrophage infiltration in A549 pulmonary metastasis. Tumor-infiltrating cells in the serial transplant studies were obtained by dissociation of tumor-bearing lung tissues. Flow cytometry was performed to identify $CD11b^+$ $F4/80^+$ macrophages and $CD11b^+$ $Ly6G^+$ neutrophils. Results are shown as mean ± SEM (n=8 per group in the 1st transplant and n=4-5 in the 3rd transplant); **p<0.01, ****p<0.0001.

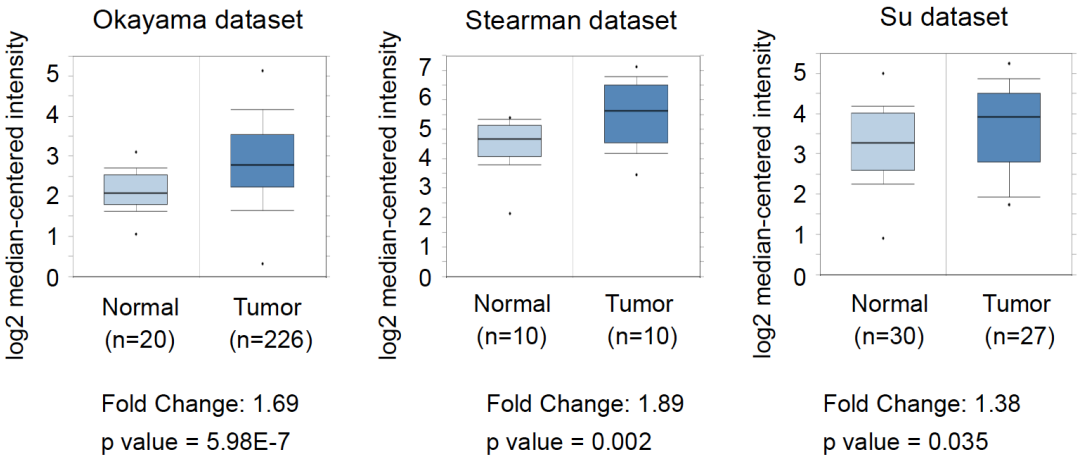

Figure 5-15. APOE is a potential tumor-promoting factor in human lung cancer. Median-centered intensity of APOE expression in three different datasets of human lung adenocarcinomas was obtained from Oncomine. Fold change is presented as relative expression compared with normal lung tissues.

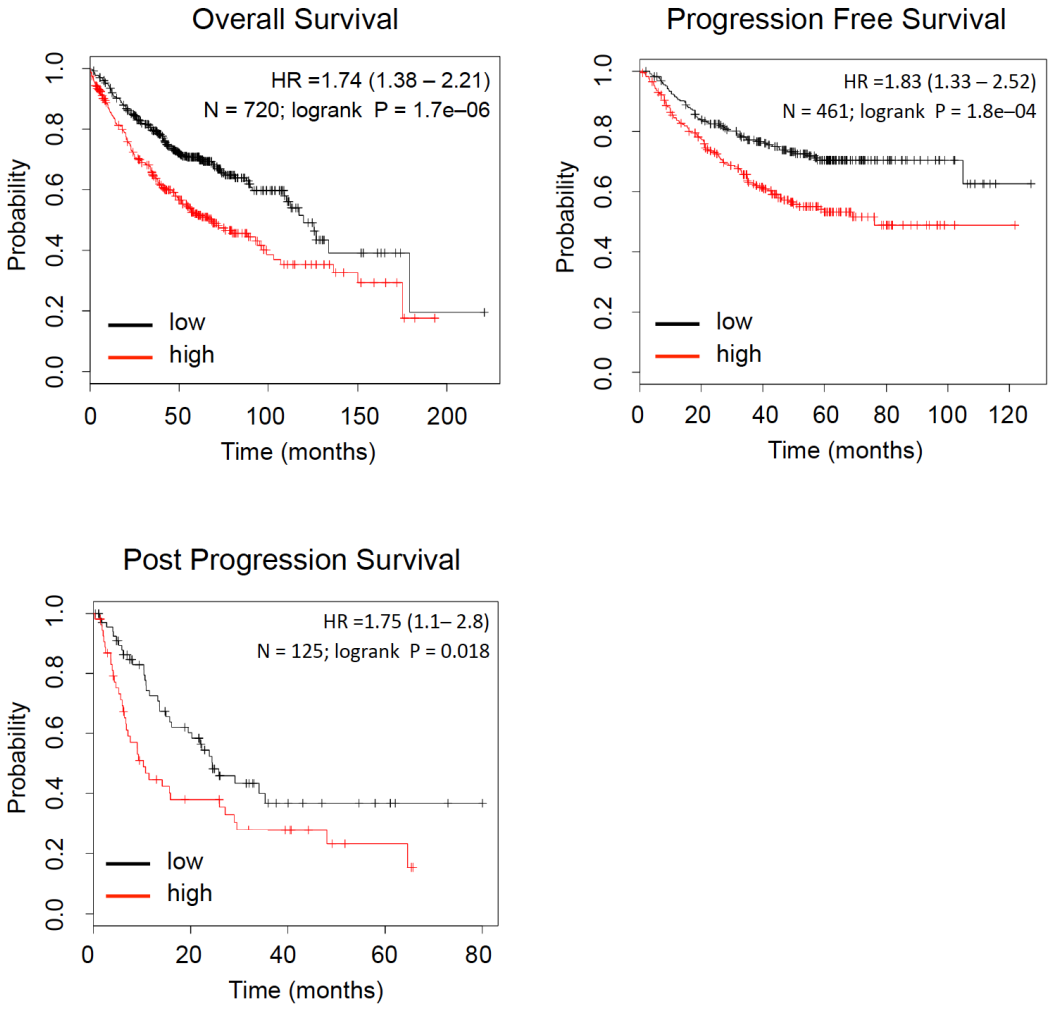

Figure 5-16. APOE is a potential negative prognostic factor in human lung cancer. Kaplan-Meier analysis of overall survival, progression free survival and post progression survival using publicly available lung adenocarcinoma microarray dataset, stratified according to APOE expression. HR = hazard ratio.

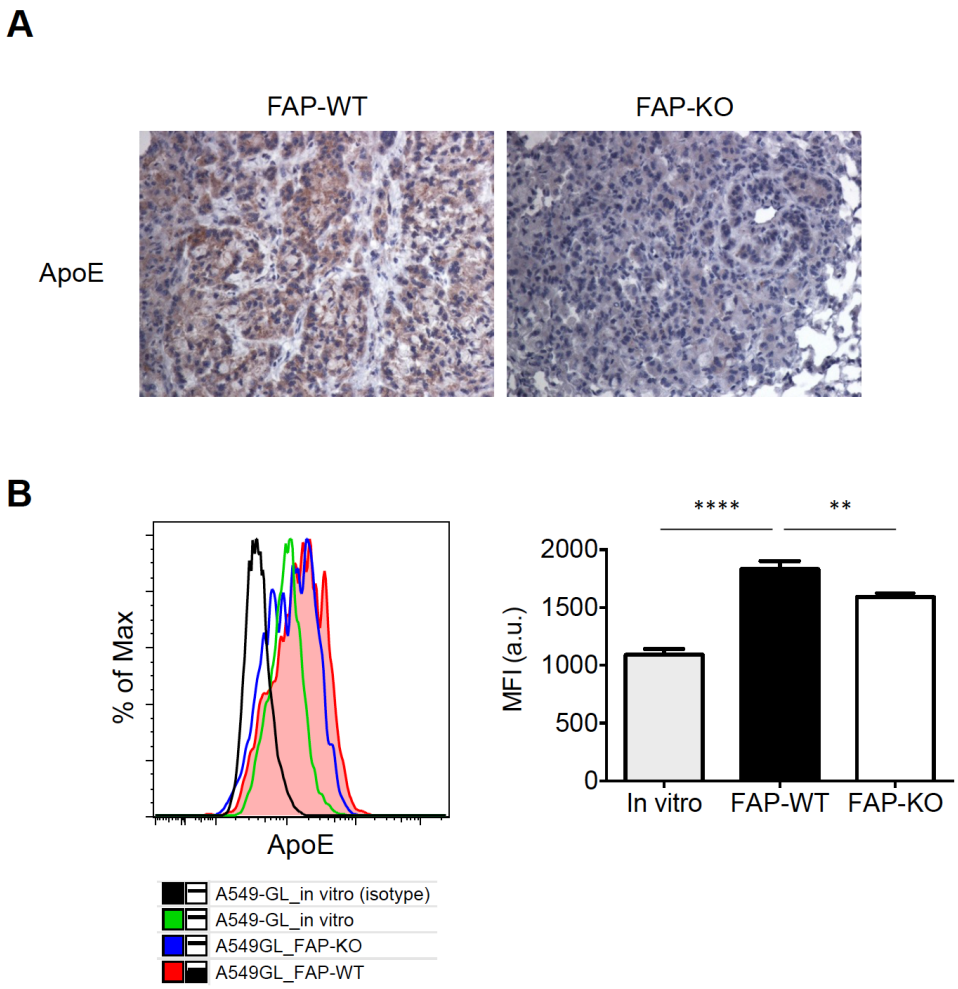

Figure 5-17. APOE expression is down-regulated in A549 tumor cells passaged in FAP-deficient mice. (A) FAP-WT and FAP-KO NSG mice were injected intravenously with A549 cells (n≥6 per group). Tumor-bearing lung tissues were harvested 30 days after tumor-cell transfer and immunohistochemical analysis was performed using anti-APOE antibodies. Representative images demonstrate that APOE is decreased in the FAP-deficient mice. (B) Tumor-bearing lung tissues were harvested and digested with a collagenase cocktail to obtain single-cell suspensions for APOE intracellular staining. Tumor cells from culture were used to demonstrate baseline APOE expression (ie, in vitro). Results are shown as mean fluorescence intensity ± SEM (n=7 per group); **p<0.01.

CHAPTER 6 – Fibroblast activation protein augments autochthonous pancreatic ductal carcinoma progression and metastasis

Introduction

Pancreatic cancer

Pancreatic ductal adenocarcinoma (PDA), characterized by extensive desmoplastic stroma and proinflammatory cell infiltration, has among the worst prognoses of all human malignancies (Hidalgo, 2010; Ryan et al., 2014). Despite significant advancements in surgery, radiotherapy, and chemotherapy, the clinical outcome for PDA remains dismal, with a median survival of less than 6 months and 5-year survival rate of less than 5%. The poor clinical outcome can be attributed to several factors. Firstly, early detection and diagnosis of pancreatic cancer is severely limited by the anatomic location and imaging characteristics of the pancreas, enabling tumors to develop relatively undetected until progression to advanced stages where surgical intervention, considered the only potentially curative therapy, is no longer feasible. Secondly, pancreatic cancer is refractory to chemotherapy as the formation of desmoplastic tumor stroma results in increased tissue solid stress and interstitial fluid pressures, both of which lead to vascular compression and dysfunction, thereby impairing drug delivery into tumors (Jacobetz et al., 2013; Olive et al., 2009; Provenzano et al., 2012; Stylianopoulos et al., 2012). Moreover, the inflammatory and immunosuppressive environment of pancreatic cancer renders it resistant to checkpoint blockade-based immunotherapy (Feig et al., 2013). Currently, PDA is the fourth-leading cause of cancer-related deaths in the United States, and is estimated to rank second by 2020 due to the ageing population and increasing

prevalence of two major risk factors, obesity and diabetes (Rahib et al., 2014). Therefore, thorough understanding of the pathogenesis and therapeutic resistance of PDA is necessary to overcome this devastating disease.

Pancreatic cancer pathogenesis

The mechanisms of pancreatic cancer initiation and progression were originally inferred from analyses of resected clinical specimens (Hruban et al., 2001; Hruban et al., 2004). Histologically, normal pancreatic ducts comprise a single layer of cuboidal ductal epithelial cells with the nucleus localized toward the basal lumen. Invasive pancreatic tumors arise from a spectrum of preneoplastic mucinous lesions with ductal-like morphology, also known as pancreatic intraepithelial neoplasia (PanIN). Based on the morphologic alterations, it can be further categorized into: PanINA, which is characterized by transition from the cuboidal morphology to a columnar phenotype with prominent mucin-containing cytoplasm; PanIN1B, which is characterized by additional papillary projections; PanIN2, which is characterized by significant loss of polarity and moderate nuclear atypia; and PanIN3, also known as carcinoma *in situ*, which is characterized by complete loss of cellular polarity, significant nuclear atypia, and budding of cell clusters into the ductal lumen. Genomics analyses of human PanINs have revealed that disease progression is paralleled by the successive accumulation of genetic mutations, including in *KRAS, TP53*, *CDKN2A* and *DPC4*, which may lead to an increasing degree of nuclear atypia and ultimately development of pancreatic cancer (Feldmann et al., 2007). The earliest detectable mutations identified in human preneoplastic lesions involve the *KRAS* gene (Kanda et al., 2012).

Mouse models of pancreatic cancer

Given the high mutation rate and the importance of KRAS signaling pathways in driving cell proliferation and survival, a genetically engineered mouse model of pancreatic cancer was developed using Cre-*loxP* recombination technology (Sauer and Henderson, 1988). Oncogenic *Kras* ($Kras^{G12D}$) is introduced into the endogenous *Kras* allele along with genetic elements upstream that inhibit transcription and translation (stop cassette) flanked by *LoxP* sites (LSL). Expression of Cre recombinase is targeted to the pancreas through the use of pancreas-specific promoters including *Pdx-1* or *Ptf1a*. This compound strain is designated as KC mouse model. Once the stop cassette is removed by Cre recombinase, oncogenic *Kras* expression is driven by the endogenous promoter at the physiological level. Expression of oncogenic *Kras* in the mouse pancreas stochastically forms preinvasive PanINs with 100% penetrance and that eventually spontaneously progress to PDA, albeit with a prolonged latency (Hingorani et al., 2003). Concomitant targeted expression of point-mutated *Trp53* allele ($Trp53^{R172H}$) in the KC mouse model accelerates pancreatic tumorigenesis and results in the development hemorrhagic ascites and widespread metastases to the liver, lung, mesentery, peritoneum and lymph nodes, as well as inciting a paraneoplastic syndrome that includes cachexia and anemia (Hingorani et al., 2005). This autochthonous pancreatic cancer mouse model, also known as KPC mice, faithfully recapitulates the clinical manifestations, histological features, metastatic profiles, chemoresistance phenotypes and immunological-tolerant hallmarks of PDA, highlighting its utility for mechanistic understanding of the pancreatic cancer biology and the development of therapeutic strategies or early detection methods for this disease.

Further genetically engineered mouse models employing conditional deletion of *Cdkn2a*, *Ink4a*, *Smad4* or *Tgfbr2* tumor suppressors also cooperate with oncogenic *Kras* to drive formation of pancreatic cancer (Aguirre et al., 2003; Bardeesy et al., 2006; Ijichi et al., 2006; Izeradjene et al., 2007; Kojima et al., 2007). Nonetheless, loss of either of these tumor suppressors does not directly induce pancreatic cancer formation, indicating that expression of oncogenic *Kras* is required for pancreatic tumorigenesis within the compound mutant models. Lineage tracing also revealed that despite the ductal appearance of pancreatic cancer lesions, acinar cells instead of ductal epithelial cells might be the origin for most pancreatic tumors (Kopp et al., 2012).

FAP protease and pancreatic cancer

Given the extensive desmoplastic stromal response associated with pancreatic cancer, it is perhaps not surprising that clinicopathological studies demonstrated that expression of fibroblast activation protein (FAP) was associated with worse clinical outcome in PDA patients (Cohen et al., 2008; Shi et al., 2012). Higher FAP expression correlated with lymph node metastasis and increased risk of tumor recurrence and death. A recent study also revealed that FAP protease is important in matrix remodeling to drive pancreatic tumor cell migration through the β1-integrin signaling pathway (Lee et al., 2011). Collectively, these data suggest that FAP protease may regulate pancreatic tumor invasion and/or metastasis. In this chapter, I describe using a genetically engineered mouse model of pancreatic cancer to study the potential impacts of FAP protease on pancreatic tumorigenesis, progression and metastasis.

Materials and methods

Animals

C57BL/6 mice were purchased from Charles River Laboratories, Inc. (Wilmington, MA). FAP-luciferase reporter mice (*Fap*$^{Luc/Luc}$) and FAP-deficient mice (*Fap*$^{DTR/DTR}$) were generated using a targeting construct originally provided by Dr. Andreas Schnapp (Boehringer-Ingelheim, Germany). *Kras*$^{LSL\text{-}G12D/+}$ and *Pdx-1-Cre* C57BL/6 mice were kindly provided by Drs. Sandra Ryeom and Robert Vonderheide, respectively, at University of Pennsylvania (Philadelphia, PA). *Trp53*$^{LSL\text{-}R172H/+}$ mice on a mixed 129/SvJae/C57BL/6 background were acquired from the Mouse Repository at the National Cancer Institute. Mice were backcrossed at least 8 generations onto a C57BL/6 genetic background and interbred to generate triple-mutant mice. Experimental protocols were approved by the Institutional Animal Care and Use Committee and were in compliance with guidelines for the care and use of animals.

Orthotopic pancreatic tumor model

Mice were anesthetized under 2% isoflurane, after which the abdomen was shaved and its skin disinfected. A laparotomy was performed with an approximately 1 cm incision in the left upper quadrant of the abdomen using a sterile scalpel. The peritoneal cavity was exposed with spreaders, and cotton swab sticks were used to displace the intestines to expose the spleen and pancreatic tail for orthotopic tumor injection. 2.5×10^5 PanO2 cells in a volume of 30 μL serum-free medium or medium only were injected using insulin syringes. After injection, all abdominal organs were carefully replaced into the peritoneal cavity using cotton swabs. The peritoneal incision was closed using a continuous chromic

gut 4-0 Vicryl suture (Covidien), followed by an interrupted Sofsilk 6-0 silk suture (Covidien) for the abdominal wall incision. The procedure typically lasted approximately 20 minutes and was well tolerated by all the animals. After the tumor cell implantation, these mice were monitored daily for signs of distress, infection or tumor formation.

Bioluminescence imaging

The IVIS Lumina III Bioluminescence and Fluorescence Imaging System (Perkin Elmer, Waltham, MA) was used for *in vivo* bioluminescent imaging. Pancreatic tumor-bearing mice and animals that underwent sham surgery were injected intraperitoneally with 150mg/kg body D-luciferin (Gold Biotechnology) suspended in PBS. Mice were imaged under isoflurane anesthesia 15 minutes post D-luciferin injection as kinetic studies demonstrated peak bioluminescent intensity of tumors around this time. Bioluminescent signal from tumor cells expressing luciferase was quantified by Living Image software and reported as units of tissue radiance (photons/second).

Ultrasound imaging

High-resolution sonography was performed using the Vevo 2100 imaging system equipped with a 55 MHz MicroScan transducer (Visual Sonics). Mice were enrolled at around 8 to 10 weeks of age for weekly ultrasound scans to detect presence of pancreatic tumors or metastatic disease. Mice were anesthetized under 2% isoflurane and transferred to the imaging stage. Fur was removed from the abdomen using a depilatory cream and the abdomen was swabbed with sterile water to remove any residuals. A thin layer of ultrasound gel was applied over the abdominal area and monitored by the transducer.

Each imaging session lasted 10-15 minutes. Mice were provided with heat support and were monitored until they recovered from anesthesia. Mice with pancreatic tumors underwent further scanning using a 3D motor to acquire serial images at either 0.076 mm (for tumors smaller than 10 mm) or 0.127 mm (for tumors larger than 10 mm) intervals through the entire tumor. Pancreatic tumors were then digitally visualized and reconstructed to determine tumor volumes using the Integrated Vevo Workstation software package. Mice were excluded from the survival study if they developed ulcerated facial or vaginal papillomas, or exhibited large thymic lymphomas. Study endpoint criteria included tumor diameter exceeding 20 mm or mice becoming moribund or showing signs of distress such as anorexia and cachexia.

Histopathological, histochemical and immunofluorescent analysis

The pancreas, pancreatic tumors and visceral organs were harvested, fixed with Prefer (Anatech), dehydrated and paraffin-embedded. Tissue sections were deparaffinized, rehydrated and stained with Masson's tricrhome, Alcian blue or H&E. H&E-stained sections were evaluated by a board-certified pathologist (Elizabeth L. Buza) at the Ryan Veterinary Hospital of the University of Pennsylvania. For each tumor sample, the predominant tumor phenotype (glandular, sarcomatoid or anaplastic) was determined by the presence of greater than 50% of the field of view for each subtype. PanIN lesions were evaluated and scored based on the 10 consecutive high power field (40X) images. For immunofluorescent staining, frozen sections were fixed in acetone, dried, washed with PBS, and incubated with 10% goat serum in 1% BSA/PBS at room temperature for an hour, and then incubated with streptavidin-biotin block (Vector Labs). An F19-FAP

antibody (20 μg/mL) was applied overnight at 4°C and incubated with biotinylated goat anti-mouse IgG antibody (10 μg/mL, Jackson ImmunoResearch) at room temperature for an hour. Bound antibodies were detected with streptavidin-TRITC (3 μg/mL, Jackson ImmunoResearch). Tissue sections were further incubated with an EpCAM antibody conjugated with Alexa488 (10 μg/mL, Cell Signaling) at room temperature for an hour. Nuclei were counterstained with DAPI for 10 minutes and sections were mounted with Slowfade (Thermo Fisher Scientific). Digital images were captured using a Nikon E600 microscope at 20X HPF.

Statistical Analyses

Statistics were calculated using GraphPad Prism 6. For studies comparing two groups, Student's *t*-test was used. For survival and tumor detection studies, log-rank tests were performed. For studies comparing outcomes between two groups, the Chi-square test was used. Data are represented as mean ± SEM. Differences were considered significant when $p < 0.05$.

Results

FAP accelerates tumor progression and decreases survival in a mouse model of pancreatic cancer

To determine whether FAP might be a therapeutic target in pancreatic cancer, we first examined the expression of FAP in clinical specimens. Immunofluorescent staining showed that the stromal cells in pancreatic tumors predominantly expressed FAP, and that expression was much lower in the adjacent pancreatic tissue (**Figure 6-1A**). This selective expression pattern was further confirmed by using *Fap* luciferase reporter mice, demonstrating that while basal FAP expression was detected in the normal pancreatic tissue, FAP was highly expressed in syngeneic pancreatic tumors (**Figure 6-1B**).

Our prior study suggested that FAP deficiency might impair tumor initiation or tumor progression in mutant *Kras*-driven lung tumors; we were therefore interested in whether FAP may also play a critical role in pancreatic cancer development. We employed an autochthonous mouse model of pancreatic cancer to determine if endogenous FAP regulates tumor initiation, progression and/or metastasis. We globally deleted *Fap* alleles by crossing FAP-deficient mice ($Fap^{DTR/DTR}$) with $Kras^{LSL\text{-}G12D/+}$, $Trp53^{LSL\text{-}R172H/+}$ and *Pdx-1-Cre* (KPC) to generate KPC-FAP heterozygous (FAP-Het) and KPC global FAP-deficient (FAP-KO) mice (**Figure 6-3**). Both genotypes of these mice were born at expected Mendelian ratios and appeared phenotypically normal at birth. FAP deletion had no impact on pancreatic development (**Figure 6-2**). We assessed pancreatic tumor formation and found pancreatic tumors arose in both KPC-FAP-Het and KPC-FAP-KO mice, and the number of tumors between these two groups was not different, indicating

that FAP is not essential for pancreatic tumor tumorigenesis driven by oncogenic *Kras* in this model (**Figure 6-6**). Remarkably however, genetic deletion of FAP prolonged the median survival of KPC mice. KPC-FAP-KO mice had a median survival of 192.5 days, compared to a median survival of 153 days for KPC-FAP-Het mice ($p<0.05$) (**Figure 6-4**). Sonographic studies revealed that FAP-deficiency delayed the onset of PDA, shifting the median time to tumor detection from 14.9 to 20.1 weeks ($p<0.05$) (**Figure 6-5**). Furthermore, histological analysis showed a lower frequency of pancreatic intraepithelial neoplasia (PanIN)-2 in 24-week-old KC-FAP-KO compared to KC-FAP-Het mice ($p<0.05$) (**Figure 6-7**). Taken together, these data indicate that FAP is not involved in the initiation of pancreatic cancer development, but rather plays a critical role in disease progression.

FAP augments pancreatic cancer resistance to necrosis and drives tumor metastasis to multiple target organs

Recent studies have shown that pancreatic tumors exhibiting poorly-differentiated and undifferentiated histologies are highly aggressive and lethal. To determine if the delayed onset of pancreatic tumors in the KPC-FAP-KO mice is associated with altered tumor histology, we performed histopathological analyses to assess the composition of the pancreatic tumors. Targeting FAP did not impact the distribution of pancreatic cancer subtypes, as 80% of the tumors in KPC-FAP-Het and KPC-FAP-KO mice exhibited primary ductal structure, while the remainder showed undifferentiated phenotypes (**Figure 6-8**).

Interestingly, sonographic and histopathological analyses revealed that pancreatic tumors from KPC-FAP-KO mice exhibited marked necrotic tumor death relative to the tumors in KPC-FAP-Het mice (**Figure 6-9 and 6-10**). We also noted that this necrotic tumor death induced by FAP deficiency was associated with increased lymphocytic cell infiltration, suggesting that FAP expression may render pancreatic tumors resistant to immune-mediated control of tumor progression.

To determine whether FAP is essential in tumor invasion and metastasis, we examined the metastatic lesions in multiple target organs. At the endpoint, primary tumor weights between the KPC-FAP-Het and KPC-FAP-KO groups were not different (1.60 ± 0.19 versus 1.53 ± 0.31 grams, **Figure 6-11A**). Interestingly, the frequency of tumor invasion and metastasis in multiple organs including liver, lung, mesentery, pleura/peritoneum and lymph nodes was decreased in KPC-FAP-KO mice, indicating FAP may regulate tumor invasion and metastasis (**Figure 6-11B**). In addition, the frequency of both liver and pulmonary macro-metastatic lesion identified at the time of necropsy was reduced in KPC-FAP-KO mice, suggesting that FAP may drive the outgrowth of the metastatic lesions. Collectively, these data indicate that FAP protease activity plays a critical role in the progression and metastasis of pancreatic cancer. The mechanisms underlying this impact of FAP deficiency on the tumor stroma and anti-tumor immunity are currently under further investigation.

Conclusions and discussion

Pancreatic cancer drives the formation of a robust desmoplastic stroma, with stromal cells and the extracellular matrix encompassing up to 90% of the total tumor volume. Stromal elements are highly expressed in clinical specimens and predict poor prognostic outcomes (Infante et al., 2007; Moffitt et al., 2015; Von Hoff et al., 2011; Whatcott et al., 2015). This widely noted stromal reaction has led researchers to emphasize studying the interaction between the tumor cells and the surrounding stromal elements (Kern et al., 2001; Mahadevan and Von Hoff, 2007). Studies employing *in vitro* culture or *in vivo* transplantation approaches have reached to an unambiguous conclusion that various stromal elements can promote pancreatic cancer proliferation, migration, invasion and metastasis (Hwang et al., 2008; Ikenaga et al., 2010; Shields et al., 2011; Xu et al., 2010). These observations, collectively, exemplify one of the hallmarks of cancer in which tumor stroma functions to support the growth of tumor (Hanahan and Weinberg, 2011).

Nonetheless, despite these lines of evidence, results from two studies challenge the current paradigm, demonstrating that stromal elements can also restrain rather than support tumor progression, at least in pancreatic cancer (Ozdemir et al., 2014; Rhim et al., 2014). Pancreas-specific deletion or pharmacological targeting of Sonic hedgehog (Shh), a soluble ligand overexpressed by pancreatic tumor cells critical for driving formation of a desmoplastic stroma, was shown to reduce stromal contents in autochthonous pancreatic tumors. However, Shh-deficient tumors developed earlier and were more aggressive, exhibiting undifferentiated histology and heightened levels of angiogenesis and proliferation. Administration of VEGFR blocking antibody improved

survival of Shh-deficient tumor-bearing mice, indicating that Hedgehog-driven stromagenesis suppresses tumor growth in part by restraining tumor angiogenesis (Rhim et al., 2014). Specific ablation of SMA^+ myofibroblasts in two autochthonous mouse models of pancreatic cancer resulted in minimal tumor growth reduction and exhibited higher mortality rate. Deletion of SMA^+ myofibroblasts was shown to promote tumor aggressiveness by inducing hypoxia, EMT and immune suppression in primary tumors, as well as increasing tumor emboli found in lung tissue. Treatment of anti-CTLA4 immunotherapy reversed disease acceleration and prolonged animal survival in the SMA^+ myofibroblasts depleted pancreatic tumors (Ozdemir et al., 2014). Together, these studies raise substantial concerns as to whether targeting the tumor stroma remains an encouraging therapeutic approach for pancreatic cancer.

My studies described in this chapter reveal that stromal FAP protease is important in pancreatic tumor progression. Specifically genetic deletion of FAP delayed the progression of pancreatic preneoplastic lesions and tumor formation. FAP deficiency did not impact pancreatic development or function. Importantly, FAP deficiency induced pancreatic tumor necrosis and impeded pancreatic tumor metastasis and outgrowth in multiple target organs. These findings support targeting FAP protease as a promising approach to treat pancreatic cancer. The mechanisms underlying the impact of FAP protease on the ECM remodeling, angiogenesis, inflammatory and immune response are currently under further investigation. My investigation will specifically focus on following key FAP-proteolysis dependent factors including collagen, TGFβ, CCL2 and

CXCL12/SDF-1α that play critical roles for stromagenesis, ECM remodeling, and macrophage and T-cell recruitment to impact tumor progression, invasion and metastasis.

The ECM provides essential signals to maintain tissue polarity and architecture, as well as regulating cell growth and turnover. In the appropriate context, the ECM is sufficient to restrain tumorigenesis (Bissell and Hines, 2011). For instance, accumulation of high molecular weight HA has been reported to protect naked mole rats against cancer by impeding malignant transformation (Tian et al., 2013). Additionally, expression of type III collagen has been shown to restrain spontaneous tumor development and inhibit the growth and metastasis of transplanted breast tumors by regulating ECM remodeling (Brisson et al., 2015). However, during tumor development and progression, the ECM becomes deregulated and disorganized resulting in the generation of distinct biochemical and biophysical signals that drive tumor proliferation, migration, invasion and metastasis (Bonnans et al., 2014; Pickup et al., 2014).

In primary pancreatic tumors, extracellular matrix deposition, such as collagen and HA, was shown to negatively correlate with patient survival. Moreover, both primary tumors and metastases of pancreatic cancer exhibited stromal fibrosis (Whatcott et al., 2015). These observations indicate that aberrant desmoplastic response may impact progression of primary tumor as well as distant metastasis. Interestingly, FAP protease-mediated remodeling of the tumor stroma was shown to promote tumor cell migration, suggesting that FAP protease may regulate early steps of the metastasis cascade i.e. tumor cell dissemination and/or invasion (Lee et al., 2011). This may in part explain our data

showing the frequency of pancreatic cancer metastasis to multiple target organs is reduced in FAP-deficient KPC mice. Future studies utilizing three-dimensional organotypic culture with fibroblast or fibroblast-derived matrix will inform whether FAP protease is essential for tumor invasion and dissemination. Another, not mutually exclusive explanation is that FAP protease play a crucial role in formation of a premetastatic niche. It will therefore be interesting to examine FAP expression level in metastasis target organs at the preneoplastic stage and determine whether disruption of FAP protease will alter the matrix modeling thereby inhibits malignant cell seeding. Furthermore, the presence of macroscopic liver and pulmonary metastases is less frequent in FAP deficient KPC mice, indicating FAP protease may drive the outgrowth of the metastatic lesions. Our prior studies indicate that disruption of FAP protease inhibits pulmonary metastatic outgrowth and this inhibition correlates with reduced macrophage infiltration, which may be due to down-regulation of CCL2 from FAP-deficient CAFs (Koczorowska et al., 2016). Further studies are required to determine if this mechanism can be extended to the pancreatic cancer metastasis.

The immune surveillance program has great potential to identify and destroy nascent tumors, thereby functions as a primary defense against cancer. Nevertheless, tumors evolve multiple strategies to prevent the generation of an effective anti-tumor immunity. In pancreatic cancer, one of such tumoral immune suppression mechanism is exclusion of effector T cells from neoplastic cells orchestrated by the desmoplastic stroma. Evidence suggests that the extracellular matrix is a contributing factor that presents a physical barrier that impairs T cell infiltration, migration and engagement with tumor cells, as

treatment with collagenase has been demonstrated to enhance T-cell mobilization to the vicinity of tumor nests (Salmon et al., 2012). Moreover, based on investigations of human pancreatic tumor specimens and the tumors-derived from KPC mice, activated pancreatic stellate cells (PSCs) was shown to reduce migration of $CD8^+$ T cells to juxtatumoral stromal compartments, thereby preventing the access of $CD8^+$ T cells to cancer cells. SDF-1α/CXCL12 secreted by activated PSCs was then identified as the key mediator that drive the $CD8^+$ T cells chemotaxis towards PSCs *in vitro*. Molecular targeting of SDF-1α/CXCL12 or pharmacological treatment of activated PSCs with all-trans retinoic acid (ATRA), a drug that rendered PSCs quiescent, abrogated $CD8^+$ T cells chemotaxis towards PSCs. Notably, ATRA treatment enhanced $CD8^+$ T cells infiltration to the proximity of the neoplastic cells in tumor-bearing KPC mice (Ene-Obong et al., 2013). In contrast to the theory mentioned above, it has been proposed that SDF-1α/CXCL12 derived from FAP^+ stromal cells could bind to the high mobility group box 1 (HMGB1) expressed by pancreatic cancer cells, and therefore excluded T cells from neoplastic cells through an unknown mechanism. Nonetheless, inhibition of CXCR4, a receptor of SDF-1α/CXCL12, by AMD3100 induced rapid T-cell accumulation among cancer cells and potentiated the efficacy of checkpoint-blockade based immunotherapy to restrain growth of pancreatic tumors (Feig et al., 2013). Based on these observations, it is interesting to address whether FAP protease is involved the regulation of T cell-exclusion in pancreatic tumors. Prior studies revealed that FAP could mediate proteolytic processing of SDF-1α/CXCL12 by its DPP acitivity (Keane et al., 2011). Truncated SDF-1α/CXCL12 (residues 3–68) was shown to act as an antagonist, losing both lymphocyte chemotactic and CXCR4-signaling properties (Proost et al., 1998). Therefore, we

hypothesize that disruption of FAP protease activity may permit T-cell recruitment and infiltration into pancreatic tumors. Preliminary histopathological observations suggest that the heightened necrotic death noted in FAP-deficient primary pancreatic tumors is associated with increased lymphocytic cell infiltration. Further immunohistochemical staining and flow cytometry analysis will be performed to better characterize immune and inflammatory cell infiltrates in tumors derived from KPC-FAP-Het and KPC-FAP-KO mice.

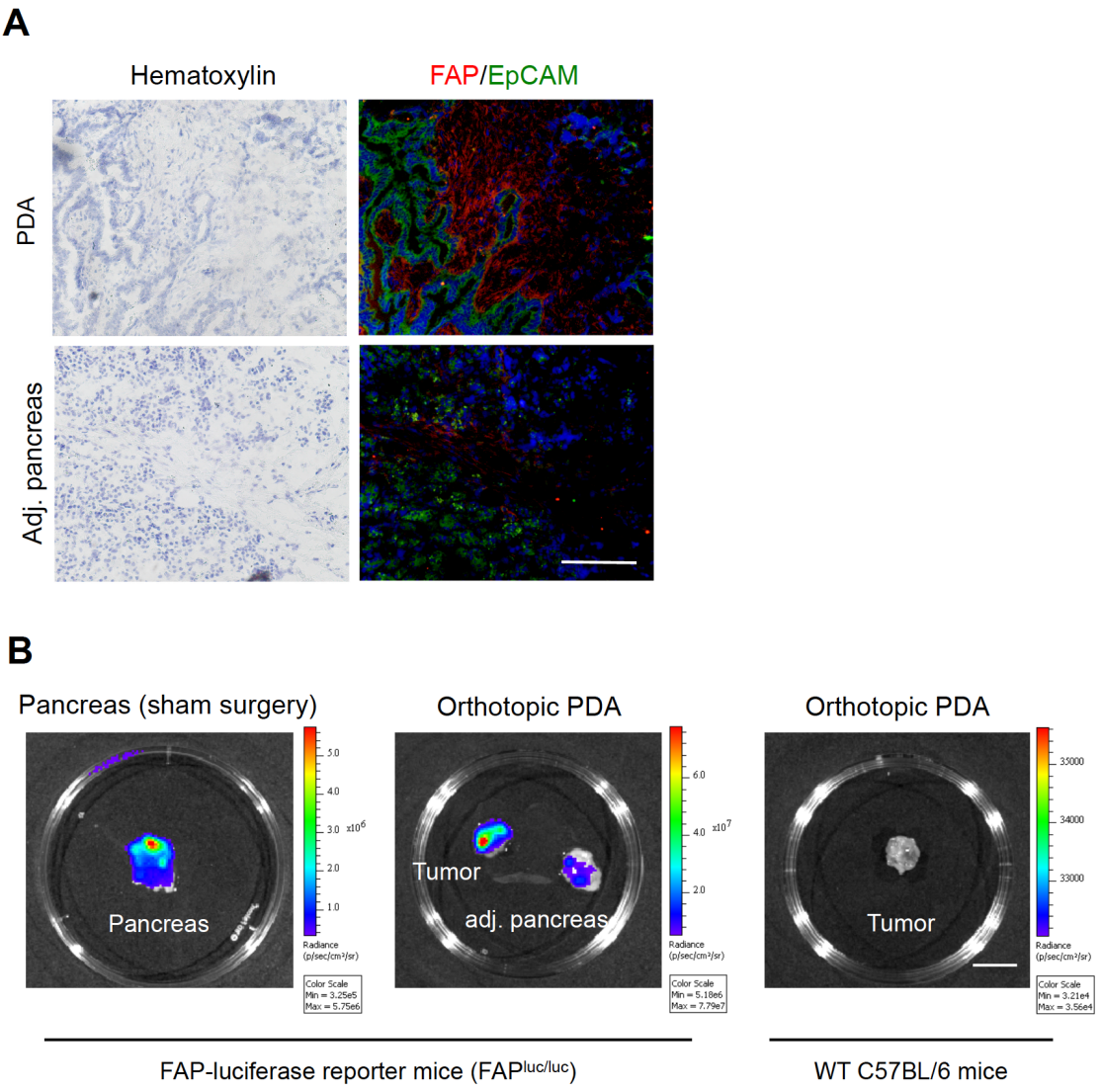

Figure 6-1. FAP is overexpressed in pancreatic ductal adenocarcinoma. (A) Human pancreatic tumors and adjacent normal pancreatic tissues were subjected to hematoxylin and immunofluorescent staining with FAP and EpCAM; scale: 100 μm. (B) FAP luciferase reporter knock-in or wild-type C57BL/6 mice were orthotopically implanted with syngeneic PanO2 pancreatic cancer cells or serum-free medium (sham surgery) into the tail of the pancreas. Tumor and adjacent pancreatic tissues were harvested and subjected to bioluminescent imaging; scale: 1 cm.

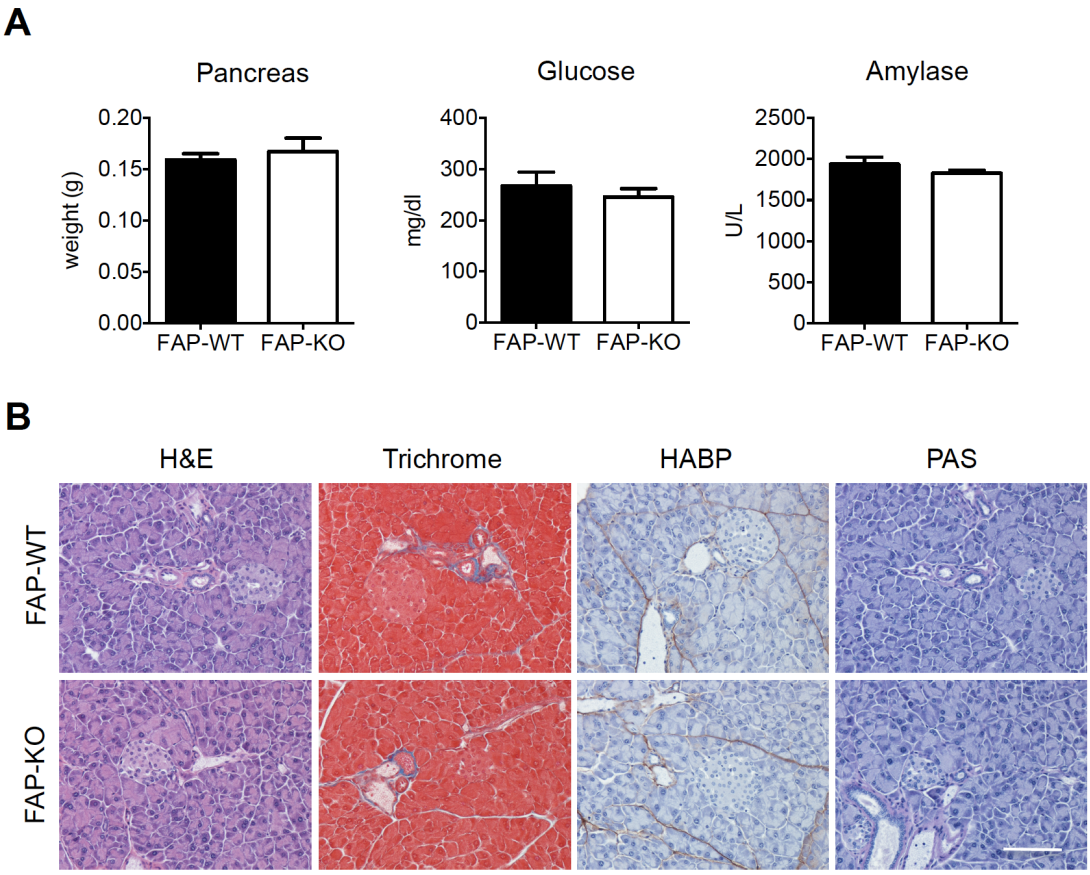

Figure 6-2. FAP is dispensable for pancreatic development. (A) The pancreas was harvested from FAP-WT and FAP-KO C57BL/6 mice and weighed. Serum glucose and circulating amylase levels were measured. Results are shown as mean ± SEM (n=6). (B) Representative hematoxylin and eosin (H&E), trichrome, hyaluronan-binding peptide (HABP) and periodic acid–Schiff (PAS)-stained pancreas from FAP-WT and FAP-KO C57BL/6 mice; scale: 100 μm. No statistical significance was found.

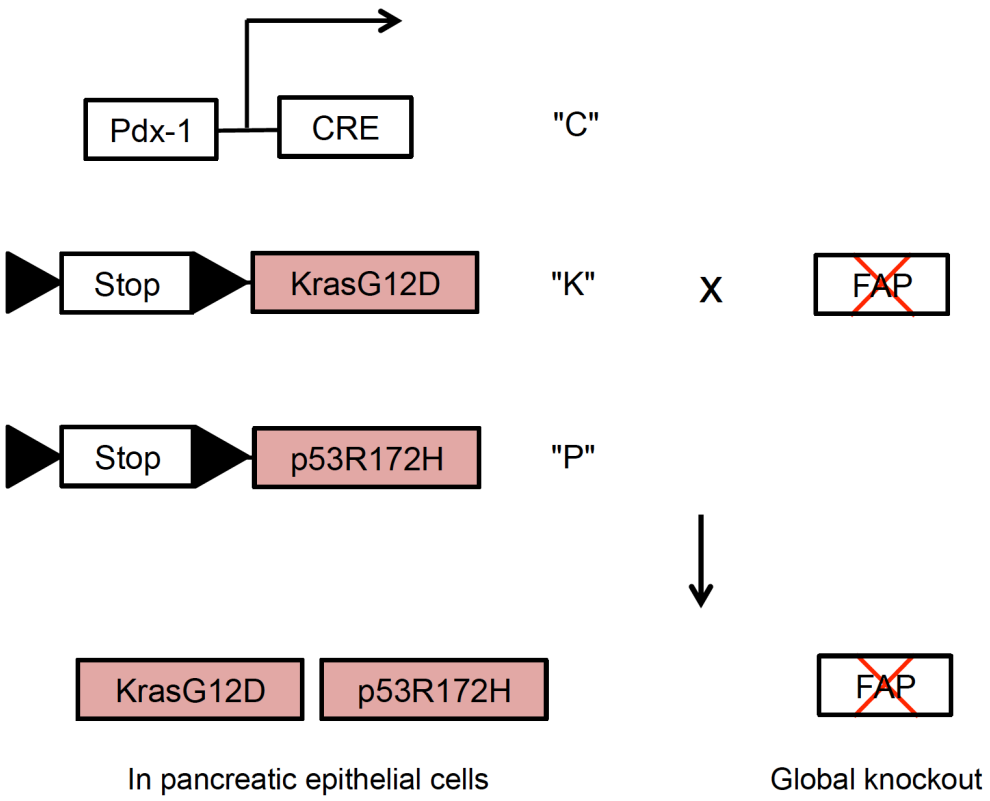

Figure 6-3. Genetic targeting of FAP in a preclinical mouse model of pancreatic ductal adenocarcinoma. *LSL-Kras*$^{G12D/+}$, *LSL-Trp53*^{R172H} and *Pdx-1-Cre* (KPC) mice were crossed with FAP-deficient mice to generate KPC-FAP heterozygous (FAP-Het) and KPC global FAP-deficient (FAP-KO) mice. Mice were backcrossed to the C57BL/6 background for at least 8 generations prior to enrollment in the experiment.

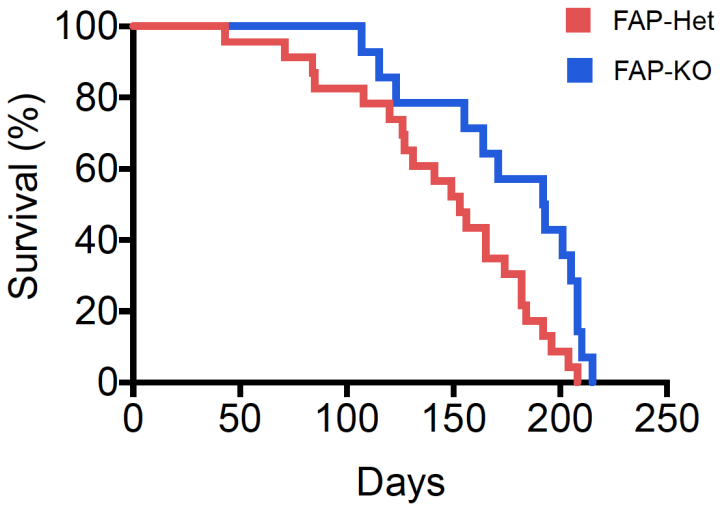

Figure 6-4. FAP protease reduces survival of KPC mice. Kaplan-Meier survival curves of KPC FAP-Het (n=23) and KPC FAP-KO (n=14) mice. All mice eventually succumbed to pancreatic cancer-related morbidity and mortality. KPC-Het mice have a median survival of 153 days, while KPC FAP-KO mice have a median survival of 192.5 days, log-rank test *$p<0.05$.

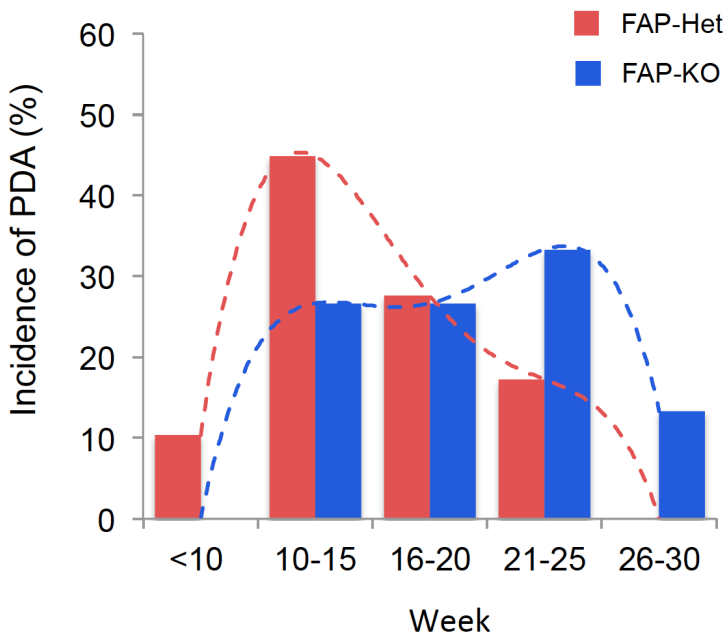

Figure 6-5. FAP protease promotes development of pancreatic ductal adenocarcinoma. KPC FAP-Het (n=29) and KPC FAP-KO (n=15) mice underwent sonographic examination to evaluate for pancreatic ductal adenocarcinoma. KPC-Het mice have a median time to tumor detection at 14.9 weeks of age, while KPC FAP-KO mice have a median time to tumor detection at 20.1 weeks of age, log-rank test: *$p<0.05$.

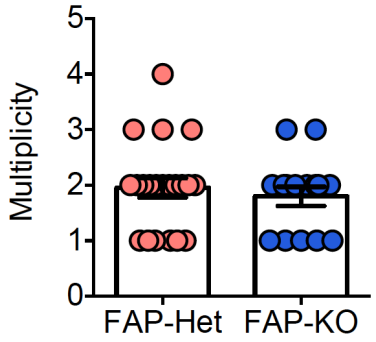

Figure 6-6. Targeting FAP does not impact the multiplicity of pancreatic tumors. The number of tumors in the KPC FAP-Het and FAP-KO mice was assessed during ultrasound scanning. Results are shown as mean ± SEM; Student T test for demonstrates no significance.

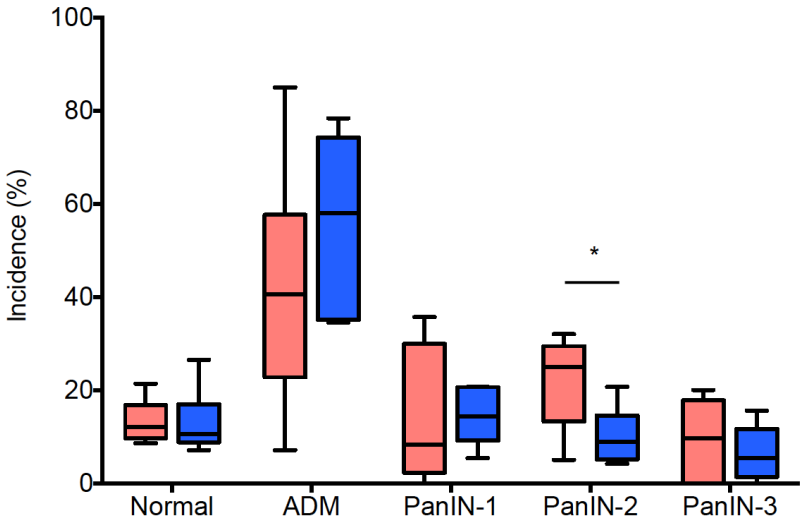

Figure 6-7. Targeting FAP delays the progression of pancreatic intraepithelial neoplasia (PanIN). Pancreas from KC FAP-Het and KC FAP-KO mice at 24-week-old were harvested for histopathological analysis. H&E stained pancreas tissues were assessed by a board-certified pathologist at the Ryan Veterinary Hospital of the University of Pennsylvania. ADM: acinar to ductal metaplasia. Results are shown as box-and-whisker plots (n=6 per group), *$p<0.05$.

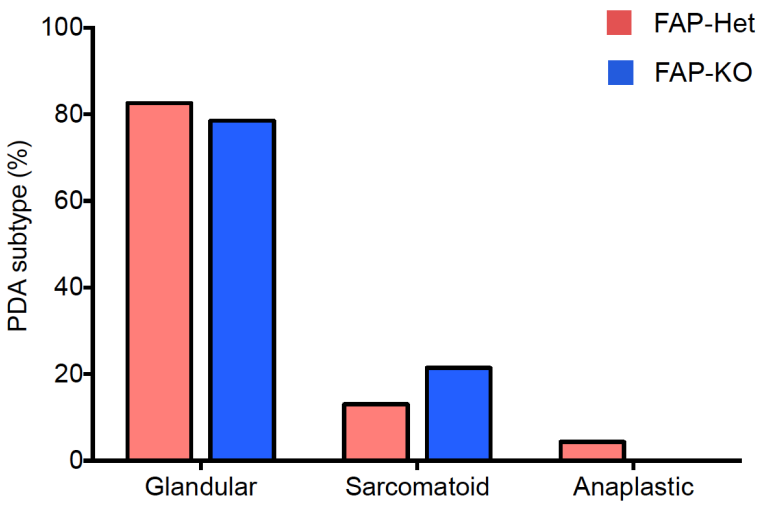

Figure 6-8. Targeting FAP does not impact the distribution of pancreatic tumor subtypes. Pancreatic tumors derived from KPC FAP-Het (n=23) and KPC FAP-KO (n=14) mice exhibit a mix of histological phenotypes (subtypes): glandular type, sarcomatoid type and anaplastic type. The predominant histology of each tumor is defined by the presence of more than 50% of a subtype within each sample as determined by a board-certified pathologist at the Ryan Veterinary Hospital of the University of Pennsylvania. Chi-square test for trend demonstrates no significance.

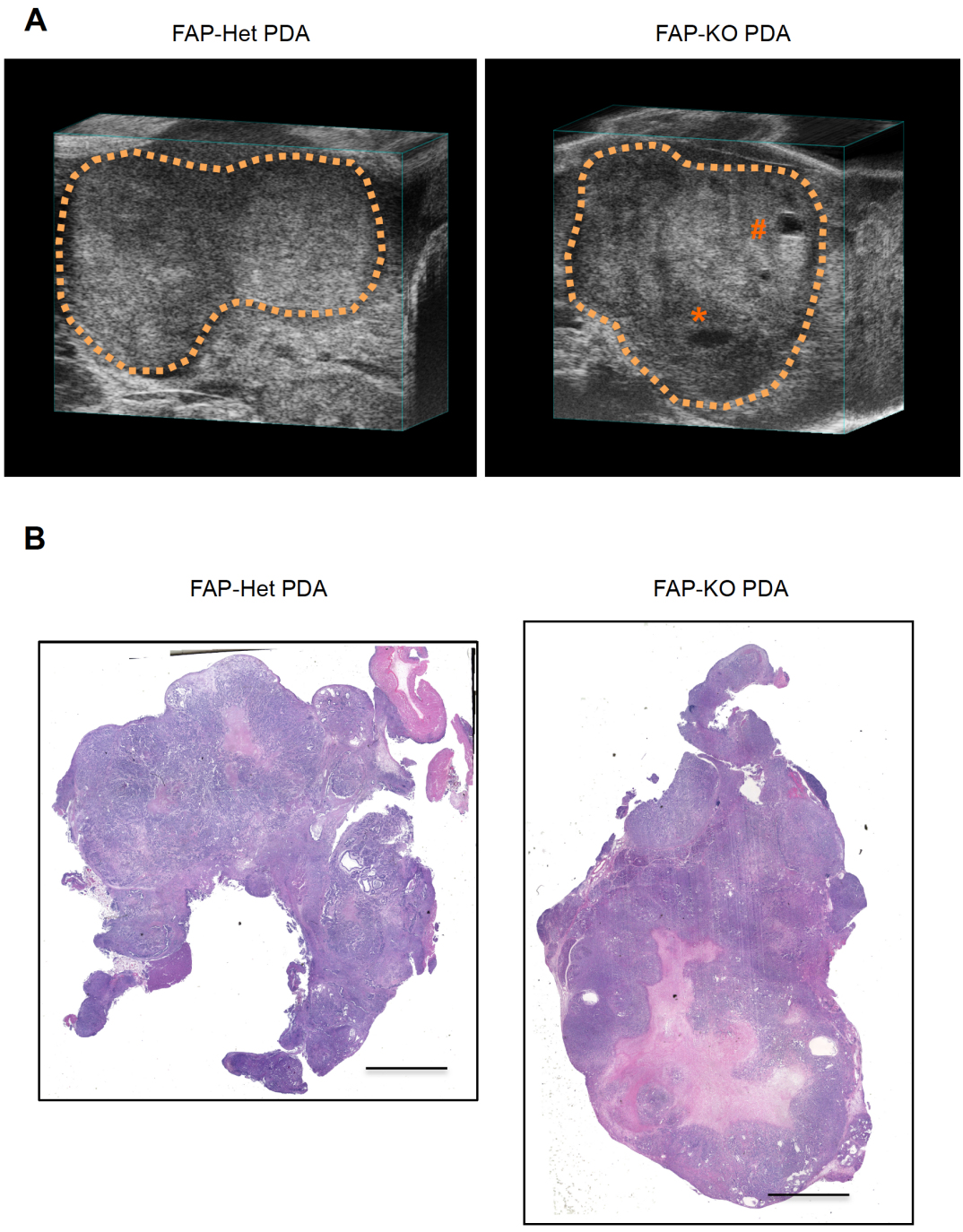

Figure 6-9. Targeting FAP alters internal tumor architecture associated with necrotic cell death. (A) Representative ultrasound images of the pancreatic tumors derived from KPC FAP-Het and KPC FAP-KO mice; * and # indicate tumor necrosis and a small cyst within the tumor, respectively. (B) Tumors were harvested at the endpoint and stained with H&E, scale: 0.5 cm.

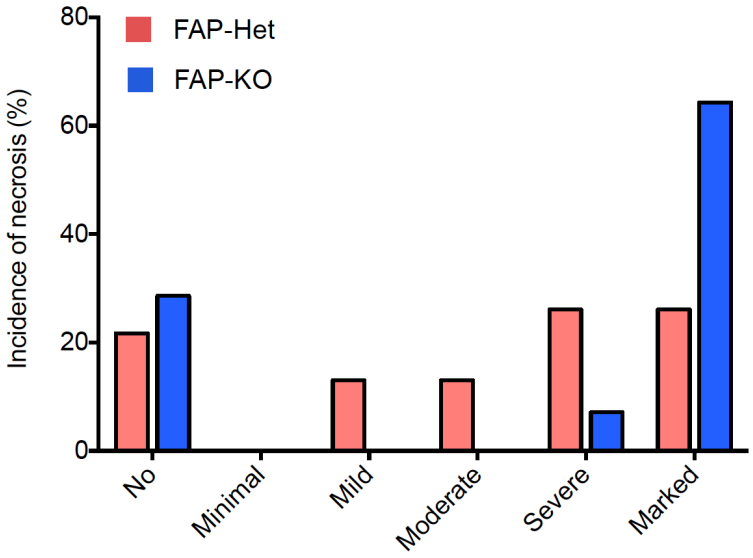

Figure 6-10. Targeting FAP results in pronounced tumor necrosis. Pancreatic tumors derived from KPC FAP-Het (n=23) and KPC FAP-KO (n=14) mice were stained with H&E. The degree of necrosis within each tumor was assessed by a board-certified pathologist at the Ryan Veterinary Hospital of the University of Pennsylvania. In the cases that exhibit various degrees of necrosis, statistical analysis was performed using the Chi-square test for trend: ***$p<0.0001$.

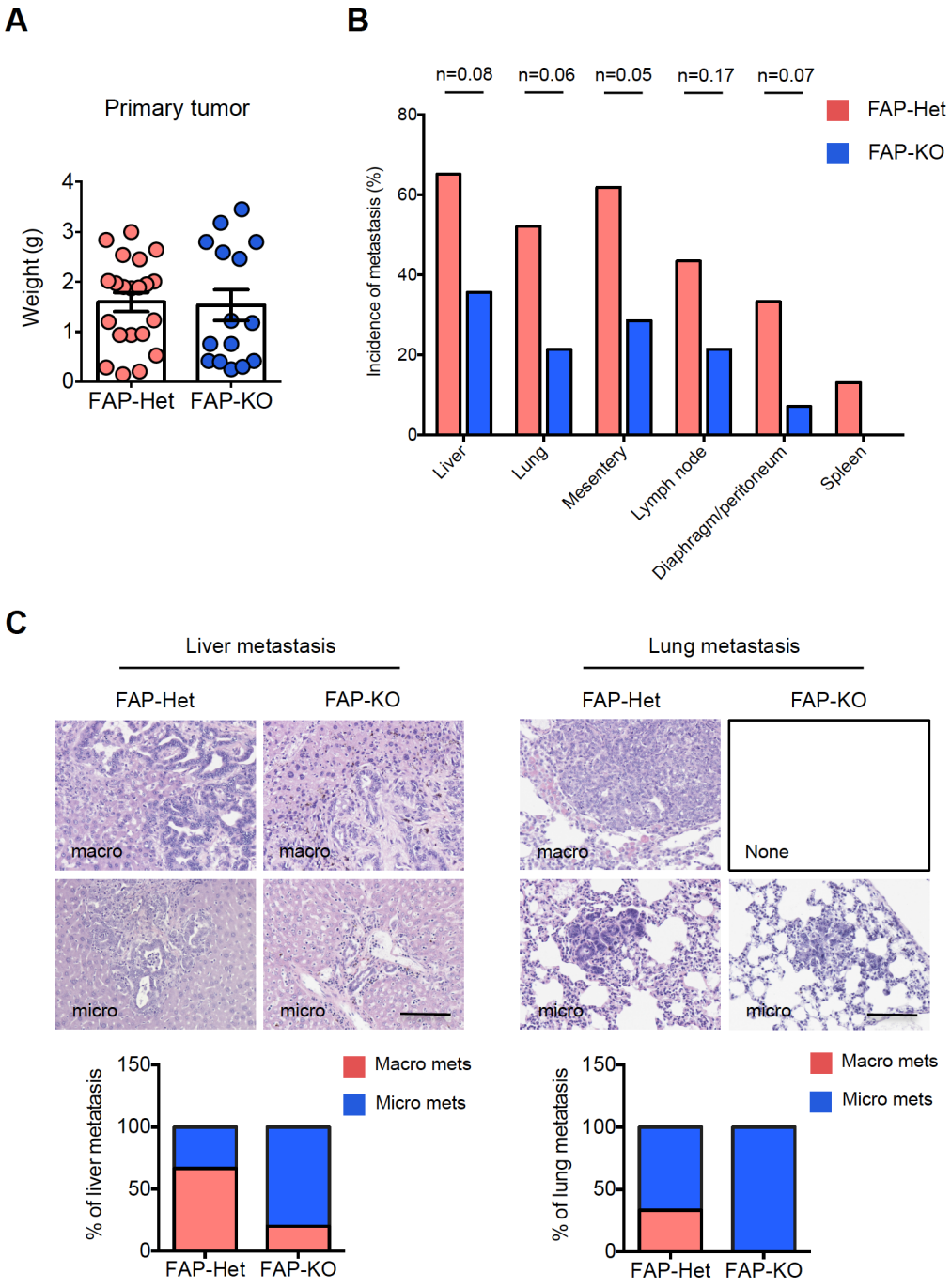

Figure 6-11. Targeting FAP impedes pancreatic cancer metastasis. (A) Pancreatic tumor weight of KPC FAP-Het and FAP-KO mice at the endpoint or death (B) Metastases in multiple organs from KPC FAP-Het (n=23) and KPC FAP-KO (n=14) mice were evaluated at necropsy and further confirmed by H&E staining. Chi-square test. (B). Liver and lung metastases were further categorized into presence of macroscopic lesions found at necrospy and micro-metastases identified by H&E staining. Scale: 100 μm.

CHAPTER 7 – Conclusion and future directions

Solid tumors are abnormal organs composed of dysregulated parenchymal tissues, mesenchymal stromal cells and connective tissue stroma. Accumulation and reprogramming of these cancer-associated mesenchymal stromal cells induces tumor desmoplasia, angiogenesis, inflammation and immune suppression, thereby contributing to tumor progression, metastasis and therapeutic resistance. Based on the tumor-promoting functions and the therapeutic resistance conferred by tumor stroma, it has been hypothesized that destruction of stromal cells and/or disruption of molecular stromal cell/ECM-dependent pathways would inhibit tumor growth and augment efficacy of other therapeutic modalities (Bhowmick et al., 2004b; Jacob et al., 2012; Kalluri and Zeisberg, 2006; Ohlund et al., 2014). Even though many studies indicate that cancer-associated mesenchymal stromal cells are functionally distinct from their normal counterparts, which is essential for inhibiting tumorigenesis and malignant progression, it is important to keep in mind the heterogeneity and potential plasticity of this compartment (Augsten, 2014; Jacob et al., 2012; Kalluri and Zeisberg, 2006; Ohlund et al., 2014; Scherz-Shouval et al., 2014; Waterman et al., 2012). Distinct mesenchymal stromal cell subpopulations may have opposing impacts on tumor growth, progression and metastasis. Subpopulations of cancer-associated mesenchymal stromal cells may retain activity of certain molecular pathways that can inhibit tumor progression (Chang et al., 2012). Based on these observations, it is possible that depletion of specific stroma cell subpopulations may have either therapeutic or detrimental effects. This impact may also depend on tumor type, stage of tumor progression, and variation in the degree of desmoplasia and tumor

immunogenicity. Therefore, careful investigation of the impact of distinct subpopulations on tumor progression and delineation of their roles in regulating desmoplasia, angiogenesis and anti-tumor immunity are required to inform the rational design of stromal cell-targeted therapies.

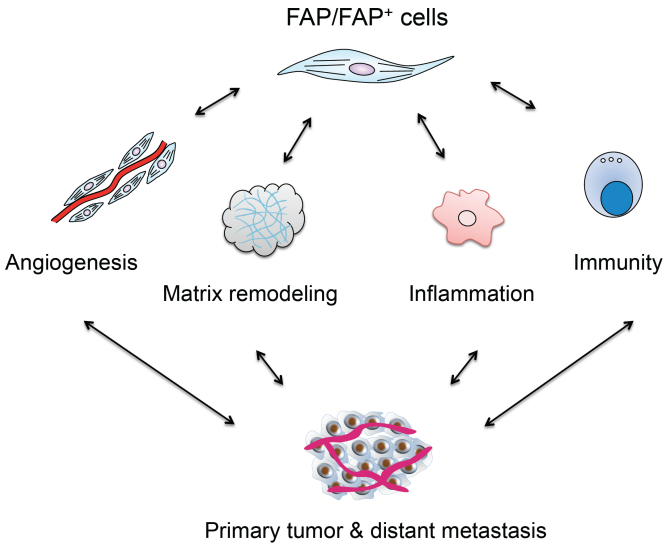

Figure 7-1. FAP/FAP$^+$ stromal cells modulate several aspects of tumor microenvironment to promote tumor progression and metastasis.

In the above chapters, I described how FAP-expressing cancer-associated stromal cells accumulate in various primary tumors and metastatic diseases and how FAP$^+$ stromal cells may drive tumor progression by themselves and/or through FAP protease activity. Conditional depletion of intratumoral FAP$^+$ stromal cells by FAP-CAR T cells inhibits tumor growth without causing systemic toxicity in multiple syngeneic transplanted tumors, xenografts and an autochthonous tumor model, suggesting that a therapeutic opportunity exists for FAP-CAR T-cell therapy. Notably, combination therapy with tumor antigen vaccination or chemotherapy can augment the therapeutic efficacy of FAP-CAR T-cell therapy. It is therefore critical to develop a human FAP knock-in mouse

model to assess the efficacy and toxicity profile of human FAP-CAR T cells before taking this approach to the clinic. In addition, my observation that tumors exhibit various degrees of desmoplasia raises several fundamental questions about the essence of the tumor desmoplastic response. For instance, what is the basis of the tumor desmoplastic response driven by FAP^+ stromal cells? Do tumors recruit the FAP^+ stromal cells and/or induce a fibroproliferative response *in vivo*? Meanwhile, targeting FAP protease activity using FAP-deficient mice also demonstrates that FAP plays a central role in pancreatic cancer progression and metastasis to multiple target organs as well as pulmonary metastases from various primaries. Although the mechanistic investigations are still underway, my studies suggest that targeting FAP protease may have the potential to impede tumor cell colonization and metastatic tumor outgrowth. In summary, I propose that FAP^+ stromal cells and FAP protease are promising treatment targets and warrant further investigation as a potential therapeutic approach for a variety of solid tumors.

As eluded earlier that the conventional view for cancer-associated stromal cells is their net pro-tumorigenic effects, nevertheless, two recent studies targeting Sonic hedgehog (Shh)-driven stromagenesis or SMA^+ myofibroblasts accelerated tumor progression and aggressiveness, thereby increasing morbidity and mortality in mouse models of pancreatic cancer (Ozdemir et al., 2014; Rhim et al., 2014). Mechanistic investigations demonstrated that Shh deficiency enhanced tumor angiogenesis and tumor cell proliferation; administration of VEGFR blocking antibody reversed malignant progression of Shh-deficient tumors (Rhim et al., 2014). Deletion of SMA^+ myofibroblasts induced hypoxia, EMT and Treg infiltration-mediated immune

suppression; treatment of anti-CTLA4 immunotherapy blocked tumor progression and prolonged survival of the SMA^+ myofibroblasts depleted pancreatic tumor-bearing animals (Ozdemir et al., 2014). Although it remains to be investigated whether those finding can be extended to other tumor types, these studies raise great concerns as to whether targeting the tumor stroma remains a suitable therapeutic approach for cancer treatment, at least for pancreatic cancer.

It is also important to note that depletion of terminally differentiated SMA^+ myofibroblasts in prior study did not alter the prevalence of FAP^+ stromal cells in pancreatic tumors (Ozdemir et al., 2014), consistent with our findings that FAP and SMA identify distinct subsets of stromal cells, with few overlapping population in either mouse or human pancreatic tumors. Moreover, analyses of matrix components in the stromal cell depletion studies indicate that while both FAP^+ and SMA^+ stromal cells regulate intratumoral collagen content, only FAP^+ stromal cells are important for the maintenance of intratumoral HA. Finally, in contrast to the immune suppression effects induced by depletion SMA^+ myofibroblasts, we and others demonstrated deletion of FAP^+ stromal cells could augment anti-tumor immunity to inhibit tumor growth (Arnold et al., 2014; Feig et al., 2013; Kraman et al., 2010; Wang et al., 2014b). Therefore, these data suggest that SMA^+ and FAP^+ stromal cells may differentially regulate tumorigenesis.

In addition to developing therapeutic strategies aiming to deplete specific stromal cell population or disrupt particular molecular stromal cell/ECM-dependent pathways, an emerging concept is to reprogram cancer-associated mesenchymal stromal cells back to

their normal homeostatic quiescent state where they may regain their tumor suppression ability and reduce therapeutic resistance induced by tumor stroma. This important new paradigm was evolved from two recent studies demonstrating the usage of Vitamin D receptor (VDR) agonists to reprogram hepatic and pancreatic stellate cells expressing VDR in context of liver fibrosis and pancreatic cancer, could reduce desmoplasia and inflammation (Ding et al., 2013; Sherman et al., 2014). The VDR-mediated pancreatic stellate cell reprogramming resulted in increased gemcitabine delivery and reduced tumor volume in autochthonous pancreatic tumors. Notably, use of the VDR agonist resulted in a 57% increase in the survival of tumor-bearing animals as compared to gemcitabine treatment only (Sherman et al., 2014). Thus, conversion of the tumor stroma to a state that is more common of normal homeostasis, such as would occur naturally during the completion of wound healing response (Dvorak, 1986; Dvorak, 2015), may be critical for restraining tumor growth and inhibiting therapeutic resistance. Future mechanistic investigations of the stromal reprogramming and identifying the factors that govern the functional and phenotypic switch of reactive tumor stroma may hold significant promise in combating cancer.

CHAPTER 8 – References

Acharya, P. S., Zukas, A., Chandan, V., Katzenstein, A. L., and Pure, E. (2006). Fibroblast activation protein: a serine protease expressed at the remodeling interface in idiopathic pulmonary fibrosis. Hum Pathol *37*, 352-360.

Aguilera, K. Y., Rivera, L. B., Hur, H., Carbon, J. G., Toombs, J. E., Goldstein, C. D., Dellinger, M. T., Castrillon, D. H., and Brekken, R. A. (2014). Collagen signaling enhances tumor progression after anti-VEGF therapy in a murine model of pancreatic ductal adenocarcinoma. Cancer Res *74*, 1032-1044.

Aguirre, A. J., Bardeesy, N., Sinha, M., Lopez, L., Tuveson, D. A., Horner, J., Redston, M. S., and DePinho, R. A. (2003). Activated Kras and Ink4a/Arf deficiency cooperate to produce metastatic pancreatic ductal adenocarcinoma. Genes Dev *17*, 3112-3126.

Arnold, J. N., Magiera, L., Kraman, M., and Fearon, D. T. (2014). Tumoral immune suppression by macrophages expressing fibroblast activation protein-alpha and heme oxygenase-1. Cancer Immunol Res *2*, 121-126.

Augsten, M. (2014). Cancer-associated fibroblasts as another polarized cell type of the tumor microenvironment. Front Oncol *4*, 62.

Bachem, M. G., Schneider, E., Gross, H., Weidenbach, H., Schmid, R. M., Menke, A., Siech, M., Beger, H., Grunert, A., and Adler, G. (1998). Identification, culture, and characterization of pancreatic stellate cells in rats and humans. Gastroenterology *115*, 421-432.

Bae, S., Park, C. W., Son, H. K., Ju, H. K., Paik, D., Jeon, C. J., Koh, G. Y., Kim, J., and Kim, H. (2008). Fibroblast activation protein alpha identifies mesenchymal stromal cells from human bone marrow. Br J Haematol *142*, 827-830.

Baird, S. K., Allan, L., Renner, C., Scott, F. E., and Scott, A. M. (2015). Fibroblast activation protein increases metastatic potential of fibrosarcoma line HT1080 through upregulation of integrin-mediated signaling pathways. Clin Exp Metastasis *32*, 507-516.

Balsamo, M., Scordamaglia, F., Pietra, G., Manzini, C., Cantoni, C., Boitano, M., Queirolo, P., Vermi, W., Facchetti, F., Moretta, A.*, et al.* (2009). Melanoma-associated fibroblasts modulate NK cell phenotype and antitumor cytotoxicity. Proc Natl Acad Sci U S A *106*, 20847-20852.

Bardeesy, N., Aguirre, A. J., Chu, G. C., Cheng, K. H., Lopez, L. V., Hezel, A. F., Feng, B., Brennan, C., Weissleder, R., Mahmood, U.*, et al.* (2006). Both p16(Ink4a) and the p19(Arf)-p53 pathway constrain progression of pancreatic adenocarcinoma in the mouse. Proc Natl Acad Sci U S A *103*, 5947-5952.

Berdiel-Acer, M., Sanz-Pamplona, R., Calon, A., Cuadras, D., Berenguer, A., Sanjuan, X., Paules, M. J., Salazar, R., Moreno, V., Batlle, E.*, et al.* (2014). Differences between CAFs and their paired NCF from adjacent colonic mucosa reveal functional heterogeneity of CAFs, providing prognostic information. Mol Oncol *8*, 1290-1305.

Bhowmick, N. A., Chytil, A., Plieth, D., Gorska, A. E., Dumont, N., Shappell, S., Washington, M. K., Neilson, E. G., and Moses, H. L. (2004a). TGF-beta signaling in fibroblasts modulates the oncogenic potential of adjacent epithelia. Science *303*, 848-851.

Bhowmick, N. A., Neilson, E. G., and Moses, H. L. (2004b). Stromal fibroblasts in cancer initiation and progression. Nature *432*, 332-337.

Bissell, M. J., and Hines, W. C. (2011). Why don't we get more cancer? A proposed role of the microenvironment in restraining cancer progression. Nat Med *17*, 320-329.

Bochet, L., Lehuede, C., Dauvillier, S., Wang, Y. Y., Dirat, B., Laurent, V., Dray, C., Guiet, R., Maridonneau-Parini, I., Le Gonidec, S.*, et al.* (2013). Adipocyte-derived fibroblasts promote tumor progression and contribute to the desmoplastic reaction in breast cancer. Cancer Res *73*, 5657-5668.

Bonnans, C., Chou, J., and Werb, Z. (2014). Remodelling the extracellular matrix in development and disease. Nat Rev Mol Cell Biol *15*, 786-801.

Brahmer, J., Reckamp, K. L., Baas, P., Crino, L., Eberhardt, W. E., Poddubskaya, E., Antonia, S., Pluzanski, A., Vokes, E. E., Holgado, E.*, et al.* (2015). Nivolumab versus Docetaxel in Advanced Squamous-Cell Non-Small-Cell Lung Cancer. N Engl J Med *373*, 123-135.

Brahmer, J. R., Tykodi, S. S., Chow, L. Q., Hwu, W. J., Topalian, S. L., Hwu, P., Drake, C. G., Camacho, L. H., Kauh, J., Odunsi, K.*, et al.* (2012). Safety and activity of anti-PD-L1 antibody in patients with advanced cancer. N Engl J Med *366*, 2455-2465.

Brennen, W. N., Rosen, D. M., Wang, H., Isaacs, J. T., and Denmeade, S. R. (2012). Targeting carcinoma-associated fibroblasts within the tumor stroma with a fibroblast activation protein-activated prodrug. J Natl Cancer Inst *104*, 1320-1334.

Brisson, B. K., Mauldin, E. A., Lei, W., Vogel, L. K., Power, A. M., Lo, A., Dopkin, D., Khanna, C., Wells, R. G., Pure, E., and Volk, S. W. (2015). Type III Collagen Directs Stromal Organization and Limits Metastasis in a Murine Model of Breast Cancer. Am J Pathol *185*, 1471-1486.

Brokopp, C. E., Schoenauer, R., Richards, P., Bauer, S., Lohmann, C., Emmert, M. Y., Weber, B., Winnik, S., Aikawa, E., Graves, K.*, et al.* (2011). Fibroblast activation protein is induced by inflammation and degrades type I collagen in thin-cap fibroatheromata. Eur Heart J *32*, 2713-2722.

Bronisz, A., Godlewski, J., Wallace, J. A., Merchant, A. S., Nowicki, M. O., Mathsyaraja, H., Srinivasan, R., Trimboli, A. J., Martin, C. K., Li, F.*, et al.* (2012). Reprogramming of the tumour microenvironment by stromal PTEN-regulated miR-320. Nat Cell Biol *14*, 159-167.

Calvo, F., Ege, N., Grande-Garcia, A., Hooper, S., Jenkins, R. P., Chaudhry, S. I., Harrington, K., Williamson, P., Moeendarbary, E., Charras, G., and Sahai, E. (2013). Mechanotransduction and YAP-dependent matrix remodelling is required for the generation and maintenance of cancer-associated fibroblasts. Nat Cell Biol *15*, 637-646.

Camerer, E., Qazi, A. A., Duong, D. N., Cornelissen, I., Advincula, R., and Coughlin, S. R. (2004). Platelets, protease-activated receptors, and fibrinogen in hematogenous metastasis. Blood *104*, 397-401.

Campbell, I., Polyak, K., and Haviv, I. (2009). Clonal mutations in the cancer-associated fibroblasts: the case against genetic coevolution. Cancer Res *69*, 6765-6768; discussion 6769.

Caruana, I., Savoldo, B., Hoyos, V., Weber, G., Liu, H., Kim, E. S., Ittmann, M. M., Marchetti, D., and Dotti, G. (2015). Heparanase promotes tumor infiltration and antitumor activity of CAR-redirected T lymphocytes. Nat Med *21*, 524-529.

Chang, P. H., Hwang-Verslues, W. W., Chang, Y. C., Chen, C. C., Hsiao, M., Jeng, Y. M., Chang, K. J., Lee, E. Y., Shew, J. Y., and Lee, W. H. (2012). Activation of Robo1 signaling of breast cancer cells by Slit2 from stromal fibroblast restrains tumorigenesis via blocking PI3K/Akt/beta-catenin pathway. Cancer Res *72*, 4652-4661.

Chen, Y., Terajima, M., Yang, Y., Sun, L., Ahn, Y. H., Pankova, D., Puperi, D. S., Watanabe, T., Kim, M. P., Blackmon, S. H.*, et al.* (2015). Lysyl hydroxylase 2 induces a collagen cross-link switch in tumor stroma. J Clin Invest *125*, 1147-1162.

Cheng, J. D., Dunbrack, R. L., Jr., Valianou, M., Rogatko, A., Alpaugh, R. K., and Weiner, L. M. (2002). Promotion of tumor growth by murine fibroblast activation protein, a serine protease, in an animal model. Cancer Res *62*, 4767-4772.

Cheng, J. D., Valianou, M., Canutescu, A. A., Jaffe, E. K., Lee, H. O., Wang, H., Lai, J. H., Bachovchin, W. W., and Weiner, L. M. (2005). Abrogation of fibroblast activation protein enzymatic activity attenuates tumor growth. Mol Cancer Ther *4*, 351-360.

Chmielewski, M., Hombach, A. A., and Abken, H. (2011). CD28 cosignalling does not affect the activation threshold in a chimeric antigen receptor-redirected T-cell attack. Gene Ther *18*, 62-72.

Christiansen, V. J., Jackson, K. W., Lee, K. N., and McKee, P. A. (2007). Effect of fibroblast activation protein and alpha2-antiplasmin cleaving enzyme on collagen types I, III, and IV. Arch Biochem Biophys *457*, 177-186.

Chung, K. M., Hsu, S. C., Chu, Y. R., Lin, M. Y., Jiaang, W. T., Chen, R. H., and Chen, X. (2014). Fibroblast activation protein (FAP) is essential for the migration of bone marrow mesenchymal stem cells through RhoA activation. PLoS One *9*, e88772.

Cohen, S. J., Alpaugh, R. K., Palazzo, I., Meropol, N. J., Rogatko, A., Xu, Z., Hoffman, J. P., Weiner, L. M., and Cheng, J. D. (2008). Fibroblast activation protein and its relationship to clinical outcome in pancreatic adenocarcinoma. Pancreas *37*, 154-158.

Comito, G., Giannoni, E., Segura, C. P., Barcellos-de-Souza, P., Raspollini, M. R., Baroni, G., Lanciotti, M., Serni, S., and Chiarugi, P. (2014). Cancer-associated fibroblasts and M2-polarized macrophages synergize during prostate carcinoma progression. Oncogene *33*, 2423-2431.

Crisanti, M. C., Wallace, A. F., Kapoor, V., Vandermeers, F., Dowling, M. L., Pereira, L. P., Coleman, K., Campling, B. G., Fridlender, Z. G., Kao, G. D., and Albelda, S. M. (2009). The HDAC inhibitor panobinostat (LBH589) inhibits mesothelioma and lung cancer cells in vitro and in vivo with particular efficacy for small cell lung cancer. Mol Cancer Ther *8*, 2221-2231.

Cuff, C. A., Kothapalli, D., Azonobi, I., Chun, S., Zhang, Y., Belkin, R., Yeh, C., Secreto, A., Assoian, R. K., Rader, D. J., and Pure, E. (2001). The adhesion receptor CD44 promotes atherosclerosis by mediating inflammatory cell recruitment and vascular cell activation. J Clin Invest *108*, 1031-1040.

Darmoul, D., Lacasa, M., Baricault, L., Marguet, D., Sapin, C., Trotot, P., Barbat, A., and Trugnan, G. (1992). Dipeptidyl peptidase IV (CD 26) gene expression in enterocyte-like colon cancer cell lines HT-29 and Caco-2. Cloning of the complete human coding

sequence and changes of dipeptidyl peptidase IV mRNA levels during cell differentiation. J Biol Chem *267*, 4824-4833.

Denton, A. E., Roberts, E. W., Linterman, M. A., and Fearon, D. T. (2014). Fibroblastic reticular cells of the lymph node are required for retention of resting but not activated CD8+ T cells. Proc Natl Acad Sci U S A *111*, 12139-12144.

Desmouliere, A., Guyot, C., and Gabbiani, G. (2004). The stroma reaction myofibroblast: a key player in the control of tumor cell behavior. Int J Dev Biol *48*, 509-517.

Desnoyers, L. R., Vasiljeva, O., Richardson, J. H., Yang, A., Menendez, E. E., Liang, T. W., Wong, C., Bessette, P. H., Kamath, K., Moore, S. J.*, et al.* (2013). Tumor-specific activation of an EGFR-targeting probody enhances therapeutic index. Sci Transl Med *5*, 207ra144.

Ding, N., Yu, R. T., Subramaniam, N., Sherman, M. H., Wilson, C., Rao, R., Leblanc, M., Coulter, S., He, M., Scott, C.*, et al.* (2013). A vitamin D receptor/SMAD genomic circuit gates hepatic fibrotic response. Cell *153*, 601-613.

Direkze, N. C., Hodivala-Dilke, K., Jeffery, R., Hunt, T., Poulsom, R., Oukrif, D., Alison, M. R., and Wright, N. A. (2004). Bone marrow contribution to tumor-associated myofibroblasts and fibroblasts. Cancer Res *64*, 8492-8495.

Dolznig, H., Schweifer, N., Puri, C., Kraut, N., Rettig, W. J., Kerjaschki, D., and Garin-Chesa, P. (2005). Characterization of cancer stroma markers: in silico analysis of an mRNA expression database for fibroblast activation protein and endosialin. Cancer Immun *5*, 10.

Draffin, J. E., McFarlane, S., Hill, A., Johnston, P. G., and Waugh, D. J. (2004). CD44 potentiates the adherence of metastatic prostate and breast cancer cells to bone marrow endothelial cells. Cancer Res *64*, 5702-5711.

Dvorak, H. F. (1986). Tumors: wounds that do not heal. Similarities between tumor stroma generation and wound healing. N Engl J Med *315*, 1650-1659.

Dvorak, H. F. (2015). Tumors: wounds that do not heal-redux. Cancer Immunol Res *3*, 1-11.

Edosada, C. Y., Quan, C., Tran, T., Pham, V., Wiesmann, C., Fairbrother, W., and Wolf, B. B. (2006). Peptide substrate profiling defines fibroblast activation protein as an endopeptidase of strict Gly(2)-Pro(1)-cleaving specificity. FEBS Lett *580*, 1581-1586.

Egeblad, M., Nakasone, E. S., and Werb, Z. (2010). Tumors as organs: complex tissues that interface with the entire organism. Dev Cell *18*, 884-901.

Ene-Obong, A., Clear, A. J., Watt, J., Wang, J., Fatah, R., Riches, J. C., Marshall, J. F., Chin-Aleong, J., Chelala, C., Gribben, J. G.*, et al.* (2013). Activated pancreatic stellate cells sequester CD8+ T cells to reduce their infiltration of the juxtatumoral compartment of pancreatic ductal adenocarcinoma. Gastroenterology *145*, 1121-1132.

Erez, N., Truitt, M., Olson, P., Arron, S. T., and Hanahan, D. (2010). Cancer-Associated Fibroblasts Are Activated in Incipient Neoplasia to Orchestrate Tumor-Promoting Inflammation in an NF-kappaB-Dependent Manner. Cancer Cell *17*, 135-147.

Erler, J. T., Bennewith, K. L., Cox, T. R., Lang, G., Bird, D., Koong, A., Le, Q. T., and Giaccia, A. J. (2009). Hypoxia-induced lysyl oxidase is a critical mediator of bone marrow cell recruitment to form the premetastatic niche. Cancer Cell *15*, 35-44.

Fedorov, V. D., Themeli, M., and Sadelain, M. (2013). PD-1- and CTLA-4-based inhibitory chimeric antigen receptors (iCARs) divert off-target immunotherapy responses. Sci Transl Med *5*, 215ra172.

Feig, C., Jones, J. O., Kraman, M., Wells, R. J., Deonarine, A., Chan, D. S., Connell, C. M., Roberts, E. W., Zhao, Q., Caballero, O. L.*, et al.* (2013). Targeting CXCL12 from FAP-expressing carcinoma-associated fibroblasts synergizes with anti-PD-L1 immunotherapy in pancreatic cancer. Proc Natl Acad Sci U S A *110*, 20212-20217.

Feldmann, G., Beaty, R., Hruban, R. H., and Maitra, A. (2007). Molecular genetics of pancreatic intraepithelial neoplasia. J Hepatobiliary Pancreat Surg *14*, 224-232.

Fiaschi, T., Marini, A., Giannoni, E., Taddei, M. L., Gandellini, P., De Donatis, A., Lanciotti, M., Serni, S., Cirri, P., and Chiarugi, P. (2012). Reciprocal metabolic reprogramming through lactate shuttle coordinately influences tumor-stroma interplay. Cancer Res *72*, 5130-5140.

Flaberg, E., Markasz, L., Petranyi, G., Stuber, G., Dicso, F., Alchihabi, N., Olah, E., Csizy, I., Jozsa, T., Andren, O.*, et al.* (2011). High-throughput live-cell imaging reveals differential inhibition of tumor cell proliferation by human fibroblasts. Int J Cancer *128*, 2793-2802.

Gaggioli, C., Hooper, S., Hidalgo-Carcedo, C., Grosse, R., Marshall, J. F., Harrington, K., and Sahai, E. (2007). Fibroblast-led collective invasion of carcinoma cells with

differing roles for RhoGTPases in leading and following cells. Nat Cell Biol *9*, 1392-1400.

Garfall, A. L., Maus, M. V., Hwang, W. T., Lacey, S. F., Mahnke, Y. D., Melenhorst, J. J., Zheng, Z., Vogl, D. T., Cohen, A. D., Weiss, B. M.*, et al.* (2015). Chimeric Antigen Receptor T Cells against CD19 for Multiple Myeloma. N Engl J Med *373*, 1040-1047.

Garin-Chesa, P., Old, L. J., and Rettig, W. J. (1990). Cell surface glycoprotein of reactive stromal fibroblasts as a potential antibody target in human epithelial cancers. Proc Natl Acad Sci U S A *87*, 7235-7239.

Garrido-Laguna, I., Uson, M., Rajeshkumar, N. V., Tan, A. C., de Oliveira, E., Karikari, C., Villaroel, M. C., Salomon, A., Taylor, G., Sharma, R.*, et al.* (2011). Tumor engraftment in nude mice and enrichment in stroma- related gene pathways predict poor survival and resistance to gemcitabine in patients with pancreatic cancer. Clin Cancer Res *17*, 5793-5800.

Gay, L. J., and Felding-Habermann, B. (2011). Contribution of platelets to tumour metastasis. Nat Rev Cancer *11*, 123-134.

Goetz, J. G., Minguet, S., Navarro-Lerida, I., Lazcano, J. J., Samaniego, R., Calvo, E., Tello, M., Osteso-Ibanez, T., Pellinen, T., Echarri, A.*, et al.* (2011). Biomechanical remodeling of the microenvironment by stromal caveolin-1 favors tumor invasion and metastasis. Cell *146*, 148-163.

Gong, D., Shi, W., Yi, S. J., Chen, H., Groffen, J., and Heisterkamp, N. (2012). TGFbeta signaling plays a critical role in promoting alternative macrophage activation. BMC Immunol *13*, 31.

Grupp, S. A., Kalos, M., Barrett, D., Aplenc, R., Porter, D. L., Rheingold, S. R., Teachey, D. T., Chew, A., Hauck, B., Wright, J. F.*, et al.* (2013). Chimeric antigen receptor-modified T cells for acute lymphoid leukemia. N Engl J Med *368*, 1509-1518.

Guerra, C., Schuhmacher, A. J., Canamero, M., Grippo, P. J., Verdaguer, L., Perez-Gallego, L., Dubus, P., Sandgren, E. P., and Barbacid, M. (2007). Chronic pancreatitis is essential for induction of pancreatic ductal adenocarcinoma by K-Ras oncogenes in adult mice. Cancer Cell *11*, 291-302.

Gupta, G. P., and Massague, J. (2006). Cancer metastasis: building a framework. Cell *127*, 679-695.

Gyorffy, B., Surowiak, P., Budczies, J., and Lanczky, A. (2013). Online survival analysis software to assess the prognostic value of biomarkers using transcriptomic data in non-small-cell lung cancer. PLoS One *8*, e82241.

Hamid, O., Robert, C., Daud, A., Hodi, F. S., Hwu, W. J., Kefford, R., Wolchok, J. D., Hersey, P., Joseph, R. W., Weber, J. S.*, et al.* (2013). Safety and tumor responses with lambrolizumab (anti-PD-1) in melanoma. N Engl J Med *369*, 134-144.

Hanahan, D., and Coussens, L. M. (2012). Accessories to the crime: functions of cells recruited to the tumor microenvironment. Cancer Cell *21*, 309-322.

Hanahan, D., and Weinberg, R. A. (2011). Hallmarks of cancer: the next generation. Cell *144*, 646-674.

Hanson, J. A., Gillespie, J. W., Grover, A., Tangrea, M. A., Chuaqui, R. F., Emmert-Buck, M. R., Tangrea, J. A., Libutti, S. K., Linehan, W. M., and Woodson, K. G. (2006).

Gene promoter methylation in prostate tumor-associated stromal cells. J Natl Cancer Inst *98*, 255-261.

Hawinkels, L. J., Paauwe, M., Verspaget, H. W., Wiercinska, E., van der Zon, J. M., van der Ploeg, K., Koelink, P. J., Lindeman, J. H., Mesker, W., ten Dijke, P., and Sier, C. F. (2014). Interaction with colon cancer cells hyperactivates TGF-beta signaling in cancer-associated fibroblasts. Oncogene *33*, 97-107.

Henry, L. R., Lee, H. O., Lee, J. S., Klein-Szanto, A., Watts, P., Ross, E. A., Chen, W. T., and Cheng, J. D. (2007). Clinical implications of fibroblast activation protein in patients with colon cancer. Clin Cancer Res *13*, 1736-1741.

Hidalgo, M. (2010). Pancreatic cancer. N Engl J Med *362*, 1605-1617.

Hingorani, S. R., Petricoin, E. F., Maitra, A., Rajapakse, V., King, C., Jacobetz, M. A., Ross, S., Conrads, T. P., Veenstra, T. D., Hitt, B. A.*, et al.* (2003). Preinvasive and invasive ductal pancreatic cancer and its early detection in the mouse. Cancer Cell *4*, 437-450.

Hingorani, S. R., Wang, L., Multani, A. S., Combs, C., Deramaudt, T. B., Hruban, R. H., Rustgi, A. K., Chang, S., and Tuveson, D. A. (2005). Trp53R172H and KrasG12D cooperate to promote chromosomal instability and widely metastatic pancreatic ductal adenocarcinoma in mice. Cancer Cell *7*, 469-483.

Hiratsuka, S., Goel, S., Kamoun, W. S., Maru, Y., Fukumura, D., Duda, D. G., and Jain, R. K. (2011). Endothelial focal adhesion kinase mediates cancer cell homing to discrete regions of the lungs via E-selectin up-regulation. Proc Natl Acad Sci U S A *108*, 3725-3730.

Hodi, F. S., O'Day, S. J., McDermott, D. F., Weber, R. W., Sosman, J. A., Haanen, J. B., Gonzalez, R., Robert, C., Schadendorf, D., Hassel, J. C*., et al.* (2010). Improved survival with ipilimumab in patients with metastatic melanoma. N Engl J Med *363*, 711-723.

Hombach, A. A., Schildgen, V., Heuser, C., Finnern, R., Gilham, D. E., and Abken, H. (2007). T cell activation by antibody-like immunoreceptors: the position of the binding epitope within the target molecule determines the efficiency of activation of redirected T cells. J Immunol *178*, 4650-4657.

Horowitz, N. A., Blevins, E. A., Miller, W. M., Perry, A. R., Talmage, K. E., Mullins, E. S., Flick, M. J., Queiroz, K. C., Shi, K., Spek, C. A*., et al.* (2011). Thrombomodulin is a determinant of metastasis through a mechanism linked to the thrombin binding domain but not the lectin-like domain. Blood *118*, 2889-2895.

Hosein, A. N., Wu, M., Arcand, S. L., Lavallee, S., Hebert, J., Tonin, P. N., and Basik, M. (2010). Breast carcinoma-associated fibroblasts rarely contain p53 mutations or chromosomal aberrations. Cancer Res *70*, 5770-5777.

Hruban, R. H., Adsay, N. V., Albores-Saavedra, J., Compton, C., Garrett, E. S., Goodman, S. N., Kern, S. E., Klimstra, D. S., Kloppel, G., Longnecker, D. S*., et al.* (2001). Pancreatic intraepithelial neoplasia: a new nomenclature and classification system for pancreatic duct lesions. Am J Surg Pathol *25*, 579-586.

Hruban, R. H., Takaori, K., Klimstra, D. S., Adsay, N. V., Albores-Saavedra, J., Biankin, A. V., Biankin, S. A., Compton, C., Fukushima, N., Furukawa, T*., et al.* (2004). An illustrated consensus on the classification of pancreatic intraepithelial neoplasia and intraductal papillary mucinous neoplasms. Am J Surg Pathol *28*, 977-987.

Hu, M., Yao, J., Cai, L., Bachman, K. E., van den Brule, F., Velculescu, V., and Polyak, K. (2005). Distinct epigenetic changes in the stromal cells of breast cancers. Nat Genet *37*, 899-905.

Huang, Y., Wang, S., and Kelly, T. (2004). Seprase promotes rapid tumor growth and increased microvessel density in a mouse model of human breast cancer. Cancer Res *64*, 2712-2716.

Hwang, R. F., Moore, T., Arumugam, T., Ramachandran, V., Amos, K. D., Rivera, A., Ji, B., Evans, D. B., and Logsdon, C. D. (2008). Cancer-associated stromal fibroblasts promote pancreatic tumor progression. Cancer Res *68*, 918-926.

Ijichi, H., Chytil, A., Gorska, A. E., Aakre, M. E., Fujitani, Y., Fujitani, S., Wright, C. V., and Moses, H. L. (2006). Aggressive pancreatic ductal adenocarcinoma in mice caused by pancreas-specific blockade of transforming growth factor-beta signaling in cooperation with active Kras expression. Genes Dev *20*, 3147-3160.

Ikenaga, N., Ohuchida, K., Mizumoto, K., Cui, L., Kayashima, T., Morimatsu, K., Moriyama, T., Nakata, K., Fujita, H., and Tanaka, M. (2010). CD10+ pancreatic stellate cells enhance the progression of pancreatic cancer. Gastroenterology *139*, 1041-1051, 1051 e1041-1048.

Infante, J. R., Matsubayashi, H., Sato, N., Tonascia, J., Klein, A. P., Riall, T. A., Yeo, C., Iacobuzio-Donahue, C., and Goggins, M. (2007). Peritumoral fibroblast SPARC expression and patient outcome with resectable pancreatic adenocarcinoma. J Clin Oncol *25*, 319-325.

Iwano, M., Plieth, D., Danoff, T. M., Xue, C., Okada, H., and Neilson, E. G. (2002). Evidence that fibroblasts derive from epithelium during tissue fibrosis. J Clin Invest *110*, 341-350.

Izeradjene, K., Combs, C., Best, M., Gopinathan, A., Wagner, A., Grady, W. M., Deng, C. X., Hruban, R. H., Adsay, N. V., Tuveson, D. A., and Hingorani, S. R. (2007). Kras(G12D) and Smad4/Dpc4 haploinsufficiency cooperate to induce mucinous cystic neoplasms and invasive adenocarcinoma of the pancreas. Cancer Cell *11*, 229-243.

Jacob, M., Chang, L., and Pure, E. (2012). Fibroblast activation protein in remodeling tissues. Curr Mol Med *12*, 1220-1243.

Jacobetz, M. A., Chan, D. S., Neesse, A., Bapiro, T. E., Cook, N., Frese, K. K., Feig, C., Nakagawa, T., Caldwell, M. E., Zecchini, H. I.*, et al.* (2013). Hyaluronan impairs vascular function and drug delivery in a mouse model of pancreatic cancer. Gut *62*, 112-120.

Jeong, J. A., Hong, S. H., Gang, E. J., Ahn, C., Hwang, S. H., Yang, I. H., Han, H., and Kim, H. (2005). Differential gene expression profiling of human umbilical cord blood-derived mesenchymal stem cells by DNA microarray. Stem Cells *23*, 584-593.

Jeong, J. A., Ko, K. M., Bae, S., Jeon, C. J., Koh, G. Y., and Kim, H. (2007). Genome-wide differential gene expression profiling of human bone marrow stromal cells. Stem Cells *25*, 994-1002.

Jiang, L., Gonda, T. A., Gamble, M. V., Salas, M., Seshan, V., Tu, S., Twaddell, W. S., Hegyi, P., Lazar, G., Steele, I.*, et al.* (2008). Global hypomethylation of genomic DNA in cancer-associated myofibroblasts. Cancer Res *68*, 9900-9908.

Johnson, L., Mercer, K., Greenbaum, D., Bronson, R. T., Crowley, D., Tuveson, D. A., and Jacks, T. (2001). Somatic activation of the K-ras oncogene causes early onset lung cancer in mice. Nature *410*, 1111-1116.

Jotzu, C., Alt, E., Welte, G., Li, J., Hennessy, B. T., Devarajan, E., Krishnappa, S., Pinilla, S., Droll, L., and Song, Y. H. (2010). Adipose tissue-derived stem cells differentiate into carcinoma-associated fibroblast-like cells under the influence of tumor-derived factors. Anal Cell Pathol (Amst) *33*, 61-79.

Kakarla, S., Chow, K. K., Mata, M., Shaffer, D. R., Song, X. T., Wu, M. F., Liu, H., Wang, L. L., Rowley, D. R., Pfizenmaier, K., and Gottschalk, S. (2013). Antitumor effects of chimeric receptor engineered human T cells directed to tumor stroma. Mol Ther *21*, 1611-1620.

Kalluri, R., and Zeisberg, M. (2006). Fibroblasts in cancer. Nat Rev Cancer *6*, 392-401.

Kanda, M., Matthaei, H., Wu, J., Hong, S. M., Yu, J., Borges, M., Hruban, R. H., Maitra, A., Kinzler, K., Vogelstein, B., and Goggins, M. (2012). Presence of somatic mutations in most early-stage pancreatic intraepithelial neoplasia. Gastroenterology *142*, 730-733 e739.

Kaplan, R. N., Riba, R. D., Zacharoulis, S., Bramley, A. H., Vincent, L., Costa, C., MacDonald, D. D., Jin, D. K., Shido, K., Kerns, S. A.*, et al.* (2005). VEGFR1-positive haematopoietic bone marrow progenitors initiate the pre-metastatic niche. Nature *438*, 820-827.

Keane, F. M., Nadvi, N. A., Yao, T. W., and Gorrell, M. D. (2011). Neuropeptide Y, B-type natriuretic peptide, substance P and peptide YY are novel substrates of fibroblast activation protein-alpha. FEBS J *278*, 1316-1332.

Keane, F. M., Yao, T. W., Seelk, S., Gall, M. G., Chowdhury, S., Poplawski, S. E., Lai, J. H., Li, Y., Wu, W., Farrell, P.*, et al.* (2013). Quantitation of fibroblast activation protein (FAP)-specific protease activity in mouse, baboon and human fluids and organs. FEBS Open Bio *4*, 43-54.

Kern, S., Hruban, R., Hollingsworth, M. A., Brand, R., Adrian, T. E., Jaffee, E., and Tempero, M. A. (2001). A white paper: the product of a pancreas cancer think tank. Cancer Res *61*, 4923-4932.

Kidd, S., Spaeth, E., Watson, K., Burks, J., Lu, H., Klopp, A., Andreeff, M., and Marini, F. C. (2012). Origins of the tumor microenvironment: quantitative assessment of adipose-derived and bone marrow-derived stroma. PLoS One *7*, e30563.

Kim, J. W., Evans, C., Weidemann, A., Takeda, N., Lee, Y. S., Stockmann, C., Branco-Price, C., Brandberg, F., Leone, G., Ostrowski, M. C., and Johnson, R. S. (2012). Loss of fibroblast HIF-1alpha accelerates tumorigenesis. Cancer Res *72*, 3187-3195.

Kitamura, T., Qian, B. Z., and Pollard, J. W. (2015a). Immune cell promotion of metastasis. Nat Rev Immunol *15*, 73-86.

Kitamura, T., Qian, B. Z., Soong, D., Cassetta, L., Noy, R., Sugano, G., Kato, Y., Li, J., and Pollard, J. W. (2015b). CCL2-induced chemokine cascade promotes breast cancer metastasis by enhancing retention of metastasis-associated macrophages. J Exp Med *212*, 1043-1059.

Kloss, C. C., Condomines, M., Cartellieri, M., Bachmann, M., and Sadelain, M. (2013). Combinatorial antigen recognition with balanced signaling promotes selective tumor eradication by engineered T cells. Nat Biotechnol *31*, 71-75.

Kobayashi, N., Miyoshi, S., Mikami, T., Koyama, H., Kitazawa, M., Takeoka, M., Sano, K., Amano, J., Isogai, Z., Niida, S.*, et al.* (2010). Hyaluronan deficiency in tumor stroma impairs macrophage trafficking and tumor neovascularization. Cancer Res *70*, 7073-7083.

Koczorowska, M. M., Tholen, S., Bucher, F., Lutz, L., Kizhakkedathu, J. N., De Wever, O., Wellner, U. F., Biniossek, M. L., Stahl, A., Lassmann, S., and Schilling, O. (2016). Fibroblast activation protein-alpha, a stromal cell surface protease, shapes key features of cancer associated fibroblasts through proteome and degradome alterations. Mol Oncol *10*, 40-58.

Kojima, K., Vickers, S. M., Adsay, N. V., Jhala, N. C., Kim, H. G., Schoeb, T. R., Grizzle, W. E., and Klug, C. A. (2007). Inactivation of Smad4 accelerates Kras(G12D)-mediated pancreatic neoplasia. Cancer Res *67*, 8121-8130.

Kojima, Y., Acar, A., Eaton, E. N., Mellody, K. T., Scheel, C., Ben-Porath, I., Onder, T. T., Wang, Z. C., Richardson, A. L., Weinberg, R. A., and Orimo, A. (2010). Autocrine TGF-beta and stromal cell-derived factor-1 (SDF-1) signaling drives the evolution of tumor-promoting mammary stromal myofibroblasts. Proc Natl Acad Sci U S A *107*, 20009-20014.

Kopp, J. L., von Figura, G., Mayes, E., Liu, F. F., Dubois, C. L., Morris, J. P. t., Pan, F. C., Akiyama, H., Wright, C. V., Jensen, K.*, et al.* (2012). Identification of Sox9-

dependent acinar-to-ductal reprogramming as the principal mechanism for initiation of pancreatic ductal adenocarcinoma. Cancer Cell *22*, 737-750.

Kordes, C., Sawitza, I., and Haussinger, D. (2009). Hepatic and pancreatic stellate cells in focus. Biol Chem *390*, 1003-1012.

Koyama, H., Hibi, T., Isogai, Z., Yoneda, M., Fujimori, M., Amano, J., Kawakubo, M., Kannagi, R., Kimata, K., Taniguchi, S., and Itano, N. (2007). Hyperproduction of hyaluronan in neu-induced mammary tumor accelerates angiogenesis through stromal cell recruitment: possible involvement of versican/PG-M. Am J Pathol *170*, 1086-1099.

Koyama, H., Kobayashi, N., Harada, M., Takeoka, M., Kawai, Y., Sano, K., Fujimori, M., Amano, J., Ohhashi, T., Kannagi, R.*, et al.* (2008). Significance of tumor-associated stroma in promotion of intratumoral lymphangiogenesis: pivotal role of a hyaluronan-rich tumor microenvironment. Am J Pathol *172*, 179-193.

Kraman, M., Bambrough, P. J., Arnold, J. N., Roberts, E. W., Magiera, L., Jones, J. O., Gopinathan, A., Tuveson, D. A., and Fearon, D. T. (2010). Suppression of antitumor immunity by stromal cells expressing fibroblast activation protein-alpha. Science *330*, 827-830.

Kurose, K., Gilley, K., Matsumoto, S., Watson, P. H., Zhou, X. P., and Eng, C. (2002). Frequent somatic mutations in PTEN and TP53 are mutually exclusive in the stroma of breast carcinomas. Nat Genet *32*, 355-357.

Labelle, M., and Hynes, R. O. (2012). The initial hours of metastasis: the importance of cooperative host-tumor cell interactions during hematogenous dissemination. Cancer Discov *2*, 1091-1099.

Larkin, J., Chiarion-Sileni, V., Gonzalez, R., Grob, J. J., Cowey, C. L., Lao, C. D., Schadendorf, D., Dummer, R., Smylie, M., Rutkowski, P., *et al.* (2015). Combined Nivolumab and Ipilimumab or Monotherapy in Untreated Melanoma. N Engl J Med *373*, 23-34.

Le, D. T., Uram, J. N., Wang, H., Bartlett, B. R., Kemberling, H., Eyring, A. D., Skora, A. D., Luber, B. S., Azad, N. S., Laheru, D., *et al.* (2015). PD-1 Blockade in Tumors with Mismatch-Repair Deficiency. N Engl J Med *372*, 2509-2520.

Leach, D. R., Krummel, M. F., and Allison, J. P. (1996). Enhancement of antitumor immunity by CTLA-4 blockade. Science *271*, 1734-1736.

Lederle, W., Hartenstein, B., Meides, A., Kunzelmann, H., Werb, Z., Angel, P., and Mueller, M. M. (2010). MMP13 as a stromal mediator in controlling persistent angiogenesis in skin carcinoma. Carcinogenesis *31*, 1175-1184.

Lee, C. H., Shah, B., Moioli, E. K., and Mao, J. J. (2010). CTGF directs fibroblast differentiation from human mesenchymal stem/stromal cells and defines connective tissue healing in a rodent injury model. J Clin Invest *120*, 3340-3349.

Lee, H. O., Mullins, S. R., Franco-Barraza, J., Valianou, M., Cukierman, E., and Cheng, J. D. (2011). FAP-overexpressing fibroblasts produce an extracellular matrix that enhances invasive velocity and directionality of pancreatic cancer cells. BMC Cancer *11*, 245.

Lee, J., Fassnacht, M., Nair, S., Boczkowski, D., and Gilboa, E. (2005). Tumor immunotherapy targeting fibroblast activation protein, a product expressed in tumor-associated fibroblasts. Cancer Res *65*, 11156-11163.

Lee, K. N., Jackson, K. W., Christiansen, V. J., Chung, K. H., and McKee, P. A. (2004). A novel plasma proteinase potentiates alpha2-antiplasmin inhibition of fibrin digestion. Blood *103*, 3783-3788.

Lee, K. N., Jackson, K. W., Christiansen, V. J., Lee, C. S., Chun, J. G., and McKee, P. A. (2006). Antiplasmin-cleaving enzyme is a soluble form of fibroblast activation protein. Blood *107*, 1397-1404.

Lee, K. W., Yeo, S. Y., Sung, C. O., and Kim, S. H. (2015). Twist1 is a key regulator of cancer-associated fibroblasts. Cancer Res *75*, 73-85.

Levental, K. R., Yu, H., Kass, L., Lakins, J. N., Egeblad, M., Erler, J. T., Fong, S. F., Csiszar, K., Giaccia, A., Weninger, W.*, et al.* (2009). Matrix crosslinking forces tumor progression by enhancing integrin signaling. Cell *139*, 891-906.

Levy, M. T., McCaughan, G. W., Abbott, C. A., Park, J. E., Cunningham, A. M., Muller, E., Rettig, W. J., and Gorrell, M. D. (1999). Fibroblast activation protein: a cell surface dipeptidyl peptidase and gelatinase expressed by stellate cells at the tissue remodelling interface in human cirrhosis. Hepatology *29*, 1768-1778.

Li, T., Yang, Y., Hua, X., Wang, G., Liu, W., Jia, C., Tai, Y., Zhang, Q., and Chen, G. (2012). Hepatocellular carcinoma-associated fibroblasts trigger NK cell dysfunction via PGE2 and IDO. Cancer Lett *318*, 154-161.

Liao, D., Luo, Y., Markowitz, D., Xiang, R., and Reisfeld, R. A. (2009). Cancer associated fibroblasts promote tumor growth and metastasis by modulating the tumor immune microenvironment in a 4T1 murine breast cancer model. PLoS One *4*, e7965.

Liao, Y., Ni, Y., He, R., Liu, W., and Du, J. (2013). Clinical implications of fibroblast activation protein-alpha in non-small cell lung cancer after curative resection: a new predictor for prognosis. J Cancer Res Clin Oncol *139*, 1523-1528.

Lin, K. Y., Guarnieri, F. G., Staveley-O'Carroll, K. F., Levitsky, H. I., August, J. T., Pardoll, D. M., and Wu, T. C. (1996). Treatment of established tumors with a novel vaccine that enhances major histocompatibility class II presentation of tumor antigen. Cancer Res *56*, 21-26.

Liu, Z., Gao, Y., Hao, F., Lou, X., Zhang, X., Li, Y., Wu, D., Xiao, T., Yang, L., Li, Q.*, et al.* (2014). Secretomes are a potential source of molecular targets for cancer therapies and indicate that APOE is a candidate biomarker for lung adenocarcinoma metastasis. Mol Biol Rep *41*, 7507-7523.

Lo, A., Wang, L. C., Scholler, J., Monslow, J., Avery, D., Newick, K., O'Brien, S., Evans, R. A., Bajor, D. J., Clendenin, C.*, et al.* (2015). Tumor-Promoting Desmoplasia Is Disrupted by Depleting FAP-Expressing Stromal Cells. Cancer Res *75*, 2800-2810.

Loeffler, M., Kruger, J. A., Niethammer, A. G., and Reisfeld, R. A. (2006). Targeting tumor-associated fibroblasts improves cancer chemotherapy by increasing intratumoral drug uptake. J Clin Invest *116*, 1955-1962.

Lujambio, A., Akkari, L., Simon, J., Grace, D., Tschaharganeh, D. F., Bolden, J. E., Zhao, Z., Thapar, V., Joyce, J. A., Krizhanovsky, V., and Lowe, S. W. (2013). Non-cell-autonomous tumor suppression by p53. Cell *153*, 449-460.

Luzzi, K. J., MacDonald, I. C., Schmidt, E. E., Kerkvliet, N., Morris, V. L., Chambers, A. F., and Groom, A. C. (1998). Multistep nature of metastatic inefficiency: dormancy of

solitary cells after successful extravasation and limited survival of early micrometastases. Am J Pathol *153*, 865-873.

Mace, T. A., Ameen, Z., Collins, A., Wojcik, S., Mair, M., Young, G. S., Fuchs, J. R., Eubank, T. D., Frankel, W. L., Bekaii-Saab, T., *et al.* (2013). Pancreatic cancer-associated stellate cells promote differentiation of myeloid-derived suppressor cells in a STAT3-dependent manner. Cancer Res *73*, 3007-3018.

Madar, S., Brosh, R., Buganim, Y., Ezra, O., Goldstein, I., Solomon, H., Kogan, I., Goldfinger, N., Klocker, H., and Rotter, V. (2009). Modulated expression of WFDC1 during carcinogenesis and cellular senescence. Carcinogenesis *30*, 20-27.

Mahadevan, D., and Von Hoff, D. D. (2007). Tumor-stroma interactions in pancreatic ductal adenocarcinoma. Mol Cancer Ther *6*, 1186-1197.

Mantoni, T. S., Lunardi, S., Al-Assar, O., Masamune, A., and Brunner, T. B. (2011). Pancreatic stellate cells radioprotect pancreatic cancer cells through beta1-integrin signaling. Cancer Res *71*, 3453-3458.

Maris, P., Blomme, A., Palacios, A. P., Costanza, B., Bellahcene, A., Bianchi, E., Gofflot, S., Drion, P., Trombino, G. E., Di Valentin, E., *et al.* (2015). Asporin Is a Fibroblast-Derived TGF-beta1 Inhibitor and a Tumor Suppressor Associated with Good Prognosis in Breast Cancer. PLoS Med *12*, e1001871.

Maroni, P., Bendinelli, P., Matteucci, E., and Desiderio, M. A. (2007). HGF induces CXCR4 and CXCL12-mediated tumor invasion through Ets1 and NF-kappaB. Carcinogenesis *28*, 267-279.

Mathew, S., Scanlan, M. J., Mohan Raj, B. K., Murty, V. V., Garin-Chesa, P., Old, L. J., Rettig, W. J., and Chaganti, R. S. (1995). The gene for fibroblast activation protein alpha (FAP), a putative cell surface-bound serine protease expressed in cancer stroma and wound healing, maps to chromosome band 2q23. Genomics *25*, 335-337.

Maude, S. L., Frey, N., Shaw, P. A., Aplenc, R., Barrett, D. M., Bunin, N. J., Chew, A., Gonzalez, V. E., Zheng, Z., Lacey, S. F.*, et al.* (2014). Chimeric antigen receptor T cells for sustained remissions in leukemia. N Engl J Med *371*, 1507-1517.

McAllister, S. S., and Weinberg, R. A. (2014). The tumour-induced systemic environment as a critical regulator of cancer progression and metastasis. Nat Cell Biol *16*, 717-727.

Milone, M. C., Fish, J. D., Carpenito, C., Carroll, R. G., Binder, G. K., Teachey, D., Samanta, M., Lakhal, M., Gloss, B., Danet-Desnoyers, G.*, et al.* (2009). Chimeric receptors containing CD137 signal transduction domains mediate enhanced survival of T cells and increased antileukemic efficacy in vivo. Mol Ther *17*, 1453-1464.

Mishra, P. J., Mishra, P. J., Humeniuk, R., Medina, D. J., Alexe, G., Mesirov, J. P., Ganesan, S., Glod, J. W., and Banerjee, D. (2008). Carcinoma-associated fibroblast-like differentiation of human mesenchymal stem cells. Cancer Res *68*, 4331-4339.

Mitra, A. K., Zillhardt, M., Hua, Y., Tiwari, P., Murmann, A. E., Peter, M. E., and Lengyel, E. (2012). MicroRNAs reprogram normal fibroblasts into cancer-associated fibroblasts in ovarian cancer. Cancer Discov *2*, 1100-1108.

Moffitt, R. A., Marayati, R., Flate, E. L., Volmar, K. E., Loeza, S. G., Hoadley, K. A., Rashid, N. U., Williams, L. A., Eaton, S. C., Chung, A. H.*, et al.* (2015). Virtual

microdissection identifies distinct tumor- and stroma-specific subtypes of pancreatic ductal adenocarcinoma. Nat Genet *47*, 1168-1178.

Moon, E. K., Carpenito, C., Sun, J., Wang, L. C., Kapoor, V., Predina, J., Powell, D. J., Jr., Riley, J. L., June, C. H., and Albelda, S. M. (2011). Expression of a functional CCR2 receptor enhances tumor localization and tumor eradication by retargeted human T cells expressing a mesothelin-specific chimeric antibody receptor. Clin Cancer Res *17*, 4719-4730.

Moon, E. K., Ranganathan, R., Eruslanov, E., Kim, S., Newick, K., O'Brien, S., Lo, A., Liu, X., Zhao, Y., and Albelda, S. M. (2015). Blockade of Programmed Death 1 Augments the Ability of Human T cells Engineered to Target NY-ESO-1 to Control Tumor Growth after Adoptive Transfer. Clin Cancer Res.

Motzer, R. J., Escudier, B., McDermott, D. F., George, S., Hammers, H. J., Srinivas, S., Tykodi, S. S., Sosman, J. A., Procopio, G., Plimack, E. R.*, et al.* (2015). Nivolumab versus Everolimus in Advanced Renal-Cell Carcinoma. N Engl J Med *373*, 1803-1813.

Mueller, B. M., Reisfeld, R. A., Edgington, T. S., and Ruf, W. (1992). Expression of tissue factor by melanoma cells promotes efficient hematogenous metastasis. Proc Natl Acad Sci U S A *89*, 11832-11836.

Mueller, B. M., and Ruf, W. (1998). Requirement for binding of catalytically active factor VIIa in tissue factor-dependent experimental metastasis. J Clin Invest *101*, 1372-1378.

Niedermeyer, J., Garin-Chesa, P., Kriz, M., Hilberg, F., Mueller, E., Bamberger, U., Rettig, W. J., and Schnapp, A. (2001). Expression of the fibroblast activation protein during mouse embryo development. Int J Dev Biol *45*, 445-447.

Niedermeyer, J., Kriz, M., Hilberg, F., Garin-Chesa, P., Bamberger, U., Lenter, M. C., Park, J., Viertel, B., Puschner, H., Mauz, M.*, et al.* (2000). Targeted disruption of mouse fibroblast activation protein. Mol Cell Biol *20*, 1089-1094.

Ohlund, D., Elyada, E., and Tuveson, D. (2014). Fibroblast heterogeneity in the cancer wound. J Exp Med *211*, 1503-1523.

Okada, H., Danoff, T. M., Kalluri, R., and Neilson, E. G. (1997). Early role of Fsp1 in epithelial-mesenchymal transformation. Am J Physiol *273*, F563-574.

Okayama, H., Kohno, T., Ishii, Y., Shimada, Y., Shiraishi, K., Iwakawa, R., Furuta, K., Tsuta, K., Shibata, T., Yamamoto, S.*, et al.* (2012). Identification of genes upregulated in ALK-positive and EGFR/KRAS/ALK-negative lung adenocarcinomas. Cancer Res *72*, 100-111.

Olive, K. P., Jacobetz, M. A., Davidson, C. J., Gopinathan, A., McIntyre, D., Honess, D., Madhu, B., Goldgraben, M. A., Caldwell, M. E., Allard, D.*, et al.* (2009). Inhibition of Hedgehog signaling enhances delivery of chemotherapy in a mouse model of pancreatic cancer. Science *324*, 1457-1461.

Orimo, A., Gupta, P. B., Sgroi, D. C., Arenzana-Seisdedos, F., Delaunay, T., Naeem, R., Carey, V. J., Richardson, A. L., and Weinberg, R. A. (2005). Stromal fibroblasts present in invasive human breast carcinomas promote tumor growth and angiogenesis through elevated SDF-1/CXCL12 secretion. Cell *121*, 335-348.

Orimo, A., and Weinberg, R. A. (2007). Heterogeneity of stromal fibroblasts in tumors. Cancer Biol Ther *6*, 618-619.

Ostermann, E., Garin-Chesa, P., Heider, K. H., Kalat, M., Lamche, H., Puri, C., Kerjaschki, D., Rettig, W. J., and Adolf, G. R. (2008). Effective immunoconjugate therapy in cancer models targeting a serine protease of tumor fibroblasts. Clin Cancer Res *14*, 4584-4592.

Osterreicher, C. H., Penz-Osterreicher, M., Grivennikov, S. I., Guma, M., Koltsova, E. K., Datz, C., Sasik, R., Hardiman, G., Karin, M., and Brenner, D. A. (2011). Fibroblast-specific protein 1 identifies an inflammatory subpopulation of macrophages in the liver. Proc Natl Acad Sci U S A *108*, 308-313.

Ozdemir, B. C., Pentcheva-Hoang, T., Carstens, J. L., Zheng, X., Wu, C. C., Simpson, T. R., Laklai, H., Sugimoto, H., Kahlert, C., Novitskiy, S. V.*, et al.* (2014). Depletion of carcinoma-associated fibroblasts and fibrosis induces immunosuppression and accelerates pancreas cancer with reduced survival. Cancer Cell *25*, 719-734.

Pallangyo, C. K., Ziegler, P. K., and Greten, F. R. (2015). IKKbeta acts as a tumor suppressor in cancer-associated fibroblasts during intestinal tumorigenesis. J Exp Med *212*, 2253-2266.

Palumbo, J. S., Kombrinck, K. W., Drew, A. F., Grimes, T. S., Kiser, J. H., Degen, J. L., and Bugge, T. H. (2000). Fibrinogen is an important determinant of the metastatic potential of circulating tumor cells. Blood *96*, 3302-3309.

Palumbo, J. S., Potter, J. M., Kaplan, L. S., Talmage, K., Jackson, D. G., and Degen, J. L. (2002). Spontaneous hematogenous and lymphatic metastasis, but not primary tumor

growth or angiogenesis, is diminished in fibrinogen-deficient mice. Cancer Res *62*, 6966-6972.

Palumbo, J. S., Talmage, K. E., Massari, J. V., La Jeunesse, C. M., Flick, M. J., Kombrinck, K. W., Hu, Z., Barney, K. A., and Degen, J. L. (2007). Tumor cell-associated tissue factor and circulating hemostatic factors cooperate to increase metastatic potential through natural killer cell-dependent and-independent mechanisms. Blood *110*, 133-141.

Pang, Y., Gara, S. K., Achyut, B. R., Li, Z., Yan, H. H., Day, C. P., Weiss, J. M., Trinchieri, G., Morris, J. C., and Yang, L. (2013). TGF-beta signaling in myeloid cells is required for tumor metastasis. Cancer Discov *3*, 936-951.

Park, J. E., Lenter, M. C., Zimmermann, R. N., Garin-Chesa, P., Old, L. J., and Rettig, W. J. (1999). Fibroblast activation protein, a dual specificity serine protease expressed in reactive human tumor stromal fibroblasts. J Biol Chem *274*, 36505-36512.

Parry, R. V., Rumbley, C. A., Vandenberghe, L. H., June, C. H., and Riley, J. L. (2003). CD28 and inducible costimulatory protein Src homology 2 binding domains show distinct regulation of phosphatidylinositol 3-kinase, Bcl-xL, and IL-2 expression in primary human CD4 T lymphocytes. J Immunol *171*, 166-174.

Patocs, A., Zhang, L., Xu, Y., Weber, F., Caldes, T., Mutter, G. L., Platzer, P., and Eng, C. (2007). Breast-cancer stromal cells with TP53 mutations and nodal metastases. N Engl J Med *357*, 2543-2551.

Pear, W. S., Miller, J. P., Xu, L., Pui, J. C., Soffer, B., Quackenbush, R. C., Pendergast, A. M., Bronson, R., Aster, J. C., Scott, M. L., and Baltimore, D. (1998). Efficient and

rapid induction of a chronic myelogenous leukemia-like myeloproliferative disease in mice receiving P210 bcr/abl-transduced bone marrow. Blood *92*, 3780-3792.

Peek, R. M., Jr., and Crabtree, J. E. (2006). Helicobacter infection and gastric neoplasia. J Pathol *208*, 233-248.

Petersen, O. W., Lind Nielsen, H., Gudjonsson, T., Villadsen, R., Ronnov-Jessen, L., and Bissell, M. J. (2001). The plasticity of human breast carcinoma cells is more than epithelial to mesenchymal conversion. Breast Cancer Res *3*, 213-217.

Pickup, M. W., Mouw, J. K., and Weaver, V. M. (2014). The extracellular matrix modulates the hallmarks of cancer. EMBO Rep *15*, 1243-1253.

Pietras, K., and Ostman, A. (2010). Hallmarks of cancer: interactions with the tumor stroma. Exp Cell Res *316*, 1324-1331.

Pikarsky, E., Porat, R. M., Stein, I., Abramovitch, R., Amit, S., Kasem, S., Gutkovich-Pyest, E., Urieli-Shoval, S., Galun, E., and Ben-Neriah, Y. (2004). NF-kappaB functions as a tumour promoter in inflammation-associated cancer. Nature *431*, 461-466.

Pine, S. R., Mechanic, L. E., Enewold, L., Chaturvedi, A. K., Katki, H. A., Zheng, Y. L., Bowman, E. D., Engels, E. A., Caporaso, N. E., and Harris, C. C. (2011). Increased levels of circulating interleukin 6, interleukin 8, C-reactive protein, and risk of lung cancer. J Natl Cancer Inst *103*, 1112-1122.

Porter, D. L., Hwang, W. T., Frey, N. V., Lacey, S. F., Shaw, P. A., Loren, A. W., Bagg, A., Marcucci, K. T., Shen, A., Gonzalez, V.*, et al.* (2015). Chimeric antigen receptor T

cells persist and induce sustained remissions in relapsed refractory chronic lymphocytic leukemia. Sci Transl Med *7*, 303ra139.

Porter, D. L., Levine, B. L., Kalos, M., Bagg, A., and June, C. H. (2011). Chimeric antigen receptor-modified T cells in chronic lymphoid leukemia. N Engl J Med *365*, 725-733.

Poulsom, R., Pignatelli, M., Stetler-Stevenson, W. G., Liotta, L. A., Wright, P. A., Jeffery, R. E., Longcroft, J. M., Rogers, L., and Stamp, G. W. (1992). Stromal expression of 72 kda type IV collagenase (MMP-2) and TIMP-2 mRNAs in colorectal neoplasia. Am J Pathol *141*, 389-396.

Procopio, M. G., Laszlo, C., Al Labban, D., Kim, D. E., Bordignon, P., Jo, S. H., Goruppi, S., Menietti, E., Ostano, P., Ala, U.*, et al.* (2015). Combined CSL and p53 downregulation promotes cancer-associated fibroblast activation. Nat Cell Biol *17*, 1193-1204.

Proost, P., Struyf, S., Schols, D., Durinx, C., Wuyts, A., Lenaerts, J. P., De Clercq, E., De Meester, I., and Van Damme, J. (1998). Processing by CD26/dipeptidyl-peptidase IV reduces the chemotactic and anti-HIV-1 activity of stromal-cell-derived factor-1alpha. FEBS Lett *432*, 73-76.

Provenzano, P. P., Cuevas, C., Chang, A. E., Goel, V. K., Von Hoff, D. D., and Hingorani, S. R. (2012). Enzymatic targeting of the stroma ablates physical barriers to treatment of pancreatic ductal adenocarcinoma. Cancer Cell *21*, 418-429.

Psaila, B., and Lyden, D. (2009). The metastatic niche: adapting the foreign soil. Nat Rev Cancer *9*, 285-293.

Qian, B., Deng, Y., Im, J. H., Muschel, R. J., Zou, Y., Li, J., Lang, R. A., and Pollard, J. W. (2009). A distinct macrophage population mediates metastatic breast cancer cell extravasation, establishment and growth. PLoS One *4*, e6562.

Qian, B. Z., Li, J., Zhang, H., Kitamura, T., Zhang, J., Campion, L. R., Kaiser, E. A., Snyder, L. A., and Pollard, J. W. (2011). CCL2 recruits inflammatory monocytes to facilitate breast-tumour metastasis. Nature *475*, 222-225.

Qian, B. Z., Zhang, H., Li, J., He, T., Yeo, E. J., Soong, D. Y., Carragher, N. O., Munro, A., Chang, A., Bresnick, A. R.*, et al.* (2015). FLT1 signaling in metastasis-associated macrophages activates an inflammatory signature that promotes breast cancer metastasis. J Exp Med *212*, 1433-1448.

Qiu, W., Hu, M., Sridhar, A., Opeskin, K., Fox, S., Shipitsin, M., Trivett, M., Thompson, E. R., Ramakrishna, M., Gorringe, K. L.*, et al.* (2008). No evidence of clonal somatic genetic alterations in cancer-associated fibroblasts from human breast and ovarian carcinomas. Nat Genet *40*, 650-655.

Quante, M., Tu, S. P., Tomita, H., Gonda, T., Wang, S. S., Takashi, S., Baik, G. H., Shibata, W., Diprete, B., Betz, K. S.*, et al.* (2011). Bone marrow-derived myofibroblasts contribute to the mesenchymal stem cell niche and promote tumor growth. Cancer Cell *19*, 257-272.

Radu, M., and Chernoff, J. (2013). An in vivo assay to test blood vessel permeability. J Vis Exp, e50062.

Rahib, L., Smith, B. D., Aizenberg, R., Rosenzweig, A. B., Fleshman, J. M., and Matrisian, L. M. (2014). Projecting cancer incidence and deaths to 2030: the unexpected

burden of thyroid, liver, and pancreas cancers in the United States. Cancer Res *74*, 2913-2921.

Rettig, W. J., Chesa, P. G., Beresford, H. R., Feickert, H. J., Jennings, M. T., Cohen, J., Oettgen, H. F., and Old, L. J. (1986). Differential expression of cell surface antigens and glial fibrillary acidic protein in human astrocytoma subsets. Cancer Res *46*, 6406-6412.

Rettig, W. J., Garin-Chesa, P., Healey, J. H., Su, S. L., Ozer, H. L., Schwab, M., Albino, A. P., and Old, L. J. (1993). Regulation and heteromeric structure of the fibroblast activation protein in normal and transformed cells of mesenchymal and neuroectodermal origin. Cancer Res *53*, 3327-3335.

Rhim, A. D., Oberstein, P. E., Thomas, D. H., Mirek, E. T., Palermo, C. F., Sastra, S. A., Dekleva, E. N., Saunders, T., Becerra, C. P., Tattersall, I. W.*, et al.* (2014). Stromal elements act to restrain, rather than support, pancreatic ductal adenocarcinoma. Cancer Cell *25*, 735-747.

Rhodes, D. R., Yu, J., Shanker, K., Deshpande, N., Varambally, R., Ghosh, D., Barrette, T., Pandey, A., and Chinnaiyan, A. M. (2004). ONCOMINE: a cancer microarray database and integrated data-mining platform. Neoplasia *6*, 1-6.

Riese, M. J., Wang, L. C., Moon, E. K., Joshi, R. P., Ranganathan, A., June, C. H., Koretzky, G. A., and Albelda, S. M. (2013). Enhanced effector responses in activated CD8+ T cells deficient in diacylglycerol kinases. Cancer Res *73*, 3566-3577.

Roberts, E. W., Deonarine, A., Jones, J. O., Denton, A. E., Feig, C., Lyons, S. K., Espeli, M., Kraman, M., McKenna, B., Wells, R. J.*, et al.* (2013). Depletion of stromal cells

expressing fibroblast activation protein-alpha from skeletal muscle and bone marrow results in cachexia and anemia. J Exp Med *210*, 1137-1151.

Ronnov-Jessen, L., and Petersen, O. W. (1993). Induction of alpha-smooth muscle actin by transforming growth factor-beta 1 in quiescent human breast gland fibroblasts. Implications for myofibroblast generation in breast neoplasia. Lab Invest *68*, 696-707.

Royal, R. E., Levy, C., Turner, K., Mathur, A., Hughes, M., Kammula, U. S., Sherry, R. M., Topalian, S. L., Yang, J. C., Lowy, I., and Rosenberg, S. A. (2010). Phase 2 trial of single agent Ipilimumab (anti-CTLA-4) for locally advanced or metastatic pancreatic adenocarcinoma. J Immunother *33*, 828-833.

Rudisch, A., Dewhurst, M. R., Horga, L. G., Kramer, N., Harrer, N., Dong, M., van der Kuip, H., Wernitznig, A., Bernthaler, A., Dolznig, H., and Sommergruber, W. (2015). High EMT Signature Score of Invasive Non-Small Cell Lung Cancer (NSCLC) Cells Correlates with NFkappaB Driven Colony-Stimulating Factor 2 (CSF2/GM-CSF) Secretion by Neighboring Stromal Fibroblasts. PLoS One *10*, e0124283.

Ryan, D. P., Hong, T. S., and Bardeesy, N. (2014). Pancreatic adenocarcinoma. N Engl J Med *371*, 1039-1049.

Salmon, H., Franciszkiewicz, K., Damotte, D., Dieu-Nosjean, M. C., Validire, P., Trautmann, A., Mami-Chouaib, F., and Donnadieu, E. (2012). Matrix architecture defines the preferential localization and migration of T cells into the stroma of human lung tumors. J Clin Invest *122*, 899-910.

Santos, A. M., Jung, J., Aziz, N., Kissil, J. L., and Pure, E. (2009). Targeting fibroblast activation protein inhibits tumor stromagenesis and growth in mice. J Clin Invest *119*, 3613-3625.

Sanz-Moreno, V., Gaggioli, C., Yeo, M., Albrengues, J., Wallberg, F., Viros, A., Hooper, S., Mitter, R., Feral, C. C., Cook, M.*, et al.* (2011). ROCK and JAK1 signaling cooperate to control actomyosin contractility in tumor cells and stroma. Cancer Cell *20*, 229-245.

Sauer, B., and Henderson, N. (1988). Site-specific DNA recombination in mammalian cells by the Cre recombinase of bacteriophage P1. Proc Natl Acad Sci U S A *85*, 5166-5170.

Scanlan, M. J., Raj, B. K., Calvo, B., Garin-Chesa, P., Sanz-Moncasi, M. P., Healey, J. H., Old, L. J., and Rettig, W. J. (1994). Molecular cloning of fibroblast activation protein alpha, a member of the serine protease family selectively expressed in stromal fibroblasts of epithelial cancers. Proc Natl Acad Sci U S A *91*, 5657-5661.

Scherz-Shouval, R., Santagata, S., Mendillo, M. L., Sholl, L. M., Ben-Aharon, I., Beck, A. H., Dias-Santagata, D., Koeva, M., Stemmer, S. M., Whitesell, L., and Lindquist, S. (2014). The reprogramming of tumor stroma by HSF1 is a potent enabler of malignancy. Cell *158*, 564-578.

Schuberth, P. C., Hagedorn, C., Jensen, S. M., Gulati, P., van den Broek, M., Mischo, A., Soltermann, A., Jungel, A., Marroquin Belaunzaran, O., Stahel, R.*, et al.* (2013). Treatment of malignant pleural mesothelioma by fibroblast activation protein-specific re-directed T cells. J Transl Med *11*, 187.

Sherman, M. H., Yu, R. T., Engle, D. D., Ding, N., Atkins, A. R., Tiriac, H., Collisson, E. A., Connor, F., Van Dyke, T., Kozlov, S.*, et al.* (2014). Vitamin D receptor-mediated stromal reprogramming suppresses pancreatitis and enhances pancreatic cancer therapy. Cell *159*, 80-93.

Shi, M., Yu, D. H., Chen, Y., Zhao, C. Y., Zhang, J., Liu, Q. H., Ni, C. R., and Zhu, M. H. (2012). Expression of fibroblast activation protein in human pancreatic adenocarcinoma and its clinicopathological significance. World J Gastroenterol *18*, 840-846.

Shields, M. A., Dangi-Garimella, S., Krantz, S. B., Bentrem, D. J., and Munshi, H. G. (2011). Pancreatic cancer cells respond to type I collagen by inducing snail expression to promote membrane type 1 matrix metalloproteinase-dependent collagen invasion. J Biol Chem *286*, 10495-10504.

Shimoda, M., Principe, S., Jackson, H. W., Luga, V., Fang, H., Molyneux, S. D., Shao, Y. W., Aiken, A., Waterhouse, P. D., Karamboulas, C.*, et al.* (2014). Loss of the Timp gene family is sufficient for the acquisition of the CAF-like cell state. Nat Cell Biol *16*, 889-901.

Sierra-Filardi, E., Nieto, C., Dominguez-Soto, A., Barroso, R., Sanchez-Mateos, P., Puig-Kroger, A., Lopez-Bravo, M., Joven, J., Ardavin, C., Rodriguez-Fernandez, J. L.*, et al.* (2014). CCL2 shapes macrophage polarization by GM-CSF and M-CSF: identification of CCL2/CCR2-dependent gene expression profile. J Immunol *192*, 3858-3867.

Smith, N. R., Baker, D., Farren, M., Pommier, A., Swann, R., Wang, X., Mistry, S., McDaid, K., Kendrew, J., Womack, C.*, et al.* (2013). Tumor stromal architecture can

define the intrinsic tumor response to VEGF-targeted therapy. Clin Cancer Res *19*, 6943-6956.

Stairs, D. B., Bayne, L. J., Rhoades, B., Vega, M. E., Waldron, T. J., Kalabis, J., Klein-Szanto, A., Lee, J. S., Katz, J. P., Diehl, J. A.*, et al.* (2011). Deletion of p120-catenin results in a tumor microenvironment with inflammation and cancer that establishes it as a tumor suppressor gene. Cancer Cell *19*, 470-483.

Stearman, R. S., Dwyer-Nield, L., Zerbe, L., Blaine, S. A., Chan, Z., Bunn, P. A., Jr., Johnson, G. L., Hirsch, F. R., Merrick, D. T., Franklin, W. A.*, et al.* (2005). Analysis of orthologous gene expression between human pulmonary adenocarcinoma and a carcinogen-induced murine model. Am J Pathol *167*, 1763-1775.

Sternlicht, M. D., Lochter, A., Sympson, C. J., Huey, B., Rougier, J. P., Gray, J. W., Pinkel, D., Bissell, M. J., and Werb, Z. (1999). The stromal proteinase MMP3/stromelysin-1 promotes mammary carcinogenesis. Cell *98*, 137-146.

Stoker, M. G., Shearer, M., and O'Neill, C. (1966). Growth inhibition of polyoma-transformed cells by contact with static normal fibroblasts. J Cell Sci *1*, 297-310.

Stromnes, I. M., Brockenbrough, J. S., Izeradjene, K., Carlson, M. A., Cuevas, C., Simmons, R. M., Greenberg, P. D., and Hingorani, S. R. (2014). Targeted depletion of an MDSC subset unmasks pancreatic ductal adenocarcinoma to adaptive immunity. Gut *63*, 1769-1781.

Stylianopoulos, T., Martin, J. D., Chauhan, V. P., Jain, S. R., Diop-Frimpong, B., Bardeesy, N., Smith, B. L., Ferrone, C. R., Hornicek, F. J., Boucher, Y.*, et al.* (2012).

Causes, consequences, and remedies for growth-induced solid stress in murine and human tumors. Proc Natl Acad Sci U S A *109*, 15101-15108.

Su, L. J., Chang, C. W., Wu, Y. C., Chen, K. C., Lin, C. J., Liang, S. C., Lin, C. H., Whang-Peng, J., Hsu, S. L., Chen, C. H., and Huang, C. Y. (2007). Selection of DDX5 as a novel internal control for Q-RT-PCR from microarray data using a block bootstrap re-sampling scheme. BMC Genomics *8*, 140.

Su, W. P., Chen, Y. T., Lai, W. W., Lin, C. C., Yan, J. J., and Su, W. C. (2011). Apolipoprotein E expression promotes lung adenocarcinoma proliferation and migration and as a potential survival marker in lung cancer. Lung Cancer *71*, 28-33.

Tchou, J., Zhang, P. J., Bi, Y., Satija, C., Marjumdar, R., Stephen, T. L., Lo, A., Chen, H., Mies, C., June, C. H.*, et al.* (2013). Fibroblast activation protein expression by stromal cells and tumor-associated macrophages in human breast cancer. Hum Pathol *44*, 2549-2557.

Terzic, J., Grivennikov, S., Karin, E., and Karin, M. (2010). Inflammation and colon cancer. Gastroenterology *138*, 2101-2114 e2105.

Tian, X., Azpurua, J., Hine, C., Vaidya, A., Myakishev-Rempel, M., Ablaeva, J., Mao, Z., Nevo, E., Gorbunova, V., and Seluanov, A. (2013). High-molecular-mass hyaluronan mediates the cancer resistance of the naked mole rat. Nature *499*, 346-349.

Torres, S., Bartolome, R. A., Mendes, M., Barderas, R., Fernandez-Acenero, M. J., Pelaez-Garcia, A., Pena, C., Lopez-Lucendo, M., Villar-Vazquez, R., de Herreros, A. G.*, et al.* (2013). Proteome profiling of cancer-associated fibroblasts identifies novel

proinflammatory signatures and prognostic markers for colorectal cancer. Clin Cancer Res *19*, 6006-6019.

Tran, E., Chinnasamy, D., Yu, Z., Morgan, R. A., Lee, C. C., Restifo, N. P., and Rosenberg, S. A. (2013). Immune targeting of fibroblast activation protein triggers recognition of multipotent bone marrow stromal cells and cachexia. J Exp Med *210*, 1125-1135.

Trimboli, A. J., Cantemir-Stone, C. Z., Li, F., Wallace, J. A., Merchant, A., Creasap, N., Thompson, J. C., Caserta, E., Wang, H., Chong, J. L.*, et al.* (2009). Pten in stromal fibroblasts suppresses mammary epithelial tumours. Nature *461*, 1084-1091.

Valencia, K., Ormazabal, C., Zandueta, C., Luis-Ravelo, D., Anton, I., Pajares, M. J., Agorreta, J., Montuenga, L. M., Martinez-Canarias, S., Leitinger, B., and Lecanda, F. (2012). Inhibition of collagen receptor discoidin domain receptor-1 (DDR1) reduces cell survival, homing, and colonization in lung cancer bone metastasis. Clin Cancer Res *18*, 969-980.

Valencia, T., Kim, J. Y., Abu-Baker, S., Moscat-Pardos, J., Ahn, C. S., Reina-Campos, M., Duran, A., Castilla, E. A., Metallo, C. M., Diaz-Meco, M. T., and Moscat, J. (2014). Metabolic reprogramming of stromal fibroblasts through p62-mTORC1 signaling promotes inflammation and tumorigenesis. Cancer Cell *26*, 121-135.

Vicent, S., Sayles, L. C., Vaka, D., Khatri, P., Gevaert, O., Chen, R., Zheng, Y., Gillespie, A. K., Clarke, N., Xu, Y.*, et al.* (2012). Cross-species functional analysis of cancer-associated fibroblasts identifies a critical role for CLCF1 and IL-6 in non-small cell lung cancer in vivo. Cancer Res *72*, 5744-5756.

Von Hoff, D. D., Ramanathan, R. K., Borad, M. J., Laheru, D. A., Smith, L. S., Wood, T. E., Korn, R. L., Desai, N., Trieu, V., Iglesias, J. L.*, et al.* (2011). Gemcitabine plus nab-paclitaxel is an active regimen in patients with advanced pancreatic cancer: a phase I/II trial. J Clin Oncol *29*, 4548-4554.

Walter, K., Omura, N., Hong, S. M., Griffith, M., and Goggins, M. (2008). Pancreatic cancer associated fibroblasts display normal allelotypes. Cancer Biol Ther *7*, 882-888.

Wang, E., Wang, L. C., Tsai, C. Y., Bhoj, V., Gershenson, Z., Moon, E., Newick, K., Sun, J., Lo, A., Baradet, T.*, et al.* (2015). Generation of Potent T-cell Immunotherapy for Cancer Using DAP12-Based, Multichain, Chimeric Immunoreceptors. Cancer Immunol Res *3*, 815-826.

Wang, H., Wu, Q., Liu, Z., Luo, X., Fan, Y., Liu, Y., Zhang, Y., Hua, S., Fu, Q., Zhao, M.*, et al.* (2014a). Downregulation of FAP suppresses cell proliferation and metastasis through PTEN/PI3K/AKT and Ras-ERK signaling in oral squamous cell carcinoma. Cell Death Dis *5*, e1155.

Wang, L. C., Lo, A., Scholler, J., Sun, J., Majumdar, R. S., Kapoor, V., Antzis, M., Cotner, C. E., Johnson, L. A., Durham, A. C.*, et al.* (2014b). Targeting fibroblast activation protein in tumor stroma with chimeric antigen receptor T cells can inhibit tumor growth and augment host immunity without severe toxicity. Cancer Immunol Res *2*, 154-166.

Wang, S. J., and Bourguignon, L. Y. (2006). Hyaluronan and the interaction between CD44 and epidermal growth factor receptor in oncogenic signaling and chemotherapy resistance in head and neck cancer. Arch Otolaryngol Head Neck Surg *132*, 771-778.

Wang, X. M., Yao, T. W., Nadvi, N. A., Osborne, B., McCaughan, G. W., and Gorrell, M. D. (2008). Fibroblast activation protein and chronic liver disease. Front Biosci *13*, 3168-3180.

Waterman, R. S., Henkle, S. L., and Betancourt, A. M. (2012). Mesenchymal stem cell 1 (MSC1)-based therapy attenuates tumor growth whereas MSC2-treatment promotes tumor growth and metastasis. PLoS One *7*, e45590.

Weinberg, R. A. (2008). Coevolution in the tumor microenvironment. Nat Genet *40*, 494-495.

Wendling, O., Bornert, J. M., Chambon, P., and Metzger, D. (2009). Efficient temporally-controlled targeted mutagenesis in smooth muscle cells of the adult mouse. Genesis *47*, 14-18.

Whatcott, C. J., Diep, C. H., Jiang, P., Watanabe, A., LoBello, J., Sima, C., Hostetter, G., Shepard, H. M., Von Hoff, D. D., and Han, H. (2015). Desmoplasia in Primary Tumors and Metastatic Lesions of Pancreatic Cancer. Clin Cancer Res *21*, 3561-3568.

Wolchok, J. D., Kluger, H., Callahan, M. K., Postow, M. A., Rizvi, N. A., Lesokhin, A. M., Segal, N. H., Ariyan, C. E., Gordon, R. A., Reed, K.*, et al.* (2013). Nivolumab plus ipilimumab in advanced melanoma. N Engl J Med *369*, 122-133.

Wu, C. Y., Roybal, K. T., Puchner, E. M., Onuffer, J., and Lim, W. A. (2015). Remote control of therapeutic T cells through a small molecule-gated chimeric receptor. Science *350*, aab4077.

Xu, Z., Vonlaufen, A., Phillips, P. A., Fiala-Beer, E., Zhang, X., Yang, L., Biankin, A. V., Goldstein, D., Pirola, R. C., Wilson, J. S., and Apte, M. V. (2010). Role of pancreatic stellate cells in pancreatic cancer metastasis. Am J Pathol *177*, 2585-2596.

Yan, L., and DeMars, L. C. (2014). Effects of a high-fat diet on spontaneous metastasis of Lewis lung carcinoma in plasminogen activator inhibitor-1 deficient and wild-type mice. PLoS One *9*, e110869.

Yokota, N., Zarpellon, A., Chakrabarty, S., Bogdanov, V. Y., Gruber, A., Castellino, F. J., Mackman, N., Ellies, L. G., Weiler, H., Ruggeri, Z. M., and Ruf, W. (2014). Contributions of thrombin targets to tissue factor-dependent metastasis in hyperthrombotic mice. J Thromb Haemost *12*, 71-81.

Yu, Q., and Stamenkovic, I. (2000). Cell surface-localized matrix metalloproteinase-9 proteolytically activates TGF-beta and promotes tumor invasion and angiogenesis. Genes Dev *14*, 163-176.

Zeisberg, E. M., Potenta, S., Xie, L., Zeisberg, M., and Kalluri, R. (2007). Discovery of endothelial to mesenchymal transition as a source for carcinoma-associated fibroblasts. Cancer Res *67*, 10123-10128.

Zhang, D., Wang, Y., Shi, Z., Liu, J., Sun, P., Hou, X., Zhang, J., Zhao, S., Zhou, B. P., and Mi, J. (2015). Metabolic reprogramming of cancer-associated fibroblasts by IDH3alpha downregulation. Cell Rep *10*, 1335-1348.

Zhang, K., Corsa, C. A., Ponik, S. M., Prior, J. L., Piwnica-Worms, D., Eliceiri, K. W., Keely, P. J., and Longmore, G. D. (2013). The collagen receptor discoidin domain

receptor 2 stabilizes SNAIL1 to facilitate breast cancer metastasis. Nat Cell Biol *15*, 677-687.

Zhao, Y., Moon, E., Carpenito, C., Paulos, C. M., Liu, X., Brennan, A. L., Chew, A., Carroll, R. G., Scholler, J., Levine, B. L.*, et al.* (2010). Multiple injections of electroporated autologous T cells expressing a chimeric antigen receptor mediate regression of human disseminated tumor. Cancer Res *70*, 9053-9061.

Zhen, E. Y., Jin, Z., Ackermann, B. L., Thomas, M. K., and Gutierrez, J. A. (2015). Circulating FGF21 Proteolytic Processing Mediated by Fibroblast Activation Protein. Biochem J.

Zigrino, P., Kuhn, I., Bauerle, T., Zamek, J., Fox, J. W., Neumann, S., Licht, A., Schorpp-Kistner, M., Angel, P., and Mauch, C. (2009). Stromal expression of MMP-13 is required for melanoma invasion and metastasis. J Invest Dermatol *129*, 2686-2693.